

Bioinspired Redox Active Pseudotetrahedral Ni(II) Thiolate and Phenolate Complexes:
Synthesis, Characterization, Alkylation Kinetics and Molecular Oxygen Activation

A dissertation presented to
the faculty of
the College of Arts and Sciences of Ohio University

In partial fulfillment
of the requirements for the degree
Doctor of Philosophy

Tapash K. Deb

December 2013

© 2013 Tapash K. Deb. All Rights Reserved.

This dissertation titled
Bioinspired Redox Active Pseudotetrahedral Ni(II) Thiolate and Phenolate Complexes:
Synthesis, Characterization, Alkylation Kinetics and Molecular Oxygen Activation

by

TAPASH K. DEB

has been approved for
the Department of Chemistry and Biochemistry
and the College of Arts and Sciences by

Michael P. Jensen

Associate Professor of Chemistry and Biochemistry

Robert Frank

Dean, College of Arts and Sciences

ABSTRACT

DEB, TAPASH K., Ph.D., December 2013, Chemistry

Bioinspired Redox Active Pseudotetrahedral Ni(II) Thiolate and Phenolate Complexes:
Synthesis, Characterization, Alkylation Kinetics and Molecular Oxygen Activation

Director of Dissertation: Michael P. Jensen

A series of new environmentally and catalytically significant bioinorganic redox active pseudotetrahedral Ni(II) thiolate and Ni(II) phenolate ($S=1$, d^8) complexes were synthesized and fully characterized as small molecular models in order to study the coordination mode of the Ni-S bond that is biologically significant in anaerobic and archaeobacterial enzymes. During this characterization a unique Ni-S ligation mode was discovered and modulated by steric titration and details were further investigated. Nickel thiolate bond reactivity towards electrophilic alkylation with methyl iodide (MeI) is briefly discussed. A series of new Ni(II) phenolate complexes were synthesized and characterized as well as their O_2 activation activity were investigated as a model for nickel substituted Copper Amine Oxidase (CAO). During this O_2 reduction investigation, depending on the ligand bulk on the parent $Tp^{Ph,Me}/Tp^{Me,Me}$ ligand (where, $Tp^{Ph,Me}$ = hydrotris{3-phenyl-5-methyl pyrazol-1-yl}borate; $Tp^{Me,Me}$ = hydrotris{3,5-dimethyl pyrazol-1-yl}borate) either a C-H or a C=C bond activation was observed. In addition, surprisingly where C-H activation was not possible, a CO_2 capture activity was observed by a reactive intermediate nickel species.

DEDICATION

*This dissertation is dedicated to my loving parents Jayanta Bhushan Deb and Tripti Deb
for their significant inspiration and sacrifices*

ACKNOWLEDGMENTS

This dissertation is a combined work of multiple related projects. One of the major publications was possible because someone in the research group inspired me to do investigative chemistry and that person is my research advisor Professor Michael P. Jensen. In a traditional environment, graduate students just follow what their advisor asks them to do mostly word for word but he also encouraged to look at similar relevant chemistry by varying different groups, metals etc. and find out the similarities and dissimilarities and dig deeper. I learned a lot from him – not only chemistry but also professional attitude and behavior.

In addition, I would like to thank the members of my dissertation committee (Prof. Jeffrey Rack, Prof. Hugh Richardson and Prof. Alexander Govorov) for their time and support. I should mention of Professor Rack in particular, who helped me in various ways- such as supporting me to go to conferences. Also, Prof. Richardson for his questions in PIG seminar that made me think deeper into the fundamental aspects of chemistry.

I would also like to thank my fellow lab mates, faculty, staff and especially former post doctoral researcher Dr. Swarup Chattopadhyay for their support and contribution. Our collaborators Prof. Jeffrey Petersen at West Virginia University and Dr. Victor G. Young also contributed to my publications with excellent X-ray crystallographic data.

Outside the department, I would like to thank my family and friends for their strong support and motivation through rough days when things did not work as planned, without their support it would have been really difficult to complete my PhD.

TABLE OF CONTENTS

	Page
Abstract.....	3
Dedication.....	4
Acknowledgments.....	5
List of Tables	9
List of Schemes.....	10
List of Figures.....	11
Chapter 1: Introduction.....	15
1.1 Other remarks	26
1.2 References.....	27
Chapter 2: Arylthiolate Coordination and Reactivity at High-spin Nickel(II): Modulation by Non-Covalent Interactions.....	31
2.1 Introduction.....	31
2.2 Experimental.....	33
2.3 Results.....	37
2.4 Discussion.....	51
2.5 Conclusions.....	53
2.6 References.....	57
Chapter 3: Steric Titration of Arylthiolate Coordination Modes at Pseudotetrahedral Nickel (II) Centers	65
3.1 Introduction.....	65
3.2 Experimental Methods.....	67
3.3 Results and Discussion	72
3.4 Conclusion	98
3.5 References.....	101
Chapter 4: Aerobic and hydrolytic decomposition of pseudotetrahedral nickel phenolate complexes	106
4.1 Introduction.....	106
4.2 Experimental.....	108
4.3 Results.....	117
4.4 Discussion and Conclusion.....	131

4.5 References.....	147
Appendix A: Permissions for figures.....	156
Appendix B: Crystal Data refinement and bond lengths for complex 2.1a	159
Appendix C: Crystal Data refinement and bond lengths 2.2c	163
Appendix D: Electronic spectra and configurational data for chapter 3.....	170
Appendix E: Crystal structure and data refinement for complex 3.5	185
Appendix F: Detailed Spectra of Oxidation of Nickel(II)phenolates	192
Appendix G: Crystal structure and data refinement for complex 4.1b	241
Appendix H: Crystal structure and data refinement for complex 4.1a	248
Appendix I: Crystal structure and data refinement for complex 4.2	256
Appendix J: Crystal structure and data refinement for complex 4.3	263
Appendix K: Crystal structure and data refinement for complex 4.4	271

LIST OF TABLES

	Page
Table 1: Curie Law fits to paramagnetic contact shifts for arylthiolate complexes.	55
Table 2: Summary of the crystal data and structure refinements.....	56
Table 3: Summary of significant bond lengths and angles.....	57
Table 4: Structural parameters for Ni(II) arylthiolate complexes of tripodal borato ligands.....	80
Table 5: Summary of X-ray crystallography.....	146
Table 6: Calculated bond lengths from computational models.....	147

LIST OF SCHEMES

	Page
Scheme 1: Thiolate Reaction Scheme.....	20
Scheme 2: Proposed mechanism of CAO.....	136
Scheme 3: Singlet oxygen degradation mechanism.....	136
Scheme 4: Proposed degradation mechanism of Ni(II)Phenolates.....	137

LIST OF FIGURES

	Page
Figure 1: ACDS A cluster β subunit.....	17
Figure 2: Ni-Fe hydrogenase active site	18
Figure 3: Interconnected carbon cycle similar to the Monsanto reaction.....	18
Figure 4: APO-CAO retains reactivity with alternative metals	24
Figure 5: Proposed mechanism of CAO by Klinman <i>et al.</i>	25
Figure 6: UV-Vis-NIR spectra at 297 K in CH_2Cl_2 solution for: $\text{Tp}^{\text{Me,Me}}\text{Ni-SPh}$ (2.1a , magenta trace); $\text{Tp}^{\text{Me,Me}}\text{Ni-SMes}$ (2.1b , red); $\text{Tp}^{\text{Ph,Me}}\text{Ni-SPh}$ (2.2a , green); and $\text{Tp}^{\text{Ph,Me}}\text{Ni-SMes}$ (2.2b , blue).....	38
Figure 7: ^1H NMR spectra recorded at 293 K in CDCl_3 solution for: $\text{Tp}^{\text{Me,Me}}\text{Ni-Cl}$ (top), labels indicate tris(pyrazolylborate) resonances, s = residual solvent, w=water; $\text{Tp}^{\text{Me,Me}}\text{Ni-SPh}$ (middle), labels indicate arylthiolate resonances; and $\text{Tp}^{\text{Me,Me}}\text{Ni-SMes}$ (bottom).....	42
Figure 8: Plot of averaged LMCT band energies of 2.1a,b and 2.2a,b versus hyperfine slopes for arylthiolate meta resonances (\blacklozenge , left axis) and 4-pyrazolyl resonances (\square , right axis).....	44
Figure 9: ORTEP plots for $\text{Tp}^{\text{Me,Me}}\text{Ni-SPh}$ (2.1a , left) and $\text{Tp}^{\text{Ph,Me}}\text{Ni-SXyl}$ (2.2c , right) with thermal ellipsoids drawn at 30% probability. A least-squares superposition of the structures is shown at center to highlight differential thiolate coordination; for clarity, only the ipso carbons of the 3-Ph substituents are shown for 2.2c	44
Figure 10: ^1H NMR spectra for reaction of $\text{Tp}^{\text{Me,Me}}\text{Ni-SMes}$ and MeI in CD_2Cl_2 at 295 K, near the start (bottom) and near equilibrium (top). Inset shows spectrum of arylmethylsulfide co-product recorded using routine acquisition parameters for a diamagnetic solvate.....	49
Figure 11: UV-visible traces for reaction of $\text{Tp}^{\text{Ph,Me}}\text{Ni-SMes}$ (2.2b , 0.5 mM) with MeI (128 mM) at 295 K in CH_2Cl_2 solution ($\Delta t = 900$ s). Limiting traces shown in blue and red are calculated spectra of the starting thiolate and product $\text{Tp}^{\text{Ph,Me}}\text{Ni-I}$ complexes,	

respectively. Inset shows a single-exponential fit by global least-squares techniques to the time-dependent optical density at 574 nm (λ_{\max} for 2.2b).....	49
Figure 12: Dependence of methyl iodide concentration on rate of decomposition ($k_{\text{obs}} = k_1 + k_2[\text{MeI}]$) for $\text{Tp}^{\text{Me,Me}}\text{Ni-SPh}$ (2.1a , \blacktriangledown , $R^2 = 0.91$) and $\text{Tp}^{\text{Ph,Me}}\text{Ni-SPh}$ (2.2b , \bullet , $R^2 = 0.99$) in CH_2Cl_2 solution at 297 K.	50
Figure 13: ORTEP diagram (50% ellipsoids) of $\text{Tp}^{\text{Me,Me}}\text{Ni-S-2,6-Ph}_2\text{C}_6\text{H}_3$ (3.5) Selected bond lengths (\AA): Ni1-N4, 1.995(1); Ni1-N2, 2.001(2); Ni1-S1, 2.2589(6); S1-C11, 1.785(2). Bond angles ($^\circ$): N4-Ni1-N4', 92.06(8); N4-Ni1-N2, 91.20(5); N4-Ni1-S1, 115.47(4); N2-Ni1-S1, 140.01(6); Ni1-S1-C11, 100.11(7).....	73
Figure 14: Illustration of sawhorse (top) and off-axis bending (bottom) on a <i>cis</i> -divacant octahedron (left column) and monovacant trigonal bipyramid (right column), as seen in two orientations of the core structures for 3.5 (top row) and 3.9 (bottom row), with <i>ortho</i> substituents on the arylthiolate rings and all but the <i>ipso</i> carbon of the 3-phenyl substituents of 3.9 omitted for clarity.	78
Figure 15: Space-filling models of 2.1a (left) and 3.5 (right), demonstrating a dominant steric role for <i>ortho</i> substitution in effecting an observed conformational switch in arylthiolate coordination.	79
Figure 16: ^1H NMR spectra of 2.1a , 3.2 and 3.5 (from bottom to top, respectively) recorded in CDCl_3 at 293 K. The peak marked (*) is residual solvent; peak assignments not labeled are listed in the experimental section. Arrows indicate shift of the resonance assigned to the <i>para</i> position of the arylthiolate rings.....	81
Figure 17: UV-visible-NIR spectra (CH_2Cl_2 solutions, 297 K) of 2.1a (black), 3.3 (green), 3.4 (red), and 3.5 (blue).....	85
Figure 18: UV-visible-NIR spectra of 3.3 in toluene as a function of temperature from 287-343 K. Spectra were normalized for changes in solvent density.....	85
Figure 19: UV-visible-NIR spectra (CH_2Cl_2 solutions, 297 K) of 2.1a (black), 3.6 (blue), 3.7 (red), and 3.8 (green)	86
Figure 20: Relevant frontier orbitals of the free PhS^- ligand, separated by symmetry class. The dashed horizontal line separates occupied and empty orbitals.	88

- Figure 21: Qualitative symmetry-derived ligand field splittings for tetrahedral (left), axial pseudotetrahedral (center), and bent arylthiolate geometries (right). 88
- Figure 22: Relevant β -spin frontier orbitals for **2.1a'** (left) and **3.5'** (right). Orbitals are distinguished by parity under imposed C_s symmetry, with a' (red) and a'' (blue) representations corresponding to respective σ and π overlap along the Ni-S bond vector. 91
- Figure 23: Sterically accessible limiting configurations for a simplified TpNiSPh model. Horizontal translation between columns corresponds to 90° rotation about the S- C_{ipso} bond, transposing the π_{ip} and π_{op} thiolate donor orbitals, and vertical translation down a column corresponds to 90° rotation about the Ni-S bond, transposing Ni $d\pi^*$ acceptor orbitals. Number in brackets indicates the relative calculated energy in kJ/mole. 94
- Figure 24: TD-DFT calculated spectra of **2.1a''** (bottom) and **3.5'** (top). Ligand field and S-Ni LMCT bands are labeled with predominant orbital contributions. For convenience, calculated lines are presented as Gaussian curves with line widths of 3 nm (corresponding to the vertical intensity scale) and 50 nm (vertical scale exaggerated with offset). 98
- Figure 25: Thermal ellipsoid plots (50% probability) of $\text{Tp}^{\text{Ph,Me}}\text{Ni-O-2,6-}^i\text{Pr}_2\text{C}_6\text{H}_3$ (**4.1a**, left) and $\text{Tp}^{\text{Me,Me}}\text{Ni-O-2,6-}^i\text{Pr}_2\text{C}_6\text{H}_3$ (**4.1b**, right). Hydrogen atoms are omitted for clarity. 138
- Figure 26: UV-Vis-NIR spectra for decomposition of **4.1a** (0.61 mM) in CH_2Cl_2 under O_2 (306 K). Inset shows traces at 476 nm (green trace, left axis) and 426 nm (red trace, right axis), corresponding to the absorption maxima of **4.1a** and 3,5,3',5'-tetrakisopropyl-4,4'-diphenoquinone, respectively. 139
- Figure 27: Thermal ellipsoid plot (30% probability) for dimeric $[(\text{Tp}^{\text{Ph,Me}^*})\text{Ni}]_2$ (**4.2**, left) and the monomeric asymmetric unit (right). Hydrogen atoms are omitted for clarity. . 139
- Figure 28: Thermal ellipsoid plot (30% probability) of $[\text{Tp}^{\text{Me,Me}}\text{Ni}]_2(\mu\text{-CO}_3)$ (**4.3**). Hydrogen atoms are omitted for clarity. 140
- Figure 29: UV-Vis spectra demonstrating reaction of **4.1a** (0.30 mM, green) with added H_2O (270 mM) to form a hydrolyzed intermediate (blue) that reacts rapidly with H_2O_2 (67 mM) to form **4.2** (red). 141

- Figure 30: UV-Vis-NIR absorption vs. time ($\Delta t = 1000$ s) following addition of O_2 to a hydrolyzed solution of **4.1a** (0.44 mM in CH_2Cl_2 , 306 K). Inset shows trace at 426 nm (red), corresponding to accumulation of 3,5,3',5'-tetraisopropyl-4,4'-diphenoquinone, and compared to data shown in Figure 26 for O_2 addition to intact **4.1a** (green) and corrected for absorption of **4.1a** (black). 141
- Figure 31: Thermal ellipsoid plot (30% probability) of $[(Tp^{Ph,Me})_2Ni]$ (**4.4**). For clarity, hydrogen atoms are omitted and carbon atoms of opposing ligands are differentially shaded. 142
- Figure 32: Optimized geometries of C_s -symmetric computational models of TpNiOPh (A), TpNiOPh(O_2) (B-D) and TpNiO $_2$ (E-I)..... 143
- Figure 33: Relevant spin-unrestricted frontier molecular orbitals in the C_s -symmetric TpNiOPh computational model (Figure 32-A), circumscribing five nickel d orbitals and the in-plane and out-of-plane phenolate donor orbitals. Red and blue orbitals and labels respectively signify symmetry (a') and antisymmetry (a'') with respect to the mirror plane. 144
- Figure 34: Relevant spin-unrestricted frontier molecular orbitals in a C_s -symmetric TpNiOPh(O_2) computational model (Figure 32-B), circumscribing five nickel d orbitals, the two phenolate donor orbitals, and two O_2 π^* orbitals. Red and blue orbitals and labels respectively signify symmetry (a') and antisymmetry (a'') with respect to the mirror plane..... 145

CHAPTER 1: INTRODUCTION

Nickel, an inexpensive abundant metal in nature, is very significant in environmental and biological chemistry¹. Nickel dependent enzymes efficiently interconvert gigatons of CO₂, CO and methane each year by utilizing redox chemistry. The National Oceanic and Atmospheric Administration (NOAA) recently reported² an all time high CO₂ level (400 ppm) in the atmosphere, and if a solution to contain the situation by finding an alternative route to fossil fuel is not found soon, the whole world will be faced with significantly difficult newer challenges. One way to face this challenge would be to better understand the basic chemistry and mechanism these bacterial enzymes exploit for their survival and then design a solution, possibly a catalyst. Hence, it is important to know how the bonding and nature of the atoms surrounding the nickel center in redox active nickel enzymes containing Ni-S_{cys} or Ni-SAr_{tyr} bonds.

From the environmental perspective, a recent article³ in *Nature* reported that a depletion of oceanic nickel due to cooling of the upper atmosphere and decreased eruption of nickel rich minerals from volcanoes caused a famine (from about 400 nM concentration around 2.7×10^9 years ago to about 9 nM around 550 mega years ago) to the most archaic methanogen bacteria that solely relied on nickel for their enzymatic activity. Even in present days gigatons of acetate and green house gases such as carbon dioxide (CO₂) and methane (CH₄) are interconverted each year by these bacterial enzymes that affect the global carbon cycle^{4,5} from an environmental aspect as well as in the energy sector⁶. It is needless to mention why nickel is so important because out of the

eight nickel centered enzymes, seven of them either use or produce CO, CO₂, CH₄, H₂, NH₃ and O₂ where nickel cycles through different redox states (+1 to +3) to catalyze these environmentally significant enzymatic reactions. This is significant in biological carbon cycles.

The main goal of my project is to better understand the mechanism of these active sites by successfully synthesizing small molecular models as well as possibly carrying out other redox chemistry along the way. The first two chapters of this dissertation describe my contribution to successfully model the histidine (His)-cysteine N₃S⁻ combination ligand system using tris(pyrazolyl)borate (Tp) to mimic the ACS/CODH enzyme active site and the discovery of unique ligation mode of nickel thiolate bond by steric modulation of ortho-substituents on the thio-aryl ring. The fourth chapter contains molecular dioxygen activation chemistry arising from phenolate ligation to the high spin nickel (II) center.

For example, carbon monoxide dehydrogenase (CODH) has Ni-S bond and it interconverts CO and CO₂ to provide a source of energy for anaerobic bacteria, Acetyl-CoA synthase (ACS) utilizes CO in conjugation with CODH, Ni-Fe hydrogenase utilizes hydrogen gas, Methyl-CoM reductase (MCR) generates methane, and nickel superoxide dismutase (Ni-SOD) generates O₂ in the process of saving cells from reactive oxygen species such as peroxides and superoxides. Charles Riordan at University of Delaware also did some relevant modeling of ACS CoA⁷ active site.

On the other hand, in many of the cases just cited, the resting active-site nickel is supported within a weak ligand field in a divalent, high-spin state (d⁸, S=1). Examples

include reduced hydrogenase^{8,9} and the ACDS A-cluster proximal nickel (Figure 1)^{10,11}; the ACS A-cluster proximal site can also adopt a tetrahedral geometry about divalent metal ions¹². Comparatively less is known about relevant organometallic and organosulfur coordination chemistry of tetrahedral high-spin nickel(II) centers.

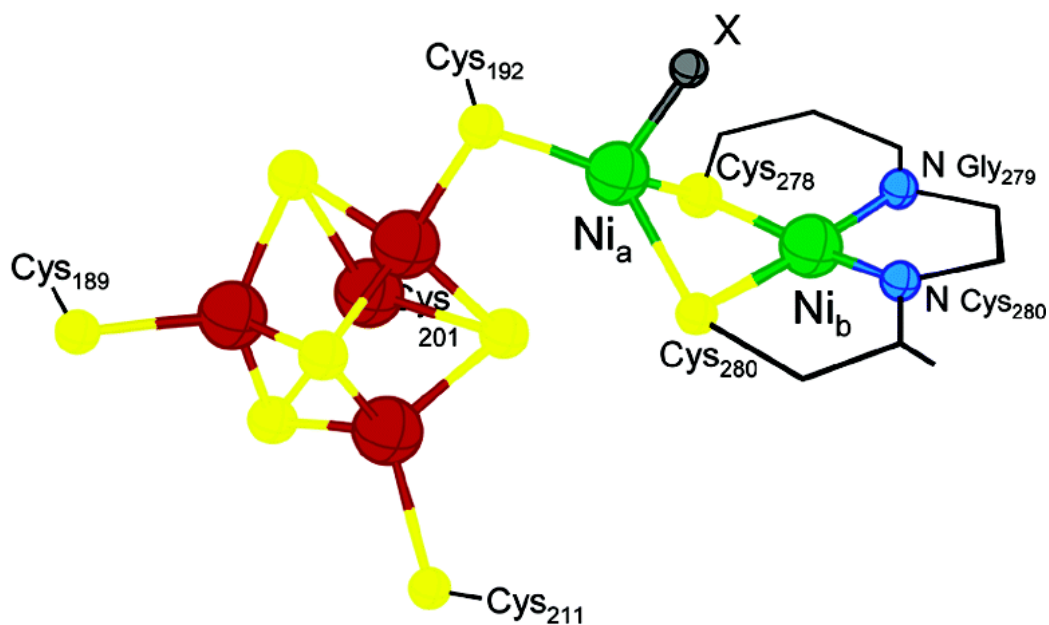


Figure 1: ACDS A cluster β subunit

(Reprinted (adapted) with permission from Tucci, G. C.; Holm, R. H. *J. Am. Chem. Soc.* **1995**, *117*, 6489–6496. Copyright 1995 American Chemical Society.)

Also not too long ago in 1997 Higuchi *et al.*¹³ published the crystal structure of the Ni-Fe hydrogenase active site that binds hydrogen at the active site and oxidizes hydrogen into two H^+ and two e^- . It is believed that the Fe center does not change its oxidation state through out the process and all the redox chemistry takes place at the Ni center. In either case, nickel is ligated to the S-atom of the Cys residue; hence this work is relevant to the understanding of Ni-S bond at its basic level.

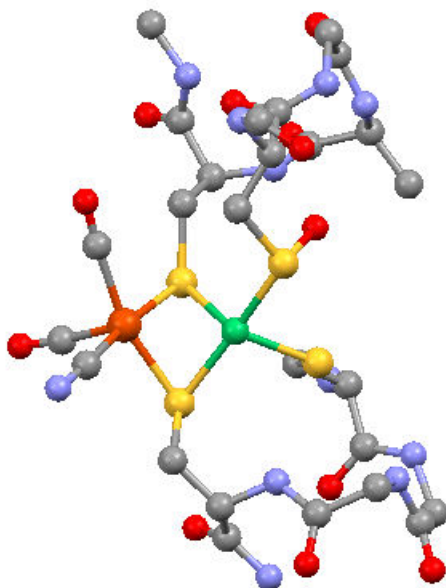


Figure 2: Ni-Fe hydrogenase active site

(Reprinted (adapted) with license number 3200970791791. Copyright 1997 Elsevier.)

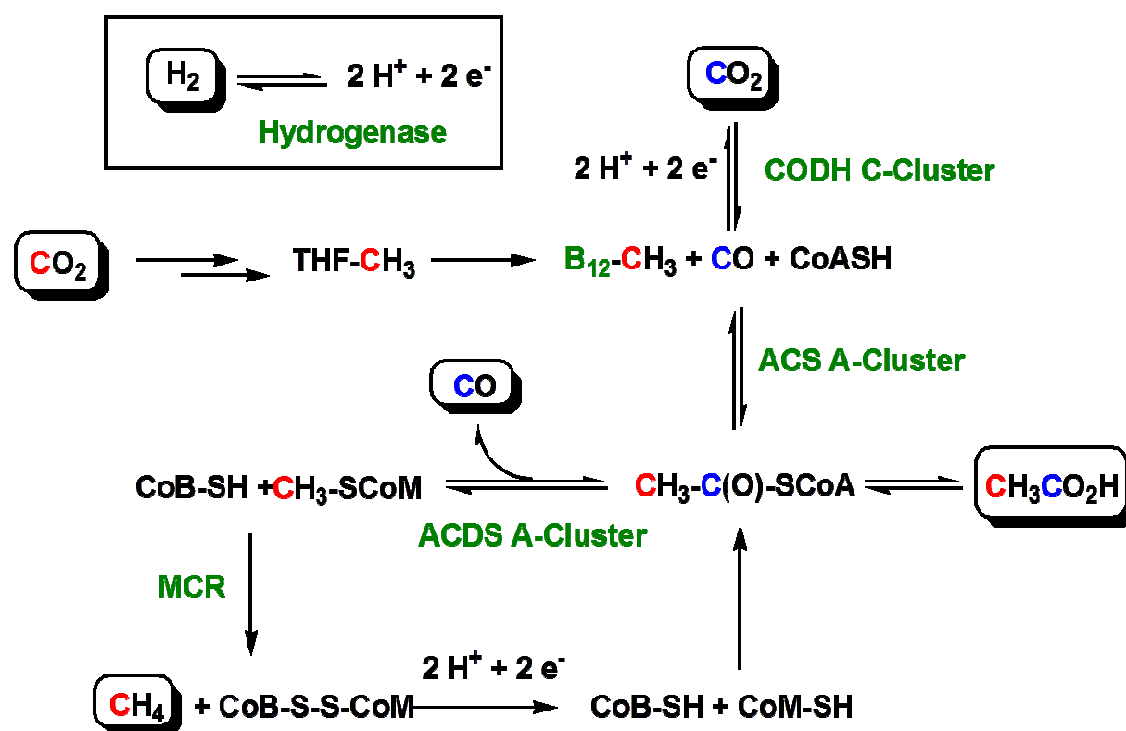


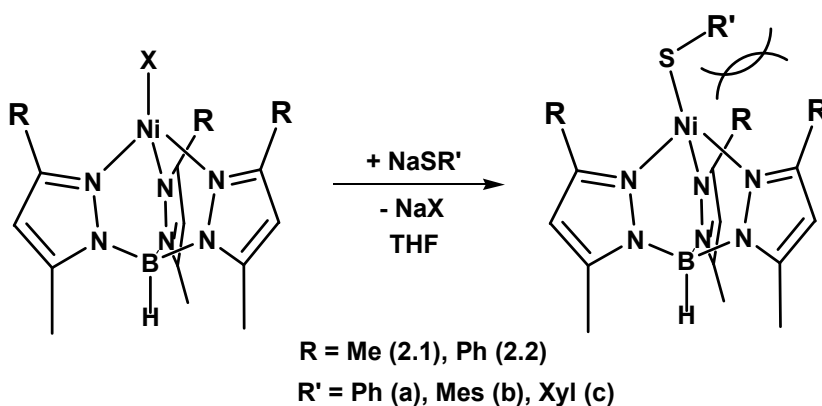
Figure 3: Interconnected carbon cycle similar to the Monsanto reaction

Figure 3, describes a complex interdependent system similar to the Monsanto acetic acid reaction where a hypothetical system could be created based on the individual reactivity of the enzymes combined to gain a working model. In this system, each product from a reaction will supply reactant or aid the process for the next reaction; for example, the hydrogenase would capture H_2 and split it into proton and electron which could then reduce CO_2 via CODH C-cluster. Simultaneously, tetrahydrofolate could reduce CO_2 in coordination with formate dehydrogenase and make $B_{12}-CH_3$, CO and CoASH that could take advantage of ACS A-cluster and make acetic acid. On the other hand, it could utilize ACDS A-cluster to release CO and transfer the methyl group to ligate with the methyl coenzyme M (Me-S-CoM) and coenzyme B (CoBSh). This could then oxidize and release methane and make a disulfide linked CoB-CoM that could get reduced by two protons to make CoBSh and CoMSH. Thus, it can re-enter the stage of $CH_3COSCoA$. This way initial acetic acid could be made that could be coupled with other carbons to make long chained synthetic hydrocarbons for fuel.

It is very difficult to study, examine and predict the exact mechanism of the original intact enzyme active site as it is surrounded by long chains of amino acid residues. Therefore, small molecular model complexes are more convenient experimentally. A Cambridge Structural Database (CSD) search returns only 59 examples of discrete terminal complexes, of which 42 are diamagnetic. Several paramagnetic complexes are found with linear,¹⁴ square-pyramidal,¹⁵⁻¹⁷ trigonal-bipyramidal,¹⁸⁻²¹ and octahedral geometries;^{18,22} pseudo-tetrahedral examples include only five complex ions of general formula $[Ni(SAr)_4]^{2-}$,²³⁻²⁶ plus five recently reported

complexes of general formula $(\kappa^3\text{-L})\text{NiSAr}$, where L is a tripodal anionic borate with appended organophosphine,²⁷ pyrazolyl²⁸ or organosulfide²⁹ donors. This clearly indicates not enough study has been conducted on paramagnetic nickel (II) complexes.

In our group we have adapted the scorpionate trispyrazolyl (Tp) ligand with varying proximal substituents to synthesize Ni(II) analogues that are known enforcers of pseudotetrahedral geometry. In particular, we vary the proximal substituent on the 3-pyrazolyl and *ortho*-arylthiolate carbons to manipulate thiolate coordination through non-covalent steric contact (Scheme). In particular, the tris(pyrazolyl)borate complexes $\text{Tp}^{\text{R,Me}}\text{Ni-SR}'$ [R = Me (**2.1**), Ph (**2.2**); R' = C₆H₅, Ph (**a**); 2,4,6-C₆H₂Me₃, Mes (**b**); 2,6-C₆H₃Me₂, Xyl (**c**)] were prepared and characterized. These series of sterically modified complexes **2.1a,b** and **2.2a-c** reveal significant and unprecedented correlations between spectroscopy, structure, and reactivity that further elucidate about metal-sulfur coordination at tetrahedral nickel(II) center.



Scheme 1: Thiolate Reaction Scheme

As the substituents are disposed in a perpendicular fashion to the N₃ donor plane, a pocket is formed about a fourth binding site for a co-ligand. This effect enables rudimentary control of co-ligand bonding through steric contact, in modest analogy to typically elegant allosteric active site control achieved in metalloenzymes through all levels of protein structure. During the synthesis and structural characterization work for the Ni(II) thiolate complexes, a distinct conformation change was observed due to steric modulation. In one case, where the Tp ligand was less bulky (Tp^{Me,Me}) a distinct trigonal pyramidal conformation was observed in the crystal structure after ligation of the 4th ligand non-bulky (thiolate), and this structure would change to a sawhorse geometry when bulky groups are placed on the *ortho* position of the thiolate ligand. But if the Tp ligand was itself bulky (Tp^{Ph,Me}) this conformation change was not observed instead an enforcement of trigonal bending was observed. The UV-Vis spectrum for the Tp^{Ph,Me} complexes red shifts indicating trigonal bending as there is no room for conformational rotation to occur. This also indicates an increasingly strong destabilizing σ^* interaction between the pyrazole N donor atom as there starts a tug of war scenario between the Ni-S bond and Ni-N bonds.

Another important aspect of my research project was to investigate molecular oxygen reduction. Molecular oxygen activation is of utter significance in transition metal catalysis and bioinorganic chemistry. A significant amount of work has been dedicated towards copper and iron complexes in recent years as there have been a few examples of enzymatic and biomimetic activation of dioxygen present in nature and literature for a long time² (such as activation by heme protein, cytochrome P450 and other

macromolecular iron complexes³⁰). For the first time, in 1955, Hayaishi *et al.*³¹ reported molecular oxygen activation by an iron containing enzyme which changed the view that scientists had at the time about how oxygen is incorporated in biomolecular systems. Copper containing enzymes were also discovered to activate molecular oxygen; in 1995 for the first time Marc Fontecave and Hans Eklund³² reported the three dimensional structure of copper amine oxidase (CAO). And since then scientists have invested significant work into studying and modeling these enzymes. But the scope of molecular oxygen activation by nickel was still limited. Recently, in 2005 Nicole Samuels and J. P. Klinman reported³³ biomimetic activity of nickel-substituted apo-CAOs. This was the inspiration for the second chapter of this dissertation which was published in the *Inorganic Chemistry* journal. Copper amine oxidases are ubiquitous in nature among both prokaryotes and eukaryotes. They catalyze oxidative deamination of primary amines to aldehydes by activating molecular dioxygen and utilizes a tyrosine residue, through a post translational modification, as a redox cofactor called topaquinoxinone (TPQ). In eukaryotes they have a wider range of functions such as cell differentiation, cell growth, cell signaling, detoxification and wound healing but in higher organism their pathways are still unclear but they are believed to play a role in diabetes in mammals.³⁴ Ground state of molecular oxygen is in triplet state ($^3\text{O}_2$) which is very stable and unreactive in most cases. But molecular oxygen in its singlet ($^1\text{O}_2$) state overcomes the spin barrier, goes to an excited state and is less stable and highly reactive. But this singlet oxygen is available only by photosensitizer organic dye such as rose bengal, methylene blue or porphyrins. But in the case of nickel-substituted CAO, J. P. Klinman *et al.*³³ reported that

molecular oxygen is activated inside the nickel containing enzyme under both ambient and dioxygen saturated conditions whereas at the same time Okajima *et al.*³⁵ reported that nickel substituted enzyme did not generate TPQ under ambient conditions but was reactive under saturated oxygen conditions. Klinman *et al.* proposed (Figure 5) a mechanism where the tyrosine residue loses its proton and binds to the metal center. After an electron transfer, molecular oxygen gets activated to superoxide anion and a nickel (II) phenoxyl radical and nickel does not change its oxidation state as the Ni-(II)-tyrosinate complex is oxidized by an outer-sphere electron transfer mechanism to O₂. But they could not completely exclude the possibility of nickel (II) phenoxyl radical stabilized via a Ni(III)-phenolate coupling structure. They suggested the generation of a radical pair by electron transfer that would overcome the spin restrictions for the oxygenation of tyrosine and allow rapid combination of the reduced oxygen species with the unpaired spin on the tyrosyl ring to form an alkyl peroxide intermediate which is a complete two electron process. It is not clear if this mechanism would work by one 2e-oxidation process or via two 1e- transfer process in a rapid manner. Afterwards, this intermediate undergoes heterolytic O-O bond cleavage with the removal of a proton at the tyrosine ring to generate dopaquinone which is then undergoes post-translational modification to form the oxidized topaquinone (TPQ) cofactor.

In recent years, some crystal structures have revealed some binding information but they are insufficient to come to a complete conclusion. For example, one of the enzymes found in *Hansenula polymorpha*³⁶ contains copper amine oxidase (CAO) which activates molecular oxygen in a similar fashion to Ni-ARD. But the actual mechanistic

details have yet to be elucidated. J. P. Klinman *et al.*³³ recently reported that CAO kinetic functionality response was significant when the active site metal was replaced by nickel compared to other alternative metals (Figure 4) such as Fe^{2+} , Fe^{3+} , Co^{2+} , Zn^{2+} , Mn^{2+} incorporated into the apo amine oxidase enzyme of *Hansenula polymorpha* (apo-HPAO). And with alternate metal nickel it showed the second highest reactivity after copper.

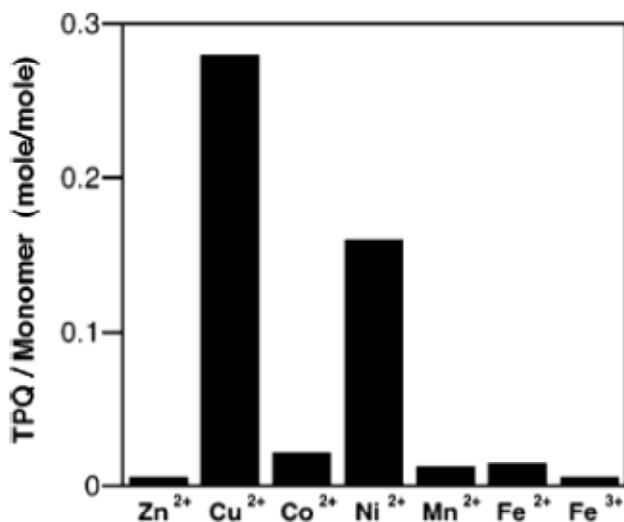


Figure 4: APO-CAO retains reactivity with alternative metals (Reprinted (adapted) with permission from Samuels, N. M.; Klinman, J. P. *Biochemistry* **2005**, *44*, 14308–14317. Copyright 2005 American Chemical Society.)

Even though this research group proposed a mechanism (Figure 5) based on crystal structures³⁷ of five of the intermediate states that have been determined by X-ray crystallography and one consensus alkylperoxo-intermediate step. But some basic questions have remained unanswered such as the fate of the protons attached to the tyrosine residue during the reaction, whether it is two one electron oxidations or 1 two-

electron oxidation remains to be elucidated. My project involved exploring and mimicking the bio-reactivity of these enzymes in small molecular models as it is very hard to pinpoint the mechanism of how the nickel center takes part in the biogenesis³⁸ process within the intact enzyme. Once the mechanism of such nickel containing enzymes could be properly understood, it could be exploited to various type of chemistry such as molecular oxygen activation in biochemistry, industrial catalysis, environmental chemistry and in the renewable energy sector.

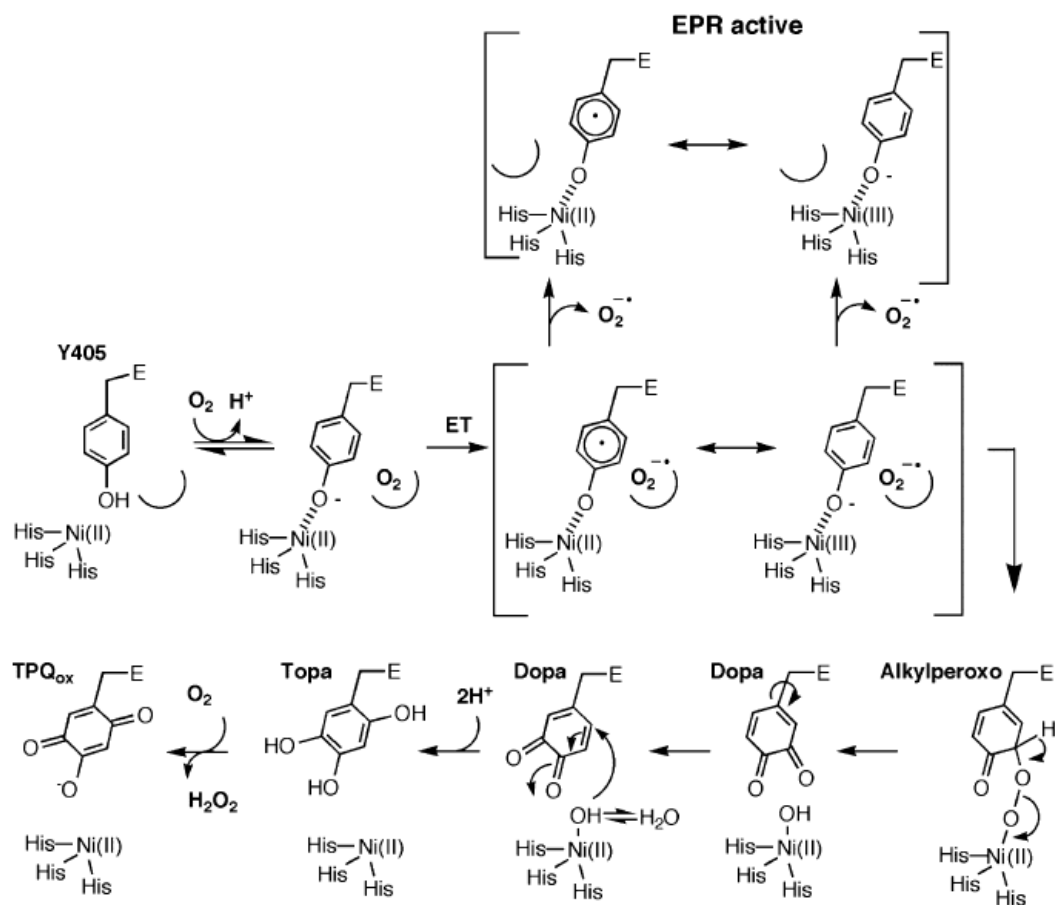


Figure 5: Proposed mechanism of CAO by Klinman *et al.*

(Reprinted (adapted) with permission from Samuels, N. M.; Klinman, J. P. *Biochemistry* **2005**, *44*, 14308–14317. Copyright 2005 American Chemical Society. Appendix A)

1.1 Other remarks

Besides the chemistry described above and discussed in detail in chapters 2-4 some other investigative and similar chemistry has been carried out in the lab. For example, in recent years, due to the push for alternative energy resources, scientists started looking into the possibilities for hydrogen storage as borohydrides and hence research interests in stable borohydride complexes have become more significant in recent years. Initially during the 60's nickel acetate was reacted with sodium borohydride to make nickel boride as colloidal particle to use as a hydrogenation catalyst³⁹. After that Hinze *et al.*⁴⁰ in the early 70's and later Furukawa *et al.*⁴¹ reported nickel catalyzed allyl transfer reactions and a few other publications were reported to use nickel borohydride as catalysts. In recent years, Desrochers *et al.*⁴² did some tremendous work on the synthesis and characterization of tripodal Tp ligand supported nickel borohydride complex and compared to its analogous borodeuteride complexes. This d^9 electron configuration of nickel(I) is also believed to be invoked in nickel-containing enzymes such as hydrogenase, CODH and methyl-S-coenzyme M reductase.^{43,44} Some work has been done in this regard but not discussed in the scope of this dissertation. Also, in regards to the O_2 activation chemistry, alternative metal reactivity has been studied. In addition, one of my fellow group members Dr. Liang made a series of half-sandwich complexes of neutral Tpm and anionic Tp ligands and O_2 activation chemistry was studied with these

complexes. Also, a series of Ni(II) sandwich complexes have been synthesized in collaboration with another group member (Mr. Wang) and he will present those results in his dissertation.

1.2 References

- (1) Mulrooney, S. B.; Hausinger, R. P. *FEMS Microbiology reviews* **2006**, *27*, 239–261.
- (2) Zabarenko, D.; Carbon dioxide level crosses milestone at Hawaii site. *Reuters.com*, **2013**.
- (3) Konhauser, K. O.; Pecoits, E.; Lalonde, S. V.; Papineau, D.; Nisbet, E. G.; Barley, M. E.; Arndt, N. T.; Zahnle, K.; Kamber, B. S. *Nature* **2009**, *458*, 750–753.
- (4) Ragsdale, S. W. *J Biol Chem* **2009**, *284*, 18571–18575.
- (5) Ermler, U. *Dalton Trans.* **2005**, 3451–3458.
- (6) Daniell, J.; Köpke, M.; Simpson, S. *Energies* **2012**, *5*, 5372–5417.
- (7) Schreiter, E. R.; Sintchak, M. D.; Guo, Y.; Chivers, P. T.; Sauer, P. T.; Drennan, C. L. *Nature Struct. Biol.* **2003**, *10*, 794-799.
- (8) Dian, C.; Schauer, K.; Kapp, U.; McSweeney, S. M.; Labigne, A.; Terradot, L. *J. Mol. Biol.* **2006**, *361*, 715-730.
- (9) Kowal, A. T.; Zambrano, I. C.; Moura, I.; Moura, J. J. G.; LeGall, J.; Johnson, M. K. *Inorg. Chem.* **1988**, *27*, 1162-1166

- (10) (a) Gu, W.; Gencic, S.; Cramer, S. P.; Grahame, D. A. *J. Am. Chem. Soc.* **2003**, *125*, 15343-15351.
- (b) Funk, T.; Gu, W.; Friedrich, S.; Wang, H.; Gencic, S.; Grahame, D. A.; Cramer, S. P. *J. Am. Chem. Soc.* **2004**, *126*, 88-95.
- (11) Tucci, G. C.; Holm, R. H. *J. Am. Chem. Soc.* **1995**, *117*, 6489-6496.
- (12) Dixon, N. E.; Gazzola, C.; Blakeley, R. L.; Zerner, B. *Journal of the American Chemical Society* **1975**, *97*, 4131-4133.
- (13) Y. Higuchi, T. Yagi, N. Yasuoka *Structure* **1997**, *5*, 1671-1680
- (14) Nguyen, T.; Panda, A.; Olmstead, M. M.; Richards, A. F.; Stender, M.; Brynda, M.; Power, P. P. *J. Am. Chem. Soc.* **2005**, *127*, 8545-8552.
- (15) Ram, M. S.; Riordan, C. G.; Ostrander, R.; Rheingold, A. L. *Inorg. Chem.* **1995**, *34*, 5884-5892.
- (16) Wilker, J. J.; Gelasco, A.; Pressler, M. A.; Day, R. O.; Maroney, M. J. *J. Am. Chem. Soc.* **1991**, *113*, 6342-6343.
- (17) Fox, D. C.; Fiedler, A. T.; Halfen, H. L.; Brunold, T. C.; Halfen, J. A. *J. Am. Chem. Soc.* **2004**, *126*, 7627-7638.
- (18) Baidya, N.; Olmstead, M.; Mascharak, P. K. *Inorg. Chem.* **1991**, *30*, 929-937.
- (19) Baidya, N.; Olmstead, M. M.; Whitehead, J. P.; Bagyinka, C.; Maroney, M. J.; Mascharak, P. K. *Inorg. Chem.* **1992**, *31*, 3612-3619.
- (20) Baidya, N.; Olmstead, M. M.; Mascharak, P. K. *J. Am. Chem. Soc.* **1992**, *114*, 9666-9668.

- (21). Marganian, C. A.; Vazir, H.; Baidya, N.; Olmstead, M. M.; Mascharak, P. K. *J. Am. Chem. Soc.* **1995**, *117*, 1584-1594.
- (22). Osakada, K.; Yamamoto, T.; Yamamoto, A.; Takenaka, A.; Sasada, Y. *Acta. Cryst. C* **1984**, *40*, 85-87.
- (23) Swenson, D.; Baenziger, N. C.; Coucouvanis, D. *J. Am. Chem. Soc.* **1978**, *100*, 1932-1934.
- (24) Rosenfield, S. G.; Armstrong, W. H.; Mascharak, P. K. *Inorg. Chem.* **1986**, *25*, 3014-3018.
- (25) Silver, A.; Koch, S. A.; Millar, M. *Inorg. Chim. Acta.* **1993**, *205*, 9-14.
- (26) Mueller, A.; Henkel, G. *Z. Naturforschung B* **1995**, *50*, 1464-1468.
- (27) Kowal, A. T.; Zambrano, I. C.; Moura, I.; Moura, J. J. G.; LeGall, J.; Johnson, M. K. *Inorg. Chem.* **1988**, *27*, 1162-1166.
- (28) Huang, Y.-H.; Moura, I.; Moura, J. J. G.; LeGall, J.; Park, J.-B.; Adams, M. W. W.; Johnson, M. K. *Inorg. Chem.* **1993**, *32*, 406-412.
- (29) Tennent, D. L.; McMillin, D. R. *J. Am. Chem. Soc.* **1979**, *101*, 2307-2311.
- (30) Groves, J. T. *PNAS* **2003**, *100*, 3569-3574.
- (31) Hayaishi, O.; Katagiri, M.; Rothberg, S. *J. Am. Chem. Soc.* **1955**, *77*, 5450-5451.
- (32) Fontecave, M.; Eklund, H. *Structure* **1995**, *3*, 1127-1129.
- (33) Samuels, N. M.; Klinman, J. P. *Biochemistry* **2005**, *44*, 14308-14317.
- (34) Boomsma, F.; Derkx, F. H.; van den Meiracker, A. H.; Man in 't Veld, A. J.; Schalekamp, M. A. *Clin. Sci.* **1995**, *88*, 675-679.

- (35) Okajima, T.; Kishishita, S.; Chiu, Y.-C.; Murakawa, T.; Kim, M.; Yamaguchi, H.; Hirota, S.; Kuroda, S.; Tanizawa, K. *Biochemistry* **2005**, *44*, 12041–12048.
- (36) Li, R.; Klinman, J. P.; Mathews, F. S. *Structure* **1998**, *6*, 293–307.
- (37) Wilmot, C. M.; Hajdu, J.; McPherson, M. J.; Knowles, P. F.; Phillips, S. E. V. *Science* **1999**, *286*, 1724–1728.
- (38) Janes, S. M.; Palcic, M. M.; Scaman, C. H.; Smith, A. J.; Brown, D. E.; Dooley, D. M.; Mure, M.; Klinman, J. P. *Biochemistry* **1992**, *31*, 12147–12154.
- (39) Brown, C. A.; Brown, H. C. *Journal of the American Chemical Society* **1964**, *85*, 1005.
- (40) Hinze, A. G.; Frost, D. J. *Journal of Catalysis* **1972**, *24*, 541–543.
- (41) Furukawa, J.; Kiji, J.; Yamamoto, K.; Tojo, T. *Tetrahedron* **1973**, *29*, 3149–3151.
- (42) Desrochers, P. J.; LeLievre, S.; Johnson, R. J.; Lamb, B. T.; Phelps, A. L.; Cordes, A. W.; Gu, W.; Cramer, S. P. *Inorg. Chem.* **2003**, *42*, 7945–7950.
- (43) Thauer, R. K. *Science* **2001**, *293*, 1264–1265.
- (44) Desrochers, P. J.; Sutton, C. A.; Abrams, M. L.; Ye, S.; Neese, F.; Telser, J.; Ozarowski, A.; Krzystek, J. *Inorganic Chemistry* **2012**, *51*, 2793–2805.

CHAPTER 2: ARYLTHIOLATE COORDINATION AND REACTIVITY AT HIGH-SPIN NICKEL(II): MODULATION BY NON-COVALENT INTERACTIONS.

Note: Asterisk () denoted complexes were initially synthesized by Dr. S. Chattopadhyay. I also published these results in Inorganic Chemistry journal DOI: 10.1021/ic702417w*

2.1 Introduction

The ongoing renaissance in structural biology has recently yielded X-ray crystallographic structures of several metalloenzymes that anaerobic bacteria and archaeobacteria utilize to support metabolic bio-organometallic reactivity, in which carbon dioxide, methane and acetate are interconverted on a gigaton/year scale, significantly impacting the global carbon cycle.^{1,2} These enzymes, including the A- and C-clusters of acetyl coenzyme-A synthase/ carbon monoxide dehydrogenase (ACS/CODH) and acetyl coenzyme-A decarbonylase/synthase (ACDS),³⁻⁸ Fe/Ni hydrogenases,^{9,10} and the F430 cofactor of methyl-coenzyme M reductase (MCR),¹¹ all feature essential nickel ions in their active sites.¹²⁻¹⁸ Moreover, the metal-centered enzymatic activities have strong evolutionary links to organosulfur chemistry, either as active-site ligation to nickel, or in essential cofactors.^{19,20} Sulfur-ligated nickel ions in weak ligand fields were recently found in a superoxide dismutase,^{21,22} and in nickel-dependent transcription factors.^{23,24} Nickel(II) ions have also been introduced into cysteine-ligated binding sites as spectroscopic and structural probes in rubredoxin,^{25,26} azurin,^{27,28} aspartate transcarbamoylase regulatory domain,²⁹ and zinc fingers.³⁰

The ACS A-cluster turnover plausibly occurs through a formally diamagnetic Ni(0)/Ni(II) couple at the proximal nickel,^{6,31-34} and several elegant ACS model reactions using synthetic diamagnetic complexes have been reported,³⁵⁻⁴¹ On the other hand, in many of the cases just cited, the resting active-site nickel is supported within a weak ligand field in a divalent, high-spin state (d^8 , $S = 1$). Examples include reduced hydrogenase^{42,43} and the ACDS A-cluster proximal nickel,^{16,17} the ACS A-cluster proximal site also adopts a tetrahedral geometry about divalent metal ions.⁶ Comparatively less is known about relevant organometallic and organosulfur coordination chemistry of tetrahedral high-spin nickel(II).

Considering the relevant example of small-molecule complexes of experimentally convenient arylthiolates, the Cambridge Structural Database presently returns only 59 examples of discrete terminal complexes, of which 42 are diamagnetic. Several high-spin structures are found in linear,⁴⁴ square-pyramidal,⁴⁵⁻⁴⁷ trigonal-bipyramidal,⁴⁸⁻⁵¹ and octahedral geometries,^{48,52} pseudo-tetrahedral examples include only five complex ions of general formula $[\text{Ni}(\text{SAr})_4]^{2-}$,⁵³⁻⁵⁶ plus five recently reported complexes of general formula $(\kappa^3\text{-L})\text{NiSAr}$, where L is a tripodal anionic borate with appended organophosphine,⁵⁷ pyrazolyl⁵⁸ or organosulfide⁵⁹ donors. Further elucidation of biomimetic organosulfur chemistry at high-spin nickel(II) thus retains significant impetus.

We describe in the present work additional examples of pseudo-tetrahedral arylthiolate complexes of nickel(II) supported by tris(pyrazolyl)borate ligands. Moreover, we have adopted a distinctive approach by focusing exclusively on complexes

in which proximal substituents on the 3-pyrazolyl and *ortho*-arylthiolate carbons are varied to manipulate thiolate coordination through non-covalent steric contact (Scheme 1). In particular, the tris(pyrazolyl)borate complexes $\text{Tp}^{\text{R,Me}}\text{Ni-SR}'$ [$\text{R} = \text{Me}$ (**2.1**), Ph (**2.2**); $\text{R}' = \text{C}_6\text{H}_5$, Ph (**a**); $2,4,6\text{-C}_6\text{H}_2\text{Me}_3$, Mes (**b**); $2,6\text{-C}_6\text{H}_3\text{Me}_2$, Xyl (**c**)] were prepared and characterized. The resulting series of sterically modified complexes **2.1a,b** and **2.2a-c** reveals significant and unprecedented correlations between spectroscopy, structure, and reactivity that further illuminate metal-sulfur coordinate bonding at high-spin nickel(II).

2.2 Experimental

2.2.1 General procedures

All materials obtained from commercial vendors were ACS reagent-grade or better and were used as received, except for drying of solvents by routine techniques. All manipulations were carried out under an inert atmosphere of prepurified argon, either in a glovebox (MBraun Unilab) or using Schlenk techniques. Known $\text{Tp}^{\text{R,Me}}\text{NiCl}$ complexes ($\text{R} = \text{Me}$, Ph) were prepared by modification of literature procedures,⁶⁰⁻⁶² from metatheses of anhydrous NiCl_2 and $\text{TiTp}^{\text{R,Me}}$ in $\text{MeOH}/\text{CH}_2\text{Cl}_2$ (**Caution:** thallium salts are extremely toxic and must be properly handled and disposed of). Aromatic thiols were purchased from Aldrich and converted to sodium salts by titration of NaNH_2 in toluene. ^1H NMR data were recorded on a Varian Unity 500 spectrometer and processed using the MestReNova software suite (Mestrelab Research, Santiago de Campostela, Spain); spectra were referenced internally to residual CHCl_3 solvent (7.24 ppm), and

experimental temperatures were calibrated by the methanol method using Varian software. FT-IR spectra were recorded from KBr pellets on a Thermo-Electron Nicolet 380 spectrophotometer. UV-visible-NIR spectra were recorded on an Agilent HP-8453 diode-array spectrophotometer; kinetic data were analyzed using the SPECFIT software package (Spectrum Software Associates, Marlborough, MA). Elemental analyses were performed by Atlantic Microlabs, Inc. (Norcross, GA).

Preparation of $Tp^{Me,Me}Ni-SPh$ (2.1a). To the solution of $Tp^{Me,Me}NiCl$ (75 mg, 0.19 mmol) in THF (20 mL) was added dropwise a solution of NaSPh (38 mg, 0.29 mmol) in THF (15 mL). The color of the solution changed from pale pink to intense red. The mixture was stirred 2 h and then solvent was removed under vacuum. The resulting red solid was extracted into toluene (20 mL). The extracts were filtered and evaporated to yield a red powder. Yield: 68 mg (76%). Anal. Calc'd. (found) for $C_{21}H_{27}BN_6NiS$: C, 54.23 (54.64); H, 5.85 (5.98); N 18.07 (18.24). $\nu(B-H)$: 2520 cm^{-1} . 1H NMR ($CDCl_3$; δ , ppm): 77.2 (3H, 4-pz); 23.3 (2H, *meta*); 6.6 (9H, 5-Me); -7.1 (9H, 3-Me); -10.7 (1H, B-H); -18.9 (2H, *ortho*); -26.6 (1H, *para*). UV-Vis (CH_2Cl_2 , λ_{max} , nm; ϵ , $mM^{-1}\text{ cm}^{-1}$): 354 (1.6); 464 (2.4); 506 (2.6); 614 (sh, 0.2); 836 (0.2).

Preparation of $Tp^{Me,Me}Ni-SMes$ (2.1b). The red complex was prepared as for **2.1a** above with NaSMes. Yield: 71 mg (73%). Anal. Calc'd. (found) for $C_{24}H_{33}BN_6NiS$: C, 56.84 (56.75); H, 6.56 (6.59); N 16.57 (17.32). $\nu(B-H)$: 2518 cm^{-1} . 1H NMR ($CDCl_3$; δ , ppm): 75.0 (3H, 4-pz); 33.3 (6H, *ortho*); 25.8 (3H, *para*); 25.3 (2H, *meta*); 5.2 (9H, 5-Me); -7.5 (9H, 3-Me); -11.3 (1H, B-H). UV-Vis (CH_2Cl_2 , λ_{max} , nm; ϵ , $mM^{-1}\text{ cm}^{-1}$): 343 (1.1); 371 (1.1); 406 (1.2); 467 (sh, 1.5); 514 (2.7); 636 (0.3); 861 (0.2).

Preparation of $Tp^{Ph,Me}Ni-SPh$ (2.2a).* The purple complex was prepared as for **2.1a** above with NaSPh. Yield: 59 mg (70%). Anal. Calc'd. (found) for $C_{36}H_{33}BN_6NiS$: C, 66.39 (67.44); H, 5.11 (5.63); N 12.90 (13.03). $\nu(B-H)$: 2548 cm^{-1} . 1H NMR ($CDCl_3$; δ , ppm): 70.8 (3H, 4-pz); 25.5 (2H, *meta*); 10.5 (6H, 3-*o*-Ph); 7.8 (6H, 3-*m*-Ph); 7.4 (3H, 3-*p*-Ph); 4.6 (9H, 5-Me); -10.6 (1H, B-*H*); -27.8 (2H, *ortho*); -37.6 (1H, *para*). UV-Vis (CH_2Cl_2 , λ_{max} , nm; ϵ , $mM^{-1} cm^{-1}$): 372 (0.9); 489 (sh, 1.0); 537 (1.7); 700 (0.2); 905 (0.2).

Preparation of $Tp^{Ph,Me}Ni-SMes$ (2.2b).* The blue complex was prepared as for **2.1a** above with NaSMes. Yield: 70 mg (78%). Anal. Calc'd. (found) for $C_{21}H_{27}BN_6NiS$: C, 67.57 (67.30); H, 5.67 (5.82); N 12.12 (11.89). $\nu(B-H)$: 2540 cm^{-1} . 1H NMR ($CDCl_3$; δ , ppm): 91.8 (6H, *ortho*); 67.0 (3H, 4-pz); 57.2 (3H, *para*); 32.2 (2H, *meta*); 9.9 (6H, 3-*o*-Ph); 7.4 (6H, 3-*m*-Ph); 7.2 (3H, 3-*p*-Ph); 2.5 (9H, 5-Me); -11.2 (1H, B-*H*). UV-Vis (CH_2Cl_2 , λ_{max} , nm; ϵ , $mM^{-1} cm^{-1}$): 352 (1.0); 378 (0.9); 551 (sh, 2.1); 574 (2.2); 884 (0.1).

Preparation of $Tp^{Ph,Me}Ni-SXyl$ (2.2c).* The purple complex was prepared as for **2.1a** above with NaSXyl. Yield: 66 mg (75%). Anal. Calc'd. (found) for $C_{21}H_{27}BN_6NiS$: C, 67.19 (67.14); H, 5.49 (5.48); N 12.37 (12.51). $\nu(B-H)$: 2543 cm^{-1} . 1H NMR ($CDCl_3$; δ , ppm): 97.1 (6H, *ortho*); 68.0 (3H, 4-pz); 32.9 (2H, *meta*); 9.9 (6H, 3-*o*-Ph); 7.4 (6H, 3-*m*-Ph); 7.2 (3H, 3-*p*-Ph); 2.5 (9H, 5-Me); -11.4 (1H, B-*H*); -43.2 (1H, *para*). UV-Vis (CH_2Cl_2 , λ_{max} , nm; ϵ , $mM^{-1} cm^{-1}$): 353 (1.3); 373 (1.3); 543 (2.2); 574 (sh, 2.0); 700 (sh, 0.2); 893 (0.2).

2.2.2 X-ray crystallography

Diffraction-quality crystals of **2.1a** and **2.2c**•2CH₃CN were grown from acetonitrile solutions at -37 °C. Data collections and refinement parameters are summarized in Table 2. Bond lengths and angles are summarized in Table 3. ORTEP diagrams of the complexes are illustrated in Figure 9.

Experimental work on **2.1a** was conducted at West Virginia University (JLP). A reddish-orange crystal (0.10 x 0.21 x 0.58 mm) was washed with perfluoroether PFO-XR75 (Lancaster) and sealed under N₂ in a glass capillary. The sample was optically aligned on the four-circle of a Siemens P4 diffractometer equipped with a graphite monochromator, a monocap collimator, a Mo Ka radiation source ($\lambda = 0.71073 \text{ \AA}$), and a SMART CCD detector. The program SMART (version 5.6)⁶³ was used for diffractometer control, frame scans, indexing, orientation matrix calculations, least-squares refinement of cell parameters, and the data collection. Raw data frames were read by SAINT (version 5/6.0)⁶³ and integrated using 3D profiling algorithms. A semi-empirical absorption correction was applied using SADABS.^{63,64} The data were corrected for Lorentz and polarization effects. Data preparation was carried out by using the program XPREP.⁶³ The structure was solved by direct methods and difference Fourier analysis with the use of SHELXTL 6.1.⁶⁵ Idealized positions for the hydrogen atoms were included as fixed contributions using a riding model with isotropic temperature factors set at 1.2 (aromatic protons and B-H) or 1.5 (methyl protons) times that of the adjacent non-hydrogen atom. A correction for secondary extinction was not applied. The linear absorption coefficient, atomic scattering factors, and anomalous dispersion

corrections were calculated from values found in the International Tables of X-ray Crystallography.⁶⁶

Experimental work on **2.2c•2CH₃CN** was done at University of Minnesota (VGY). A purple needle (0.45 x 0.15 x 0.15 mm) was placed on the tip of a 0.1 mm diameter glass capillary and mounted on a Bruker AXS diffractometer equipped with a CCD area detector for a data collection at 173(2) K.⁶³ The data collection was carried out using Mo K α radiation ($\lambda = 0.71073$ Å, graphite monochromator). The intensity data were corrected for absorption and decay (SADABS).^{63,64} Final cell constants were calculated from 2796 strong reflections from the actual data collection after integration (SAINT).⁶³ The structure was solved by direct methods and difference Fourier analysis and refined using Bruker SHELXTL.⁶⁵ The space group P2₁/c was determined based on systematic absences and intensity statistics. All non-hydrogen atoms were refined with anisotropic displacement parameters. All hydrogen atoms were placed in ideal positions and refined as riding atoms with relative isotropic displacement parameters, except the borate hydrogen was allowed to refine positionally with a constrained Uiso relative to the host boron atom.

2.3 Results

2.3.1 General remarks.

Arylthiolate complexes were prepared by metathesis reactions of known complexes Tp^{R,Me}Ni-Cl with sodium thiolate salts in weakly polar THF solvent (Scheme

1). To prevent dissociation of the N-SR bond, the lipophilic product complexes were isolated by subsequent extraction into nonpolar toluene. Elemental analyses on isolated products were consistent with formulation as $\text{Tp}^{\text{R,Me}}\text{Ni-SR}'$ (Scheme 1), and spectroscopic data described below were uniquely consistent with pseudo-tetrahedral complexes in high-spin ($S = 1$) d^8 electron configurations. This was confirmed for **2.1a** and **2.2c** by X-ray structure determinations. Electrochemical measurements were negated by thiolate dissociation in electrolytic solutions.

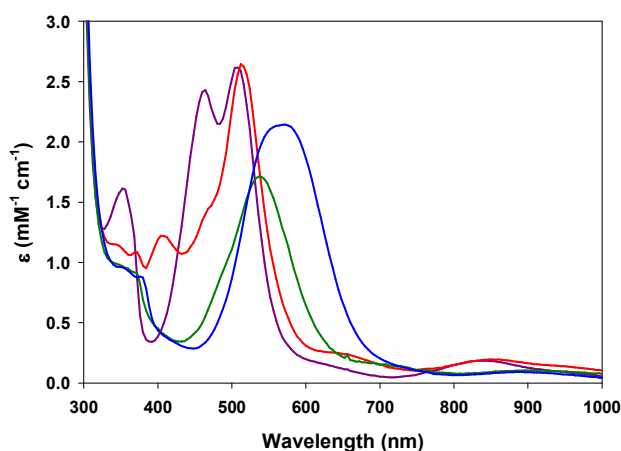


Figure 6: UV-Vis-NIR spectra at 297 K in CH_2Cl_2 solution for: $\text{Tp}^{\text{Me,Me}}\text{Ni-SPh}$ (**2.1a**, magenta trace); $\text{Tp}^{\text{Me,Me}}\text{Ni-SMes}$ (**2.1b**, red); $\text{Tp}^{\text{Ph,Me}}\text{Ni-SPh}$ (**2.2a**, green); and $\text{Tp}^{\text{Ph,Me}}\text{Ni-SMes}$ (**2.2b**, blue).

2.3.2 Electronic spectroscopy

Successful formation of the various thiolate complexes in reaction solutions was initially signified by appearance of intense coloration arising from S-Ni $p\pi-d\pi^*$ LMCT transitions at visible wavelengths (Figure 6). Similar bands were observed the spectra of

$\text{Tp}^{\text{iPr,iPr}}\text{Ni-SC}_6\text{F}_5$ (430 nm),^{58,67} Ni(II)-substituted rubredoxin (360, 450 nm),^{25,26} Ni(II)-aspartate transcarbamoylase (360, 440 nm),²⁹ and $[\text{Ni}(\text{SPh})_4]^{2-}$ in CH_3CN solution (460, 510 nm).^{26,27} Given the weak ligand field and electron-rich thiolates utilized in the present work, the LMCT transitions are correspondingly red-shifted. Thus, complexes supported by $\text{Tp}^{\text{Me,Me}}$ (**2.1a,b**) are bright red, while those of $\text{Tp}^{\text{Ph,Me}}$ (**2.2a-c**) are dark purple or blue.

In contrast to the single LMCT transition reported for $\text{Tp}^{\text{iPr,iPr}}\text{Ni-SC}_6\text{F}_5$ and related synthetic complexes,⁵⁷⁻⁵⁹ two strong absorption bands with separations of 1000-2000 cm^{-1} were observed: **2.1a**, $\lambda_{\text{max}} = 464$ and 506 nm; **2.1b**, 467(sh) and 514 nm; **2.2a**, 489(sh) and 537 nm; and **2.2b**, 551 and 574 nm. These bands retained essentially equivalent positions and intensities in toluene, CH_2Cl_2 , and CH_3CN solutions for all four complexes. The two bands of **2.1a**, **2.2b**, and **2.2c** had approximately equivalent extinctions, but those of **2.1b** and **2.2a** exhibited disparate values. A separate LMCT transition based on the second half-filled nickel orbital and a Ni-S $\text{p}\sigma\text{-d}_{z^2}$ bonding interaction was not suggested by DFT electronic structure calculations on $\text{Tp}^{\text{iPr,iPr}}\text{Ni-SC}_6\text{F}_5$,⁶⁷ so these observations may indicate unexpected complexity in the underlying photophysics. Nickel-thiolate stretching modes exhibit much lower energies,⁶⁷ so resolved vibrational structure within a single transition is not expected. Ligand field absorptions of $\text{Tp}^{\text{R,Me}}\text{Ni-Cl}$ (R = Me, Ph), include a strong band at 482 nm,⁶⁸ and the thiolate complexes should have an analogous band under the charge transfer features; such a band is indeed evident ($\lambda_{\text{max}} = 498$ nm, $\epsilon = 875 \text{ M}^{-1} \text{ cm}^{-1}$) as a shoulder on the relatively blue-shifted CT band of $\text{Tp}^{\text{iPr,iPr}}\text{Ni-SC}_6\text{F}_5$.⁶⁷ Given the low symmetry of the thiolate complexes, configuration

interaction between ligand field and charge transfer states may be possible, giving rise to the strong split absorptions.

Additional ligand field bands were evident at longer wavelength from the edge of the CT band: **2.1a**, $\lambda_{\text{max}} = 614$ and 836 nm; **2.1b**, $\lambda_{\text{max}} = 636$ and 861 nm; and **2.2a**, $\lambda_{\text{max}} = 700$ and 905 nm. Broad NIR absorptions were also found for **2.1a,b** at 1580 nm. Thus, the ligand field bands approximately coincide with those reported for high-spin $\text{Tp}^{\text{R,Me}}\text{Ni-Cl}$ complexes of approximate C_{3v} pseudo-tetrahedral geometry.^{62,68} Additional bands of intermediate extinction in the near UV are absent in the chloride complex precursors, and thus can be plausibly assigned to intraligand transitions within the aromatic thiolate substituents.

A red-shift of the LMCT and ligand field bands can be noted in order of increasing steric bulk of the $\text{Tp}^{\text{R,Me}}\text{Ni-SR}'$ complexes. For example, the LMCT features lie at notably lower energies for $\text{R} = \text{Ph}$ compared to $\text{R} = \text{Me}$, as also observed in trigonal-pyramidal complexes,⁶⁰ and secondarily for $\text{R}' = \text{Mes}$ compared to Ph as well. This trend might reflect weaker pyrazolyl σ -donor strength afforded to nickel(II) due to an opened ligand bite accommodating the larger 3-pyrazolyl substituent for $\text{R}' = \text{Ph}$, as well as enhanced thiolate basicity for $\text{R} = \text{Mes}$. However, the presence of *ortho*-thiolate substituents alone induces the LMCT shift evident between spectra of **2.2a** and **2.2b,c**. We conclude that contact between the 3-pyrazolyl and *ortho*-thiolate substituents perturbs Ni-S bonding, resulting in a significant contribution to observed LMCT red shifts.

2.3.3 ^1H NMR spectroscopy

Complexes **2.1a,b**, **2.2a-c**, and their precursor chloride complexes all exhibited well-resolved ^1H NMR spectra at room temperature in CDCl_3 solutions, notwithstanding their paramagnetic electronic configurations (Figure 7). Tp^*NiCl exhibited four expected signals: a relatively sharp resonance at 6.0 ppm assigned to the 5-methyl protons; a much broader resonance at -8.1 ppm assigned to the 3-methyl protons proximal to the metal ion; a borohydride resonance at -12.9 ppm, and a 4-pyrazolyl ring proton resonance shifted significantly downfield to 81.9 ppm. Compared to the chloride complex, the spectrum of **2.1a** in CDCl_3 contains three additional signals at 23.7, -18.9, and -26.6 ppm respectively assigned to the *meta*, *ortho*, and *para* protons of the phenylthiolate ligand on the basis of their relative intensities and linewidths in relation to expected spatial separation from the $S=1$ nickel(II) ion. The alternating upfield, downfield, upfield pattern in the arylthiolate proton shifts reflects a predominant contact shift mediated by spin polarization,^{45,54,59,69,70} consistent with residence of the unpaired electrons in a nondegenerate configuration exhibiting S-Ni $p\pi-d\pi^*$ overlap.⁶⁷ Introduction of *ortho* and *para* methyl substituents on the mesitylthiolate ligand of **2.1b** causes expected reversal of the spin polarity at these positions, resulting in three downfield signals at 33.27 (*ortho*), 25.8 (*para*) and 25.3 (*meta*). Analogous results were also obtained for the series of $\text{Tp}^{\text{Ph,Me}}$ complexes. Thus, the precursor chloride complex exhibited six resonances: signals at 78.6, 4.4, and -13.7 ppm correspond to the 4-pyrazolyl, 5-methyl, and borohydride protons; three more at 9.7, 8.7, and 8.0 ppm correspond to the *ortho*, *meta* and *para* protons of the 3-phenyl substituents. The latter three signals increasingly

broaden with increasing proximity to the metal center, with the *ortho* resonance being particularly broad. The complexes **2.2a-c** exhibit three additional resonances due to the arylthiolate protons, with contact shifts again determined by spin polarization.

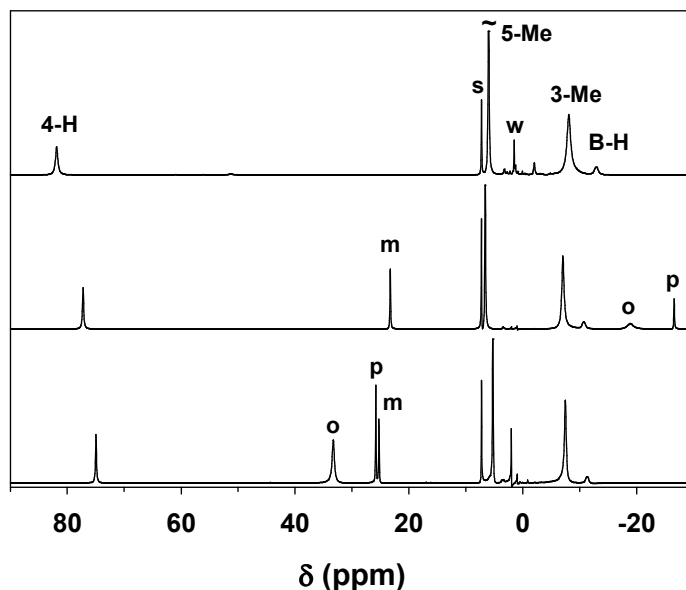


Figure 7: ^1H NMR spectra recorded at 293 K in CDCl_3 solution for: $\text{Tp}^{\text{Me,Me}}\text{Ni-Cl}$ (top), labels indicate tris(pyrazolylborate) resonances, s = residual solvent, w=water; $\text{Tp}^{\text{Me,Me}}\text{Ni-SPh}$ (middle), labels indicate arylthiolate resonances; and $\text{Tp}^{\text{Me,Me}}\text{Ni-SMes}$ (bottom)

In comparing the various ^1H NMR spectra, shifts of the tris(pyrazolyl) ligand resonances are smaller in magnitude for $\text{Tp}^{\text{Ph,Me}}$ complexes compared to $\text{Tp}^{\text{Me,Me}}$ analogs, and also for thiolate complexes compared to their chloride complex precursors. For example, the chemical shifts of the 4-pyrazolyl protons of $\text{Tp}^{\text{Me,Me}}\text{Ni-Cl}$, **2.1a** and **2.1b** are 81.9, 77.2, and 75.0 ppm respectively (Figure 2), compared to 78.6, 70.8, and 67.0 ppm for their respective $\text{Tp}^{\text{Ph,Me}}$ analogs. Conversely, the arylthiolate protons show an opposing trend; the common arylthiolate *meta* protons resonate at 23.3, 25.3, 25.5, 32.2,

and 32.9 ppm for **2.1a-b**, **2.2a-c**, respectively. The latter effect is particularly dramatic for **2.2b,c** which incorporate both the bulkier $\text{Tp}^{\text{Ph,Me}}$ ligand and an *ortho*-disubstituted arylthiolate: the *ortho*-methyl protons of **2.2b-c** resonate at 92 and 97 ppm respectively, compared to 33 ppm for **2.1b**. These trends may arise from competing factors. Steric contact between the thiolate and the pyrazolyl substituents may reduce covalency of the Ni-N coordinate bonds, attenuating spin density on the pyrazolyl rings. Such steric contacts may alternatively perturb thiolate coordination, causing the arylthiolate ligands to accept more spin density through enhanced covalency in the S-Ni $p\pi-d\pi^*$ bond, reducing shifts of the tris(pyrazolyl)borate ligand protons relative to a chloride complex.

In order to clearly delineate these trends, chemical shifts were determined as a function of temperature over a 265-300 K range for the 4-pyrazolyl protons on the Tp ligands, and the *ortho*, *meta*, and *para* positions of the arylthiolates for complexes **2.1a,b** and **2.2a,b**. The data were fit by least-squares techniques to linear functions according to the Curie law, and the results are summarized in Table 1. Obtained slopes (*i.e.*, hyperfine constants) correlate with the averaged S-Ni $p\pi-d\pi^*$ LMCT energies for each complex (Figure 8). The absence of significant shift effects from zero-field splitting was evident from linearity of the Curie plots, and the observed trends also suggest predominance of through-bond contact shifts over dipolar shifts, both consistent with spin Hamiltonian parameters reported for $\text{Tp}^{\text{Me,Me}}\text{Ni-Cl}$.⁶⁸ An inverse dependence was evident in the common *meta* resonance on the arylthiolate ligands (*i.e.*, **2.1a** < **2.1b** < **2.2a** < **2.2b**), thus implying a significant steric effect on Ni-SR' covalency, consistent with an opposing

trend for the 4-pyrazolyl protons (*i.e.*, **2.1a** \geq **2.2a** \geq **2.2b**). These results are consistent with significant steric perturbation of the nickel-thiolate coordinate bond.

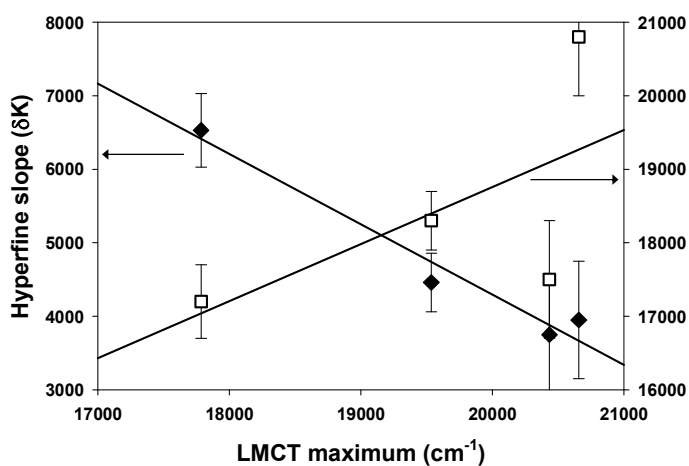


Figure 8: Plot of averaged LMCT band energies of **2.1a,b** and **2.2a,b** versus hyperfine slopes for arylthiolate meta resonances (♦, left axis) and 4-pyrazolyl resonances (□, right axis).

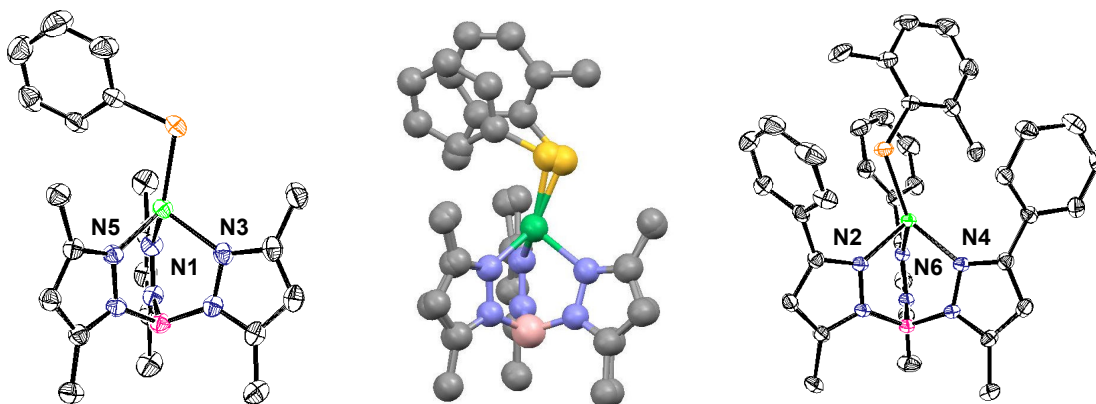


Figure 9: ORTEP plots for $\text{Tp}^{\text{Me,Me}}\text{Ni-SPh}$ (**2.1a**, left) and $\text{Tp}^{\text{Ph,Me}}\text{Ni-SXyl}$ (**2.2c**, right) with thermal ellipsoids drawn at 30% probability. A least-squares superposition of the structures is shown at center to highlight differential thiolate coordination; for clarity, only the ipso carbons of the 3-Ph substituents are shown for **2.2c**.

2.3.4 X-ray Crystallography.

To further elucidate this steric effect, structures were determined by X-ray crystallography for complexes **2.1a** and **2.2c** (Figure 9 and Table 3). Both complexes adopt severely distorted pseudotetrahedral geometries in which the Ni-S bonds are significantly bent from an ideal trigonal axis towards one pyrazole ring, as previously reported for $\text{Tp}^{\text{iPr,iPr}}\text{Ni-SC}_6\text{F}_5$.⁵⁸ The aromatic thiolate substituents are disposed backward over the edge between the two distal pyrazoles, and are nearly coplanar with the Ni-S bonds (torsion angles: $\pm 15.2^\circ$ for **2.1a**; $\pm 16.4^\circ$ for **2.2c**), yielding approximate C_s symmetry. The Ni-S bond length of **2.1a** is slightly longer than that of **2.2c**, 2.216(1) and 2.1978(5) Å respectively. Conversely, the Ni-N bonds of **2.1a** are very slightly shorter than those of **2.2b**, averaging 1.986(7) and 2.027(7) Å respectively, compared to 1.98(2) and 1.99(1) Å in the chloride complex precursors $\text{Tp}^{\text{R,Me}}\text{Ni-Cl}$, (R = Me, Ph respectively).^{61,62} Moreover, the N-Ni-N angles remain close to 90° for both complexes (averaging $90.7(8)^\circ$ for **2.2c** and $92(1)^\circ$ for **2.1a**), owing to the constrained bite imposed upon the Tp ligand by the borate tether. Given displacement of the thiolate donors off the trigonal axis, the N-Ni-S angles vary widely (Table 3).

Reflecting the increased basicity of the arylthiolates utilized in the present work compared to the perfluoroaryl analog, the Ni-S bond lengths of **2.1a** and **2.2c** are significantly shorter than that of $\text{Tp}^{\text{iPr,iPr}}\text{Ni-SC}_6\text{F}_5$ (2.259(2) Å),⁵⁸ and also those of $[\text{Ni}(\text{SAr})_4]^{2-}$ (2.26-2.33 Å),⁵³⁻⁵⁶ consistent with reduced complex charge. Ni-S bond lengths of 2.236(1) Å and 2.187(1) Å were recently reported for $\text{PhB}(\text{CH}_2\text{S}^t\text{Bu})_3\text{Ni-SAr}$ (Ar = $-\text{C}_6\text{F}_5$ and C_6H_5 , respectively).⁵⁹ A shorter Ni-S bond length of 2.119(1) Å was

found in the pseudotetrahedral complex $\text{PhB}(\text{CH}_2\text{PPh}_2)_3\text{Ni-SC}_6\text{H}_4\text{-}i^t\text{Bu}$; aside from the distinctive donor set of this complex, the Ni-S coordinate bond is bent over an edge between donor atoms and the arylthiolate substituent adopts a perpendicular orientation (torsion angles: 113° , -69°).

As anticipated from spectroscopic results, there are clear and instructive differences between the sterically unhindered arylthiolate ligation of **2.1a** and that of the more encumbered **2.2c** (Figure 9, center). Most obviously, the bond angle at sulfur (*i.e.*, Ni-S-C) is significantly increased, from $103.84(8)^\circ$ in **2.1a** to $116.51(7)^\circ$ in **2.2c**, and tilting of the thiolate bond off the trigonal axis towards a proximal pyrazole nitrogen becomes even more pronounced ($\text{N3-Ni1-S1} = 113.26(6)^\circ$ in **2.1a**, $\text{N2-Ni1-S1} = 103.05(5)^\circ$ in **2.2c**). The Cambridge Database presently returns exactly 100 values for bond angles about sulfur for terminal arylthiolate ligands on nickel; these range from 99.146° to 121.038° , of which only nine are smaller than that of **2.1a** and only three exceed that of **2.2c**. Hence, **2.1a** and **2.2c** together nearly span the known coordination space available to arylthiolates at a single nickel center. The steric hindrance in **2.2c** arises from short contacts between the thiolate and the 3-phenyl substituents on the supporting ligand, which are rotationally disposed to form a three-sided box about the xylyl substituent. The sulfur atom itself is wedged against the central 3-phenyl ring, resulting in a distance of only 3.29 \AA to the *ipso* carbon. This distance plausibly represents the sum of van der Waals radii. Distances between the inner *ortho*-xylyl carbon on the thiolate and the two flanking 3-Ph rings include carbon-carbon contacts as short as 3.45 \AA .

The nickel ion itself also provides a short contact to the *ortho* methyl at a distance of 3.10 Å, supporting a Ni...H-C distance of 2.56 Å that is disposed nearly axially towards the proximal pyrazole (N2-Ni1...H38A = 163.9°). Similarly short *ortho*-fluorine contacts (ca. 2.56-2.64 Å) within related perfluoroarylthiolate complexes were previously dismissed as non-bonding.⁷¹ While unusual low-energy $\nu(\text{C-H})$ IR modes indicative of agostic bonding were not observed in the present work,^{72,73} weak electrostatic (“anagostic”)⁷⁴ interaction with the hydrocarbyl substituents does seem plausible.⁷⁵⁻⁷⁷ Moreover, the dissimilar dispositions of arylthiolate ligands in **2.1a** and **2.2c** place their respective *ortho* and xylyl methyl carbons in nearly equivalent positions relative to nickel (Figure 9, center), so a short Ni...H-C distance of 2.72 Å is also found in **2.1c** between the *ortho* proton and nickel, at an angle of 173.1° to N3 on the proximal pyrazole.

2.3.5 Electrophilic alkylation.

Initial observed reactivities of **2.1a** and **2.2b** with methyl iodide were reported in this publication but more elaboration is to come out as a form of publication in near future. Alkylation kinetics was examined to further probe the steric manipulation of their respective nickel-thiolate bonds. Addition of excess MeI to a CD₂Cl₂ solution of **2.1b** at room temperature resulted in clean decomposition to form a paramagnetic halide complex and free MeSMes as observed by ¹H NMR spectroscopy (Figure 10). Conversion of **2.1a** and **2.2b** to respective Tp^{R,Me}Ni-I (R = Me, Ph) product complexes was monitored by UV-visible spectrophotometry (Figure 11); the equilibrium spectrum of the Tp^{Me,Me}Ni-I concurred with previous results,⁶⁸ while the identity of Tp^{Ph,Me}Ni-I was

inferred by comparison to the chloride complex.^{60,68} But later independent synthesis was carried out to characterize all the Tp halide products. Kinetic measurements for alkylations were made under pseudo-first-order conditions (equation (i))

$$-d[\text{Tp}^{\text{R,Me}}\text{Ni-SR}']/dt = k_{\text{obs}}[\text{Tp}^{\text{R,Me}}\text{Ni-SR}'],$$

$$\text{Where, } k_{\text{obs}} = k_1 + k_2[\text{MeI}]_0; \dots\dots\dots \text{(i)}$$

$$[\text{Tp}^{\text{R,Me}}\text{Ni-SR}']_0 = 0.5 \text{ mM},$$

$$[\text{MeI}]_0 = 16\text{-}128 \text{ mM),}$$

and linear dependences for observed rate as a function of methyl iodide concentrations were obtained by global least-squares fittings to single exponentials for both complexes (Figure 12). The second-order rate constant obtained for the sterically hindered complex **2.2b** was ten-fold larger, $k_2 = 1.23(8) \times 10^{-3} \text{ M}^{-1} \text{ s}^{-1}$ vs. $1.20(3) \times 10^{-4} \text{ M}^{-1} \text{ s}^{-1}$ for **2.1a**. A zero-order intercept was extrapolated for **2.2b**, $k_1 = 3.3(6) \times 10^{-5} \text{ s}^{-1}$, while that for **2.1a** was again smaller, $5(2) \times 10^{-6} \text{ s}^{-1}$.

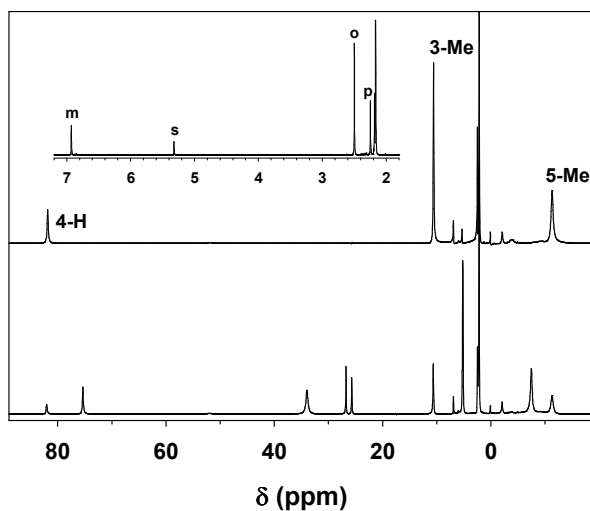


Figure 10: ^1H NMR spectra for reaction of $\text{Tp}^{\text{Me,Me}}\text{Ni-SMes}$ and MeI in CD_2Cl_2 at 295 K, near the start (bottom) and near equilibrium (top). Inset shows spectrum of arylmethylsulfide co-product recorded using routine acquisition parameters for a diamagnetic solvate.

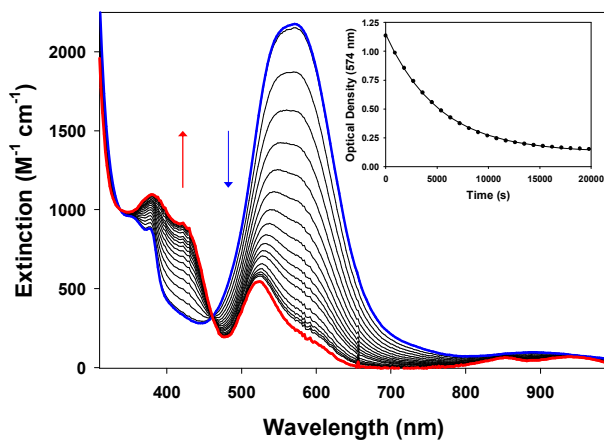


Figure 11: UV-visible traces for reaction of $\text{Tp}^{\text{Ph,Me}}\text{Ni-SMes}$ (**2.2b**, 0.5 mM) with MeI (128 mM) at 295 K in CH_2Cl_2 solution ($\Delta t = 900$ s). Limiting traces shown in blue and red are calculated spectra of the starting thiolate and product $\text{Tp}^{\text{Ph,Me}}\text{Ni-I}$ complexes, respectively. Inset shows a single-exponential fit by global least-squares techniques to the time-dependent optical density at 574 nm (λ_{max} for **2.2b**).

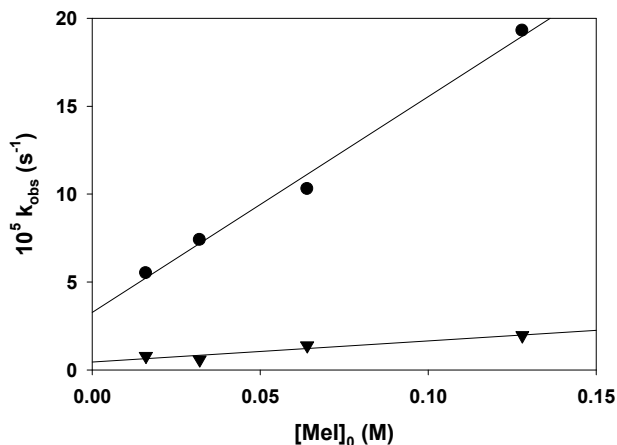


Figure 12: Dependence of methyl iodide concentration on rate of decomposition ($k_{\text{obs}} = k_1 + k_2[\text{MeI}]$) for $\text{Tp}^{\text{Me,Me}}\text{Ni-SPh}$ (**2.1a**, ▼, $R^2 = 0.91$) and $\text{Tp}^{\text{Ph,Me}}\text{Ni-SPh}$ (**2.2b**, ●, $R^2 = 0.99$) in CH_2Cl_2 solution at 297 K.

These results demonstrate a significant steric effect on reaction kinetics, consistent with perturbation of Ni(II)-SAr coordinate bonding already evident in the spectroscopic and structural data. Initially in this paper the intercept was interpreted to represent an unprecedented superposition of competing mechanisms but later it revealed that was not the case (manuscript in progress) bimolecular nucleophilic reaction between intact complex and methyl iodide that gives rise to the first-order (i.e., linear) rate dependence.⁴⁷ The distinctive color of the thiolate complexes were observed to slowly discharge in solution even without addition of MeI and further investigation probed that is due to oxygenation of these complexes as the cuvettes do not stay sealed for long period of time. Moreover, decompositions were observed to speed up dramatically in more polar solvents, consistent with accumulation of significant charge in the rate-limiting steps.

2.4 Discussion

The prominent feature of the thiolate complex structures is the tilting of the Ni-S bond vector off the trigonal axis, which is accentuated by steric effects in the bulkier complex **2.2c**. In light of the attendant spectroscopic trends already elucidated, the effects of this geometric distortion on the electronic structure of the complexes can be considered in a qualitative sense based on symmetry considerations. Cogent DFT analyses have already been reported for spectroscopy and bonding of arylthiolates at high-spin complexes in tetrahedral and square pyramidal geometries,^{47,67} which serve as a starting point for such deliberation. The pseudo-tetrahedral chloride complex precursors exhibit nearly perfect three-fold symmetry,^{61,62} but the arylthiolate substituents break axial symmetry, enabling the observed reduction in symmetry from C_{3v} to C_s . The thiolate ligands accordingly present two unhybridized sulfur p orbitals toward the metal ion of σ and π symmetry; the sulfur $p\sigma$ orbital is destabilized by interaction with a lower-lying, filled nickel $d\sigma$ orbital, the other p orbital effects net covalent $p\pi-d\pi^*$ bonding with a half-filled d orbital, and the second half-filled d orbital is essentially non-bonding.⁶⁷ Of course, the σ and π symmetries and bonding interactions are exactly reversed in a square pyramid.⁴⁷ Tilting of the Ni-S bond vector off the trigonal axis toward one vertex will reduce the destabilizing axial $p\sigma-d\sigma^*$ overlap in a pseudo-tetrahedron, but the cylindrical symmetry of the single $p\pi-d\pi^*$ bonding interaction would be unaffected. Therefore, covalency of the Ni-SR' coordinate bond should increase with the degree of tilting and indeed, a slightly shortened bond distance is observed in **2.2c** compared to **2.1a**. The

orbital effects of an opposing tilt, away from a trigonal vertex towards an edge between nitrogen donors, were explicitly modeled for isoelectronic TpCo(CO) using Extended Hückel theory;⁷⁸ such a structure has been observed experimentally in PhB(CH₂PPh₂)₃Ni-SC₆H₄-*p*-^tBu.⁵⁷ Steric effects can profoundly perturb the geometric and electronic structures, for example axial Jahn-Teller distortion can be preferentially enforced over trigonal bending by the presence of very bulky arylthiolate substituents in the low spin ($S = \frac{1}{2}$) state of related cobalt(II) complexes.⁷⁹

Electrophilic alkylation of thiolate complexes are of interest in regard to analogous biological alkyl transfers to zinc thiolate centers such as that in the Ada DNA repair protein.⁸⁰⁻⁸³ Comparative reactivities of zinc and nickel model complexes have been studied to determine kinetic and mechanistic effects arising from covalency of the Ni-S bond.^{45,47} Direct bimolecular reactions (*i.e.*, k_2 in equation (i)) of intact neutral complexes (κ^3 -L)Zn-SR,⁸³ as well as of cationic complexes [$(\kappa^4$ -L)M-SR]⁺ (M = Ni, Zn).⁴⁷ The dianionic charge of the former assists a unique thiolate dissociation pathway,⁸² and as mentioned above, the effects of solvent polarity (*i.e.*, DMSO) also should be considered.⁴⁵

We were initially puzzled by the k_1 intercept in reactivity of the neutral pseudo-tetrahedral nickel(II) complexes and believed it to be a competing mechanism only later to discover that this is more plausibly due to oxygenation (publication manuscript in progress) and other side reactions. In contrast, square-pyramidal RSRS-[(κ^4 -tmc)Ni-SPh]⁺ (tmc = 1,4,8,11-tetra-*N*-methyl-tetraazacyclotetradecane) with a shorter Ni-SPh bond reacts 300-fold more slowly with C₂H₅I than the RRSS isomer.⁴⁵ Significant effects

within pseudo-tetrahedral complexes arising from varied thiolate substituents and tripodal supporting ligands were previously reported for bimolecular reaction rates of neutral zinc complexes;⁸³ the observed rate of reaction for MeI with $\text{Tp}^{\text{Ph,Me}}\text{Zn-SPh}$ (the analog of **2.2a**) was $2.0 \times 10^{-3} \text{ M}^{-1} \text{ s}^{-1}$ (in CHCl_3 at 300 K), approximating the value of k_2 observed for **2.2b**. Curiously, the bulkier $\text{Tp}^{\text{tBu,Me}}\text{Zn-SPh}$ complex reacted 200 times more slowly than $\text{Tp}^{\text{Ph,Me}}\text{Zn-SPh}$, reflecting steric protection of the Zn-S bond from MeI within a hydrophobic pocket. Similar rates of reaction were also observed for reaction of benzyl bromide in CH_3CN with a pair of square-pyramidal complex analogs ($\kappa^4\text{-L}$)M-SAr [M = Ni, Zn, L = 1,5-bis(2-pyridylmethyl)-1,5-diazacyclooctane].⁴⁷

The disparate effects of complex charge, geometry, bonding and sterics on the Ni-SR' bond stabilities underscore the rich mechanistic behavior of the superficially straightforward alkylation reactivity. Full elucidation of the factors controlling this chemistry will be discussed in a publication in a ACS journal.

2.5 Conclusions

Five high-spin nickel(II) arylthiolate complexes $\text{Tp}^{\text{R,Me}}\text{Ni-SR}'$ (R = Me, Ph; R' = Ph, 2,4,6-Mes, 2,6-Xyl) were prepared and fully characterized. Manipulation of steric bulk at the opposing 3-pyrazoyl and *ortho*-arylthiolate positions within this series gives rise to a range of electronic structures as revealed by UV-visible-NIR and paramagnetic ^1H NMR spectra, as well as by X-ray crystallography of two examples at steric extremes of this series. Increasing steric bulk gives rise to structural distortion of the nickel(II)-

thiolate bond consisting of a significantly increased tilting of the Ni-S bond from trigonal symmetry and increased linearity of the Ni-S-R angle. This distortion alters covalency of the Ni-S coordinate bond, as revealed by red-shifted LMCT bands and enhanced hyperfine contacts onto the arylthiolate substituent. Reactivity of the nickel-thiolate linkage towards electrophilic alkylation was also studied showing most a pseudo first order dependency on the alkylating reagent.

2.5.1 Acknowledgment:

I acknowledge Dr. Swarup Chattopadhyay and Dr. Michael P Jensen for their support and contribution on this work. This work was supported by a startup grant from Ohio University (MPJ).

2.5.2 Appendix section information:

Appendix B and Appendix C contains data refinement, detailed bond length and bond angle information for **2.1a** and **2.2c**. Also, crystallographic data for $\text{Tp}^{\text{Me,Me}}\text{Ni-SC}_6\text{H}_5$ (**2.1a**) and $\text{Tp}^{\text{Ph,Me}}\text{NiS-2,6-C}_6\text{H}_3(\text{CH}_3)_2 \cdot 2\text{CH}_3\text{CN}$ (**2.2c**•**2CH₃CN**) in CIF format is available at the CSD database and via internet at at <http://pubs.acs.org>.

Table 1: Curie Law fits to paramagnetic contact shifts for arylthiolate complexes.

Complex	Resonance			
	H-4	<i>Ortho</i>	<i>meta</i>	<i>para</i>
2.1a intercept slope	$R^2 = 0.995$ $\delta = 7(3)$ $+ 20.8(8) \times 10^3/T$	$R^2 = 0.996$ $\delta = 3.7(8)$ $- 6.7(2) \times 10^3/T$	$R^2 = 0.994$ $\delta = 10.0(6)$ $+ 4.0(2) \times 10^3/T$	$R^2 = 0.996$ $\delta = 2(1)$ $- 8.4(3) \times 10^3/T$
2.1b	$R^2 = 0.994$ $\delta = 16(3)$ $+ 17.5(8) \times 10^3/T$	$R^2 = 0.996$ $\delta = -4(2)$ $+ 11.0(4) \times 10^3/T$	$R^2 = 0.994$ $\delta = 12.7(6)$ $+ 3.8(2) \times 10^3/T$	$R^2 = 0.995$ $\delta = 5(1)$ $+ 6.4(3) \times 10^3/T$
2.2a	$R^2 = 0.999$ $\delta = 9(1)$ $+ 18.3(4) \times 10^3/T$	$R^2 = 0.998$ $\delta = -4.9(7)$ $- 6.8(2) \times 10^3/T$	$R^2 = 0.999$ $\delta = 10.4(3)$ $+ 4.5(1) \times 10^3/T$	$R^2 = 0.999$ $\delta = -1.8(6)$ $- 10.6(2) \times 10^3/T$
2.2b	$R^2 = 0.997$ $\delta = 10(2)$ $+ 17.2(5) \times 10^3/T$	$R^2 = 0.998$ $\delta = -17(3)$ $+ 32.5(9) \times 10^3/T$	$R^2 = 0.998$ $\delta = 10.3(7)$ $+ 6.5(2) \times 10^3/T$	$R^2 = 0.998$ $\delta = 2(2)$ $+ 16.4(4) \times 10^3/T$

Table 2: Summary of the crystal data and structure refinements.

Complex	Tp ^{Me,Me} Ni-SPh (2.1a)	Tp ^{Ph,Me} Ni-SXyl (2.2c)•2CH ₃ CN
Empirical formula	C ₂₁ H ₂₇ BN ₆ NiS	C ₄₂ H ₄₃ BN ₈ NiS
Formula weight	465.07	762.42
Crystal size, mm	0.10 x 0.21 x 0.58	0.45 x 0.15 x 0.15
T, K	293(2)	173(2)
Crystal system	orthorhombic	monoclinic
Space group	Pbca	P2 ₁ /c
a, Å	15.259(2)	10.8543(3)
b, Å	14.427(1)	39.977(3)
c, Å	21.182(2)	10.1747(8)
α, deg	90	90
β, deg	90	114.972(1)
γ, deg	90	90
V, Å ³	4662.9(8)	4002.3(5)
Z	8	4
D _{calc} , g cm ⁻³	1.325	1.264
2θ range, deg	2.17 – 27.49	2.04 – 27.51
μ (Mo Kα), mm ⁻¹	0.941	0.577
R1, wR2 (I > 2σ(I))	0.0401, 0.1061	0.0402, 0.0949
R1, wR2 (all data)	0.0614, 0.1246	0.0579, 0.1008

Table 3: Summary of significant bond lengths and angles.

Complex			
TP^{Me,Me}Ni-SPh (2.1a)		TP^{Ph,Me}Ni-SXyl (2.2c)	
Bond lengths			
Ni1-S1	2.216(1)	Ni1-S1	2.1978(5)
Ni1-N3	1.992(2)	Ni1-N2	2.032(2)
Ni1-N1	1.978(2)	Ni1-N4	2.019(2)
Ni1-N5	1.988(2)	Ni1-N6	2.030(2)
S1-C16	1.771(2)	S1-C31	1.775(2)
Bond Angles			
S1-Ni1-N3	113.26(6)	S1-Ni1-N2	103.05(5)
S1-Ni1-N1	134.69(6)	S1-Ni1-N4	135.73(5)
S1-Ni1-N5	122.69(6)	S1-Ni1-N6	129.95(5)
N1-Ni1-N3	90.25(8)	N2-Ni1-N4	89.70(6)
N3-Ni1-N5	92.49(8)	N2-Ni1-N6	91.02(6)
N1-Ni1-N5	92.48(8)	N4-Ni1-N6	91.23(6)
Ni1-S1-C16	103.84(8)	Ni1-S1-C31	116.51(7)

2.6 References

- (1) Drennan, C. L.; Doukov, T. I.; Ragsdale, S. W. *J. Biol. Inorg. Chem.* **2004**, *9*, 511-515.
- (2) Ermler, U. *Dalton Trans.* **2005**, 3451-3458.
- (3) Drennan, C. L.; Heo, J.; Sintchak, M. D.; Schreiter, E.; Ludden, P. W. *Proc. Nat'l. Acad. Sci. USA* **2001**, *98*, 11973-11978.
- (4) Dobbek, H.; Svetlitchnyi, V.; Gremer, L; Huber, R.; Meyer, O. *Science* **2001**, *293*, 1281-1285.
- (5) Doukov, T. I.; Iverson, T. M.; Seravalli, J.; Ragsdale, S. W.; Drennan, C. L. *Science* **2002**, *298*, 567-572.

- (6) Darnault, C.; Volbeda, A.; Kim, E. J.; Legrand, P.; Vernède, X.; Lindahl, P. A.; Fontecilla-Camps, J. C. *Nature Struct. Biol.* **2003**, *10*, 271-279.
- (7) Svetlitchnyi, V.; Dobbek, H.; Meyer-Klaucke, W.; Meins, T.; Thiele, B.; Römer, P.; Huber, R.; Meyer, O. *Proc. Nat'l. Acad. Sci. USA* **2004**, *101*, 446-451.
- (8) Jeoung, J.-H.; Dobbek, H. *Science* **2007**, *318*, 1461-1464.
- (9) Volbeda, A.; Charon, M.-H.; Piras, C.; Hatchikian, E. C.; Frey, M.; Fontecilla-Camps, J. C. *Nature* **1995**, *373*, 580-587.
- (10) Fontecilla-Camps, J. C.; Volbeda, A.; Cavazza, C.; Nicolet, Y. *Chem. Rev.* **2007**, *107*, 4273-4303.
- (11) Ermler, U.; Grabarse, W.; Shima, S.; Goubeaud, M.; Thauer, R. K. *Science* **1997**, *278*, 1457-1462.
- (12) Bramlett, M. R.; Tan, X.; Lindahl, P. A. *J. Am. Chem. Soc.* **2003**, *125*, 9316-9317.
- (13) Tan, X.; Bramlett, M. R.; Lindahl, P. A. *J. Am. Chem. Soc.* **2004**, *126*, 5954-5955.
- (14) Seravalli, J. Xiao, Y.; Gu, W.; Cramer, S. P.; Antholine, W. E.; Krymov, V.; Gerfen, G. J.; Ragsdale, S. W. *Biochemistry* **2004**, *43*, 3944-3955.
- (15) Gencic, S.; Grahame, D. A. *J. Biol. Chem.* **2003**, *278*, 6101-6110.
- (16) Gu, W.; Gencic, S.; Cramer, S. P.; Grahame, D. A. *J. Am. Chem. Soc.* **2003**, *125*, 15343-15351.
- (17) Funk, T.; Gu, W.; Friedrich, S.; Wang, H.; Gencic, S.; Grahame, D. A.; Cramer, S. P. *J. Am. Chem. Soc.* **2004**, *126*, 88-95.

- (18) Dey, M.; Telser, J.; Kunz, R. C.; Lees, N. S.; Ragsdale, S. W.; Hoffman, B. M. *J. Am. Chem. Soc.* **2007**, *129*, 11030-11032.
- (19) Huber, C.; Wächtershäuser, G. *Science* **1997**, *276*, 245-247.
- (20) Russell, M. J.; Martin, W. *Trends. Biochem. Sci.* **2004**, *29*, 358-363.
- (21) Barondeau, D. P.; Kassman, C. J.; Bruns, C. K.; Tainer, J. A.; Getzoff, E. D. *Biochemistry* **2004**, *43*, 8038-8047.
- (22) Wuerges, J.; Lee, J.-W.; Yim, Y.-I.; Yim, H.-S.; Kang, S.-O.; Carugo, K. D. *Proc. Nat'l. Acad. Sci. USA* **2004**, *101*, 8569-8574.
- (23) Schreiter, E. R.; Sintchak, M. D.; Guo, Y.; Chivers, P. T.; Sauer, P. T.; Drennan, C. L. *Nature Struct. Biol.* **2003**, *10*, 794-799.
- (24) Dian, C.; Schauer, K.; Kapp, U.; McSweeney, S. M.; Labigne, A.; Terradot, L. *J. Mol. Biol.* **2006**, *361*, 715-730.
- (25) Kowal, A. T.; Zambrano, I. C.; Moura, I.; Moura, J. J. G.; LeGall, J.; Johnson, M. K. *Inorg. Chem.* **1988**, *27*, 1162-1166.
- (26) Huang, Y.-H.; Moura, I.; Moura, J. J. G.; LeGall, J.; Park, J.-B.; Adams, M. W. W.; Johnson, M. K. *Inorg. Chem.* **1993**, *32*, 406-412.
- (27) Tennent, D. L.; McMillin, D. R. *J. Am. Chem. Soc.* **1979**, *101*, 2307-2311.
- (28) Hannan, J. P.; Davy, S. L.; Moore, G. R.; Eady, R. R.; Andrew, C. R.; *J. Biol. Inorg. Chem.* **1998**, *3*, 282-291.
- (29) Johnson, R. S.; Schachman, H. K. *Proc. Nat'l. Acad. Sci. USA* **1980**, *77*, 1995-1999.
- (30) Krizek, B. A.; Berg, J. M. *Inorg. Chem.* **1992**, *31*, 2984-2986.

- (31) Lindahl, P. A. *J. Biol. Inorg. Chem.* **2004**, *9*, 516-524.
- (32) Webster, C. E.; Darensbourg, M. Y.; Lindahl, P. A.; Hall, M. B. *J. Am. Chem. Soc.* **2004**, *126*, 3410-3411.
- (33) Tan, X.; Surovtsev, I. V.; Lindahl, P. A. *J. Am. Chem. Soc.* **2006**, *128*, 12331-12338.
- (34) Bramlett, M. R.; Stubna, A.; Tan, X.; Surovtsev, I. V.; Münck, E.; Lindahl, P. A. *Biochemistry* **2006**, *45*, 8674-8685.
- (35) Stavropoulos, P.; Carrié, M.; Muetterties, M. C.; Holm, R. H. *J. Am. Chem. Soc.* **1990**, *112*, 5385-5387.
- (36) Stavropoulos, P.; Muetterties, M. C.; Carrié, M.; Holm, R. H. *J. Am. Chem. Soc.* **1991**, *113*, 8485-8492.
- (37) Hsiao, Y.-M.; Chojnacki, S. S.; Hinton, P.; Reibenspies, J. H.; Darensbourg, M. Y. *Organometallics* **1993**, *12*, 870-875.
- (38) Matsunaga, P. T.; Hillhouse, G. L. *Angew. Chem. Int. Ed.* **1994**, *106*, 1841-1843.
- (39) Tucci, G. C.; Holm, R. H. *J. Am. Chem. Soc.* **1995**, *117*, 6489-6496.
- (40) Sellmann, D.; Häussinger, D.; Knoch, F.; Moll, M. *J. Am. Chem. Soc.* **1996**, *118*, 5386-5374.
- (41) Eckert, N. A.; Dougherty, W. G.; Yap, G. P. A.; Riordan, C. G. *J. Am. Chem. Soc.* **2007**, *129*, 9286-9287.
- (42) Wang, H.; Ralston, C. Y.; Patil, D. S.; Jones, R. M.; Gu, W.; Verhagen, M.; Adams, M.; Ge, P.; Riordan, C.; Marganian, C. A.; Mascharak, P.; Kovacs, J.; Miller, C.

- G.; Collins, T. J.; Brooker, S.; Croucher, P. D.; Wang, K.; Stiefel, E. I.; Cramer, S. P. *J. Am. Chem. Soc.* **2000**, *122*, 10544-10552.
- (43) Fan, H.-J.; Hall, M. B. *J. Am. Chem. Soc.* **2002**, *124*, 394-395.
- (44) Nguyen, T.; Panda, A.; Olmstead, M. M.; Richards, A. F.; Stender, M.; Brynda, M.; Power, P. P. *J. Am. Chem. Soc.* **2005**, *127*, 8545-8552.
- (45) Ram, M. S.; Riordan, C. G.; Ostrander, R.; Rheingold, A. L. *Inorg. Chem.* **1995**, *34*, 5884-5892.
- (46) Wilker, J. J.; Gelasco, A.; Pressler, M. A.; Day, R. O.; Maroney, M. J. *J. Am. Chem. Soc.* **1991**, *113*, 6342-6343.
- (47) Fox, D. C.; Fiedler, A. T.; Halfen, H. L.; Brunold, T. C.; Halfen, J. A. *J. Am. Chem. Soc.* **2004**, *126*, 7627-7638.
- (48) Baidya, N.; Olmstead, M.; Mascharak, P. K. *Inorg. Chem.* **1991**, *30*, 929-937.
- (49) Baidya, N.; Olmstead, M. M.; Whitehead, J. P.; Bagyinka, C.; Maroney, M. J.; Mascharak, P. K. *Inorg. Chem.* **1992**, *31*, 3612-3619.
- (50) Baidya, N.; Olmstead, M. M.; Mascharak, P. K. *J. Am. Chem. Soc.* **1992**, *114*, 9666-9668.
- (51) Marganian, C. A.; Vazir, H.; Baidya, N.; Olmstead, M. M.; Mascharak, P. K. *J. Am. Chem. Soc.* **1995**, *117*, 1584-1594.
- (52) Osakada, K.; Yamamoto, T.; Yamamoto, A.; Takenaka, A.; Sasada, Y. *Acta Cryst. C* **1984**, *40*, 85-87.
- (53) Swenson, D.; Baenziger, N. C.; Coucouvanis, D. *J. Am. Chem. Soc.* **1978**, *100*, 1932-1934.

- (54) Rosenfield, S. G.; Armstrong, W. H.; Mascharak, P. K. *Inorg. Chem.* **1986**, *25*, 3014-3018.
- (55) Silver, A.; Koch, S. A.; Millar, M. *Inorg. Chim. Acta.* **1993**, *205*, 9-14.
- (56) Mueller, A.; Henkel, G. *Z. Naturforschung B* **1995**, *50*, 1464-1468.
- (57) MacBeth, C. E.; Thomas, J. C.; Betley, T. A.; Peters, J. C. *Inorg. Chem.* **2004**, *43*, 4645-4662.
- (58) Matsunaga, Y.; Fujisawa, K.; Ibi, N.; Miyashita, Y.; Okamoto, K.-i. *Inorg. Chem.* **2005**, *44*, 325-335.
- (59) Cho, J.; Yap, G. P. A.; Riordan, C. G. *Inorg. Chem.* **2007**, *46*, 11308-11315.
- (60) Desrochers, P. J.; Cutts, R. W.; Rice, P. K.; Golden, M.; Graham, J. B.; Barclay, T. M.; Cordes, A. W. *Inorg. Chem.* **1999**, *38*, 5690-5694.
- (61) Uehara, K.; Hikichi, S.; Akita, M. *J. Chem. Soc., Dalton Trans.* **2002**, 33529-3538.
- (62) Desrochers, P. J.; LeLievre, S.; Johnson, R. J.; Lamb, B. T.; Phelps, A. L.; Cordes, A. W.; Gu, W.; Cramer, S. P. *Inorg. Chem.* **2003**, *42*, 7945-7950.
- (63) SMART V5.054 Bruker Analytical X-ray Systems, Madison, WI, 2001.
- (64) An empirical correction for absorption anisotropy, R. Blessing, *Acta Cryst. A* **1995**, *51*, 33-38.
- (65) SHELXTL V6.14, Bruker Analytical X-ray Systems, Madison, WI, **2001**.
- (66) International Tables for X-ray Crystallography, Vol. 4, Kynoch Press, Birmingham, **1974**.

- (67) Gorelsky, S. I.; Basumallick, L.; Vura-Weis, J.; Sarangi, R.; Hodgson, K. O.; Hedman, B.; Fujisawa, K.; Solomon, E. I. *Inorg. Chem.* **2005**, *44*, 4947-4960.
- (68) Desrochers, P. J.; Telsler, J.; Zvyagin, S. A.; Ozarowski, A.; Krzystek, J.; Vivic, D. A. *Inorg. Chem.* **2006**, *45*, 8930-8941.
- (69) Jesson, J. P. *J. Chem. Phys.* **1967**, *47*, 582-591.
- (70) Horrocks, W. DeW., Jr.; Greenberg, E. S. *Inorg. Chem.* **1971**, *10*, 2190-2194.
- (71) Thompson, J. S.; Sorrell, T.; Marks, T. J.; Ibers, J. A. *J. Am. Chem. Soc.* **1979**, *101*, 4193-4200.
- (72) Trofimenko, S.; Calabrese, J. C.; Thompson, J. S. *Inorg. Chem.* **1992**, *31*, 974-979.
- (73) Alvarez, H. M.; Krawiec, M.; Donovan-Merkert, B. T.; Fouzi, M.; Rabinovich, D. *Inorg. Chem.* **2001**, *40*, 5736-5737.
- (74) Brookhart, M.; Green, M. L. H.; Parkin, G. *Proc. Nat'l Acad. Sci. USA* **2007**, *104*, 6908-6914.
- (75) Soong, S.-L.; Hain, J. H., Jr.; Millar, M.; Koch, S. A. *Organometallics* **1988**, *7*, 556-557.
- (76) Youngs, W. J.; Kinder, J. D.; Bradshaw, J. D.; Tessier, C. A. *Organometallics* **1993**, *12*, 2406-2407.
- (77) Shan, X.-F.; Wu, L.-Z.; Liu, X.-Y.; Zhang, L.-P.; Tung, C.-H. *Eur. J. Inorg. Chem.* **2007**, 3315-3319.
- (78) Detrich, J. L.; Konečný, R.; Vetter, W. M.; Doren, D.; Rheingold, A. L.; Theopold, K. H. *J. Am. Chem. Soc.* **1996**, *118*, 1703-1712.

- (79) Jenkins, D. M.; Peters, J. C. *J. Am. Chem. Soc.* **2005**, *127*, 7148-7165.
- (80) Parkin, G. *Chem. Rev.* **2004**, *104*, 699-767.
- (81) Wilker, J. J.; Lippard, S. J. *J. Am. Chem. Soc.* **1995**, *117*, 8682-8683.
- (82) Wilker, J. J.; Lippard, S. J. *Inorg. Chem.* **1997**, *36*, 969-978.
- (83) Rombach, M.; Seebacher, J.; Ji, M.; Zhang, G.; He, G.; Ibrahim, M. M.; Benkmil, B.; Vahrenkamp, H. *Inorg. Chem.* **2006**, *45*, 4571-4575.

CHAPTER 3: STERIC TITRATION OF ARYLTHIOLATE COORDINATION MODES AT PSEUDOTETRAHEDRAL NICKEL (II) CENTERS

(Note: Asterisk () denoted complexes were initially synthesized by Dr. Swarup Chattopadhyay and was highly significant. I also published these results in Inorganic Chemistry journal DOI: 10.1021/ic901347p)*

3.1 Introduction

Active site nickel ions are found in a number of bacterial and archaeobacterial enzymes that catalyze organometallic reactions, including H₂ oxidation,¹ methane synthesis,^{2,3} CO₂ reduction and acetate synthesis.^{2,4,5} This enzymology is environmentally significant in the global carbon cycle,² and may also represent precedent for sustainable energy technologies.^{6,7} Recent structural work has elucidated a variety of active sites for nickel, typically with low-coordinate ligand fields in non-classical geometries, valence and spin states, and with sulfur ligands and cofactors.⁸ These structures pose questions regarding dynamics and reactivity of novel active sites. As small molecule modeling is an established paradigm to examine these questions, we are accordingly interested in developing small-molecule coordination chemistry of paramagnetic nickel complexes with sulfur ligands.⁹⁻¹¹

The initial focus of our efforts has been pseudotetrahedral arylthiolate complexes supported by tris(pyrazolyl)borates.⁹ A key advantage afforded by these tripodal supporting ligands is the ability to add substituents to the facially tridentate pyrazole rings, enabling manipulation of electronic and steric properties of the ligand.¹² As the substituents are disposed “vertically” (*i.e.*, perpendicular to the N₃ donor plane), a pocket

is formed about a fourth binding site for a co-ligand. This effect enables rudimentary control of co-ligand bonding through steric contact, in modest analogy to typically elegant allosteric active site control achieved in metalloenzymes through all levels of protein structure.

We previously observed that the relatively large substituents of tris(3-phenyl,5-methylpyrazolyl)borate (*i.e.*, $\text{Tp}^{\text{Ph,Me}}$) forced significant bending of a Ni(II)-SXyl bond; the observed Ni-S-Ar bond angle increased from $103.84(8)^\circ$ for $\text{Tp}^{\text{Me,Me}}\text{Ni-SPh}$ (**2.1a**) to $116.51(7)^\circ$ for $\text{Tp}^{\text{Ph,Me}}\text{Ni-SXyl}$ in respective X-ray crystal structures.⁹ The arylthiolate coordination was otherwise quite similar in the two complexes, with the thiophenolate sulfur displaced off the three-fold axis toward one pyrazole, and the aryl substituent oriented vertically (*i.e.*, aligned between 3-substituents on the other two pyrazole rings). Several related complexes of various tripodal borate ligands have been reported. Similar vertical geometries were observed for $\text{Tp}^{\text{iPr,iPr}}\text{Ni-SC}_6\text{F}_5$,¹³ an analogous tripodal borate complex with thioether donors,¹⁴ and its $\text{C}_6\text{H}_5\text{S}^-$ congener.¹⁴ In contrast, a tripodal borate with diphenylphosphinomethyl donor arms yielded a different motif, with the sulfur atom disposed between donors and the substituent significantly rotated towards horizontal,¹⁵ as typically found for complexes with planar tetradentate supporting ligands.¹⁶ Another class of $[\text{Ni}(\text{SAr})_4]^{2-}$ complexes exhibit tetragonal (D_{2d}) distortion,¹⁷⁻²⁰ and a linear $\text{Ni}(\text{SAr})_2$ complex has also been reported.²¹ The distinctive features of these structures demonstrate disparate coordination modes for arylthiolates in pseudotetrahedral Ni(II) complexes.

In this chapter, we probed arylthiolate ligation at $\text{Tp}^{\text{Me,Me}}\text{Ni}^{\text{II}}$ centers by selectively modifying the arylthiolate on the parent $\text{Tp}^{\text{Me,Me}}\text{Ni-SPh}$ complex (**2.1a**), either with increasingly bulky *ortho* groups (**3.2-3.5**), or with electronically significant *para* substituents (**3.6-3.8**). These complexes demonstrate a primary role for steric interaction with the tris(pyrazolyl) pocket in eliciting two disparate arylthiolate bonding modes, which have been structurally characterized and distinguished by spectroscopy and DFT calculations.

3.2 Experimental Methods

3.2.1 General and synthetic procedures.

All manipulations were carried out under an inert atmosphere of prepurified argon, either in a glovebox (MBraun Unilab) or using Schlenk techniques. ^1H NMR data were recorded on a Varian Unity 500 spectrometer and processed using the MestReNova 5.1.0 software suite (Mestrelab Research, Santiago de Compostela, Spain); spectra were referenced internally to residual solvent. Solution magnetic moments were determined by the Evans NMR method in CDCl_3 at 295 K.²² UV-visible-NIR spectra were recorded on an Agilent HP-8453 diode-array spectrophotometer. Elemental analyses were performed by Atlantic Microlabs, Inc. (Norcross, GA). $\text{Tp}^{\text{Me,Me}}\text{NiCl}$ was prepared by metathesis of anhydrous NiCl_2 and $\text{TlTp}^{\text{Me,Me}}$ in $\text{MeOH}/\text{CH}_2\text{Cl}_2$ (**caution**: thallium salts are extremely toxic and must be properly handled and disposed of).²³ 2,6-diphenyl- and 2,4,6-tris(isopropyl)phenylthiol were prepared by literature procedures,²⁴⁻²⁶ and other

thiols were obtained from a commercial vendor (Aldrich). The thiols were converted to respective sodium salts by titration of NaNH₂ in toluene, and reacted with Tp^{Me,Me}NiCl in THF to obtain target complexes in 65-80% yields following toluene extraction as previously described.⁹ Characterizations of product complexes are summarized below. All other materials were obtained from commercial vendors as ACS reagent-grade or better and used as received, except for drying of solvents by routine techniques.

Tp^{Me,Me}Ni-SC₆H₅ (**2.1a**).⁹ Anal. Calc'd. (found) for C₂₁H₂₇BN₆NiS: C, 54.23 (54.64); H, 5.85 (5.98); N 18.07 (18.24). UV-Vis (CH₂Cl₂, λ_{max}, nm; ε, mM⁻¹ cm⁻¹): 354 (1.6); 464 (2.4); 506 (2.6); 614 (sh, 0.2); 836 (0.2); 970 (sh, 0.1). ¹H NMR (CDCl₃, 295 K; δ, ppm): 77.2 (3H, 4-pz); 23.3 (2H, *meta*); 6.6 (9H, 5-Me); -7.1 (9H, 3-Me); -10.7 (1H, B-*H*); -18.9 (2H, *ortho*); -26.6 (1H, *para*); μ_{eff} = 2.92 μ_B.

Tp^{Me,Me}Ni-S-2,6-Me₂C₆H₃ (**3.2**). Anal. Calc'd. (found) for C₂₃H₃₁BN₆NiS•H₂O: C, 54.05 (54.24); H, 6.51 (6.71); N 16.44 (16.57). UV-Vis (toluene, λ_{max}, nm; ε, mM⁻¹ cm⁻¹): 342 (0.9); 368 (0.9); 411 (1.1); 471 (sh, 1.4); 511 (2.2); 640 (0.2); 856 (0.1), 958 (0.1). ¹H NMR (CDCl₃; δ, ppm): 75.3 (3H, 4-pz); 31.7 (6H, *ortho*); 25.2 (2H, *meta*); 5.5 (9H, 5-Me); -7.5 (9H, 3-Me); -10.4 (1H, *para*); -11.3 (1H, B-*H*).

Tp^{Me,Me}Ni-S-2,4,6-Me₃C₆H₂ (**3.3**).⁹ Anal. Calc'd. (found) for C₂₄H₃₃BN₆NiS: C, 56.84 (56.75); H, 6.56 (6.59); N 16.57 (17.32). UV-Vis (CH₂Cl₂, λ_{max}, nm; ε, mM⁻¹ cm⁻¹): 343 (1.1); 371 (1.1); 406 (1.2); 467 (sh, 1.5); 514 (2.7); 636 (sh, 0.2); 861 (0.2). ¹H NMR (CDCl₃; δ, ppm): 75.0 (3H, 4-pz); 33.3 (6H, *ortho*); 25.8 (3H, *para*); 25.3 (2H, *meta*); 5.2 (9H, 5-Me); -7.5 (9H, 3-Me); -11.3 (1H, B-*H*); μ_{eff} = 3.01 μ_B.

$Tp^{Me,Me}Ni-S-2,4,6-iPr_3C_6H_2$ (**3.4**)*. Anal. Calc'd. (found) for $C_{30}H_{45}BN_6NiS$: C, 60.94 (61.03); H, 7.67 (7.83); N 14.21 (14.25). UV-Vis (CH_2Cl_2 , λ_{max} , nm; ϵ , $mM^{-1} cm^{-1}$): 338 (sh, 1.1); 414 (2.2); 516 (2.8); 665 (0.3); 870 (0.2); 954 (0.1). 1H NMR ($CDCl_3$; δ , ppm): 75.3 (3H, 4-pz); 24.5 (2H, *meta*); 19.7 (2H, 2,6-*CHMe*₂); 8.8 (1H, 4-*CHMe*₂); 8.0 (12H, 2,6-*CHMe*₂); 5.3 (9H, 5-Me); 2.3 (6H, 2,6-*CHMe*₂); -8.1 (9H, 3-Me); -11.8 (1H, B-*H*).

$Tp^{Me,Me}Ni-S-2,6-Ph_2C_6H_3$ (**3.5**)*. Anal. Calc'd. (found) for $C_{33}H_{35}BN_6NiS$: C, 64.21 (64.27); H, 5.72 (5.79); N 13.62 (13.57). UV-Vis (CH_2Cl_2 , λ_{max} , nm; ϵ , $mM^{-1} cm^{-1}$): 357 (sh, 0.8); 422 (1.8); 516 (1.8); 657 (0.3); 867 (0.2); 942 (0.1). 1H NMR ($CDCl_3$; δ , ppm): 76.5 (3H, 4-pz); 24.6 (2H, *meta*); 15.1 (4H, 2,6-*ortho*); 7.4 (2H, 2,6-*para*); 6.8 (4H, 2,6-*meta*); 5.9 (9H, 5-Me); 1.4 (1H, *para*); -9.4 (9H, 3-Me); -11.7 (1H, B-*H*); $\mu_{eff} = 2.89 \mu_B$.

$Tp^{Me,Me}Ni-S-C_6H_4-4-OCH_3$ (**3.6**)*. Anal. Calc'd. (found) for $C_{24}H_{33}BN_6NiS$: C, 53.37 (53.46); H, 5.90 (5.89); N 16.98 (17.21). UV-Vis (CH_2Cl_2 , λ_{max} , nm; ϵ , $mM^{-1} cm^{-1}$): 348 (1.8); 484 (sh, 2.4); 517 (3.1); 843 (0.2); 1000(sh, 0.1). 1H NMR ($CDCl_3$; δ , ppm): 75.5 (3H, 4-pz); 22.5 (2H, *meta*); 6.3 (9H, 5-Me); -6.9 (9H, 3-Me); -8.3 (3H, OMe); -10.3 (1H, B-*H*); -21.0 (2H, *ortho*).

$Tp^{Me,Me}Ni-S-C_6H_4-4-CH_3$ (**3.7**)*. Anal. Calc'd. (found) for $C_{24}H_{33}BN_6NiS$: C, 55.16 (55.18); H, 6.10 (6.16); N 17.54 (17.63). UV-Vis (CH_2Cl_2 , λ_{max} , nm; ϵ , $mM^{-1} cm^{-1}$): 353 (1.7); 475 (2.4); 513 (3.2); 624 (sh, 0.2); 841 (0.1); 970 (sh, 0.1). 1H NMR ($CDCl_3$; δ , ppm): 75.7 (3H, 4-pz); 38.1 (3H, *para-CH*₃); 23.1 (2H, *meta*); 6.4 (9H, 5-Me); -6.9 (9H, 3-Me); -10.4 (1H, B-*H*); -19.9 (2H, *ortho*).

$Tp^{Me,Me}Ni-S-C_6H_4-4-Cl$ (**3.8**)*. Anal. Calc'd. (found) for $C_{24}H_{33}BN_6NiS$: C, 50.50 (50.65); H, 5.25 (5.35); N 16.83 (16.70). UV-Vis (CH_2Cl_2 , λ_{max} , nm; ϵ , $mM^{-1} cm^{-1}$): 361 (1.9); 464 (2.7); 510(2.8); 615 (sh, 0.2); 835 (0.2); 970 (sh, 0.1). 1H NMR ($CDCl_3$; δ , ppm): 77.0 (3H, 4-pz); 23.7 (2H, *meta*); 7.1 (9H, 5-Me); -6.9 (9H, 3-Me); -10.5 (1H, B-H); -20.3 (2H, *ortho*).

3.2.2 X-ray crystallography.

The structure of $Tp^{Me,Me}Ni-S-2,6-Ph_2C_6H_3 \cdot 2.0THF$ (**3.5**) was solved at the University of Minnesota (VGY). Suitable crystals were grown from a concentrated THF solution cooled to $-36^\circ C$. An orange block ($0.35 \times 0.30 \times 0.30 \text{ mm}^3$) was placed onto the tip of a 0.1 mm diameter glass capillary and mounted on a Bruker AXS diffractometer equipped with a CCD area detector.²⁷ The data collection was carried out at 123(2) K using $MoK\alpha$ radiation ($\lambda = 0.71073 \text{ \AA}$, graphite monochromator). The intensity data were corrected for absorption and decay (SADABS).²⁸ Final cell constants were calculated from 2761 strong reflections from the actual data collection after integration (SAINT).²⁹ The structure was solved and refined using Bruker SHELXTL.³⁰ The space group Pnma was determined based on systematic absences and intensity statistics. A direct-methods solution was calculated which provided most non-hydrogen atoms from the E-map; full-matrix least squares difference Fourier cycles were performed which located the remaining non-hydrogen atoms. All non-hydrogen atoms were refined with anisotropic displacement parameters. All hydrogen atoms were placed in ideal positions and refined as riding atoms with relative isotropic displacement parameters. The

molecule is bisected by the crystallographic mirror plane so that half appears in one asymmetric unit. There is also one molecule of THF solvent per asymmetric unit disordered over two positions in the same region of space in a 0.68:0.32 ratio. There is some indication that at least one THF fragment also has “envelope flap” disorder. It appears that the THF oxygen atoms were correctly placed for both disordered fragments. A total of 46783 reflections were collected, with 4718 being independent ($R_{\text{int}} = 0.0323$) and 4062 observed. The refinement converged to give $R1 = 0.0411$, $wR2 = 0.1042$ (all data), $\text{GoF} = 1.122$. Crystal data: $\text{C}_{41}\text{H}_{51}\text{BN}_6\text{NiO}_2\text{S}_2$, formula weight 761.46, orthorhombic, Pnma , $a = 15.984(2) \text{ \AA}$, $b = 23.499(3) \text{ \AA}$, $c = 10.685(1) \text{ \AA}$, $V = 4013.4(8) \text{ \AA}^3$, $Z = 4$, $D_{\text{calc}} = 1.260 \text{ g/cm}^3$, $\mu = 5.78 \text{ cm}^{-1}$.

3.2.3 DFT calculations.

All calculations were carried out using the Amsterdam Density Functional software package (version 2007.01, Scientific Computing and Modeling NV).^{31,32} Atomic coordinates were imported from the experimental structures of **2.1a** and **3.5** and reduced to simple TpNi-SPh models **2.1a'** and **3.5'** by replacement of the pyrazole and *ortho*-arylthiolate substituents with hydrogen atoms in ideal positions. The model geometries were optimized under imposed C_s symmetry, with the Ni-S- C_{ipso} angle of **3.5'** constrained to the experimental value to prevent inward bending in the absence of the 3-pyrazole and *ortho*-arylthiolate substituents. Furthermore, a full series of configurational models spanning arylthiolate coordination with equatorial or axial sulfur ligation and horizontal or vertical substituent orientations was obtained by manipulating the $N_{\text{axial-Ni}}$

S-C_{ipso} and Ni-S-C_{ipso}-C_{ortho} torsion angles of **3.5'** with subsequent geometry optimization under appropriate symmetry (*i.e.*, C_1 or C_s) without additional constraints. Finally, a **2.1a''** model optimized under experimental C_1 symmetry was also included in TD-DFT calculations. Spin-unrestricted geometry optimizations, single point and TD-DFT^{33,34} calculations were performed using the Vosko-Wilk-Nussair LDA exchange-correlation functional,³⁵ the Becke-Perdew GGA correction,^{36,37} and the Slater-type orbital TZP (triple zeta with single polarization) basis set available in the ADF library, with frozen atomic cores and default convergence criteria. A solvation model and relativistic correction were not applied. Spin-restricted calculations on the free phenylthiolate anion were performed similarly, starting from a suitable crystal structure fragment.

3.3 Results and Discussion

3.3.1 General Comments.

We prepared several derivatives of our previously reported parent complex $\text{Tp}^{\text{Me,Me}}\text{Ni-SPh}$ (**2.1a**),⁹ modified along steric and electronic vectors: a series of complexes with enhanced bulk at the *ortho* arylthiolate positions, $\text{Tp}^{\text{Me,Me}}\text{Ni-SAr}$ [Ar = C₆H₅ (**2.1a**), 2,6-Me₂-C₆H₃ (**3.2**), 2,4,6-Me₃-C₆H₂ (**3.3**), 2,4,6-*i*-Pr₃C₆H₂ (**3.4**), 2,6-Ph₂-C₆H₃ (**3.5**)]; and a second series with *para* substituents of varying electronic donor strength, $\text{Tp}^{\text{Me,Me}}\text{Ni-S-C}_6\text{H}_4\text{-4-X}$ [X = OCH₃ (**3.6**), CH₃ (**3.7**), H (**2.1a**) and Cl (**3.8**)]. The complexes were prepared by metatheses of $\text{Tp}^{\text{Me,Me}}\text{NiCl}$ with respective sodium thiolate salts in THF, resulting in appearance of intense coloration due to characteristic Ni-SAr

LMCT bands (*vide infra*). The complexes were characterized by elemental analyses, ^1H NMR and UV-Vis-NIR spectroscopy. In all cases, the results were consistent with pseudotetrahedral complexes exhibiting a paramagnetic ($S = 1$) d^8 electron configuration. The structure of **3.5** was also determined.

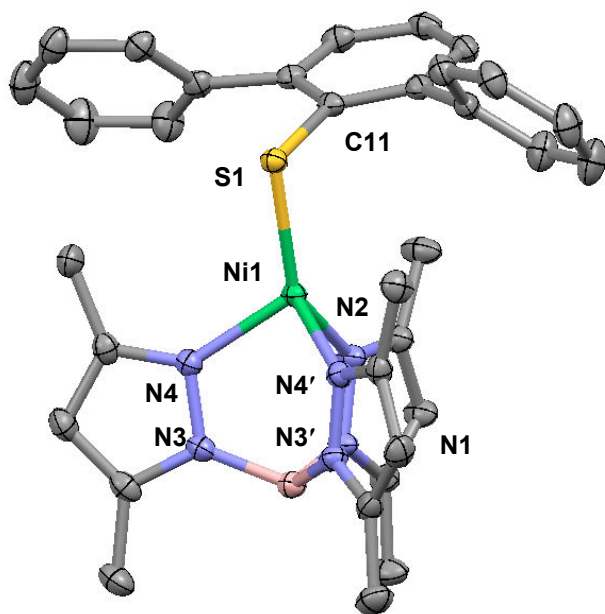


Figure 13: ORTEP diagram (50% ellipsoids) of $\text{Tp}^{\text{Me,Me}}\text{Ni-S-2,6-Ph}_2\text{C}_6\text{H}_3$ (**3.5**) Selected bond lengths (\AA): Ni1-N4, 1.995(1); Ni1-N2, 2.001(2); Ni1-S1, 2.2589(6); S1-C11, 1.785(2). Bond angles ($^\circ$): N4-Ni1-N4', 92.06(8); N4-Ni1-N2, 91.20(5); N4-Ni1-S1, 115.47(4); N2-Ni1-S1, 140.01(6); Ni1-S1-C11, 100.11(7).

3.3.2 X-ray crystallography.

The previously reported structures of $\text{Tp}^{\text{Me,Me}}\text{NiSPh}$ (**2.1a**) and the bulkier analog $\text{Tp}^{\text{Ph,Me}}\text{Ni-S-2,6-Me}_2\text{C}_6\text{H}_3$ (**3.9**) analog consisted of distorted pseudotetrahedral N_3S ligand fields with the Ni-S bond bent off the three-fold $\text{H-B}\cdots\text{Ni}$ axis particularly towards one of the pyrazolyl arms, giving a trigonal pyramidal shape with an N_2S

equatorial plane.⁹ The arylthiolate substituents were disposed over unoccupied axial sites and nearly vertical between 3-pyrazole substituents on opposing equatorial donor arms. In the present work, we introduced steric bulk at the arylthiolate *ortho* positions while retaining the smaller 3-pyrazole methyl substituents. This elicited a distinct arylthiolate coordination mode, revealed by the crystal structure of $\text{Tp}^{\text{Me,Me}}\text{Ni-S-2,6-Ph}_2\text{C}_6\text{H}_3$ (**3.5**), which is distorted by off-axis thiolate bending toward a sawhorse geometry, with axial sulfur and pyrazole donors (*i.e.*, S1 and N2) and an open equatorial site (Figure 13). The Ni-S bond in **3.5** is bent between pyrazole donors, and the arylthiolate substituent is displaced backward over the third pyrazole and the vacant equatorial site, rotating into a rigorously horizontal orientation (molecular C_s symmetry is enforced by a crystallographic mirror plane). The outer 2,6-phenyl ring planes are rotated 55.89° from co-planarity, giving short contacts between each of the pyrazole 3-methyl substituents and an opposing aromatic ring on the arylthiolate, 3.330 and 3.503 Å to the inner and outer centroids, respectively. The unique N-Ni-S angle from the axial pyrazole increases from $113.26(6)^\circ$ in **2.1a** to $140.01(6)^\circ$ in **3.5**, with further opening possibly constrained by the equatorial 3-methyl substituents, given short $\text{S}\cdots\text{HC}$ contacts of 2.883 Å. The Ni-S bond length is slightly longer in **3.5** than in **2.1a**, 2.2589(6) vs. 2.216(1) Å, while the Ni-S-Ar angle is less obtuse, $100.11(7)$ vs. $103.84(8)^\circ$.

3.3.3 Ni-SAr structural configurations.

Tris(pyrazolyl)borates and related tripodal ligands have been referred to as “tetrahedral enforcers” for the four-coordinate, half-sandwich geometry they typically

support.^{38,39,40} However, the tetrahedral ligand fields are typically distorted (hence “pseudotetrahedral”), and several unique distortional modes have been identified by symmetry mapping of four-coordinate metal centers.⁴¹ A universal $T_d \rightarrow C_{3v}$ umbrella distortion is enforced by the constrained ligand bite, in which N-Ni-N angles are reduced to *ca.* 90°, and the angle to the trigonal H-B•••Ni axis is concordantly increased to *ca.* 124° for the tris(pyrazolyl)borate ligand. Such facially tridentate ligands are perhaps more appropriately assigned as filling one face of an octahedron, particularly when an apical co-ligand can donate six electrons utilizing orthogonal lone pairs of π symmetry, such as CO or halide anions.³⁸⁻⁴⁰ The borate chelate also constrains $T_d \rightarrow D_{2d}$ spread and pincer distortions, the former having been observed for $[\text{Ni}(\text{SAr}_4)]^{2-}$ complexes,¹⁷⁻²⁰ but the apical arylthiolate ligand is still susceptible to $T_d \rightarrow C_s$ off-axis and $T_d \rightarrow C_{2v}$ sawhorse bendings.⁴¹ With three positions defined by constrained facial pyrazolyl nitrogens, the off-axis and sawhorse bendings are limited to opposing motions of the sulfur toward or away from a particular pyrazole ring. These will respectively lead to a unique N-Ni-S angle that is smaller or larger than the average umbrella angle.

Relevant geometric parameters for the seven structurally characterized arylthiolate complexes of Ni(II) supported by tripodal borate ligands can be summarized within this model (Table 4).^{9,13-15} A significant umbrella distortion is indicated in each case by the pseudotetrahedral angle formed between the three-fold H-B•••Ni axis and the coordinate bond vectors to the borate tripod donors, ranging from 120.4° to 124.8° compared to the ideal tetrahedral value of 109.47°. Further distortion by off-axis or sawhorse bending of the arylthiolate is indicated by distribution of L-Ni-S angles about

this value. As predicted in limiting cases, one of the three L-Ni-S angles is unique, being smaller (*e.g.*, **3.9**) or larger (*e.g.*, **3.5**) than the pseudotetrahedral angle.

The sawhorse distortion has been structurally analyzed in terms of a *cis*-divacant octahedron (Figure 14, left),^{39,40} in which Ni-S bending towards an edge of the L₃ donor triangle leads to a staggered geometry, illustrated for the core structure of **3.5** (Figure 14, top). Off-axis bending can be interpreted in the opposite direction, towards a vertex that yields an eclipsed geometry typified by **3.9** (Figure 14, bottom). Since a *bent* arylthiolate ligand can donate only four electrons, these distortions can be alternatively considered on the surface of a monovacant trigonal bipyramid (Figure 14, right),^{13,14,38,42} overlooking the constrained bite of the equatorial nitrogens. Nevertheless, bending of sulfur toward distinct axial or equatorial sites gives the same two limiting geometries. The Ni-S bond is directly bent over a donor in the trigonal/eclipsed/equatorial geometry, and directly away in the sawhorse/staggered/axial geometry. Equivalence of the octahedral and trigonal bipyramidal models can be observed by rotation of the corresponding core structures of **3.5** and **3.9** about the axial pyrazole nitrogen. The trigonal bipyramidal nomenclature (*i.e.*, axial and equatorial) seems the most descriptive of the ligand field and will be used exclusively henceforth, with “axial” coordination denoting distortion towards a trigonal bipyramidal vertex as opposed to a site along the H-B•••Ni umbrella axis.

The limiting axial and equatorial configurations just defined are further differentiated by orthogonal orientations of the aryl substituent (Figure 14). The substituent is usually folded backwards over the vacated site and rotated to minimize

steric contact with the opposing tripodal ligand substituents. The axial thiolate configurations of **3.5** and the PhBP₃Ni-S-C₆H₄-4-^tBu complex reported by MacBeth, *et al.*¹⁵ are associated with a “horizontal” disposition of the aryl substituent, denoted by large Ni-S-C_{ipso}-C_{ortho} torsion angles (Table 4), while an equatorial, vertical orientation is observed in the other structures.

The magnitudes of distortions of tetracoordinate complexes from tetrahedral towards a trigonal monopyramid have been quantified either by a τ parameter ranging from zero to unity, based on the difference of apical and basal bond angles,⁴² or inversely by metal separation from an equatorial N₂S basal plane.¹³ A uniquely large N-Ni-S angle consistent with a sawhorse geometry gives an undefined τ value. However, a different τ_4 parameter defined by the two largest bond angles encompasses both distortions, such that unity corresponds to a tetrahedron (reduced to 0.78-0.85 by the umbrella distortion), while a sawhorse and a trigonal pyramid are independently defined as 0.64 (with 90° N-Ni-N angles).⁴³ These various parameters are also summarized for each tripodal arylthiolate complex (Table 4).

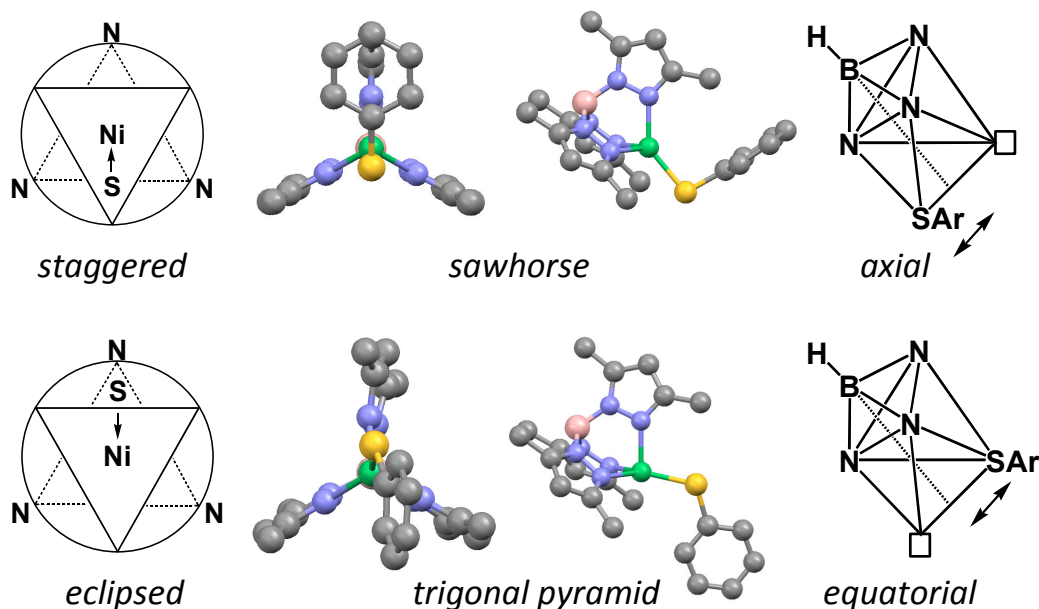


Figure 14: Illustration of sawhorse (top) and off-axis bending (bottom) on a *cis*-divacant octahedron (left column) and monovacant trigonal bipyramid (right column), as seen in two orientations of the core structures for **3.5** (top row) and **3.9** (bottom row), with *ortho* substituents on the arylthiolate rings and all but the *ipso* carbon of the 3-phenyl substituents of **3.9** omitted for clarity.

As discussed previously, the off-axis and sawhorse bendings are energetically favored for a d^8 electron configuration by reduction of destabilizing overlap in the filled Ni-S $d\sigma-p\sigma^*$ interaction.⁴⁰ While electronic in origin, the direction and magnitude of the bending can be manipulated by steric contacts. We previously demonstrated enhanced trigonal bending from **2.1a** to **3.9** ($\tau = 0.60$ and 0.81 respectively, Table 4) by substituting bulky 3-pyrazole substituents (*i.e.*, $Tp^{Ph,Me}$) proximal to added *ortho*-methyl substituents on the arylthiolate ring.⁹ The rigid 3-phenyl rings enforced retention of a vertical 2,6-xylyl substituent orientation in **3.9**, leaving the sulfur in an equatorial configuration with enhanced off-axis bending. With retention of the smaller $Tp^{Me,Me}$ ligand substituents,

rotation of the arylthiolate ring is enabled, and the bulky thiolate of **3.5** adopts an axial/horizontal configuration. We hypothesize that the equatorial/vertical configuration lies somewhat lower in energy for **2.1a**, but is destabilized by enhanced steric contact with *ortho*-phenyl substituents, thus effecting a conformational switch (Figure 15). This suggests a dynamic equilibrium between the configurations can be manipulated by changing the size of added *ortho* arylthiolate substituents. Spectroscopic evidence supporting this interpretation was obtained across the series **2.1a**, **3.2-3.5** encompassing added 2,6-Me₂, -^{*i*}Pr₂, and -Ph₂ arylthiolate disubstitution of **2.1a**.

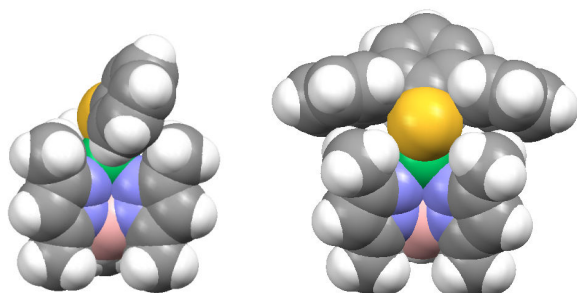


Figure 15: Space-filling models of **2.1a** (left) and **3.5** (right), demonstrating a dominant steric role for *ortho* substitution in effecting an observed conformational switch in arylthiolate coordination.

Table 4: Structural parameters for Ni(II) arylthiolate complexes of tripodal borato ligands.

Complex	Umbrella angle (°) ^(a)	L-Ni-S angles (°)	Ni-S-C _{ipso} -C _{ortho} torsion angles (°)	d (Å) ^(b)	τ ^(c)	τ_4 ^(d)	Ref.
Tp ^{Ph,Me} Ni-S-2,6-Me ₂ C ₆ H ₃ (3.9)	124.8	135.73(5), 129.95(5), 103.05(5)	15.14, 15.19	0.20	0.81	0.67	9
PhTt ^{tBu} Ni-SC ₆ F ₅ ^(e)	122.9	130.29(2), 128.52(2), 105.13(2)	5.35, 7.15	0.28	0.74	0.70	14
Tp ^{iPr,iPr} Ni-SC ₆ F ₅ ^(f)	123.8	132.7(1), 128.9(1), 106.8(1) 132.8(1), 128.4(1), 106.4(1)	10.41, 11.62 10.84, 11.90	0.28	0.72	0.70	13
PhTt ^{tBu} Ni-SPh ^(e)	122.3	129.94(4), 129.00(4), 104.49(4)	1.03, 1.66	0.31	0.69	0.72	14
Tp ^{Me,Me} Ni-SPh (2.1a)	124.0	134.96(6), 122.69(6), 113.26(6)	16.11, 16.64	0.37	0.60	0.73	9
Tp ^{Me,Me} Ni-S-2,6-Ph ₂ C ₆ H ₃ (3.5)	124.2	140.01(6), 115.47(4), 115.47(4)	89.46, 89.46	0.42	(g)	0.74	(h)
PhBP ₃ Ni-S-C ₆ H ₄ -4- ^t Bu ⁽ⁱ⁾	120.4	151.84(3), 109.79(3), 101.54(3)	67.32, 68.66	0.32	(g)	0.70	15

(a) The average umbrella angle between the three-fold H-B•••Ni axis and the L-Ni bond vectors (*i.e.*, 109.47° for T_d symmetry).

(b) Displacement of Ni from an equatorial L₂S plane, see ref. 13.

(c) [Σ <(apical-basal) - Σ <(basal-basal)]/90, see ref. 42.

(d) (360° - α - β)/141°, where α and β are the two largest interligand angles, see ref. 43.

(e) PhTt^{tBu} = phenyltris(tert-butylthiomethyl)borate, [Ph(CH₂S^tBu)₃].

(f) Two independent molecules.

(g) Undefined.

(h) This work.

(i) PhBP₃ = phenyltris(diphenylphosphinomethyl)borate, [Ph(CH₂PPh₂)₃].

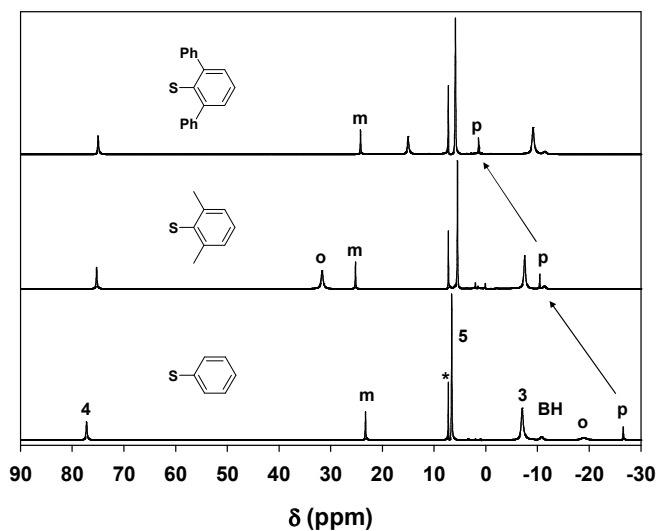


Figure 16: ^1H NMR spectra of **2.1a**, **3.2** and **3.5** (from bottom to top, respectively) recorded in CDCl_3 at 293 K. The peak marked (*) is residual solvent; peak assignments not labeled are listed in the experimental section. Arrows indicate shift of the resonance assigned to the *para* position of the arylthiolate rings.

3.3.4 ^1H NMR spectroscopy.

NMR spectra obtained for paramagnetic complexes **2.1a**, **3.2-3.8** were consistent with their formulations, notwithstanding significant paramagnetic shifts induced by unpaired electrons ($S = 1$) on high-spin Ni(II). A prominent feature common to all the spectra was a single resonance for three equivalent 4-pyrazole protons with a pronounced downfield shift (Figure 16). Equivalent 3- and 5-methyl resonances were also observed much closer to the diamagnetic region, with the former significantly broadened by the proximal paramagnet. A borohydride resonance and additional signals consistent with the various aryl substituents were also observed. Compared to the static crystal structures, equivalence of all three pyrazoles and both arylthiolate faces is indicative of rapid

migration of the arylthiolate on the NMR timescale, minimally between equivalent binding sites about the three-fold H-B•••Ni axis.

The alternating upfield and downfield shifts for the arylthiolate protons of **2.1a**, as well as reversal of *ortho* and *para* polarization with methyl substitution in **3.3**, are consistent with hyperfine contact shifting due to electron spin delocalization onto the arylthiolate by a π -polarization pathway.⁹ The *para* protons of **3.2** and **3.5** exhibit a striking attenuation of upfield shift, consistent with quenching of the π -polarization upon orthogonal rotation of the aryl substituent evident between the crystal structures of **2.1a** and **3.5**. Thus, the solid state structures of **2.1a** and **3.5** are plausibly maintained as predominant conformations in solution, with **3.2** partitioning in a dynamic equilibrium between these two limits. The 3-pyrazole methyl protons also exhibited a much smaller monotonic increase in upfield shift with increasing steric bulk of **2.1a**, **3.2-3.5**, which may represent differential diamagnetic shifts arising from aromatic ring currents on the proximal thiolate, consistent with the proposed conformation change. In contrast, the *meta* protons of **2.1a**, **3.2-3.5** maintain a nearly constant downfield shift, indicative of a second mechanism, such as direct spin delocalization through σ bonds. J-coupling between the assigned *meta* and *para* protons of **3.2** and **3.5** were established by COSY techniques (see Appendix D, E).

The series of *para*-substituted arylthiolate complexes **3.6-3.8** was also examined. Not surprisingly, ¹H NMR spectra were nearly identical to that of **2.1a**, absent the upfield *para* proton resonance and addition of either a broad upfield methoxy resonance in **3.6** or a downfield methyl resonance in **3.7**. The remaining resonances exhibited comparable chemical shifts to those of **2.1a**, except for a slight upfield shift of the 4-pyrazole protons

in **3.6** and **3.7**. These observations demonstrate the absence of significant electronic effects on Ni-S bonding, with the structure of **2.1a** retained over the series **3.6-3.8**.

3.3.5 Electronic spectroscopy.

The previously reported UV-Vis-NIR spectrum of **2.1a** in CH₂Cl₂ revealed multiple transitions, with three strong bands (354, 464, and 506 nm) apparently exhibiting S-Ni LMCT character.⁹ The three spin-allowed ligand field transitions of a tetrahedral d⁸ metal ion were split by the effective C_s symmetry, yielding several relatively weak and broad bands at lower energy (614, 836, 970, and 1580 nm) and obfuscating more precise assignment. Analysis of absorption and MCD spectra for Tp^{iPr,iPr}Ni-SC₆F₅ in cyclohexane yielded qualitatively similar assignments,⁴⁴ and comparable ligand field bands under C_{3v} symmetry were also reported for Tp^{Me,Me}NiCl in CH₂Cl₂.⁴⁵

Compared to **2.1a**, the *ortho*-disubstituted arylthiolate complexes **3.3-3.5** yielded dramatically different UV-Vis spectra (Figure 17). The 506 nm CT band was retained, but the 464 and 354 nm bands seemed to progressively collapse in **3.3-3.5**, while a new feature appeared at intermediate wavelengths. The ligand field bands also shifted dramatically, with emergence of a broad band near 660 nm. Taken together, the overlaid spectra give the appearance of a titration plot, presumably representing distributions of the two distinct conformations already elucidated. Complex **2.1a** and **3.5** would retain the respective equatorial/vertical and axial/horizontal configurations defined in the solid state, while **3.3** and **3.4** with intermediate steric bulk would partition between these configurations. Of course, the features of **3.3-3.5** would display minor differences in

energy and extinction due to chemical modification of the arylthiolate, and legitimate isosbestic points are not observed.

To test this hypothesis, spectra of the mesityl complex **3.3** were recorded in toluene over a temperature range of 287-343 K (Figure 18). Fully reversible temperature-dependent absorption changes were observed with at least four isosbestic points, consistent with perturbation of two-state equilibrium. In particular, a CT feature at 412 nm emerged with increasing temperature at the expense of flanking bands, analogous to the preceding comparison of **2.1a** and **3.5** (Figure 17). The spectral features of **3.3** show surprisingly little difference between CH₂Cl₂ and toluene solutions despite a significant change in solvent polarity.

To further probe the charge transfer features of **2.1a**, spectra were obtained for the series of *para*-substituted arylthiolate complexes Tp^{Me,Me}Ni-S-C₆H₄-*p*-X (X = OMe, **3.6**; Me, **3.7**; H, **2.1a**; and Cl, **3.8**, Figure 19). All four spectra yielded similar ligand field bands, exhibiting only a slight red-shift in the order **3.8** < **2.1a** < **3.7** < **3.6**, paralleling the overall donor strength of the arylthiolates. This result is again indicative of a common solution structure. In contrast, the strong charge transfer features at 464 and 506 nm were more noticeably red shifted, with the former band showing a larger effect, in the order **2.1a** < **3.8** < **3.7** < **3.6**, following relative π -donor strengths consistent with S-Ni $p\pi-d\pi^*$ LMCT character. Finally, the weaker CT band at 354 nm displayed a reversed red-shift pattern, **3.6** < **3.7** < **2.1a** < **3.8**, with retention of the poorly resolved fine structure. The contrasting behaviors of the three strong CT bands indicate complexity in the nickel-arylthiolate bonding interaction.

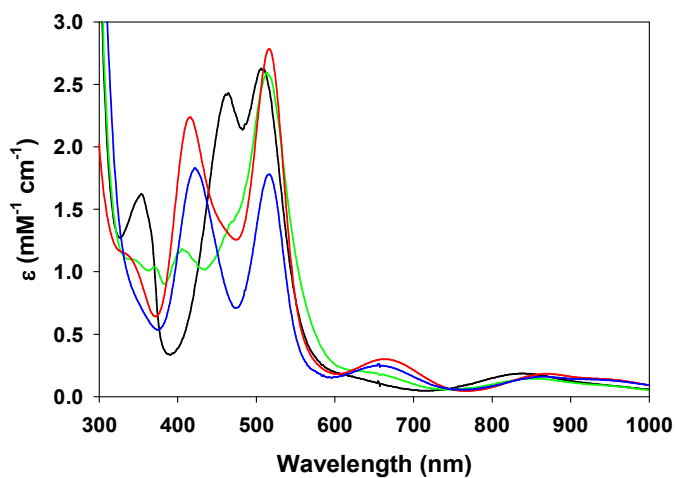


Figure 17: UV-visible-NIR spectra (CH_2Cl_2 solutions, 297 K) of **2.1a** (black), **3.3** (green), **3.4** (red), and **3.5** (blue).

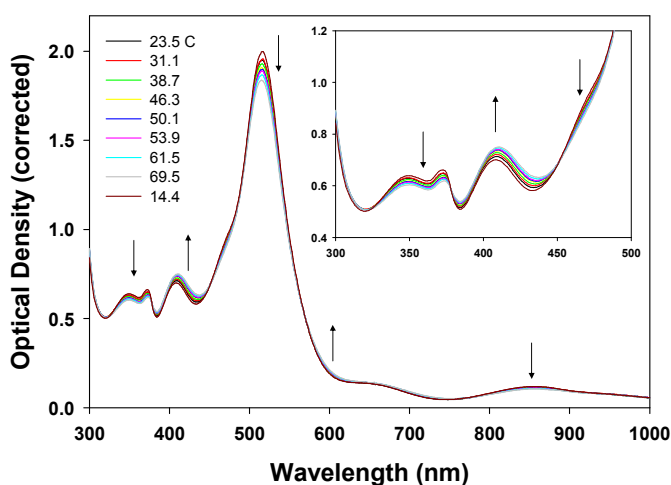


Figure 18: UV-visible-NIR spectra of **3.3** in toluene as a function of temperature from 287-343 K. Spectra were normalized for changes in solvent density.

Raw data are shown in Appendix D and E.

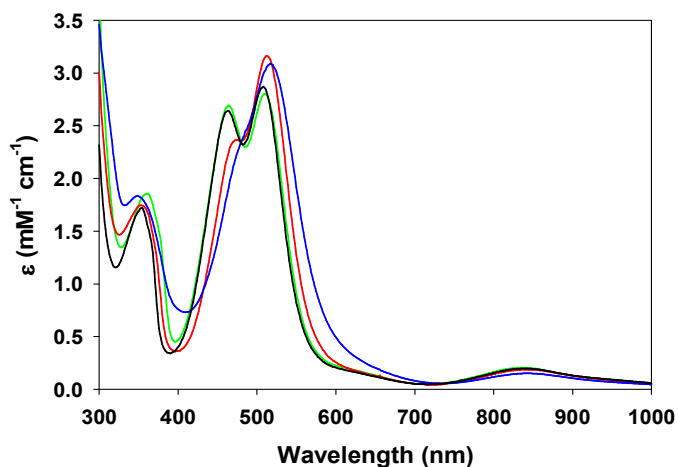


Figure 19: UV-visible-NIR spectra (CH_2Cl_2 solutions, 297 K) of **2.1a** (black), **3.6** (blue), **3.7** (red), and **3.8** (green)

3.3.6 DFT calculations

To further rationalize the divergent arylthiolate configurations and spectroscopic results observed for **2.1a** and **3.5**, spin-unrestricted DFT calculations were performed on simplified TpNiSPh computational models **2.1a'** and **3.5'** constructed from the respective crystal structures by substitution of hydrogen atoms for pyrazole and arylthiolate substituents and geometry optimization under imposed C_s symmetry. Orbital energies and allowed electronic transitions were calculated for both models. Of principal interest in Ni-SAr bonding are eight β -spin frontier orbitals corresponding to the five d orbitals split by the ligand field and three arylthiolate donor orbitals. The metal and thiolate fragments are first discussed separately, and then together as Ni-SR complexes. An expanded range of limiting arylthiolate configurations incorporating **2.1a'** and **3.5'** was defined on the basis of Ni-SAr bending and scaled by calculated relative energies, and TD-DFT calculations were performed to assign CT features in electronic spectra.

3.3.6.1 Arylthiolate donor orbitals.

Spin-restricted calculations were performed for the free $C_6H_4S^-$ anion after geometry optimization under C_{2v} symmetry (Figure 20). Of the three sulfur 3p orbitals available for bonding with nickel, one is coincident with the S- C_{ipso} bond vector and significantly stabilized ($15a_1$). The other two comprise nearly degenerate lone pairs at high energy (*i.e.*, HOMO and HOMO-1), one coplanar with the phenyl ring ($9b_1$, 93% S), and the other perpendicular to the ring and delocalized onto it. The symmetry and intermediate energy of the latter atomic orbital with respect to the one- and two-node Hückel π orbitals on the substituent ring results in bonding ($3b_2$, 16% S), non-bonding ($4b_2$, 69% S) and anti-bonding ($5b_2$, 13% S) combinations. The $4b_2$ HOMO is destabilized by only 0.07 eV relative to $9b_1$. These two donor orbitals have been referred to respectively as π_{op} and π_{ip} in previous work,^{15,21,47,48} although one of these must adopt a pseudo- σ orientation for a bent thiolate,⁴⁴ depending on the configurational geometry. The $3b_2$ orbital is stabilized by 2.06 eV compared to the $4b_2$ HOMO, and by 0.37 eV relative to its symmetry-isolated Hückel congener ($1a_2$). Despite this stabilization and consequent attenuation of S 3p contribution, the $3b_2$ orbital exhibits the same symmetry as π_{op} , and subsequent calculations on the arylthiolate complexes suggest a role for this third donor orbital in differentiating the bonding and spectroscopy of the two arylthiolate bonding modes of **2.1a** and **3.5** (*vide infra*).

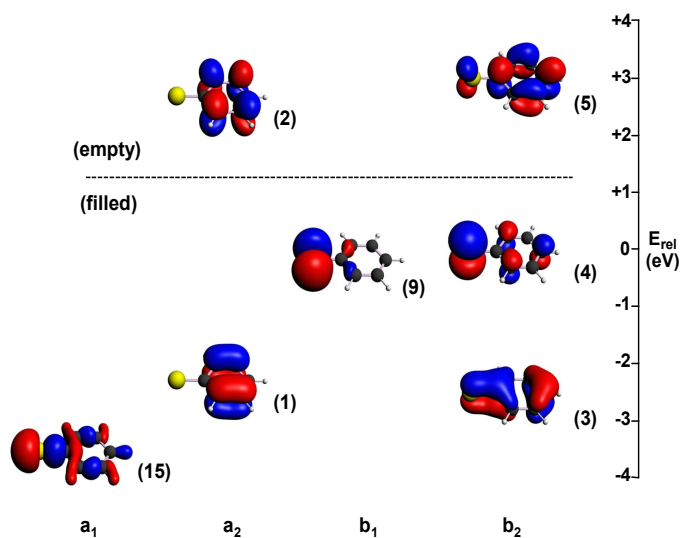


Figure 20: Relevant frontier orbitals of the free PhS^- ligand, separated by symmetry class. The dashed horizontal line separates occupied and empty orbitals.

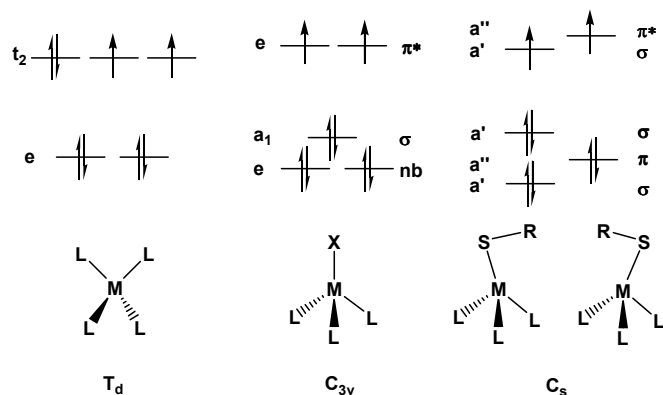


Figure 21: Qualitative symmetry-derived ligand field splittings for tetrahedral (left), axial pseudotetrahedral (center), and bent arylthiolate geometries (right).

3.3.6.2 Nickel acceptor *d* orbitals.

Ligand field splitting of *d* orbitals for a pseudotetrahedral Ni(II) ion can be qualitatively anticipated by symmetry reduction from T_d , with upper t_2 (d_{xy} , d_{xz} , d_{yz}) and lower e ($d_{x^2-y^2}$, and d_{z^2}) sets (Figure 21, left). Umbrella distortion yields C_{3v} symmetry

with reduced N-Ni-N angles, causing axial destabilization that is offset in the perpendicular equatorial plane. This gives rise to an axial d_{z^2} orbital sandwiched between e sets (d_{xz} , d_{yz} over d_{xy} , $d_{x^2-y^2}$; Figure 21, center).⁴⁵ The former exhibit π symmetry towards the axial ligand, while the filled d_{z^2} orbital assumes σ symmetry, and the equatorial d_{xy} , $d_{x^2-y^2}$ pair is non-bonding.^{15,45} Off-axis or sawhorse bending further reduces symmetry to C_s , breaking the equatorial degeneracy. The e orbital pairs are slightly split; within each pair, one orbital adopts σ symmetry while the other exhibits π overlap (Figure 21, right). Consequent elaboration of σ interactions stabilizes the distortion. The standard setting of the C_s point group invokes an x,y mirror plane containing the nickel-sulfur bond. The d_{xy} , $d_{x^2-y^2}$, and d_{z^2} orbitals are symmetric under reflection and encompass Ni-SPh σ bonding under a' symmetry, while antisymmetric d_{xz} , d_{yz} orbitals are π bonding under a'' symmetry.

3.3.6.3 Ni-SAr bonding.

Spin unrestricted calculations were performed on TpNiSPh models **2.1a'** and **3.5'** under enforced C_s symmetry, focusing on eight β -spin molecular orbitals corresponding to the five nickel d orbitals and three arylthiolate donor orbitals. These are illustrated for both models (Figure 22). Bonding in **2.1a'** and **3.5'** were considered in detail to elucidate the differences between the diametrically opposed equatorial/vertical and axial/horizontal configurations. Previous calculations on TpNi-SC₆F₅ in the equatorial/vertical coordination mode analogous to **2.1a'** assigned thiolate π_{ip} and π_{op} donor orbitals intermediate energies with respect to the d orbital manifold; the π_{op} orbital was stabilized

by a $p\pi-d\pi^*$ interaction with a half-filled Ni d orbital, while the perpendicular π_{ip} orbital was destabilized by a filled-filled interaction of pseudo- σ symmetry.⁴⁴ A qualitatively similar electronic structure was found for **2.1a'** (Figure 22, left), with the arylthiolate π_{op} and π_{ip} donor orbitals (21a'' and 40a', respectively) retaining analogous bonding roles. In the axial/horizontal configuration of **3.5'**, these donor orbitals (24a'' and 37a') necessarily exchange their roles due to orthogonal rotation of the arylthiolate substituent, and bonding overlap is altered by displacement of the sulfur atom within the ligand field. These combined symmetry effects must be the root cause of the spectroscopic differences between **2.1a** and **3.5** in their distinctive configurations. The two highest molecular orbitals (*i.e.*, 41a' and 22a'' in **2.1a'** and 38a' and 25a'' in **3.5'**) are primarily nickel-centered d orbitals destabilized by strong Ni-N σ^* interactions, and are unoccupied, consistent with a d^8 electron count for Ni(II) and a paramagnetic, $S = 1$ ground state in both complexes.

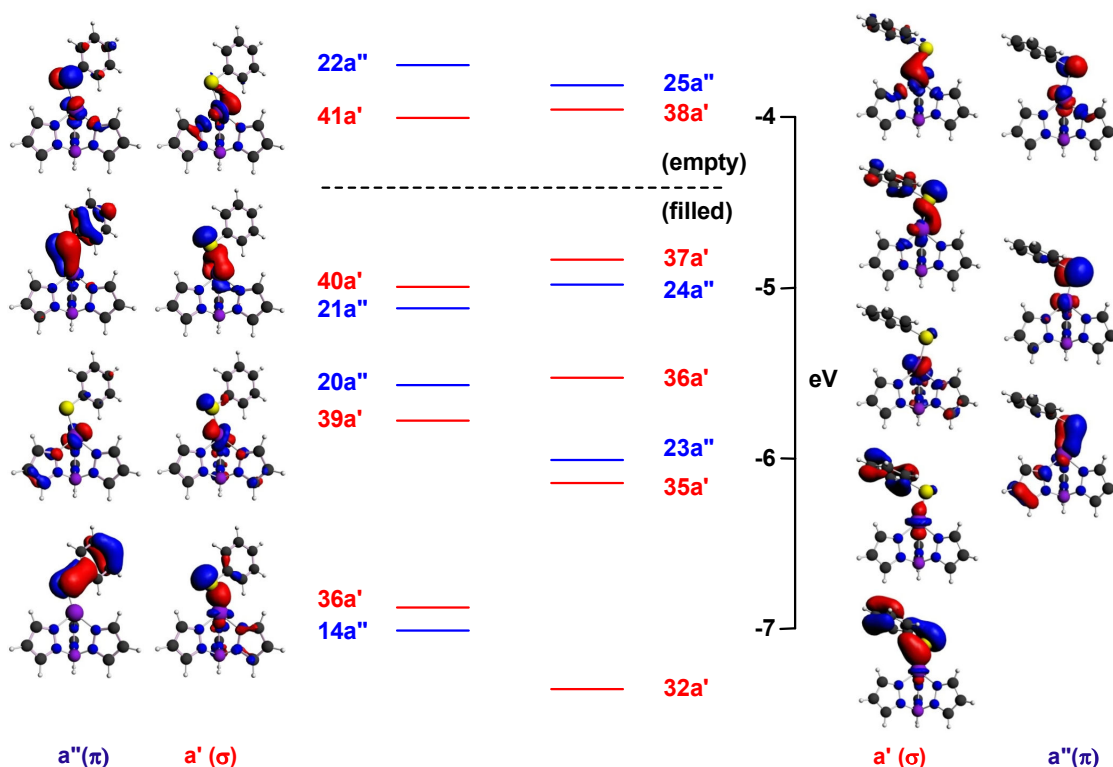


Figure 22: Relevant β -spin frontier orbitals for **2.1a'** (left) and **3.5'** (right). Orbitals are distinguished by parity under imposed C_s symmetry, with a' (red) and a'' (blue) representations corresponding to respective σ and π overlap along the Ni-S bond vector.

Three β -spin frontier orbitals exhibit Ni-S π -bonding symmetry in the axial/horizontal thiolate coordination of **3.5'** ($23a''$ - $25a''$; Figure 22, right). The highest orbital is unoccupied and metal-centered ($25a''$: 59% Ni d_{yz} ; 19% S p_z), representing Ni-S $d\pi$ - $p\pi^*$ character. The intermediate orbital represents the π_{ip} orbital with a minor non-bonding metal contribution ($24a''$: 22% Ni d_{xz} , 15% d_{yz} ; 47% S p_z). The lowest orbital is a metal centered π -bond ($23a''$: 41% Ni d_{xz} ; 22% S p_z). Overlap in this orbital is favorably directed towards the axial sulfur, but minimized in the empty $25a''$ antibonding orbital that is directed toward the vacant equatorial site. Significant Ni-S π covalency is therefore indicated.

The five other relevant β -spin orbitals of **3.5'** (32a' and 35a'-38a') exhibit a' symmetry appropriate for Ni-S σ bonding. Two of the orbitals are primarily metal-centered (36a': 39% d_{z^2} , 31% $d_{x^2-y^2}$; 38a': 44% $d_{x^2-y^2}$, 21% d_{z^2}) and present nodal planes toward the sulfur atom, rendering them essentially non-bonding (<4% S p_x). Similar to 25a'', the latter is destabilized by a Ni-N σ^* interaction and is unoccupied. The third d orbital (35a': 39% d_{xy} , 12% d_{z^2}) is properly aligned to overlap with the π_{op} orbital (37a': 33% d_{xy} ; 28% S p_x). However, this orbital is lacking any sulfur contribution (*ca.* 1% S p_x), despite obvious delocalization onto the aryl substituent. The third arylthiolate donor orbital, specifically the one-node Hückel donor orbital 3b₂ (32a': 13% d_{xy} ; 33% S p_x), brackets the d manifold from below, and with the π_{op} donor orbital above, forms a stack of three σ orbitals with bonding, non-bonding and anti-bonding character. The σ bonding can be described as a three-center interaction between nickel, sulfur, and the aryl substituent. The intermediate non-bonding orbital exhibits significant Ni d character and a node on the central sulfur atom, while the bonding orbital (32a') is fully delocalized and stabilized by an additional 0.8 eV below the symmetry-isolated one-node Hückel congener (21a', not shown in Figure 22; *cf.*, 1a₂ in Figure 20). As all three orbitals are filled; no net Ni-S $d\sigma$ - $p\sigma^*$ bonding can be obtained.

The difference in arylthiolate coordination in **2.1a'** compared to **3.5'** is displacement of sulfur from an axial to an equatorial position, with a concordant back-flip and orthogonal rotation of the aryl substituent from horizontal to vertical. This perturbs several aspects of Ni-SAr bonding elucidated for **3.5'** (Figure 22, left). Aryl substituent rotation swaps the pseudo- σ and π bonding roles of the thiolate π_{op} and π_{ip} donor orbitals

(21a'' and 40a' in **2.1a'**, respectively); the third thiolate 3b₂ donor orbital is also transformed from σ to π symmetry in **2.1a'** (14a''), stabilizing the overall σ manifold. The Ni-S π bonding is also perturbed by hopping of sulfur from an axial to an equatorial position, which enhances overlap in the empty antibonding orbital (22a'') at the expense of the filled bonding orbital (20a'') and destabilizes both orbitals. The opposing effects on σ - and π -bonding yield a relatively small difference in total bonding energy between **2.1a'** and **3.5'**, supporting a relatively flat energy surface consistent with the dynamic structural rearrangement in solution, as evidenced in NMR spectra.

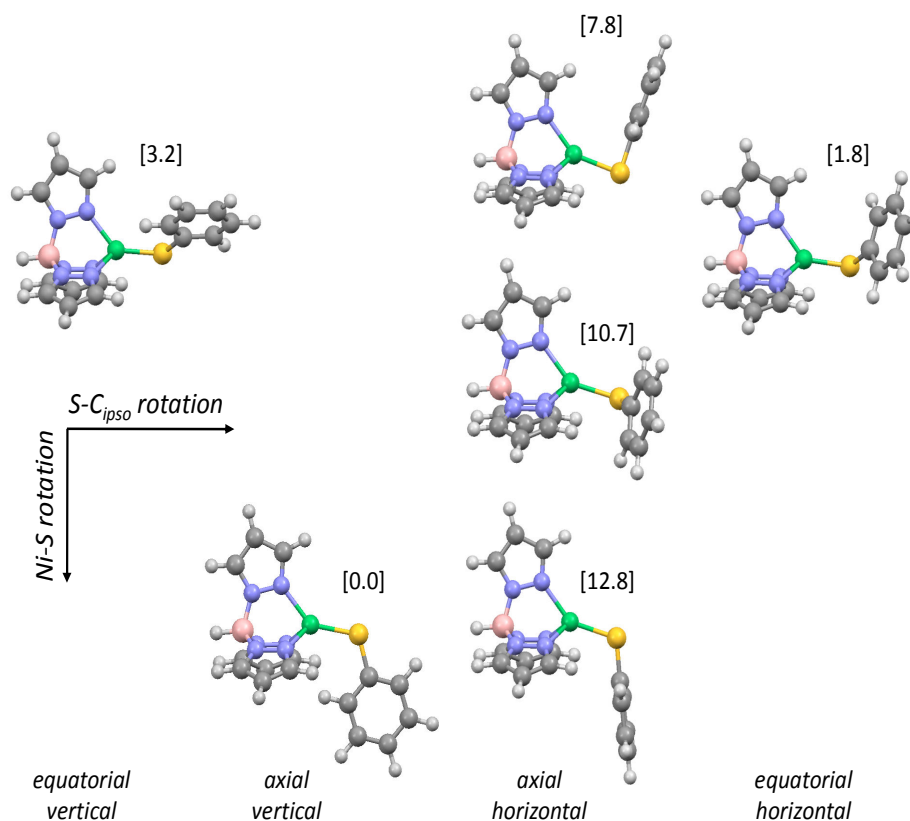


Figure 23: Sterically accessible limiting configurations for a simplified TpNiSPh model. Horizontal translation between columns corresponds to 90° rotation about the $S-C_{ipso}$ bond, transposing the π_{ip} and π_{op} thiolate donor orbitals, and vertical translation down a column corresponds to 90° rotation about the Ni-S bond, transposing Ni $d\pi^*$ acceptor orbitals. Number in brackets indicates the relative calculated energy in kJ/mole.

3.3.6.4 Conformational energetics.

Including the respective equatorial/vertical and axial/horizontal configurations of **2.1a'** and **3.5'**, a total of 16 limiting bonding configurations are possible for a bent thiolate. The sulfur can adopt axial or equatorial positions, and orthogonal rotation between the vertical and horizontal orientations exchanges the respective σ and π overlap symmetries of the π_{ip} and π_{op} donor orbitals. Furthermore, the substituent can rotate away from the Ni-S bond in 90° increments, exchanging π overlap with orthogonal nickel

d acceptor orbitals (e.g., 25a'' and 38a' of **3.5'**, Figure 22); this additional factor yields the aforementioned sixteen orientations (i.e., equatorial/axial \times horizontal/vertical \times 0/90/180/270°). However, the 90° and 270° rotations are enantiomorphous, so only 12 configurations are energetically unique. Such rotation is evident in the structure of PhBP₃Ni-S-C₆H₄-4-^tBu reported by MacBeth, *et al.*¹⁵ Even for the minimal TpNiSPh models with no substituents, only six of these configurations are sterically accessible as local minima (Figure 23), excluding from consideration the thirteenth umbrella configuration, with a linear thiolate and both π_{ip} and π_{op} in a π -bonding orientation. Added substituents presumably would further reduce the number of assessible configurations. Optimization of the six model conformations suggests a relatively flat energy surface within 13 kJ/mole of the global minimum; the absolute accuracy of the calculations is unknown, although calculations on isomeric configurations of the same complex would presumably cancel some systematic error. Three of these six configurations have been observed experimentally. Five of the seven known tripodal thiolate structures adopt the equatorial/vertical/0° configuration (Table 4),^{9,13,14} which is calculated to lie only 5-8 KJ/mole below the axial/horizontal configurations adopted by **3.5** and PhBP₃Ni-S-C₆H₄-4-^tBu.¹⁵ Only small enhancement of steric contact at the *ortho* position should suffice to tip the minimum from the equatorial/vertical configuration observed for **2.1a** into the axial/horizontal configuration of **3.5**. The modest substitution of **3.2-3.4** would accordingly enable equilibration between both bonding configurations. Other configurations have yet to be observed, including an axial/vertical/180° configuration identified as the global minimum for TpNiSPh. However, this

configuration was recently observed in a crystal structure of a tripodal copper(II) phenolate.⁴⁸

3.3.6.5 TD-DFT calculations and electronic spectra.

TD-DFT calculations were performed on models **2.1a''** and **3.5'** under respective experimental C_I and C_s symmetry, in order to provide a basis for assignment of the observed CT bands already described in electronic spectra (Figure 12). The vacant β -spin orbitals of σ symmetry (41a' and 38a' in **2.1a'** and **3.5'**, respectively) exhibit little contribution from the thiolate sulfur (3.1 and 3.7 % S p, respectively). The TD-DFT calculations accordingly predict that the strongest transitions arise within the Ni-S π bond manifolds. The next set of empty acceptor orbitals are π^* orbitals localized on the pyrazole and arylthiolate substituent rings; as these lie 3.5-3.8 eV above the highest occupied orbitals, they would support MLCT and π - π^* transitions deeper into the UV.

The three-orbital π stack in **3.5'** yields two CT excitations (Figure 24, top), one at 783 nm (25a'' \leftarrow 24a'') and the other at 476 nm (25a'' \leftarrow 23a''). Several weaker pyrazole-centered LMCT bands are calculated to fall in the range of *ca.* 400-600 nm;⁴⁹ two such transitions are evident on the high-energy side of the 476 nm LMCT band. The three most prominent ligand field bands fall at 1261, 712, and 571 nm. Calculations on **2.1a''** (Figure 24, bottom) also predict two strong CT bands arising from the Ni-S π interaction at 674 (63a \leftarrow 60a, corresponding to 22a'' \leftarrow 21a'' under C_s symmetry) and 560 nm (63a \leftarrow 58a), plus a third band at 359 nm arising from the 3b₂ donor orbital (63a \leftarrow 49a; 22a'' \leftarrow 14a''). Owing to the reduced symmetry, the intermediate band is actually a ligand field transition that gains intensity by configuration interaction with the nearby CT

transition ($63a \leftarrow 59a$; $22a'' \leftarrow 20a''$) at 612 nm. The remaining features are pyrazole LMCT and ligand field bands comparable to those described for **3.5'**.

The calculations qualitatively reproduce the differences observed between the CT spectra of **2.1a** and **3.5**, which arise from the difference in Ni-S π overlap in their respective equatorial and axial conformations. This demonstrates that UV-visible-NIR spectroscopy can distinguish the various Ni-SAr configurations (Figure 17). The assignments just given also rationalize the comparative shifts in band energies across the Hammett series **3.6-3.8** (Figure 19). However, while calculated ligand field energies appear to be reasonably accurate, Ni-S LMCT energies calculated herein depart from experimental results by an average of 0.6 ± 0.2 eV, in line with the present state of the art.³⁴ The low symmetry can also enable configuration interactions, and the energies of the relevant orbitals will be perturbed by arylthiolate substitution, a continuum of possible substituent rotations, steric interactions and σ^* interactions with the supporting tripodal ligand. Hence, while unique TD-DFT results were computed for the various limiting conformations of TpNiSPh (see Supporting Information), these may not be fully predictive of spectra for structures obtained experimentally.

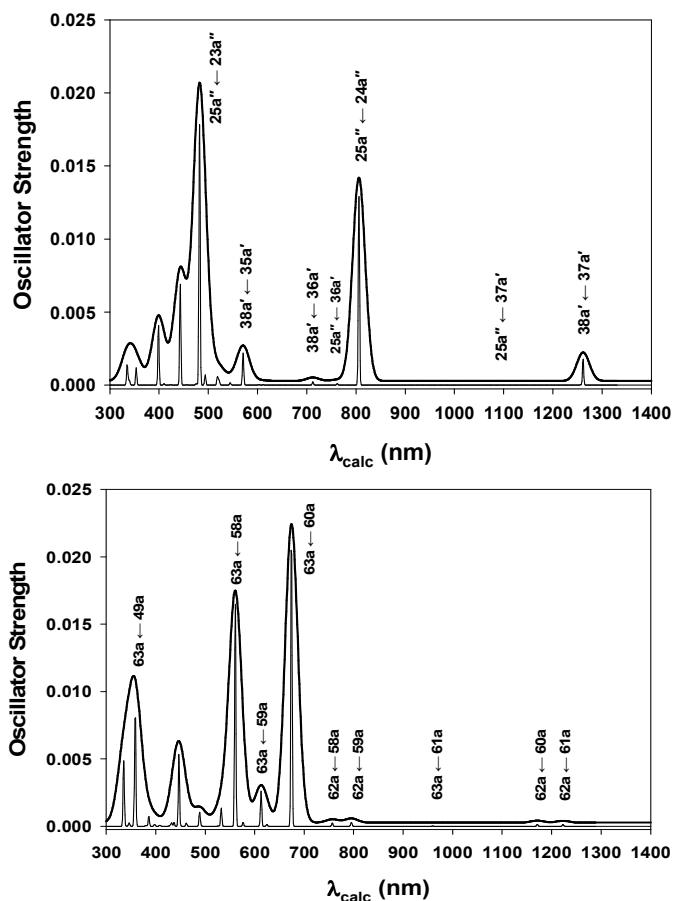


Figure 24: TD-DFT calculated spectra of **2.1a''** (bottom) and **3.5'** (top). Ligand field and S-Ni LMCT bands are labeled with predominant orbital contributions. For convenience, calculated lines are presented as Gaussian curves with line widths of 3 nm (corresponding to the vertical intensity scale) and 50 nm (vertical scale exaggerated with offset).

3.4 Conclusion

We have elicited structurally distinct axial/horizontal and equatorial/vertical configurations for bent arylthiolate ligands at a pseudotetrahedral Ni(II) center using steric interactions. The resulting conformers can be distinguished by spectroscopy in solution, and we rationalized this result on the basis of divergent electronic structures arising from differential Ni-S π overlap. Sterically unhindered arylthiolate ligands

coordinate to a $[\text{Tp}^{\text{Me,Me}}\text{Ni}(\text{II})]^+$ center in an equatorial position within an axially vacant trigonal bipyramidal ligand field. Steric contact from increasingly bulky *ortho* substitution displaces the arylthiolate ligand into the axial position. Limiting equatorial and axial configurations were structurally and spectroscopically defined for **2.1a** and **3.5**, while complexes **3.2-3.4** appear to be distributed between the limiting structures in solution. Thus, the series of complexes **2.1a**, **3.2-3.5** can be taken to be a steric titration, in which increasing size of the *ortho* arylthiolate disubstitution (*i.e.*, H, Me, *i*Pr, Ph) destabilizes preferred equatorial/vertical coordination. In contrast, sterically innocent *para* modification with substituents of varying electronic donor strength (*i.e.*, OMe, Me, Cl) effect informative spectroscopic perturbation of CT features in **3.6-3.8** without altering the coordination geometry from that of **2.1a**.

Only a handful of other pseudotetrahedral Ni(II) arylthiolate complexes have been structurally characterized, and the majority of these are tetragonally distorted (*i.e.*, D_{2d} symmetry) $[\text{Ni}(\text{SR})_4]^{2-}$ salts.¹⁷⁻²⁰ Also noteworthy is a linear $\text{Ni}(\text{SAr})_2$ complex.²¹ The others are monothiolate complexes supported by anionic tripodal borate ligands. These examples include $\text{PhB}(\text{CH}_2\text{PPh}_2)_3\text{Ni-S-4-C}_6\text{H}_4^t\text{Bu}$,¹⁵ $\text{Tp}^{\text{iPr,iPr}}\text{Ni-SC}_6\text{F}_5$,¹³ $\text{PhB}(\text{CH}_2\text{S}^t\text{Bu})_3\text{Ni-SC}_6\text{F}_5$,¹⁴ $\text{PhB}(\text{CH}_2\text{S}^t\text{Bu})_3\text{Ni-SC}_6\text{H}_5$,¹⁴ and $\text{Tp}^{\text{Ph,Me}}\text{Ni-S-2,6-Me}_2\text{C}_6\text{H}_3$.⁹ The first complex was the first example of an axial/horizontal configuration like **3.5**, but also uniquely twisted toward a 90° sidesaddle configuration. The arylthiolate is bent off-axis into an equatorial/vertical orientation analogous to **2.1a** in all the other complexes. In the last complex, the relatively large 3-Ph pyrazole moieties enforce retention of a vertical orientation even with the same *ortho* substituents as **3.2**.

The recent structural characterization of two Cu(II) phenolate complexes, $\text{Tp}^{\text{iPr,iPr}}\text{Cu-O-}p\text{-C}_6\text{H}_4\text{F}$ and $\text{Tp}^{\text{tBu,iPr}}\text{Cu-O-}p\text{-C}_6\text{H}_4\text{F}$, which are sterically distinguished by the proximal 3-pyrazole positions rather than substitution on the phenolate co-ligand, provides another relevant example.⁴⁸ The phenolate ligand binds axially in both complexes; however, in the $\text{Tp}^{\text{iPr,iPr}}$ complex, the substituent is again twisted toward a sidesaddle orientation, while the bulkier 3-*t*Bu substituents force the latter complex into an axial/vertical/180° conformation. This switches phenolate donor orbitals between the complexes, and as for **2.1a** and **3.5**, significant differences were observed in the electronic spectra of these complexes.

More recently, structural characterization of a pseudotetrahedral alkylperoxo complex $\text{Tp}^{\text{iPr,iPr}}\text{Ni-OO}^t\text{Bu}$ was reported.⁵⁰ The Ni-O bond was displaced from the H-B•••Ni axis toward one pyrazole, with the OR substituent folded back between the other two pyrazoles and approaching η^2 coordination. The geometry and bonding of this complex are analogous to equatorial/vertical arylthiolate coordination, and an axial conformation with a reversed alkylperoxo ligand can be predicted on this basis.

In concert with these results, our study suggests an expanded range of bonding configurations is accessible to arylthiolates and isolobal ligands at pseudotetrahedral metal centers. Structural characterization of disparate coordination geometries underscores the potential to elicit rich coordination chemistry by steric manipulation at the periphery of these ligand fields. As the conformers can be distinguished by routine spectroscopy, a full range of ligand configurations can be eventually observed and their effects on complex reactivity elucidated.

3.4.1 Acknowledgment

I acknowledge Dr. S. Chattopadhyay and Dr. M. P. Jensen for their significant contribution on this work. This work was supported by startup funding provided by Ohio University (MPJ).

3.4.2 Appendix/Supporting Information

TD-DFT spectra and Cartesian coordinates for six geometry optimized conformations of TpNiSPh is available in the Appendix (D and E) section. Crystallographic data in CIF format is available at the CSD database and free of charge via internet at <http://pubs.acs.org>.

3.5 References

- (1) Fontecilla-Camps, J. C.; Volbeda, A.; Cavazza, C.; Nicolet, Y. *Chem. Rev.* **2007**, *107*, 4273-4303.
- (2) Ragsdale, S. W. *J. Inorg. Biochem.* **2007**, *101*, 1657-1666.
- (3) Ermler, U. *Dalton Trans.* **2005**, 3451-3458.
- (4) Jeoung, J.-H.; Dobbek, H. *Science* **2007**, *318*, 1461-1464.
- (5) Drennan, C. L.; Doukov, T. I.; Ragsdale, S. W. *J. Biol. Inorg. Chem.* **2004**, *9*, 511-515.
- (6) Smith, M. C.; Barclay, J. E.; Davies, S. C.; Hughes, D. L.; Evans, D. J. *Dalton Trans.* **2003**, 4147-4151.

- (7) Benson, E. E.; Kubiak, C. P.; Sathrum, A. J.; Smieja, J. M. *Chem. Soc. Rev.* **2009**, 89-99.
- (8) Maroney, M. J. *Curr. Opinion. Chem. Biol.* **1999**, 3, 188-199.
- (9) Chattopadhyay, S.; Deb, T.; Ma, H.; Petersen, J. L.; Young, V. G., Jr.; Jensen, M. P. *Inorg. Chem.* **2008**, 47, 3384-3392.
- (10) Ma, H.; Chattopadhyay, S.; Petersen, J. L.; Jensen, M. P. *Inorg. Chem.* **2008**, 47, 7966-7968.
- (11) Ma, H.; Wang, G.; Yee, G. T.; Petersen, J. L.; Jensen, M. P. *Inorg. Chim. Acta* **2009**, 362, 4563-4569.
- (12) Trofimenko, S. *Chem. Rev.* **1993**, 93, 943-980.
- (13) Matsunaga, Y.; Fujisawa, K.; Ibi, N.; Miyashita, Y.; Okamoto, K.-i. *Inorg. Chem.* **2005**, 44, 325-335.
- (14) Cho, J.; Yap, G. P. A.; Riordan, C. G. *Inorg. Chem.* **2007**, 46, 11308-11315.
- (15) MacBeth, C. E.; Thomas, J. C.; Betley, T. A.; Peters, J. C. *Inorg. Chem.* **2004**, 43, 4645-4662.
- (16) Fox, D. C.; Fiedler, A. T.; Halfen, H. L.; Brunold, T. C.; Halfen, J. A. *J. Am. Chem. Soc.* **2004**, 126, 7627-7638.
- (17) Swenson, D.; Baenziger, N. C.; Coucouvanis, D. *J. Am. Chem. Soc.* **1978**, 100, 1932-1934.
- (18) Rosenfeld, S. G.; Armstrong, W. H.; Mascharak, P. K. *Inorg. Chem.* **1986**, 25, 3014-3018.
- (19) Silver, A.; Koch, S. A.; Millar, M. *Inorg. Chim. Acta* **1993**, 205, 9-14.
- (20) Mueller, A.; Henkel, G. Z. *Naturforsch. B* **1995**, 50, 1464-1468.

- (21) Nguyen, T.; Panda, A.; Olmstead, M. M.; Richards, A. F.; Stender, M.; Brynda, M.; Power, P. P. *J. Am. Chem. Soc.* **2005**, *127*, 8545-8552.
- (22) Evans, D. F.; Jakubovic, D. A. *J. Chem. Soc., Dalton Trans.* **1988**, 2927-2933.
- (23) Santi, R.; Romano, A. M.; Sommazzi, A.; Grande, M.; Bianchini, C.; Mantovani, G. *J. Mol. Cat. A* **2005**, *229*, 191-197.
- (24) Blower, P. J.; Dilworth, J. R.; Hutchinson, J. P.; Zubieta, J. A. *J. Chem. Soc., Dalton Trans.* **1985**, 1533-1541.
- (25) Newton, A. *J. Am. Chem. Soc.* **1943**, *65*, 2439-2441.
- (26) Bishop, P. T.; Dilworth, J. R.; Nicholson, T.; Zubieta, J. *J. Chem. Soc., Dalton Trans.* **1991**, 385-392.
- (27) SMART V5.054, **2001**, Bruker Analytical X-ray Systems, Madison, WI.
- (28) An empirical correction for absorption anisotropy, Blessing, R. *Acta Cryst.* **1995**, *A51*, 33-38.
- (29) SAINT+ V6.45. **2003**, Bruker Analytical X-Ray Systems, Madison, WI.
- (30) SHELXTL V6.14. **2000**, Bruker Analytical X-Ray Systems, Madison, WI.
- (31) ADF 2007.01, Scientific Computing and Modelling NV, Vrije Universiteit, Amsterdam, The Netherlands.
- (32) te Velde, G.; Bickelhaupt, F. M.; van Gisbergen, S. J. A.; Fonseca Guerra, C.; Baerends, E. J.; Snijder, J. G.; Ziegler, T. *J. Computational Chem.* **2001**, *22*, 931-967.
- (33) van Gisbergen, S. J. A.; Snijders, J. G.; Baerends, E. J. *Comput. Phys. Commun.* **1999**, *118*, 119-138.
- (34) Ziegler, T.; Wang, F. *Mol. Phys.* **2004**, *102*, 2585-2595.
- (35) Vosko, S. J.; Wilk, M.; Nussair, M. *Can. J. Phys.* **1980**, *58*, 1200-1211.

- (36) Becke, A. *Phys. Rev.* **1988**, *A38*, 3098-3100.
- (37) Perdew, J. P. *Phys. Rev.* **1986**, *B33*, 8822-8824.
- (38) Jenkins, D. M.; Peters, J. C. *J. Am. Chem. Soc.* **2005**, *127*, 7148-7165.
- (39) Kersten, J. L.; Kucharczyk, R. R.; Yap, G. P. A.; Rheingold, A. L.; Theopold, K. H. *Eur. J. Chem.* **1997**, *3*, 1668-1674
- (40) Detrich, J. L.; Konečný, R.; Vetter, W. M.; Doren, D.; Rheingold, A. L.; Theopold, K. H. *J. Am. Chem. Soc.* **1996**, *118*, 1703-1712.
- (41) Cirera, J.; Alemany, P.; Alvarez, S. *Eur. J. Chem.* **2004**, *10*, 190-207.
- (42) Vela, J.; Stoian, S.; Flaschenriem, C. J.; Münck, E.; Holland, P. L. *J. Am. Chem. Soc.* **2004**, *126*, 4522-4523.
- (43) Yang, L.; Powell, D. R.; Houser, R. P. *Dalton Trans.* **2007**, 955-964.
- (44) Gorelsky, S. I.; Basumallick, L.; Vura-Weis, J.; Sarangi, R.; Hodgson, K. O.; Hedman, B.; Fujisawa, K.; Solomon, E. I. *Inorg. Chem.* **2005**, *44*, 4947-4960.
- (45) Desrochers, P. J.; Telser, J.; Zvyagin, S. A.; Ozarowski, A.; Krzystek, J.; Vivic, D. A. *Inorg. Chem.* **2006**, *45*, 8930-8941.
- (46) Kashiwagi, H.; Hashimoto, T.; Tanaka, Y.; Makita, T. *Int. J. Thermophysics* **1982**, *3*, 201-215.
- (47) Davis, M. I.; Orville, A. M.; Neese, F.; Zaleski, J. M.; Lipscomb, J. D.; Solomon, E. I. *J. Am. Chem. Soc.* **2002**, *124*, 602-614.
- (48) Ghosh, S.; Cirera, J.; Vance, M. A.; Ono, T.; Fujisawa, K.; Solomon, E. I. *J. Am. Chem. Soc.* **2008**, *130*, 16262-16499.
- (49) Randall, D. W.; George, S. D.; Hedman, B.; Hodgson, K. O.; Fujisawa, K.; Solomon, E. I. *J. Am. Chem. Soc.* **2000**, *122*, 11620-11631.

(50) Hikichi, S.; Okuda, H.; Ohzu, Y.; Akita, M. *Angew. Chem. Int. Ed.* **2009**, *48*,

188-191.

CHAPTER 4: AEROBIC AND HYDROLYTIC DECOMPOSITION OF PSEUDOTETRAHEDRAL NICKEL PHENOLATE COMPLEXES

*(Note: I have published the results of this study on ACS journal Inorganic chemistry;
DOI: 10.1021/ic300551z)*

4.1 Introduction

Dioxygen activation is fundamentally important in catalysis and bioinorganic chemistry. Significant work has been directed at enzymatic and biomimetic iron and copper centers that react with O₂,¹⁻¹⁰ yet nickel/O₂ chemistry and biochemistry are relatively limited in scope. Only one nickel-dependent oxidase enzyme has been characterized so far, namely acireductone dioxygenase (Ni-ARD),¹¹ for which functional turnover modeling has been elicited from synthetic Ni(II) complexes of aryl-appended tris(pyridylmethyl)amine (TPA) ligands.¹² Synthetic Ni(II) complexes of electron-rich tris(oximato)amine and diamido macrocyclic ligands catalyze aerobic substrate oxidations,^{13,14} and macrocyclic complexes of Ni(II) catalyze oxygen atom transfer from suitable precursors to organic substrates.¹⁵⁻¹⁷ Stoichiometric oxygenation reactions of Ni(II)-thiolato complexes are also known.¹⁸ Superoxo,¹⁹⁻²⁶ peroxy,²⁵⁻³¹ and oxo³¹⁻⁴² complexes supported by diketimine (nacnac),^{21,22,43} TPA,^{24,25,27,35,36,40-42} hydrotris(pyrazolyl)borate (Tp),³⁰⁻³⁴ tetraazamacrocycles (e.g., tetramethylcyclam, tmc),^{20,26,28,29} and related polydentate ligands^{19,23,37-39,44} have been prepared, either by stoichiometric O₂ addition to Ni(I),^{19-23,28,29,37-39,43-45} or H₂O₂ addition to Ni(II) precursors.^{20,24-27,32-36,40-42} No biological role for nickel has been established in humans, but nickel toxicology is of interest.⁴⁶⁻⁴⁸ Elevated intracellular levels are associated with

mutagenesis, and one proposed mechanism involves catalytic depletion of cellular antioxidants, which implies formation of reduced oxygen species.⁴⁸

Copper amine oxidases (CAOs) activate O₂ to effect post-translational oxidation of an active-site tyrosine residue in the expressed apoenzyme to a catalytically essential 2,4,5-trihydroxyphenylalanine quinone (i.e., TPQ) cofactor in the active holoenzyme (Scheme 2).⁴⁹⁻⁵² Our present work was inspired by reports that TPQ biogenesis is also observed in apoenzymes reconstituted with nickel, comprising a second example of biological dioxygenase activity for this metal.^{53,54} X-ray crystallography revealed a pseudotetrahedral N₃O donor set in the apoenzyme active site, derived from three histidine imidazoles and one tyrosine sidechain, which is the TPQ precursor.⁴⁹ Following active-site binding of copper and O₂, a Cu(II)-phenolate LMCT species intermediate absorbing at 350 nm was observed, which exhibited isosbestic decay to a 480 nm chromophore characteristic of TPQ in the mature holoenzyme.⁵⁰ Other consensus intermediates include an unobserved Cu(II)-peroxyquinone complex,⁴⁹⁻⁵² which undergoes heterolysis to a structurally characterized dopaquinone intermediate,⁴⁹ but mechanistic details of the O₂ activation step remained to be elucidated.

TpCu(II)-OAr complexes with pseudotetrahedral N₃O ligand fields have been reported as CAO models,^{52,55} wherein the Tp ligands model the facial array of imidazole donors and the phenolate co-ligand completes a N₃O ligand field akin to the CAO active site. However, the complexes Tp^{tBu,R}Cu-O-C₆H₄-4-F (R = ⁱPr, ^tBu) were unreactive with O₂,⁵² while analogs with *ortho*-disubstituted phenolates decomposed even under inert atmosphere.⁵⁵ Similar behavior was also reported for (nacnac)Cu-OAr complexes.⁵⁶ Compared to the TpCu-OAr complexes, nickel analogs might be expected to exhibit

higher stability owing to relatively cathodic Ni(I/II) redox couples, but such complexes have not been reported. Building on previous work with O₂-sensitive Ni(II)-arylthiolate complexes Tp^{R,Me}Ni-SAr,⁵⁷⁻⁶¹ we report herein the bioinspired complexes Tp^{R,Me}Ni-OAr (Tp^{R,Me} = hydrotris{3-R-5-Me-pyrazol-1-yl}borate: R = Ph (**4.1a**),⁶² Me (**4.1b**),⁶³ Ar = -2,6-ⁱPr₂C₆H₃). These are thermally stable in anaerobic solutions, but decompose under O₂. Observed organic products were consistent with formation of phenoxy radical and concurrent reduction of O₂, and subsequent aromatic oxidation chemistry was observed, at either a 3-Ph pyrazole substituent of **4.1a** or the phenolato ring of **4.1b**. Taken together, these reactions are analogous to oxidase and monooxygenase activities leading to TPQ biogenesis in nickel-substituted apo-CAO. Pro-oxidant chemistry through formation of reduced oxygen species catalyzed by interaction of nickel with biological phenols and thiols would also be of interest with respect to the toxicology of the metal.⁴⁸ Recently, a biomimetic Cu(II) complex was reported to react with O₂ and transform a phenol ligand substituent into a TPQ analog.⁶⁴ Attention is called to analogous intramolecular hydroxylations of ligand substituents upon addition of H₂O₂ to Ni(II) complexes,⁴⁰⁻⁴² and oxidative transformations of substituted phenols by a discrete (nacnac)NiO₂ complex.²²

4.2 Experimental

4.2.1 General procedure

All materials were obtained from commercial vendors and used as received, except for drying of solvents by routine techniques. Syntheses were carried out under

pre-purified argon, either in a glovebox (MBraun Unilab) or using Schlenk techniques. $\text{Tp}^{\text{R,Me}}\text{NiCl}$ complexes (R=Me,Ph) were prepared from anhydrous NiCl_2 and $\text{TTp}^{\text{R,Me}}$ in $\text{MeOH}/\text{CH}_2\text{Cl}_2$ as previously described (**Caution:** Thallium salts are extremely toxic and must be properly handled and disposed of!).^{58,59,65,66} 2,6-diisopropylphenol (Alfa Aesar) was reacted with NaH in toluene to afford the sodium salt of the conjugate base. ^1H NMR data were recorded on Bruker 300 Ultrashield and Varian Unity 500 spectrometers and processed using the MestReNova software suite (Mestrelab Research, Santiago de Compostela, Spain); spectra were referenced internally to residual CHCl_3 , CHDCl_2 and $\text{C}_6\text{D}_5\text{CHD}_2$ solvents (7.24, 5.32 and 2.08 ppm, respectively). Solution magnetic moments were determined by the Evans NMR method.⁶⁷ FT-IR spectra were recorded from KBr pellets on a Thermo-Electron Nicolet 380 spectrophotometer. UV-Vis-NIR spectra were recorded on an Agilent HP-8453 diode-array spectrophotometer. Elemental analyses were performed by Atlantic Microlabs (Norcross, GA). Spectroscopic data for complexes **4.1a,b** are shown in Figures S1-S8 and summarized below.

*Synthesis of $\text{Tp}^{\text{Ph,Me}}\text{Ni-O-2,6-}^i\text{Pr}_2\text{C}_6\text{H}_3$ (**4.1a**).* A sample of $\text{Tp}^{\text{Ph,Me}}\text{NiCl}$ (150 mg, 0.26 mmol) dissolved in dichloromethane (10 mL) was added to a slurry of NaO-2,6- $^i\text{Pr}_2\text{C}_6\text{H}_3$ (57 mg, 0.29 mmol) in CH_2Cl_2 (10 mL). The color changed from pale pink to dark green when the solutions were combined. After stirring 2.0 h, the solution was filtered and evaporated to dryness. The filtrate was re-dissolved in a minimal amount of CH_2Cl_2 and green crystals were obtained by slow diffusion of *n*-hexane at $-30\text{ }^\circ\text{C}$. Yield: 171 mg (0.24 mmol, 92%). Anal. Calcd. (found) for $\text{C}_{42}\text{H}_{45}\text{BN}_6\text{NiO}$, **4.1a**: C, 70.13 (70.27); H, 6.31 (5.88); N, 11.68 (11.69). ^1H NMR (CD_2Cl_2 , 293 K; δ , ppm): 74.1 (3H,

4-pz); 42 (2H, br, -CHMe₂); 39.3 (2H, *meta*); 14.4 (6H, br, 3-*ortho*); 8.9 (3H, 3-*para*); 7.1 (6H, 3-*meta*); 2.7 (12H, br, -CHMe₂); -2.2 (9H, 5-Me); -19.9 (1H, B-*H*); -43.4 (1H, *para*). $\mu_{\text{eff}} = 2.72 \mu_{\text{B}}$ (CDCl₃, 293 K). UV-vis-NIR (CH₂Cl₂; λ_{max} , nm; ϵ , M⁻¹ cm⁻¹): 476 (1900); 612 (800); 995 (200). IR (KBr, cm⁻¹): 2543, ν (B-H).

Synthesis of Tp^{Me,Me}Ni-O-2,6-ⁱPr₂C₆H₃ (4.1b). A sample of Tp^{Me,Me}NiCl (150 mg, 0.38 mmol) dissolved in dichloromethane (10 mL) was added to a slurry of NaO-2,6-ⁱPr₂C₆H₃ (75 mg, 0.38 mmol) in CH₂Cl₂ (10 mL). The color changed from pale pink to dark orange immediately after the solutions were combined. After stirring 2.0 h, the solution was filtered and evaporated to dryness. The filtrate was re-dissolved in a minimal amount of CH₂Cl₂ and orange crystals were obtained by slow diffusion of *n*-hexane at -30 °C. Yield: 186 mg (0.35 mmol, 91%). Anal. Calcd. (found) for C₂₇H₃₉BN₆NiO, **4.1b**: C, 60.83 (60.79); H, 7.37 (7.36); N, 15.76 (15.50). ¹H NMR (CD₂Cl₂, 293 K; δ , ppm): 76.9 (3H, 4-pz); 30.3 (2H, *meta*); 26.5 (2H, br, -CHMe₂); 3.9 (12H, br, -CHMe₂); -0.8 (9H, 3-Me); -6.6 (9H, 5-Me); -19.0 (1H, B-*H*); -28.0 (1H, *para*). ¹H NMR (C₆D₅CD₃, 293 K; δ , ppm): 75.5 (3H, 4-pz); 31.5 (2H, *meta*); 28.0 (2H, br, -CHMe₂); 4.0 (12H, br, -CHMe₂); -1.3 (9H, 3-Me); -6.5 (9H, 5-Me); -19.2 (1H, B-*H*); -29.5 (1H, *para*). $\mu_{\text{eff}} = 3.09 \mu_{\text{B}}$ (CDCl₃, 293 K). UV-vis-NIR (CH₂Cl₂; λ_{max} , nm; ϵ , M⁻¹ cm⁻¹): 326 (sh, 700); 421 (sh, 770); 449 (1000); 514 (330); 810 (80); 940 (120). IR (KBr, cm⁻¹): 2523, ν (B-H).

4.2.2 Synthesis of organic standards

3,3',5,5'-tetrakis(isopropyl)-4,4'-diphenoquinone and 2,6-diisopropyl-1,4-benzoquinone were prepared by oxidation of 2,6-diisopropylphenol according to

literature procedures,⁶⁸ reduced dihydroquinones were then obtained by sequential addition of dilute hydrochloric acid and zinc dust to solutions of either quinone in aqueous methanol, followed by filtration and removal of solvent under vacuum. Spectroscopic data are summarized below and shown in Figures 4-S9-4-S22; plots use a labeling scheme A-F, including a naphthalene standard (A) and others as indicated.

2,6-diisopropylphenol (B). ¹H NMR (300 MHz, CDCl₃, 293 K; δ, ppm): 7.05 (d, 7.6 Hz, 2H); 6.90 (t, 7.6 Hz, 1H); 4.76 (s, 1H); 3.15 (septet, 6.8 Hz; 2H); 1.27 (d, 6.8 Hz, 12 H). UV-vis-NIR (CH₂Cl₂; λ_{max}, nm; ε, M⁻¹ cm⁻¹): 273 (1600).

2,6-diisopropyl-1,4-benzoquinone (C). ¹H NMR (300 MHz, CDCl₃, 293 K; δ, ppm): 6.45 (s, 2H); 3.05 (septet, 6.9 Hz, 2H); 1.11 (d, 6.9 Hz, 12H). UV-vis-NIR (CH₂Cl₂; λ_{max}, nm; ε, M⁻¹ cm⁻¹): 325 (320); 414 (40).

2,6-diisopropyl-1,4-benzodihydroquinone (D). ¹H NMR (300 MHz, CDCl₃, 293 K; δ, ppm): 6.52 (s, 2H), 4.60 (s, 1H); 4.43 (s, 1H); 3.11 (septet, 6.8 Hz, 2 H); 1.22 (d, 6.8 Hz, 12H). UV-vis-NIR (CH₂Cl₂; λ_{max}, nm; ε, M⁻¹ cm⁻¹): 289 (8400).

3,5,3',5'-tetraisopropyl-4,4'-diphenoquinone (E). ¹H NMR (300 MHz, CDCl₃, 293 K; δ, ppm): 7.64 (s, 4H); 3.22 (septet, 6.9 Hz; 4H); 1.20 (d, 6.9 Hz; 24 H); UV-vis-NIR (CH₂Cl₂; λ_{max}, nm; ε, M⁻¹ cm⁻¹): 426 (71000).

3,5,3',5'-tetraisopropyl-4,4'-diphenodihydroquinone (F). ¹H NMR (300 MHz, CDCl₃, 293 K; δ, ppm): 7.17 (s, 4 H); 4.74 (s, 2H); 3.19 (septet, 6.9 Hz, 4H); 1.31 (d, 6.9 Hz, 24 H). UV-vis-NIR (CH₂Cl₂; λ_{max}, nm; ε, M⁻¹ cm⁻¹): 265 (17000).

Aerobic decomposition of Tp^{Ph,Me}Ni-O-2,6-ⁱPr₂C₆H₃ (4.1a); isolation of [(Tp^{Ph,Me})Ni]₂ (4.2)*. A sample of **4.1a** (96 mg, 0.13 mmol) was dissolved in CH₂Cl₂ (18

mL) and sealed in a vial with a rubber septum under argon. The solution was purged for approximately 5 s with a stream of O₂ gas flowing from a needle after passage through a column of CaH₂, anhydrous CaSO₄ and MgSO₄ to assure removal of trace H₂O. The punctured septum was then covered with silicone grease to exclude atmospheric moisture. The green color of the solution slowly deepened on standing overnight. After 24 h, *n*-hexane was introduced by vapor diffusion. Green crystals of product complex **4.2**, identified as di[hydro{bis(3-phenyl-5-methyl-pyrazol-1-yl)(3-*ortho*-phenolato-5-methyl-pyrazol-1-yl) borato}nickel(II)], formed after standing 3 d, and these were recovered by filtration (yield: 40 mg, 0.04 mmol, 53%); organic co-products remaining in the reddish-brown mother liquor were identified and quantified by independent synthesis and GC-MS (*vide infra*). Spectra of **4.2** are shown in Figures 4-S30-4-S34. Anal. Calcd. (found) for C₆₀H₅₈B₂N₁₂Ni₂O₄, (**4.2**)•2H₂O: C, 62.65 (63.05); H, 5.08 (4.91); N, 14.61 (14.62). ¹H NMR (CDCl₃, 293 K; δ, ppm): 76.0 (1H); 64.6 (2H); 46.4 (1H); 30.2 (1H); -3.6 (6H); -10.2 (1H); -25.5 (1H); -30.4 (1H); plus unassigned peaks. μ_{eff} = 2.42 μ_B (CDCl₃, 293 K). UV-Vis-NIR (CH₂Cl₂; λ_{max}, nm; ε, M⁻¹ cm⁻¹): 268 (23000); 306 (sh, 8700); 317 (9000); 420 (3100); 598 (60); 755 (30); 935 (30). IR (KBr, cm⁻¹): 2547, ν(B-H).

*Aerobic decomposition of Tp^{Ph,Me}Ni-O-2,6-ⁱPr₂C₆H₃ (**4.1a**); identification and quantification of organic co-products.* The mother liquor from the sample of decomposed Tp^{Ph,Me}Ni-O-2,6-ⁱPr₂C₆H₃ (**4.1a**) (*vide supra*) was evaporated to give a yellow-orange amorphous residue. Naphthalene was added as an internal standard, and the solids were redissolved in dichloromethane (4.0 mL), and filtered through a plug of silica gel. The solution was injected into a Shimadzu GCMS-QP2010S instrument at 270

°C, with the column initially at 50 °C, and then ramped upward at 10 °C/min for 5 min, 15 °C/min for 10 min, 20 °C/min for 3 min and then held at 310 °C (Figures 4-S24, 4-S25). The first peak observed was the naphthalene standard at 8.0 min (**A**, $m/z = 128$), followed by additional peaks of 2,6-diisopropylphenol at 9.6 min (**B**, $m/z = 178$), 2,6-diisopropyl-1,4-benzoquinone at 10.1 min (**C**, $m/z = 192$), 3,5,3',5'-tetraisopropyl-4,4'-diphenodihydroquinone at 17.80 min (**E**, $m/z = 354$), and 3,5,3',5'-tetraisopropyl-4,4'-diphenodihydroquinone at 17.83 min (**F**, $m/z = 354$). A peak at the independently determined retention time (12.3 min) of 2,6-diisopropyl-1,4-benzo-dihydroquinone (**D**, $m/z = 194$) was not observed. An unknown peak at 12.4 min (**U1**, $m/z = 158$) was assigned to 3-phenyl-5-methylpyrazole (0.20 equiv), and a second unknown peak at 15.6 min (**U2**, $m/z = 354$) may represent 4-hydroxy-3,5-diisopropylphenyl-2,6-diisopropyl ether, the product of head-to-tail phenoxy radical coupling. All assignments except **U2** were confirmed by comparison to the authentic standards described above (Figures 4-S9-4-S22). Qualitatively similar results were observed by ^1H NMR spectroscopy of CD_2Cl_2 extracts (Figures 4-S26-S29).

*Aerobic decomposition of $\text{Tp}^{\text{Me,Me}}\text{Ni-O-2,6-}i\text{Pr}_2\text{C}_6\text{H}_3$ (**4.1b**); isolation of $[\text{Tp}^{\text{Me,Me}}\text{Ni}]_2(\mu\text{-CO}_3)$ (**4.3**).* A sample of **4.1b** (42 mg, 0.08 mmol) was dissolved in CH_2Cl_2 (10 mL) and reacted with O_2 as described for **4.1a** above. The solution changed color from orange to dark green within 3 h (Figure 4-S35). Green crystals of $[\text{Tp}^{\text{Me,Me}}\text{Ni}]_2(\mu\text{-CO}_3)$ (**4.3**) were grown by diffusion of *n*-hexane (yield: 16 mg, 0.02 mmol, 51%). Spectra of **4.3** are shown in Figures 4-S45-4-S48. Anal. Calcd. (found) for $\text{C}_{31}\text{H}_{44}\text{B}_2\text{N}_{12}\text{Ni}_2\text{O}_3$, **4.3**: C, 48.24 (47.88); H, 5.75 (5.75), N, 21.78 (21.52). ^1H NMR (CD_2Cl_2 , 293 K; δ , ppm): 43.4 (6H, 4-pz); 1.7 (18H, 3-Me); -4.7 (2H, B-H); -5.5 (18H,

5-Me). $\mu_{\text{eff}} = 2.22 \mu_{\text{B}}$ (CDCl_3 , 293 K). UV-Vis-NIR (CH_2Cl_2 ; λ_{max} , nm; ϵ , $\text{M}^{-1} \text{cm}^{-1}$): 412 (400); 657 (80); 839 (50). IR (KBr, cm^{-1}): 2504, $\nu(\text{B-H})$; 1577, $\nu(\text{CO}_3)$.

*Hydrolytic decomposition of $\text{Tp}^{\text{Ph,Me}}\text{Ni-O-2,6-}^i\text{Pr}_2\text{C}_6\text{H}_3$ (**4.1a**); isolation of $[(\text{Tp}^{\text{Ph,Me}})_2\text{Ni}]$ (**4.4**).* A sample of **4.1a** (31 mg, 0.04 mmol) was dissolved under argon in dichloromethane (8 mL). Degassed H_2O (30 μL , 1.7 mmol) was injected and the dark green solution turned to a pale blue-green color within 15 min. The solvent was removed under vacuum, the residue was extracted with dichloromethane, and the extracts were filtered. Pale blue-green crystals of **4.4** were obtained by diffusion of *n*-hexane. Yield: 24 mg (0.02 mmol, 100%). Spectra of **4.4** are shown in Figures 4-S57-4-S60. Anal. Calcd. (found) for $\text{C}_{60}\text{H}_{56}\text{B}_2\text{N}_{12}\text{Ni}$, **4.4**: C, 70.27 (70.15); H, 5.50 (5.65); N, 16.39 (16.35). ^1H NMR (CDCl_3 , 293 K; δ , ppm): 55.1 (3H, 4-pz); 7.3 (6H, 3-Ph); 5.9 (9H, 3-Ph); -1.7 (18H, 5-Me); -8.0 (1H, B-H). $\mu_{\text{eff}} = 3.16 \mu_{\text{B}}$ (CDCl_3 , 293 K). UV-vis-NIR (CH_2Cl_2 ; λ_{max} , nm; ϵ , $\text{M}^{-1} \text{cm}^{-1}$): 370 (sh, 15); 416 (10, sh); 603 (7.4); 762 (2.9); 992 (4.5). IR (KBr, cm^{-1}): 2549, $\nu(\text{B-H})$.

4.2.3 DFT calculations.

A simplified TpNiOPh model was derived from our previous TpNiSPh models by replacement of sulfur with oxygen, adjustment of the resulting Ni-O and O-C_{ipso} bond lengths to experimental values, and geometry optimization.⁵⁹ Hypothetical O_2 adducts were modeled by manipulating the N-Ni-OAr and Ni-O-Ar angles within the mirror plane and inserting the oxygen atoms into the resulting gap. All geometry optimizations were restrained to C_s point symmetry. Spin-unrestricted calculations were performed using the Amsterdam Density Functional software package (version 2008.01, Scientific Computing

and Modelling NV),^{69,70} using the Vosko–Wilk–Nusair LDA functional,⁷¹ the Becke–Perdew GGA correction,^{72,73} and the Slater-type TZP orbital basis set available in the ADF library, with frozen atomic cores and default convergence criteria. A solvation model and relativistic correction were not applied.

4.2.4 X-ray crystallography.

Suitable crystals were placed onto the tips of 0.1 mm diameter glass capillaries and mounted on a Bruker APEX-II CCD diffractometer.⁷⁴ In each case, a preliminary set of cell constants was calculated from reflections harvested from three sets of 12 frames. These initial sets of frames were oriented such that orthogonal wedges of reciprocal space were surveyed. This produced initial orientation matrices determined from 38-384 reflections. The data collection was carried out using MoK α radiation (graphite monochromator) with a frame time of 20-60 seconds and a detector distance of 6.0 cm. A randomly oriented region of reciprocal space was surveyed to the extent of one sphere and to a resolution of 0.77 Å. Four major sections of frames were collected with 0.50° steps in ω at four different ϕ settings and a detector position of -28° in 2θ . The intensity data were corrected for absorption and decay (SADABS).⁷⁵ Final cell constants were calculated from strong reflections from the actual data collection after integration (SAINT).⁷⁶

Structures were solved using SHELXS-97 (Sheldrick, 1990) and refined using SHELXL-97 (Sheldrick, 1997).⁷⁷ Space groups were determined based on systematic absences and intensity statistics. Direct-methods solutions were calculated which provided most non-hydrogen atoms from the E-maps. Full-matrix least squares /

difference Fourier cycles were performed which located the remaining non-hydrogen atoms. All remaining non-hydrogen atoms were refined with anisotropic displacement parameters. Hydrogen atoms were placed in ideal positions and refined as riding atoms with relative isotropic displacement parameters. The final full matrix least squares refinements converged to acceptable R values. Crystal and refinement information are summarized in Table 5 and additional comments specific to individual structure solutions are summarized below. Thermal ellipsoid plots are shown in Figure 25, Figure 27, Figure 28 and Figure 31⁷⁸ relevant bond lengths and angles are given in the captions.

For **4.1b**, the hydrogen atom on boron was located in a similar manner to the non-hydrogen atoms and refined isotropically. The dimeric structure of **4.2** sits on an inversion center, and only one half of the molecule is unique. The diffraction data of **4.3** were initially indexed to a C-centered orthorhombic unit cell with twice the volume of the final monoclinic unit cell. XPREP suggested space group $C222_1$, which is rare, and no solution could be found in it. The reassigned monoclinic unit cell has nearly equivalent *a*- and *c*-axes, yet CHECKCIF and other routines found no additional symmetry. The crystal was twinned, and the twin element is a 180° rotation about [101]. A test was performed to determine the twin law. There are two twin components related by $[0\ 0\ 1 / 0\ 1\ 0 / 1\ 0\ 0]$ in a ratio of 0.455:0.545. This implies the twins are enantiomorphs. The refinement yielded a Flack parameter of 0.00(2). The nickel atom of **4.4** is located on a special position (2-fold rotation axis), so that one-half of the molecule is the asymmetric unit. The structure of **4.4** is isomorphous with the cobalt analog (LUSQOF.cif).⁷⁹ The hydrogen atom bonded to boron was located and refined with isotropic displacement parameters.

4.3 Results

4.3.1 General remarks.

Photochemical generation of singlet ($^1\Delta_g$) dioxygen in the presence of 2,6-diisopropylphenol results in a one-electron redox reaction through net hydrogen atom abstraction to yield superoxide and phenoxyl radicals.⁶⁸ The latter decomposes by competitive dimerization and O₂ coupling to yield a mixture of 3,5,3',5'-tetraisopropyl-4,4'-diphenoquinone and 2,6-diisopropyl-1,4-benzoquinone, respectively representing 2- and 4-electron oxidations per phenol precursor (Scheme 3). We hypothesized that substitution of the phenolic proton with paramagnetic [Tp^{R,Me}Ni(II)]⁺ would provide the means to overcome the spin barrier of ground-state ($^3\Sigma_g^-$) O₂ and obtain analogous thermal reactivity. Reduced O₂ species would then be captured for aromatic oxidation akin to the CAO active site, although the phenolate *ortho* sites are blocked by substituents. We accordingly prepared and characterized pseudotetrahedral Tp^{R,Me}Ni-OAr complexes (R = Ph, **4.1a**; Me, **4.1b**), which are thermally stable under inert atmosphere, but decompose when exposed to O₂. Products consistent with phenoxyl radical formation were observed, as well as aromatic oxidation reactions, either on the supporting ligand of **4.1a**, or on the phenolate ring of **4.1b**. However, 2,6-disubstituted phenolates will undergo free radical autoxidation to diphenoquinones under alkaline conditions,⁸⁰ and therefore hydrolyses of **4.1a,b** and subsequent oxidation reactions with O₂ and H₂O₂ were also examined.

4.3.2 Synthesis and characterization of $\text{Tp}^{\text{R,Me}}\text{Ni-O-2,6-}^i\text{Pr}_2\text{C}_6\text{H}_3$ (**4.1a,b**).

The phenolate complexes (R = Ph, **4.1a**; Me, **4.1b**) were obtained as crystalline solids following deprotonation of the phenol with sodium hydride and metatheses with known $\text{Tp}^{\text{R,Me}}\text{Ni-Cl}$ precursor complexes.^{65,66} Structures of **4.1a,b** were determined by X-ray diffraction (Figure 25). As expected, the N_3O ligand fields adopt pseudotetrahedral geometries that are nearly identical for both complexes. Constrained $\text{Tp}^{\text{R,Me}}$ ligand chelation yields average N-Ni-N angles of $92(3)^\circ$ in **4.1a** and $91(1)^\circ$ in **4.1b**, resulting in umbrella distortions with Ni-N bond vectors at respective angles of $123.9(3)^\circ$ and $124.5(3)^\circ$ from an ideal three-fold axis. The phenolate oxygen is then slightly displaced off this trigonal axis, with N-Ni-O angles ranging from $119.72(5)^\circ$ to $130.14(6)^\circ$ for **4.1a**, and from $118.99(9)^\circ$ to $129.92(9)^\circ$ for **4.1b**, giving τ_4 values of 0.77 for **4.1a** and 0.75 for **4.1b**.⁸¹ The Ni-OAr bond lengths are 1.821(1) and 1.841(2) Å, and Ni-O-C_{ipso} bond angles are $147.8(1)^\circ$ and $138.9(2)^\circ$, in **4.1a,b** respectively. Average Ni-N bond lengths of 2.03(2) and 2.00(2) Å in **4.1a,b** compare to values of 1.98(2) and 1.99(2) Å in the respective $\text{Tp}^{\text{R,Me}}\text{NiCl}$ precursors.^{66,82}

Spectroscopic data of **4.1a,b** are consistent with the solid-state structures. IR spectra of **4.1a,b** exhibit $\nu(\text{B-H})$ modes at 2543 and 2523 cm^{-1} respectively (Figures 4-S1-4-S4), indicative of $\kappa^3\text{-Tp}^{\text{R,Me}}$ chelation.⁸³ The complexes exhibit intense green (**4.1a**) and orange (**4.1b**) colors, reflecting visible phenolate-Ni(II) LMCT bands, as well as weaker ligand field bands in the near-IR, with extinctions consistent with the non-centrosymmetric geometries (Figures 4-S5, 4-S6). The LMCT bands are similar to those of the arylthiolate analogs, with somewhat attenuated extinctions.^{58,59} The ligand field bands are similar to both the arylthiolate analogs and the chloride complex precursors,

although small blueshifts in energies are evident in the order: -SAr > -Cl > -OAr;

$\text{Tp}^{\text{Me,Me}} \geq \text{Tp}^{\text{Ph,Me}}$.^{58,59} In view of the low symmetry and lack of near-IR data, rigorous assignments of the ligand field bands of **4.1a,b** are not offered, although such analyses were reported previously for $\text{Tp}^{\text{iPr,iPr}}\text{Ni-SC}_6\text{F}_5$ and $\text{Tp}^{\text{Me,Me}}\text{Ni-Cl}$.^{57,84} Magnetic susceptibilities in CDCl_3 solutions, determined by the Evans NMR method,⁶⁷ gave values of 2.72 and 3.09 μ_{B} at 293 K for **4.1a,b** respectively, indicative of an orbitally non-degenerate paramagnetic ground state (i.e., $\mu_{\text{S}} = 2.83 \mu_{\text{B}}$ for $S = 1$) and similar to both the chloride complex precursors and several arylthiolate analogs.^{58,59} ^1H NMR resonances of **4.1a,b** accordingly exhibit significant contact shifts, but the spectra were nonetheless consistent with the assigned formulations (Figures 4-S7, 4-S8). As with the arylthiolate analogs,^{58,59} spin delocalization by π -polarization leads to pronounced upfield shifting of the phenolate *para* protons, with the *meta* and isopropyl methine protons shifted downfield, and the isopropyl methyl resonance nearer to the diamagnetic limit. Pyrazole resonances of the supporting Tp ligands are unremarkable. However, the borohydride resonances of **4.1a,b** both exhibit pronounced upfield shifts (-20 and -19 ppm at 293 K, respectively) compared to the chloride complex precursors (-14 and -13 ppm, respectively) and several arylthiolate analogs (typically -10 to -11 ppm),^{58,59} reflecting the trend in ligand field bands. All three pyrazoles, as well as both sides of the phenolate rings, are spectroscopically equivalent in ^1H NMR spectra of **4.1a,b**, indicative of fluxionality in solution.

4.3.3 Reactivity; oxygenation of 4.1a,b.

The phenolate complex **4.1a** was indefinitely stable in dilute solution of dry, anaerobic CH₂Cl₂ (Figure S23). However, rapid saturation of the solution of **4.1a** with O₂ resulted in monotonic bleaching of the absorption bands ($t_{1/2} \approx 2$ h at 306 K, Figure 26), coincident with growth of an intense band at 426 nm, assigned to 3,5,3',5'-tetraisopropyl-4,4'-diphenoquinone (0.05 equiv, 10 mol%).⁶⁸ The induction period apparent in growth of this band reflects bleaching of coincident CT absorption of **4.1a** (Figure 26, inset), and presumably the initial accumulation of the dihydroquinone intermediate (Scheme 3), which disrupts the isosbestic points. GC-MS analysis of a decomposed aerobic solution (Figures 4-S24, 4-S25) revealed a small fraction of unmodified 2,6-diisopropylphenol (14 mol%), as well as 2,6-diisopropyl-1,4-benzoquinone (15 mol%) and 3,5,3',5'-tetraisopropyl-4,4'-diphenodihydroquinone (46 mol% combined with the overlapping oxidized quinone); the combined yield of phenol equivalents was 76 mol%. Two additional unknown peaks were assigned as 3-phenyl-5-methylpyrazole (**U1**, $m/z = 158$, 0.20 equiv) and 4-hydroxy-3,5-diisopropylphenyl-2,6-diisopropyl ether (**U2**, $m/z = 354$), the product of head-to-tail phenoxy radical coupling. Assignments of **B-F** were confirmed by comparison to authentic standards (Figures 4-S18-4-S22), and qualitatively similar results were observed by ¹H NMR spectroscopy of CD₂Cl₂ extracts (Figures 4-S26-4-S29), except the diphenodihydroquinone was oxidized. Thus, the organic product mixture is analogous to that previously reported for oxidation of phenol by singlet oxygen,⁶⁸ consistent with formation of phenoxy radical and obligating concomitant generation of reduced oxygen species (Scheme 3). Further

evidence for a reactive oxygen intermediate was obtained from isolation of product complex **4.2**, with an oxidized ligand.

Product complex **4.2** was obtained as pale green crystals in 53% yield and characterized by X-ray crystallography (Figure 27). A dimeric structure was found; the dimer occupies a crystallographic inversion center, so only one-half of the molecule is unique. Both nickel atoms are ligated with a modified $\text{Tp}^{\text{Ph,Me}}$ ligand resulting from C-H bond hydroxylation at the *ortho* position of one 3-phenyl substituent (i.e., $\text{Tp}^{\text{Ph,Me}^*}$), a two-electron oxidation. The planar $\text{Ni(II)}_2(\text{OR})_2$ core adopts a $\text{Ni}\cdots\text{Ni}$ separation of 3.1207(5) Å and an $\text{O}\cdots\text{O}$ separation of 2.587(3) Å, with internal O-Ni-O and Ni-O-Ni angles of 79.32(8)° and 100.68(8)°, respectively. The phenolate rings are disposed parallel to the $\text{Ni1}\cdots\text{Ni1}'$ vector, with bent $\text{Ni1-O1-C10}_{\text{ipso}}$ and $\text{Ni1-O1'-C10}'_{\text{ipso}}$ angles of 130.0(2)° and 126.8(2)°. The Ni1-O1 bond length within the κ^4 -chelate is longer than the bridging Ni1-O1' bond length, 2.043(2) vs. 2.010(2) Å. These core metrical parameters are similar to those of previously characterized $[\text{TpNi}(\mu\text{-OH})]_2$ complexes,³²⁻³⁴ with somewhat longer Ni-O, Ni-O' and $\text{O}\cdots\text{O}$ distances likely reflecting the relative basicities of phenolate and hydroxo ligands, the enhanced steric bulk of the 3-pyrazole substituents, as well as constraints imposed by rigid κ^4 -chelation of the $\text{Tp}^{\text{Ph,Me}^*}$ ligand. The installed phenolate donor results in a dianionic tetradentate ligand that binds Ni(II) in a distorted trigonal pyramidal geometry ($\tau_4 = 0.65$)⁸¹ with an axial N2 donor atom on the same tripodal arm as the equatorial phenolate (i.e., O1). The Ni1-N2 bond is shorter than the Ni1-N4 and Ni1-N6 bonds, 2.000(2) vs. 2.054(2) and 2.134(2) Å, respectively. The open coordination site is filled by the opposing phenolate oxygen (i.e., O1') in the assembled dimer, giving an N2-Ni1-O1' angle of 164.81(8)° along the trigonal bipyramidal axis.

However, the plane of the central Ni₂O₂ core is canted 12.6° relative to the axial B-N1-N2-Ni1-O1' least-squares planes, with the two tripodal ligands offset and disposed over opposite faces. This results in diverging N4-Ni1-O1 and N6-Ni1-O1 bond angles of 122.82(8)° and 145.73(8)°, respectively, so the overall (N₃O₂)²⁻ ligand field is better described as a distorted square pyramid ($\tau = 0.32$)⁸⁵ with an axial N4 donor.

Six-coordinate Fe(III) complexes of Tp^{Ph,Me*} and Tp^{Ph,Ph*} ligands were obtained previously,^{86,87} by oxidation with O₂ or H₂O₂, and resonance Raman spectroscopy of the latter derivative revealed vibrational modes of the *ortho*-phenolate ring.⁸⁷ The solid-state IR spectrum of **4.2** contains several analogous bands, as well as a single $\nu(\text{B-H})$ mode at 2547 cm⁻¹, consistent with κ^3 -pyrazole ligation and ideal C_{2h} point symmetry (Figures 4-S30, 31). The UV-Vis-NIR spectrum of **4.2** in CH₂Cl₂ contains intense bands at 306, 317 and 420 nm, which can be assigned as LMCT transitions arising from the installed phenolate moieties,^{41,42,88} as well as weaker ligand field bands at longer wavelengths (Figure 4-S32). The band at 420 nm exhibits a reversible, temperature-dependent red-shift (Figure 4-S33), suggesting a solution-phase equilibrium. Notwithstanding antiferromagnetic coupling of Ni(II) ions in the dimeric complex ($\mu_{\text{eff}} = 2.42 \mu_{\text{B}}$ in CDCl₃), the ¹H NMR spectrum in CDCl₃ exhibits signals over a significant range of chemical shifts comparable to **4.1a,b** (ca. -30 to 80 ppm, Figure 4-S34). Thus, dissociation of **4.2** to monomeric (Tp^{Ph,Me*})Ni in solution is suggested. However, further analysis was complicated by the low solubility of the isolated crystalline solids, and the NMR spectrum was not fully assigned.

Aerobic decomposition of **4.1b** appeared similar to that of **4.1a** by UV-Vis-NIR spectroscopy (Figure 4-S35), albeit at a ca. 10-fold faster rate (at 293 K vs. 303 K) and

with a diminished yield of diphenoquinone (ca. 6 mol%). A slight increase in optical density broadly centered near 642 nm likely reflects accumulation of $[\text{Tp}^{\text{Me,Me}}\text{Ni}(\mu\text{-OH})]_2$.³⁴ As for decomposition of **4.1a**, GC-MS analysis of the organic products revealed formation of diphenoquinone with traces of benzoquinone and unmodified phenol (Figures 4-S36, 4-S37), and this was confirmed by ^1H NMR spectroscopy (Figures 4-S38, 4-S39). However, two significant unknown species **U3** and **U4** were also observed. The unknown components were isolated by chromatography on silica and characterized by ^1H NMR spectroscopy in CD_2Cl_2 solution (Figures 4-S40-4-S44). The data for the major product **U4** unambiguously indicate loss of ring aromaticity and symmetry, as the three ring protons shifted to 6.77 (1H, d, $J = 4.3$ Hz), 3.72 (1H, d, $J = 4.0$ Hz) and 3.59 (1H, dd). A fourth proton resonance, presumably arising from phenol tautomerization, appeared at 3.67 ppm (1H, s). Moreover, the isopropyl groups also lost equivalence, exhibiting distinct methine septets at 2.80 and 1.88 ppm, each coupled to pairs of diastereotopic methyl signals. This spectrum appears to be consistent with assignment of **U4** as 3,4-dihydro-3,4-dihydroxy-2,6-diisopropyl-cyclohex-5-enone, which apparently has not been reported previously. This product is consistent with aromatic dihydroxylation of phenol by addition of H_2O_2 or its equivalent across *meta* and *para* ring positions, a two-electron oxidation distinct from the aromatic C-H bond hydroxylation that yields **4.2**. The spectrum of the minor product **U3** was not fully resolved, and a structure was not assigned.

Also isolated from a solution of aerobically decomposed **4.1b** was a dimeric carbonato-bridged complex with unmodified scorpionate ligands, $[\text{Tp}^{\text{Me,Me}}\text{Ni}]_2(\mu\text{-CO}_3)$ (**4.3**) as pale green crystals in 51% yield. This complex presumably arises from the

previously reported $[\text{Tp}^{\text{Me,Me}}\text{Ni}(\mu\text{-OH})]_2$ by CO_2 capture during workup under air.^{34,89}

Complex **4.3** was characterized by X-ray diffraction (Figure 28). The nickel atoms of **4.3** lie on the same side of the carbonato ligand plane, in contrast to the previously reported Tp^{iPr_2} analog,⁸⁹ and are more trigonally distorted ($\tau = 0.27$ and 0.20 for Ni1 and Ni2, respectively, vs. 0.16 and 0.14). The Ni-O bonds to the bridging oxygen are longer than those to the unshared oxygens in **4.3**, $2.104(7)$ and $2.144(7)$ Å vs. $2.021(7)$ and $1.963(6)$ Å, similar to a Tp^{Cy} -supported dimer,⁹⁰ but reversed from the Tp^{iPr_2} -supported complex.⁸⁹ The bridging Ni-O-Ni angle is correspondingly decreased, from $178.0(1)^\circ$ in the latter,⁸⁹ to $169.7(4)^\circ$ in **4.3**. Within the carbonato ligand, the carbon-oxygen bond to the bridging oxygen in **4.3** is longer than those to the two terminal oxygens, $1.37(1)$ Å vs. $1.27(1)$ and $1.22(1)$ Å. The IR spectrum of **4.3** contains a band at 1577 cm^{-1} assigned to the carbonato ligand (Figures 4-S45, 4-S46), compared to 1568 and 1581 cm^{-1} in the respective Tp^{iPr_2} - and Tp^{Cy} -supported analogs.^{89,90} UV-Visible-NIR (Figure 4-S47) and ^1H NMR spectra of **4.3** (Figure 4-S48) are also consistent with these prior results,⁸⁹ with the latter exhibiting attenuated contact shifting due to antiferromagnetic coupling through the carbonato bridge ($\mu_{\text{eff}} = 2.22\ \mu_{\text{B}}$).

4.3.4 Reactivity; hydrolyses of 4.1a,b and subsequent oxidations with O_2 and H_2O_2

Given the basicity of the phenolate ligands, complexes **4.1a,b** are susceptible to hydrolysis. This fact complicates interpretation of the oxygenation experiments already described; while considerable care was taken to inject only dry oxygen, the possibility cannot be excluded that the observed decompositions are actually rate-limiting hydrolyses due to accidental introduction of H_2O . Rapid autoxidation of free phenol

might then yield H₂O₂, and precedent exists for peroxide activation and oxidative chemistry at TpNi(II) centers.³⁰⁻³⁴ Therefore, hydrolysis reactions were carried out in which excess H₂O was deliberately added to solutions of **4.1a** and **4.1b** in CH₂Cl₂. This resulted in simple bleaching of the LMCT bands in both cases (Figure 26 and 4-S49). A UV-Vis-NIR spectrum of the hydrolyzed solution of **4.1b** at equilibrium was consistent with a mixture of previously reported [Tp^{Me,Me}Ni(μ-OH)]₂ (70 mol% based on reported extinctions)³⁴ and an unknown minor species that exhibits ligand field bands typical of a pseudotetrahedral TpNi-X complex (Figure S49). Attempts to isolate the immediate product complex from hydrolysis of **4.1a**, putatively the unknown monomeric analog [Tp^{Ph,Me}Ni-OH], instead gave the previously unreported and spectroscopically distinct sandwich complex [(Tp^{Ph,Me})₂Ni] (**4.4**) as pale blue-green crystals in quantitative yield (i.e., 0.5 equiv). Subsequent addition of excess H₂O₂ to the solution of hydrolyzed **4.1a** rapidly generated complex **4.2** in quantitative spectroscopic yield (Figure 29), as confirmed by ¹H NMR (Figure 4-S50) and FTIR (Figures 4-S51, 4-S52) spectroscopy, without accumulation of diphenoquinone. Treatment of **4.4** with excess H₂O₂ also resulted in conversion to **4.2**, albeit much more slowly (Figure 4-S53).

Notwithstanding the above results, phenol oxidation following hydrolyses of **4.1a,b** and O₂ addition was slow and inefficient (Figure 30 and 4-S54). Exposure of hydrolyzed **4.1a,b** to O₂ resulted in relatively slow generation of weak absorption bands at 426 nm, consistent with significantly diminished accumulation (≤ 3.0 mol%) of diphenoquinone (Figure 30 and 4-S54, insets). GC-MS analysis of the product mixtures after standing 24 h demonstrated that the balance of organic product was unmodified 2,6-diisopropylphenol (Figures 4-S55, 4-S56). Autoxidation of free phenol is plausible, but

accumulation of diphenoquinone, and hence reduction of O₂, is faster and more extensive without added H₂O (Figure 26 and 4-S35). Unless the added H₂O also acts as a significant inhibitor of phenol autoxidation, it would be necessary to ascribe the difference in O₂ chemistry without added H₂O to oxidation of intact **4.1a,b**.

A crystal structure of complex **4.4** confirmed the sandwich structure, [(Tp^{Ph,Me})₂Ni] (Figure 31). Despite the steric bulk of opposing 3-phenyl substituents, the nickel ion resides in a pseudo-octahedral, ideally D_{3d} N₆ ligand field afforded by κ³-*fac* ligation of the two ligands. The average Ni-N bond length of 2.18(4) Å and non-bonded Ni···B distances of 3.057(2) Å can be compared to several previously reported sandwich structures: (Tp^{4Bo})₂Ni, 2.087(4) and 3.161(6) Å;⁹¹ (Tp)₂Ni, 2.093(7) and 3.165(3) Å;⁹² (Tp^{Me})₂Ni, molecule 1, 2.11(2) and 3.140(7) Å;⁹³ (Tp^{Me})₂Ni, molecule 2, 2.096(6) and 3.16(1) Å;⁹³ (Tp^{Me,Cl,Me})₂Ni, molecule 1, 2.10(1) and 3.13(1) Å;⁹⁴ (Tp^{Me,Cl,Me})₂Ni, molecule 2, 2.11(1) and 3.143(7) Å;⁹⁴ (Tp^{Np})₂Ni, 2.12(1) and 3.089(6) Å;⁹⁵ (Tp^{Me,Me})₂Ni, 2.13(2) and 3.055(6) Å;⁹⁶ (Tp^{CO₂Et,Me})₂Ni, 2.14(6) and 3.105(6) Å;⁹⁷ (Tp^{3py})₂Ni, 2.15(7) and 3.078(2) Å;⁹⁸ (Tp^{4bz})₂Ni, 2.18(5) and 3.115(7) Å;⁹⁹ (4Bo, 4,5-fused benzo ring {i.e., indazolyl vs. pyrazolyl}; Np, neopentyl, CH₂C(CH₃)₃; 3-py, *meta*-C₅H₄N; 4bz, *para*-C₆H₄-C≡N). An inverse and counter-intuitive trend in Ni-N and Ni···B distances can be inferred from these data, in which increased steric bulk of 3- and 5-pyrazole substituents favors longer Ni-N bonds within a more compact sandwich. The structure of **4.4** represents a new extreme, which is accommodated by significant B-N-N-Ni torsion angles in the pyrazole ring chelation, 15.2(1) to 19.5(1)°. The intraligand *cis*-N-Ni-N bond angles remain close to right angles, 89.17(4) to 91.48(4)°, but the interligand angles diverge, 82.71(4) to 97.25(4)° and the *trans* angles depart from linearity, 169.84(4) to

171.31(6)°. The Ni-N5 bond lengths of 2.226(1) Å, disposed *trans* along one axis, are elongated compared to orthogonal Ni-N1 and Ni-N3 bond lengths, 2.149(1) and 2.157(1) Å, respectively. The crystal lattice of **4.4** is isomorphous with the (Tp^{Ph,Me})₂Co analog, which exhibits a nearly identical structure with an average Co-N bond length of 2.21(5) Å and Co···B distances of 3.10(1) Å.⁷⁹

Spectral data of **4.4** are consistent with the sandwich structure. The IR spectrum of **4.4** contains a single $\nu_{\text{as}}(\text{B-H})$ mode at 2549 cm⁻¹ (A_{2u} under D_{3d} symmetry), indicative of dual $\kappa^3\text{-Tp}^{\text{Ph,Me}}$ ligation (Figures S57, S58). The electronic spectrum of **4.4** in CH₂Cl₂ solution is typical of a pseudo-octahedral Tp₂Ni sandwich (Figure S59).^{91,100} Weak bands consistent with spin-allowed ligand field transitions were observed at 990 (3A_{2g} → 3T_{2g}) and 603 nm (3A_{2g} → 3T_{1g}); a spin-forbidden band (3A_{2g} → 1E_g) was also observed at 762 nm. The energy of the lowest transition corresponds to $\Delta_{\text{O}} = 10,100 \text{ cm}^{-1}$ and alignment of the observed transitions on a Tanabe–Sugano diagram yields B = 770 cm⁻¹, placing the third spin-allowed (3A_{2g} → 3T_{1g}{P}) band at 380 nm, where it is obscured by tailing of stronger bands from the UV. Electronic spectra of Tp₂Ni and (Tp^{4B₀})₂Ni are blue-shifted, $\Delta_{\text{O}} = 12,000$ and 12,890 cm⁻¹ respectively,^{91,100} consistent with their shorter Ni-N bonds (*vide supra*).^{91,92} The solution magnetic susceptibility of **4.4** (3.16 μ_B) is consistent with the assigned ground state.¹⁰⁰ Compared to half-sandwich complexes (e.g., **4.1a**), resonances in the ¹H NMR spectrum of **4.4** exhibit smaller paramagnetic contact shifts, reflecting delocalization of comparable spin over two Tp^{Ph,Me} ligands (Figure S60). Equivalence of various protons on the pyrazoles of both ligands reflects ideal two- and three-fold symmetries.

4.3.5 DFT calculations.

Oxidation of intact phenolate complexes with O₂ was suggested as a reaction mechanism leading to phenoxyl radical formation, but complex intermediates were not observed during aerobic decompositions of **4.1a,b**. Therefore, geometric and electronic models were sought for hypothetical inner-sphere O₂ adducts. Spin-unrestricted DFT calculations were performed first on a simplified TpNi-OPh model (Figure 32A), related to the crystal structure of **4.1a,b** by replacement of scorpionate and phenolate ligand substituents with hydrogen. The O₂ adducts [TpNi(OPh)(O₂)] (Figure 32B-D) and [TpNi(O₂)] (Figure 32E-I) were modeled in turn, with the latter reflecting loss of phenoxyl radical subsequent to O₂ ligation. To simplify the computations and their interpretation, geometry optimizations were constrained to C_s symmetry in all cases. Calculated geometric parameters are summarized and compared (Table 6), and noteworthy features of the electronic structures are discussed below.

Geometry optimization of TpNiOPh yielded a sawhorse configuration comparable to the experimental structure of **4.1b** (Table 6, Figure 32A and Figure 4-S61), with one large axial N-Ni-O bond angle of 134° and two smaller N-Ni-O bond angles of 121° ($\tau_4 = 0.74$). The average Ni-N bond length was 2.05(1) Å, the Ni-O bond length was 1.84 Å, and the Ni-O-C_{ipso} bond angle was 149°; comparable values in **4.1b** are 2.00(2) Å, 1.841(2) Å, and 138.9(2)°, respectively. Frontier orbitals of interest included the five atomic d orbitals on nickel, as well as the in-plane and out-of-plane phenolate oxygen donor orbitals (i.e., β -spin orbitals 21a'' and 37a', respectively), which were separated by 1.8 eV (Figure 33).⁵² The electronic structure of TpNiOPh was similar to prior calculations on the arylthiolate analogs, except the relatively upright conformation of the

phenolate disposes the ligand for π overlap of both donor orbitals, in contrast to the pseudo- σ interaction of bent arylthiolates.^{57,59} Consistent with the imposed spin state ($S = 1$), the two lowest unfilled orbitals were β -spin (41a' and 22a''), composed predominantly of atomic d orbitals on nickel (69% and 62%, respectively) and exhibiting σ^* interactions with the pyrazole N2 donor atoms and π^* interaction with the phenolate. The remaining β -spin Ni d orbitals (40a', 39a' and 20a'') were stabilized by an average of 1.8 eV and were filled, as were all five α -spin analogs. The α -spin HOMO-LUMO gap was 3.6 eV, and the latter was comprised entirely of pyrazole π^* interactions (not shown). The α - and β -spin HOMOs, presumably the redox-active orbitals in a one-electron oxidation, both exhibited major contributions from the out-of-plane phenolate π donor orbital.

After benchmarking the TpNiOAr model against the experimental data for **4.1a,b**, we calculated possible structures for a hypothetical O₂ adduct, [TpNi(OPh)(O₂)] (Figure 32B-D). Ordinary unrestricted calculations were performed, without consideration for effects of magnetic coupling between spins localized on nickel and the O₂ ligand. Four conformations are possible under C_s symmetry, with the phenolate ligand displaced *cis* or *trans* with respect to the axial pyrazole (defined as occupying the mirror plane) and O₂ introduced either end-on or side-on into the opened coordination site. Calculations with imposed low-spin ($S = 0$) states failed to converge, while high-spin ($S = 2$) states converged by dissociation of O₂ and return of the TpNiOPh fragment towards its previously described structure. In contrast, computations with intermediate spin ($S = 1$) converged in three of the four cases (Figure 32B-D), failing only for a trigonal prismatic

geometry with an equatorial phenolate and side-on O₂. Of the three other models, the unique octahedral conformation with side-on O₂ and an axial phenolate (Figure 32B) was predicted to exhibit significant elongations of the Ni-OAr and *trans* Ni-N bonds along an axial vector (Table 6), suggesting Jahn–Teller distortion of a low-spin Ni(III) ion (d⁷, *S* = 1/2). A relatively long O-O bond was also predicted (Table 6), presumably facilitated by the side-on coordination. Four unoccupied orbitals were found at low energy (Figure 34): a pair of α- and β-spin σ* orbitals (25a'') delocalized over the NiO₂ core; one β-spin orbital (45a') consisting predominantly of the axially-oriented dσ* orbital on nickel; and a third β-spin hole (24a'') delocalized over both the O₂ and OPh ligands. The nature of the latter hole may facilitate phenoxide/superoxo and phenoxyl/peroxide valence isomerism. Taken as a whole, the octahedral conformation seems poised for facile homolysis of phenoxyl radical. The end-on conformations (Figure 32C,D) exhibited analogous electronic structures (Figures S62, S63), notwithstanding their trigonal bipyramidal geometries, but the predicted O-O and Ni-OAr bond lengths were shorter. The end-on conformations may be disposed towards intramolecular coupling of superoxo and phenoxo moieties,⁵¹ perhaps constituting an origin for divergent aromatic oxidation pathways.

Loss of phenoxyl radical from the O₂ adduct would generate [TpNiO₂], and calculations were performed on three limiting conformations, end-on (pseudotetrahedral) and side-on (trigonal bipyramidal or square pyramidal), in both quartet (*S* = 3/2, Figure 32E-G) and doublet states (*S* = 1/2, Figure 32H-I). Assignment of oxidation states was complicated by the high degree of NiO₂ covalency, but calculated O-O bond lengths in the high-spin structures were typically consistent with superoxo ligands (Table 6).

Accordingly, three vacant β -spin orbitals were found at low energy for the high-spin side-on models, two predominantly nickel-centered $d\sigma^*$ orbitals and one O_2 -centered π^* orbital. However, these orbitals exhibited decreased nickel d character in the end-on conformation, suggesting a shift toward univalent nickel (Figures 4-S64-4-S66). The low-spin calculations were more opaque. The initially end-on model converged to a trigonal bipyramidal geometry that appears to enforce anti-ferromagnetic coupling in a superoxo-Ni(II) valence state (Figure 4-S67), while an initially trigonal bipyramidal model converged with significantly contracted bond lengths, plausibly interpreted as peroxo-Ni(III) (Figure 4-S68). The square pyramidal conformation failed to converge. Several Ni-O₂ adducts exhibiting low-spin EPR signals were recently reported, and DFT calculations supported similarly divergent experimental assignments of ground states, depending on the supporting ligand.^{19-21,23,25,26}

4.4 Discussion and Conclusion

Inspired by the dioxygenase activity of nickel-substituted apo-CAO,^{54,55} we prepared and characterized the pseudotetrahedral phenolate complexes $Tp^{R,Me}Ni-OAr$ (R = Ph, **4.1a**; Me, **4.1b**; Ar = 2,6-*i*Pr₂C₆H₃). These novel complexes are thermally robust in anaerobic, anhydrous CH₂Cl₂, but decompose upon exposure to O₂ or H₂O to yield several novel organic and complex products (i.e., **4.2-4.4**). The organic oxidation products are consistent with formation of phenoxyl radical and reduction of O₂, which results in distinct two-electron aromatic oxidation reactions, either hydroxylation of an aromatic C-H bond on a 3-phenyl pyrazole substituent of **4.1a** or dihydroxylation of the

phenol ring of **4.1b**. In contrast, oxygenation of hydrolyzed **4.1a,b** leads to relatively slow autoxidation of free phenol, although addition of H₂O₂ also gives the intramolecular aromatic hydroxylation to form **4.2**. Taken together, the O₂ reduction and aromatic oxidations may be relevant to TPQ generation in nickel-substituted apo-CAO, and to toxicology arising from oxidative stress mediated by xenobiotic interaction of nickel with intracellular thiols and phenols.

Four different reaction mechanisms can be proposed that explain the phenol oxidation and concurrent O₂ reduction: (i) homolysis of the Ni-OAr bond leading to phenoxy radical and Ni(I), which captures O₂;⁴³⁻⁴⁵ (ii) hydrolysis of the Ni-OAr bond and autoxidation of free phenol; (iii) outer-sphere oxidation of intact phenolate complexes by O₂, followed by Ni(III)-OAr bond homolysis; or (iv) inner-sphere ligation and activation of O₂. With regards to initial Ni(II)-OAr bond homolysis (mechanism i), we clearly demonstrated the thermal stability of **4.1a** in dry CH₂Cl₂. Deliberate addition of H₂O to **4.1a,b** confirmed that the Ni-OAr bonds are susceptible to hydrolysis (mechanism ii); moreover, addition of H₂O₂ to hydrolyzed **4.1a** yielded the same product complex **4.2** as decomposition under O₂. However, aerobic oxidation of the free phenol was observed to be slow and inefficient. Unless phenol autoxidation is inhibited by the presence of excess H₂O, it seems necessary to propose that a majority of the oxidation chemistry observed in dry CH₂Cl₂ results from reaction of O₂ with the intact phenolate complexes. Direct O₂ reduction by **4.1a,b** might entail one-electron transfer, either by an outer-sphere mechanism to form superoxide and [TpNi-OAr]^{+,•} radical intermediates (mechanism iii), or by formation of an inner-sphere adduct [TpNi(OAr)(O₂)] (mechanism iv). In either case, the complex intermediate would decompose by Ni(III)-OAr bond

homolysis, with subsequent phenoxyl radical and reduced O₂ chemistry proceeding as already described (Scheme 3).⁶⁷

Although nickel complex intermediates were not observed to accumulate during aerobic decompositions of **4.1a,b**, a number of possible intermediates arising along competitive oxidation and hydrolysis pathways of the TpNiOAr complexes can be proposed (Scheme 4). Hydrolyses of the starting complexes generate free phenol and intermediate TpNi-OH species (Scheme 4, left). The latter give rise to the characterized product complexes **4.3** and **4.4**, with the former derived from the known dimeric complex [Tp^{Me,Me}Ni(μ-OH)]₂.³⁴ As demonstrated by conversion to **4.2**, the hydroxo complexes may dimerize and capture H₂O₂ to form the oxidizing species [TpNi(μ-O)]₂; complex analogs of this intermediate have been structurally characterized and are known to decompose by intramolecular ligand oxidation.³²⁻³⁴ However, phenol oxidation, and thus reduction of oxygen, was inefficient in the presence of excess water. Therefore, an alternative route to [TpNi(μ-O)]₂ involving direct reaction of O₂ with **4.1a,b** is proposed (Scheme 4, right). Possible electronic and geometric structures for an initial [TpNi(OPh)(O₂)] adduct, which was not observed experimentally, were obtained by DFT calculations (Figure 32B-D). As in proposed TPQ biogenesis mechanisms,⁵⁰⁻⁵⁴ this intermediate might undergo intramolecular collapse, resulting in oxidative modification of the phenolate ring. Competing phenoxyl radical homolysis, perhaps assisted by enhanced steric contact between *ortho*-phenolate and 3-pyrazole substituents in a high-coordinate adduct, would generate a reactive TpNiO₂ intermediate, for which a range of computational structures was also obtained (Figure 32E-I). Similar complexes were recently isolated and structurally characterized;¹⁹⁻²⁶ in one case, an isolated (nacnac)NiO₂

complex was found to carry out aromatic hydroxylation of a 2,6-disubstituted phenol.²² A low-spin TpNiO₂ complex, formally a radical species, might otherwise dimerize to generate [TpNi(μ-O₂)]₂, a bis(μ-1,2-superoxo) intermediate akin to TPA-supported analogs.^{24,25} O₂ extrusion would then effect net superoxide dismutation to yield a peroxo-bridged dimer [TpNi]₂(μ-O₂) akin to an analog supported by tmc,²⁹ and finally the [TpNi(μ-O)]₂ valence isomer, the same intermediate obtained by hydrolysis and H₂O₂ capture.³⁴ Moreover, intramolecular C-H bond hydroxylation was reported to be relatively slow for [Tp^{Me,Me}Ni(μ-O)]₂,³⁴ which may afford the ultimate opportunity for convergence of hydrolysis and oxygenation pathways (Scheme 4), as well as diversion of oxidation chemistry away from the supporting Tp ligand and onto the phenol ring in the case of **4.1b**. Other pathways may be possible, and any of the proposed activated oxygen complexes (Scheme 4, right) might effect the observed aromatic oxidations.^{22,24}

Regardless of the mechanistic details of O₂ reduction, it is clear this chemistry occurs at the expense of the phenolate moiety during decomposition of **4.1a,b**; both this chemistry and the subsequent aromatic oxidations may be relevant to nickel-catalyzed TPQ biogenesis in apo-CAO. Oxidation of **4.1a** leads to C-H bond hydroxylation of a 3-phenylpyrazole substituent on the supporting Tp^{Ph,Me} ligand, while oxidation of **4.1b** leads to a different modification of the phenolate ring. Thus, another significant question remaining to be explored is the selectivity of the oxidation chemistry in the case of **4.1a**, where two different aromatic substrates are present and a peroxide shunt was also demonstrated.

In summary, we prepared bioinspired TpNi-OAr complexes **4.1a,b** that closely approximate the N₃O (His₃Tyr) ligand field of apo-CAO. Similar to TPQ biogenesis

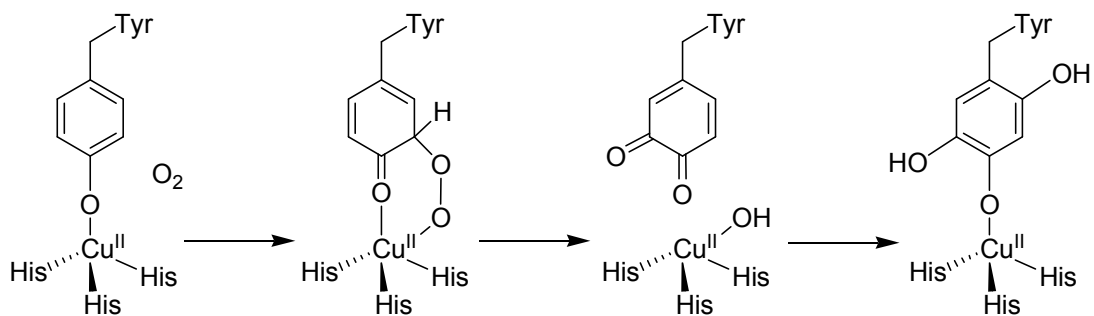
(Scheme 2), **4.1a,b** decompose in aerobic solutions, leading to phenoxy radical generation, O₂ reduction and oxidation of aromatic substrates. Hydrolysis products were identified, and subsequent phenol autoxidation and H₂O₂ activation were demonstrated. Having identified several organic and complex products in a complicated network of competitive reaction pathways (Schemes 3 and 4), we are positioned to address fundamental kinetic and mechanistic questions in future studies. Relevant issues raised by this investigation include the nature of the O₂ reduction, the identity of the reactive nickel and reduced oxygen intermediates, and how these yield the divergent oxidative modifications of aromatic substrates.

4.4.1 Acknowledgment

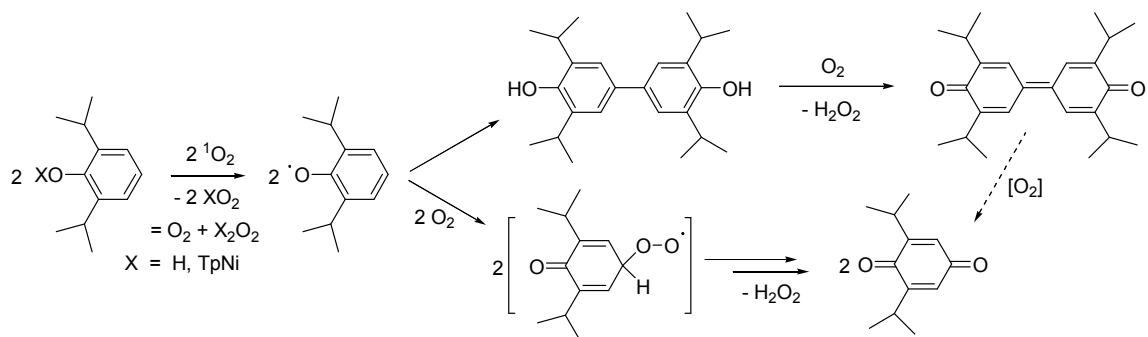
The authors acknowledge the donors of the American Chemical Society Petroleum Research Fund (49296-DNI3) for support of this research. We also thank the Ohio University 1804 Fund for support in acquiring the hardware and software for DFT computations.

4.4.2 Appendices/Supporting Information

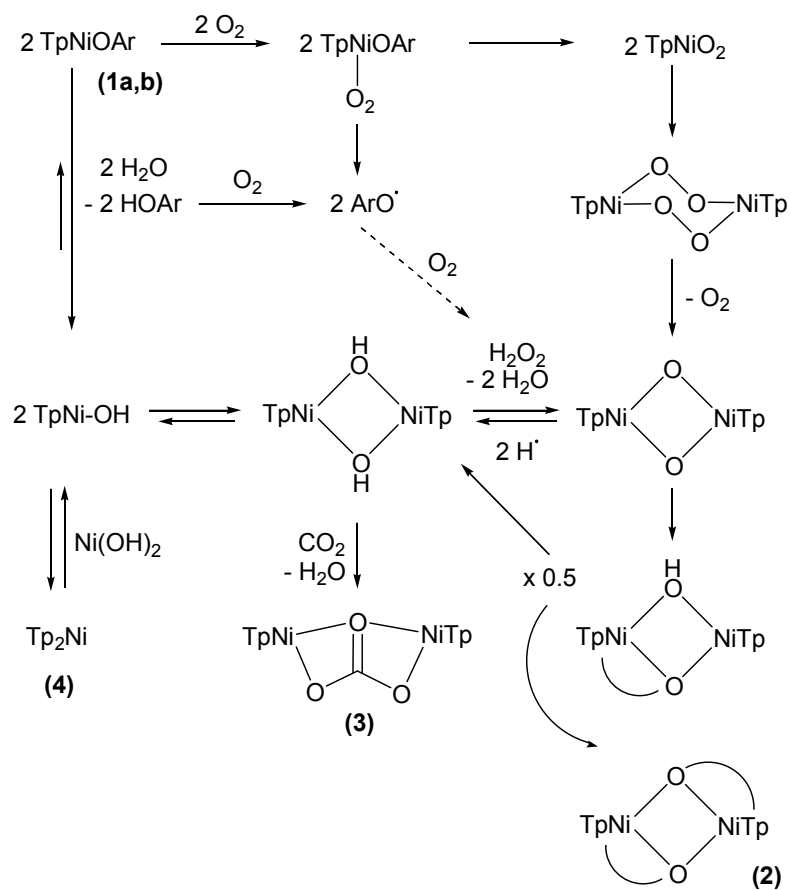
Supporting information includes details of the reactions, product characterizations and DFT calculations and provided in Appendix sections F-K. X-ray crystallographic bond length and bond angle data for **4.1a**, **4.1b** and **4.2-4.4**. Original data files (.cif) are available online at <https://pubs.acs.org>



Scheme 2: Proposed mechanism of CAO



Scheme 3: Singlet oxygen degradation mechanism



Scheme 4: Proposed degradation mechanism of Ni(II)Phenolates

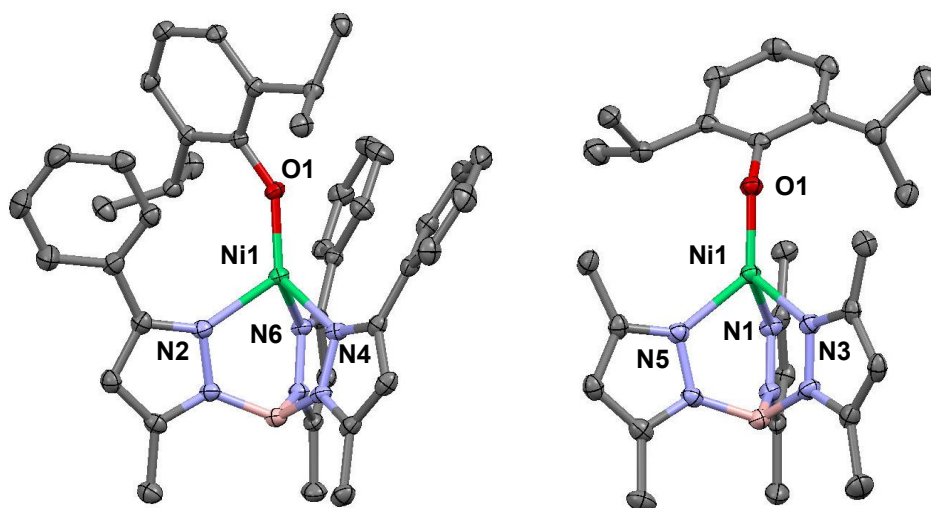


Figure 25: Thermal ellipsoid plots (50% probability) of $\text{Tp}^{\text{Ph,Me}}\text{Ni-O-2,6-}i\text{Pr}_2\text{C}_6\text{H}_3$ (**4.1a**, left) and $\text{Tp}^{\text{Me,Me}}\text{Ni-O-2,6-}i\text{Pr}_2\text{C}_6\text{H}_3$ (**4.1b**, right). Hydrogen atoms are omitted for clarity. Relevant bond lengths (Å) and angles (°) for **4.1a**: Ni1-N2, 2.046(2); Ni1-N4, 2.017(1); Ni1-N6, 2.025(1); Ni1-O1, 1.821(1); N2-Ni1-N4, 91.52(6); N2-Ni1-N6, 95.53(6); N4-Ni1-N6, 88.63(6); N2-Ni1-O1, 121.91(5); N4-Ni1-O1, 130.14(6); N6-Ni1-O1, 119.72(5); Ni1-O1-C31, 147.8(1). For **4.1b**: Ni1-N1, 2.005(2); Ni1-N3, 1.982(2); Ni1-N5, 2.014(2); Ni1-O1, 1.841(2); N1-Ni1-N3, 91.71(9); N1-Ni1-N5, 91.37(9); N3-Ni1-N5, 90.09(9); N1-Ni1-O1, 118.99(9); N3-Ni1-O1, 124.41(9); N5-Ni1-O1, 129.92(9); Ni1-O1-C16, 138.9(2).

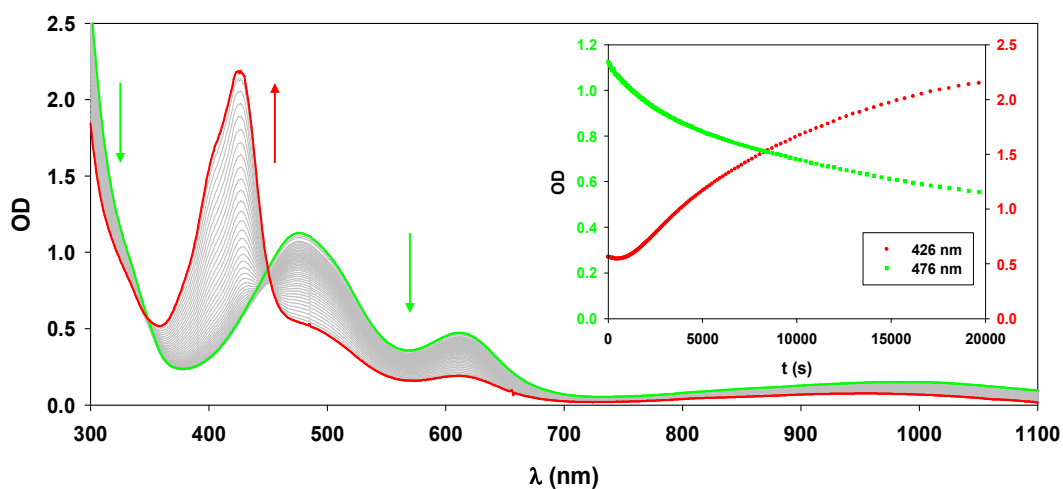


Figure 26: UV-Vis-NIR spectra for decomposition of **4.1a** (0.61 mM) in CH_2Cl_2 under O_2 (306 K). Inset shows traces at 476 nm (green trace, left axis) and 426 nm (red trace, right axis), corresponding to the absorption maxima of **4.1a** and 3,5,3',5'-tetraisopropyl-4,4'-diphenoquinone, respectively.

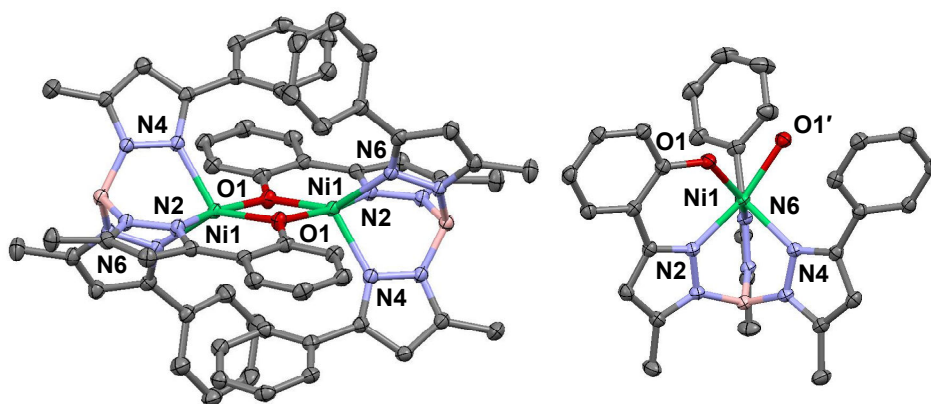


Figure 27: Thermal ellipsoid plot (30% probability) for dimeric $[(\text{Tp}^{\text{Ph,Me}^*})\text{Ni}]_2$ (**4.2**, left) and the monomeric asymmetric unit (right). Hydrogen atoms are omitted for clarity.

Relevant bond lengths (Å) and angles (°): Ni1-N2, 2.000(2); Ni1-N4, 2.054(2); Ni1-N6, 2.134(2); Ni1-O1, 2.043(2); Ni1-O1', 2.010(2); Ni1...Ni1', 3.1207(5); O1...O1', 2.587(3); N2-Ni1-N4, 89.78(8); N2-Ni1-N6, 89.40(8); N4-Ni1-N6, 90.97(8); N2-Ni1-O1, 85.55(8); N4-Ni1-O1, 122.82(8); N6-Ni1-O1, 145.73(8); N2-Ni1-O1', 164.81(8); N4-

Ni1-O1', 99.54(8); N6-Ni1-O1', 102.32(7); O1-Ni1-O1', 79.32(8); Ni1-O1-Ni1',
100.68(8); Ni1-O1-C10, 130.0(2); Ni1-O1'-C10', 126.8(2).

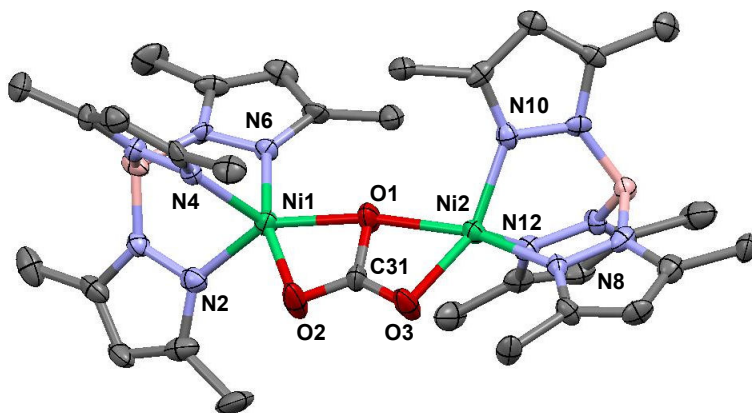


Figure 28: Thermal ellipsoid plot (30% probability) of $[\text{Tp}^{\text{Me,Me}}\text{Ni}]_2(\mu\text{-CO}_3)$ (**4.3**). Hydrogen atoms are omitted for clarity.

Relevant bond lengths (Å) and angles (°): Ni1-N2, 2.016(8); Ni1-N4, 2.009(7); Ni1-N6, 2.021(6); Ni1-O1, 2.104(7); Ni1-O2, 2.021(7); Ni2-N8, 2.054(6); Ni2-N10, 1.955(8); Ni2-N12, 2.041(8); Ni2-O1, 2.144(7); Ni2-O3, 1.963(6); C31-O1, 1.37(1); C31-O2, 1.27(1); C31-O3, 1.22(1); N2-Ni1-N4, 90.6(3); N2-Ni1-N6, 91.8(3); N4-Ni1-N6, 91.6(3); N2-Ni1-O1, 146.9(3); N2-Ni1-O2, 95.0(3); N4-Ni1-O1, 118.3(3); N4-Ni1-O2, 103.9(3); N6-Ni1-O1, 102.3(2); N6-Ni1-O2, 162.9(3); O1-Ni1-O2, 64.2(2); O1-C31-O2, 112.5(8); O1-C31-O3, 116.1(8); O2-C31-O3, 131.(8); N8-Ni2-N10, 90.5(3); N8-Ni2-N12, 90.9(3); N10-Ni2-N12, 92.4(3); N8-Ni2-O1, 161.1(2); N8-Ni2-O3, 97.5(3); N10-Ni2-O1, 102.2(3); N10-Ni2-O3, 149.0(3); N12-Ni2-O1, 102.3(3); N12-Ni1-O3, 117.2(3); O1-Ni2-O3, 64.5(3); Ni1-O1-Ni2, 169.7(4).

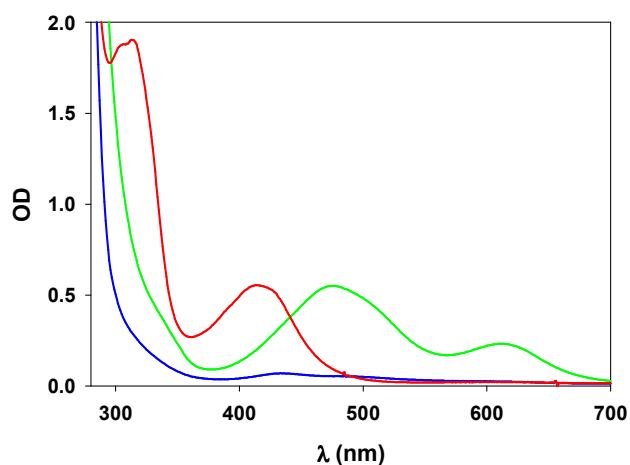


Figure 29: UV-Vis spectra demonstrating reaction of **4.1a** (0.30 mM, green) with added H₂O (270 mM) to form a hydrolyzed intermediate (blue) that reacts rapidly with H₂O₂ (67 mM) to form **4.2** (red).

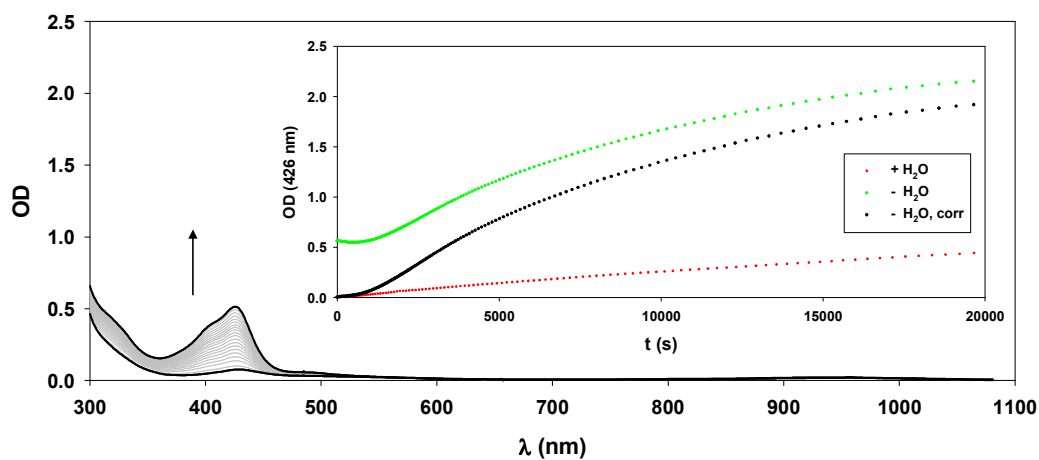


Figure 30: UV-Vis-NIR absorption vs. time ($\Delta t = 1000$ s) following addition of O₂ to a hydrolyzed solution of **4.1a** (0.44 mM in CH₂Cl₂, 306 K). Inset shows trace at 426 nm (red), corresponding to accumulation of 3,5,3',5'-tetraisopropyl-4,4'-diphenylquinone, and compared to data shown in Figure 26 for O₂ addition to intact **4.1a** (green) and corrected for absorption of **4.1a** (black).

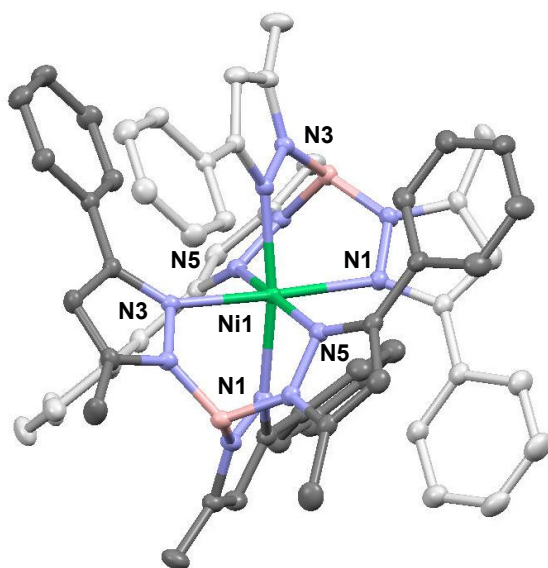


Figure 31: Thermal ellipsoid plot (30% probability) of $[(\text{Tp}^{\text{Ph,Me}})_2\text{Ni}]$ (**4.4**). For clarity, hydrogen atoms are omitted and carbon atoms of opposing ligands are differentially shaded.

Relevant bond lengths (Å) and angles (°): Ni1-N1, 2.149(1); Ni1-N3, 2.157(1); Ni1-N5, 2.226(1); N1-Ni1-N3, 89.96(4); N1-Ni1-N5, 91.48(4); N3-Ni1-N5, 89.17(4); N1-Ni1-N1', 96.32(6); N1-Ni1-N3', 169.84(4); N1-Ni1-N5', 82.71(4); N3-Ni1-N3', 85.00(6); N3-Ni1-N5', 97.25(4); N5-Ni1-N5', 171.31(6), where the prime symbol denotes a nitrogen atom on the opposing ligand.

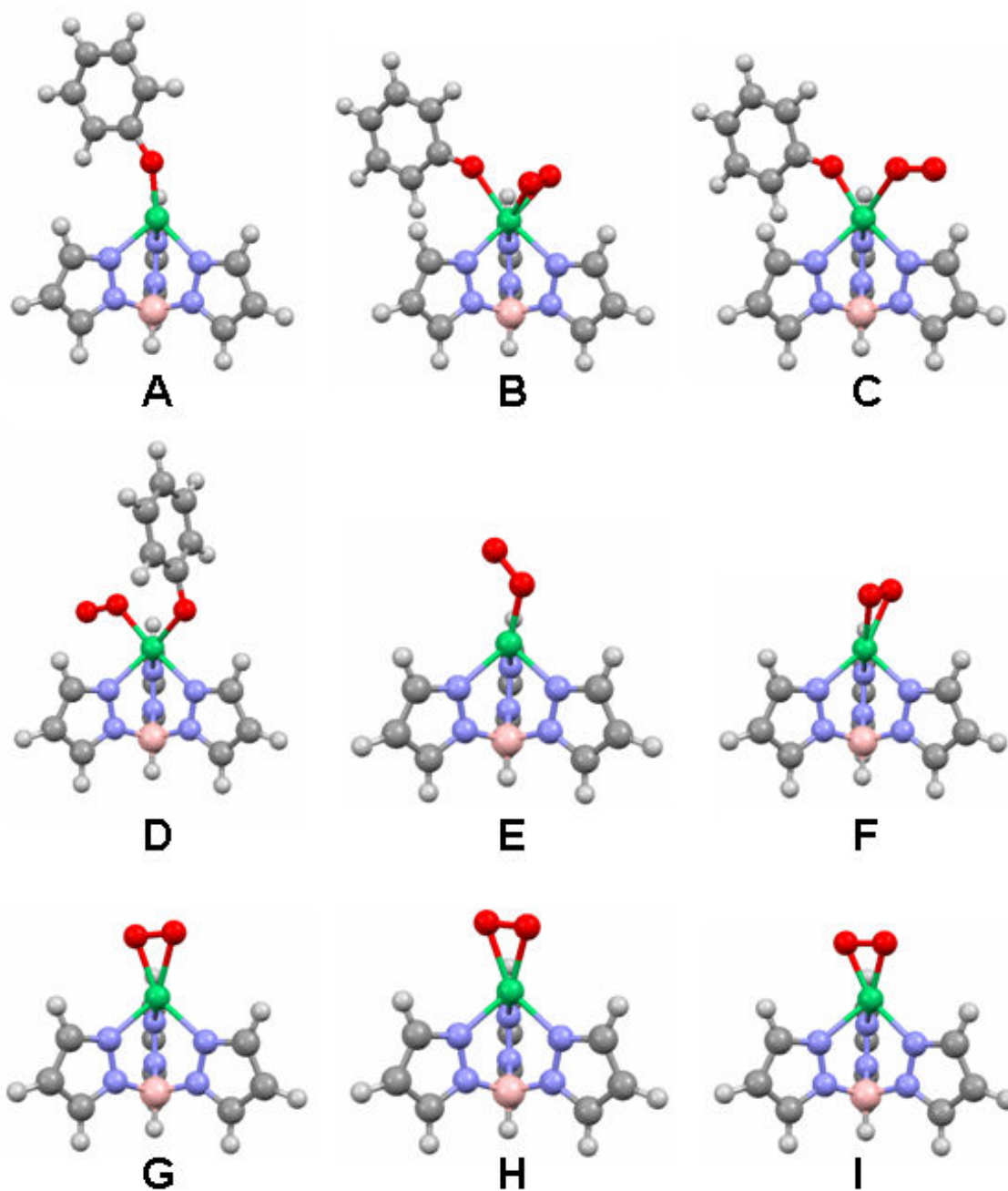


Figure 32: Optimized geometries of C_s -symmetric computational models of TpNiOPh (A), TpNiOPh(O₂) (B-D) and TpNiO₂ (E-I).

More details are provided in Appendix F.

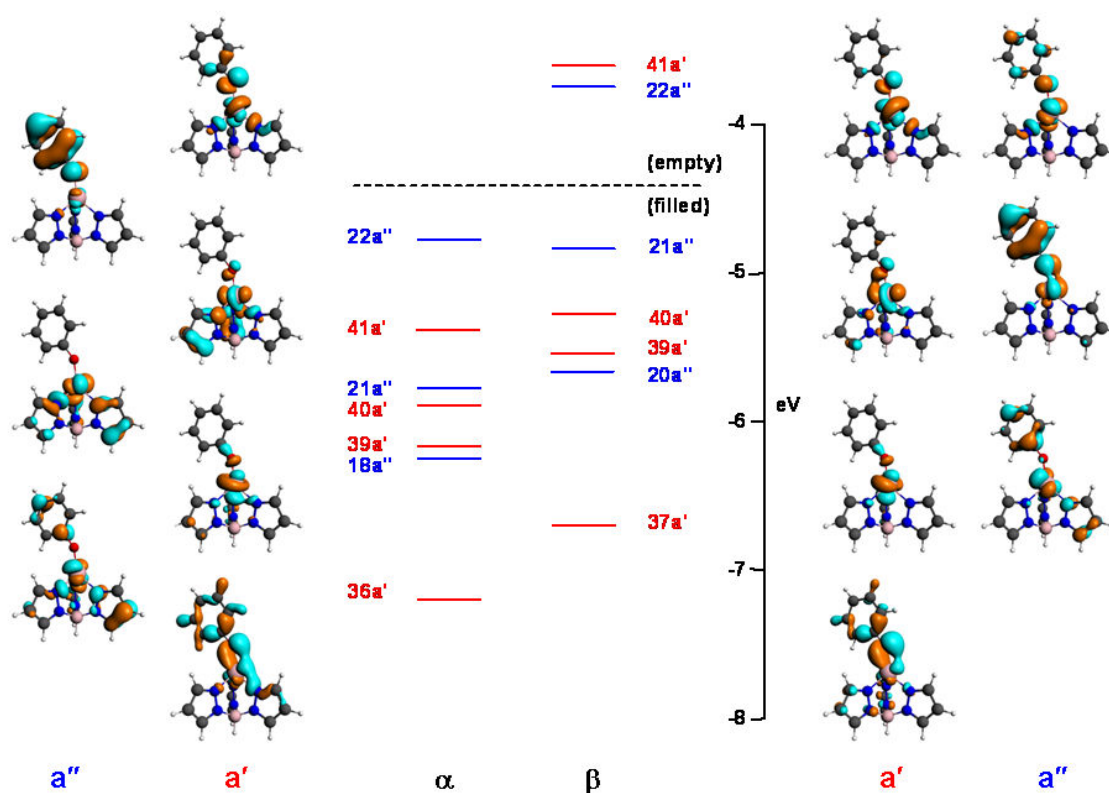


Figure 33: Relevant spin-unrestricted frontier molecular orbitals in the C_s -symmetric TpNiOPh computational model (Figure 32-A), circumscribing five nickel d orbitals and the in-plane and out-of-plane phenolate donor orbitals. Red and blue orbitals and labels respectively signify symmetry (a') and antisymmetry (a'') with respect to the mirror plane.

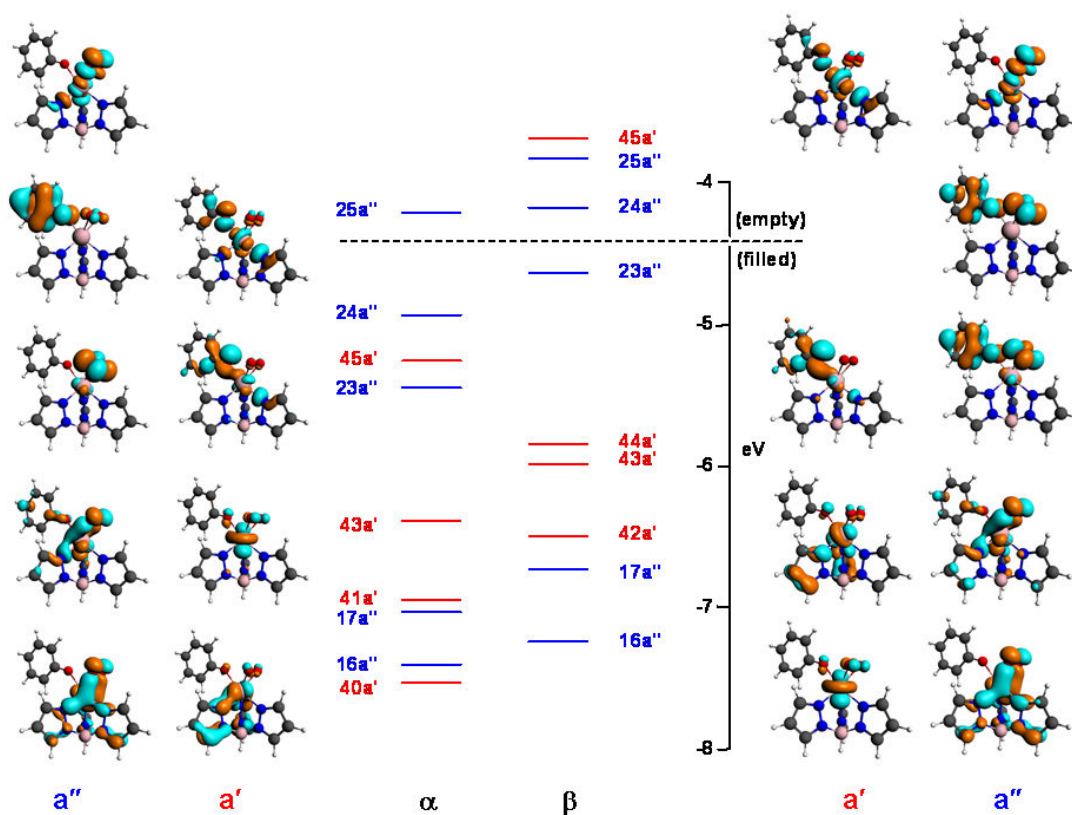


Figure 34: Relevant spin-unrestricted frontier molecular orbitals in a C_s -symmetric $\text{TpNiOPh}(\text{O}_2)$ computational model (Figure 32-B), circumscribing five nickel d orbitals, the two phenolate donor orbitals, and two O_2 π^* orbitals. Red and blue orbitals and labels respectively signify symmetry (a') and antisymmetry (a'') with respect to the mirror plane.

Table 5: Summary of X-ray crystallography.

Compound	Tp ^{Ph,Me} Ni O-2,6- iPr ₂ C ₆ H ₃ (4.1a)	Tp ^{Me,Me} Ni O-2,6- iPr ₂ C ₆ H ₃ (4.1b)	[(Tp ^{Ph,Me*})Ni] ₂ (4.2)	(Tp ^{Me,Me} Ni) ₂ (μ-CO ₃) (4.3)	(Tp ^{Ph,Me}) ₂ Ni (4.4)
Empirical formula	C ₄₂ H ₄₅ BN ₆ NiO	C ₂₇ H ₃₉ BN ₆ NiO	C ₆₀ H ₅₄ B ₂ N ₁₂ Ni ₂ O ₂	C ₃₁ H ₄₄ B ₂ N ₁₂ Ni ₂ O ₃	C ₆₀ H ₅₆ B ₂ N ₁₂ Ni ₂
Formula weight	719.36	533.16	1114.19	771.82	1025.50
Temperature (K)	123(2)	123(2)	173(2)	173(2)	173(2)
Crystal system	Triclinic	Monoclinic	Tetragonal	Monoclinic	Monoclinic
Space group	P-1	P2 ₁ /n	P4 ₂ /n	P2 ₁	C2/c
a (Å)	10.7698(9)	8.803(1)	19.682(2)	8.053(5)	18.0500(9)
b (Å)	11.111(1)	29.373(3)	19.682(2)	30.94(2)	13.7439(7)
c (Å)	12.251(2)	10.630(1)	13.541(1)	8.073(5)	21.985(2)
α (deg)	84.405(1)	90	90	90	90
β (deg)	78.857(1)	91.832(1)	90	113.820(6)	111.505(1)
γ (deg)	65.717(1)	90	90	90	90
V (Å ³)	1845.8(3)	2747.2(5)	5245.5(8)	1840(2)	5074.3
Z	2	4	4	2	4
Density (calc, g/cm ³)	1.294	1.289	1.411	1.393	1.342
Absorption coefficient (mm ⁻¹)	0.568	0.737	0.776	1.073	0.437
Crystal color, morphology	Green, block	Orange, irregular	Green, needle	Green, block	Green, block
Crystal size (mm)	0.22 x 0.12 x 0.10	0.25 x 0.12 x 0.05	0.45 x 0.12 x 0.10	0.45 x 0.12 x 0.10	1.13 x 1.07 x 0.44
Reflections collected	22004	30891	60638	14999	28593
Independent reflections (R _{int})	8349 (0.0310)	6280 (0.0751)	5365 (0.0500)	6484 (0.0528)	5818 (0.0221)
Observed reflections	6959	4388	4145	5206	5209
Data/restraints/parameters	8349/0/467	6280/0/339	5365/0/355	6484/1/464	5818/0/346
GoF	1.047	1.037	1.020	1.061	1.032
R1, wR2 [I > 2σ(I)]	0.0364, 0.0806	0.0476, 0.1056	0.0389/0.0983	0.0525, 0.1114	0.0308, 0.0776
R1, wR2 (all data)	0.0471, 0.0859	0.0803, 0.1190	0.0559/0.1088	0.0718, 0.1194	0.0356, 0.0805
Difference peak, hole (e/ Å ³)	0.596, -0.353	0.661, -0.503	0.436, -0.260	0.579, -0.627	0.268, -0.325

Table 6: Calculated bond lengths from computational models.

Model	Structure (a)	S	O-O (Å)	Ni- O ₂ (Å) ^(b)	Ni- OPh (Å)	Ni-N _{ax} (Å) ^(b)	Ni-N _{eq} (Å) ^(b)	Relative energy (eV)
TpNiOPh + O ₂	A	1 ± 1	1.23	∞	1.84	2.05	2.06	0.00
TpNiOPh(O ₂)	B	1	1.33	1.94	2.11	2.14	1.99	+ 0.05
TpNiOPh(O ₂)	C	1	1.28	2.09	1.91	2.02	2.09	+ 0.18
TpNiOPh(O ₂)	D	1	1.28	1.91	1.89	2.06	2.06	- 0.30
TpNiO ₂ + PhO [•]	E	3/2 ± 1/2	1.31	1.87	∞	2.01	2.06	+ 0.98
TpNiO ₂ + PhO [•]	F	3/2 ± 1/2	1.35	2.04	∞	2.03	2.07	+ 0.69
TpNiO ₂ + PhO [•]	G	3/2 ± 1/2	1.34	1.99 (ax) 2.11 (eq)	∞	2.08	2.04	+ 0.73
TpNiO ₂ + PhO [•]	H	1/2 ± 1/2	1.35	2.10 (ax) 2.01 (eq)	∞	2.06	2.03	+ 0.90
TpNiO ₂ + PhO [•]	I	1/2 ± 1/2	1.37	1.89 (ax) 1.84 (eq)	∞	1.96	2.08	+ 0.46

(a) Figure 32. (b) axial positions defined as pyrazole occupying the mirror plane and trans coordination site.

4.5 References

- (1) Sono, M.; Roach, M. P.; Coulter, E. D.; Dawson, J. H. *Chem. Rev.* 1996, 96, 2841-2888.
- (2) Costas, M.; Mehn, M. P.; Jensen, M. P.; Que, L., Jr. *Chem. Rev.* 2004, 104, 939-986.

- (3) Kovaleva, E. G.; Neibergall, M. B.; Chakrabarty, S.; Lipscomb, J. D. *Acc. Chem. Res.* 2007, 40, 475-483.
- (4) Krebs, C.; Fujimori, D. G.; Walsh, C. T.; Bollinger, J. M., Jr. *Acc. Chem. Res.* 2007, 40, 484-492.
- (5) Tshuva, E. Y.; Lippard, S. J. *Chem. Rev.* 2004, 104, 987-1012.
- (6) Decker, A.; Solomon, E. I. *Curr. Opin. Chem. Biol.* 2005, 9, 152-163.
- (7) Korendovych, I. V.; Kryatov, S. V.; Rybak-Akimova, E. V. *Acc. Chem. Res.* 2007, 40, 510-521.
- (8) Mirica, L. M.; Ottenwaelder, X.; Stack, T. D. P. *Chem. Rev.* 2004, 104, 1013-1046.
- (9) Lewis, E. A.; Tolman, W. B. *Chem. Rev.* 2004, 104, 1047-1076.
- (10) Kim, E.; Chufán, E. E.; Kamaraj, K.; Karlin, K. D. *Chem. Rev.* 2004, 104, 1077-1134.
- (11) Ju, T.; Goldsmith, R. B.; Chai, S. C.; Maroney, M. J.; Pochapsky, S. S.; Pochapsky, T. C. *J. Mol. Biol.* 2006, 363, 823-834.
- (12) Szajna, E.; Arif, A. M.; Berreau, L. M. *J. Am. Chem. Soc.* 2005, 127, 17186-17187.
- (13) Kimura, E.; Sakonaka, A.; Machida, R.; Kodama, M. *J. Am. Chem. Soc.* 1982, 104, 4255-4257.
- (14) Edison, S. E.; Hotz, R. P.; Baldwin, M. J. *Chem. Commun.* 2004, 1212-1213.
- (15) Koola, J. D.; Kochi, J. K. *Inorg. Chem.* 1987, 26, 908-916.
- (16) Kinneary, J. F.; Albert, J. S.; Burrows, C. J. *J. Am. Chem. Soc.* 1988, 110, 6124-6129.

- (17) Nagataki, T.; Tachi, Y.; Itoh, S. *Chem. Commun.* 2006, 4016-4018.
- (18) Grapperhaus, C. A.; Darensbourg, M. Y. *Acc. Chem. Res.* 1998, 31, 451-459.
- (19) Fujita, K.; Schenker, R.; Gu, W.; Brunold, T. C.; Cramer, S. P.; Riordan, C. G. *Inorg. Chem.* 2004, 43, 3324-3326.
- (20) Kieber-Emmons, M. T.; Annaraj, J.; Seo, M. S.; Van Heuvelen, K. M.; Tosha, T.; Kitagawa, T.; Brunold, T. C.; Nam, W.; Riordan, C. G. *J. Am. Chem. Soc.* 2006, 128, 14230-14231.
- (21) Yao, S.; Bill, E.; Milsman, C.; Wieghardt, K.; Driess, M. *Angew. Chem., Int. Ed.* 2008, 47, 7110-7113.
- (22) Company, A.; Yao, S.; Ray, K.; Driess, M. *Chem.–Eur. J.* 2010, 16, 9669-9675.
- (23) Pietrzyk, P.; Podolska, K.; Mazur, T.; Sojka, Z. *J. Am. Chem. Soc.* 2011, 133, 19931-19943.
- (24) Shiren, K.; Ogo, S.; Fujinami, S.; Hayashi, H.; Suzuki, M.; Uehara, A.; Watanabe, Y.; Moro-oka, Y. *J. Am. Chem. Soc.* 2000, 122, 254-262.
- (25) Cho, J.; Furutachi, H.; Fujinami, S.; Tosha, T.; Ohtsu, H.; Ikeda, O.; Suzuki, A.; Nomura, M.; Uruga, T.; Tanida, H.; Kawai, T.; Tanaka, K.; Kitagawa, T.; Suzuki, M. *Inorg. Chem.* 2006, 45, 2873-2885.
- (26) Cho, J.; Sarangi, R.; Annaraj, J.; Kim, S. Y.; Kubo, M.; Ogura, T.; Solomon, E. I.; Nam, W. *Nat. Chem.* 2009, 1, 568-572.
- (27) Cho, J.; Furutachi, H.; Fujinami, S.; Suzuki, M. *Angew. Chem., Int. Ed.* 2004, 43, 3300-3303.
- (28) Kieber-Emmons, M. T.; Schenker, R.; Yap, G. P. A.; Brunold, T. C.; Riordan, C. G. *Angew. Chem., Int. Ed.* 2004, 43, 6716-6718.

- (29) Schenker, R.; Kieber-Emmons, M. T.; Riordan, C. G.; Brunold, T. C. *Inorg. Chem.* 2005, 44, 1752-1762.
- (30) Hikichi, S.; Kobayashi, C.; Yoshizawa, M.; Akita, M. *Chem.–Asian J.* 2010, 5, 2086-2092.
- (31) Hikichi, S.; Okuda, H.; Ohzu, Y.; Akita, M. *Angew. Chem., Int. Ed.* 2009, 48, 188-191.
- (32) Hikichi, S.; Yoshizawa, M.; Sasakura, Y.; Akita, M.; Moro-oka, Y. *J. Am. Chem. Soc.* 1998, 120, 10567-10568.
- (33) Hikichi, S.; Yoshizawa, M.; Sasakura, Y.; Komatsuzaki, H.; Akita, M.; Moro-oka, Y. *Chem. Lett.* 1999, 979-980.
- (34) Hikichi, S.; Yoshizawa, M.; Sasakura, Y.; Komatsuzaki, H.; Moro-oka, Y.; Akita, M. *Chem.–Eur. J.* 2001, 7, 5011-5028.
- (35) Itoh, S.; Bandoh, H.; Nagatomo, S.; Kitagawa, T.; Fukuzumi, S. *J. Am. Chem. Soc.* 1999, 121, 8945-8946.
- (36) Itoh, S.; Bandoh, H.; Nakagawa, M.; Nagatomo, S.; Kitagawa, T.; Karlin, K. D.; Fukuzumi, S. *J. Am. Chem. Soc.* 2001, 123, 11168-11178.
- (37) Bag, B.; Mondal, N.; Rosair, G.; Mitra, S. *Chem. Commun.* 2000, 1729-1730.
- (38) Mandimutsira, B. S.; Yamarik, J. L.; Brunold, T. C.; Gu, W.; Cramer, S. P.; Riordan, C. G. *J. Am. Chem. Soc.* 2001, 123, 9194-9195.
- (39) Schenker, R.; Mandimutsira, B. S.; Riordan, C. G.; Brunold, T. C. *J. Am. Chem. Soc.* 2002, 124, 13842-13855.

- (40) Honda, K.; Cho, J.; Matsumoto, T.; Roh, J.; Furutachi, H.; Tosha, T.; Kubo, M.; Fujinami, S.; Ogura, T.; Kitagawa, T.; Suzuki, M. *Angew. Chem., Int. Ed.* 2009, 48, 3304-3307.
- (41) Kunishita, A.; Doi, Y.; Kubo, M.; Ogura, T.; Sugimoto, H.; Itoh, S. *Inorg. Chem.* 2009, 48, 4997-5004.
- (42) Tano, T.; Doi, Y.; Inosako, M.; Kunishita, A.; Kubo, M.; Ishimaru, H.; Ogura, T.; Sugimoto, H.; Itoh, S. *Bull. Chem. Soc. Jpn.* 2010, 83, 530-538.
- (43) Yao, S.; Driess, M. *Acc. Chem. Res.* 2012, 45, 276-287.
- (44) Kieber-Emmons, M. T.; Riordan, C. G. *Acc. Chem. Res.* 2007, 40, 618-625.
- (45) Suzuki, M. *Acc. Chem. Res.* 2007, 40, 609-617.
- (46) Cheng, C.-C.; Rokita, S. E.; Burrows, C. J. *Angew. Chem., Int. Ed. Engl.* 1993, 32, 277-278.
- (47) Liang, Q.; Ananias, D. C.; Long, E. C. *J. Am. Chem. Soc.* 1998, 120, 248-257.
- (48) Kasprzak, K. S.; Salnikow, K. *Met. Ions Life Sci.* 2007, 2, 619-660.
- (49) Kim, M.; Okajima, T.; Kishishita, S.; Yoshimura, M.; Kawamori, A. Tanizawa, K.; Yamaguchi, H. *Nat. Struct. Biol.* 2002, 9, 591-596(50) DuBois, J. L.; Klinman, J. P. *Biochemistry* 2005, 44, 11381-11388.
- (51) Prabhakar, R.; Siegbahn, P. E. M. *J. Am. Chem. Soc.* 2004, 126, 3996-4006.
- (52) Ghosh, S.; Cirera, J.; Vance, M. A.; Ono, T.; Fujisawa, K.; Solomon, E. I. *J. Am. Chem. Soc.* 2008, 130, 16262-16273.
- (53) Okajima, T.; Kishishita, S.; Chiu, Y.-C.; Murakawa, T.; Kim, M.; Yamaguchi, H.; Hirota, S.; Kuroda, S.; Tanizawa, K. *Biochemistry* 2005, 44, 12041-12048.
- (54) Samuels, N. M.; Klinman, J. P. *Biochemistry* 2005, 44, 14308-14317.

- (55) Fujisawa, K.; Iwata, Y.; Kitajima, N.; Higashimura, H.; Kubota, M.; Miyashita, Y.; Yamada, Y.; Okamoto, K.; Moro-oka, Y. *Chem. Lett.* 1999, 739-740.
- (56) Jazdzewski, B. A.; Holland, P. L.; Pink, M.; Young, V. G., Jr.; Spencer, D. J. E.; Tolman, W. B. *Inorg. Chem.* 2001, 40, 6097-6107.
- (57) Gorelsky, S. I.; Basumallick, L.; Vura-Weis, J.; Sarangi, R.; Hodgson, K. O.; Hedman, B.; Fujisawa, K.; Solomon, E. I. *Inorg. Chem.* 2005, 44, 4947-4960.
- (58) Chattopadhyay, S.; Deb, T.; Ma, H.; Petersen, J. L.; Young, V. G., Jr.; Jensen, M. P. *Inorg. Chem.* 2008, 47, 3384-3392.
- (59) Chattopadhyay, S.; Deb, T.; Petersen, J. L.; Young, V. G., Jr.; Jensen, M. P. *Inorg. Chem.* 2010, 49, 457-467.
- (60) Desrochers, P. J.; Cutts, R. W.; Rice, P. K.; Golden, M. L.; Graham, J. B.; Barclay, T. M.; Cordes, A. W. *Inorg. Chem.* 1999, 38, 5690-5694.
- (61) Nakazawa, J.; Ogiwara, H.; Kashiwazaki, Y.; Ishii, A.; Imamura, N.; Samejima, Y.; Hikichi, S. *Inorg. Chem.* 2011, 50, 9933-9935.
- (62) Rheingold, A. L.; Ostrander, R. L.; Haggerty, B. S.; Trofimenko, S. *Inorg. Chem.* 1994, 33, 3666-3676.
- (63) Trofimenko, S. *J. Am. Chem. Soc.* 1967, 89, 6288-6294.
- (64) Tabuchi, K.; Ertem, M. Z.; Sugimoto, H.; Kunishita, A.; Tano, T.; Fujieda, N.; Cramer, C. J.; Itoh, S. *Inorg. Chem.* 2011, 50, 1633-1647.
- (65) Santi, R.; Romano, A. M.; Sommazzi, A.; Grande, M.; Bianchini, C.; Mantovani, G. *J. Mol. Catal. A* 2005, 229, 191-197.
- (66) Uehara, K.; Hikichi, S.; Akita, M. *J. Chem. Soc., Dalton Trans.* 2002, 3529-3538.

- (67) Evans, D. F.; Jakubovic, D. A. *J. Chem. Soc., Dalton Trans.* 1988, 2927-2933.
- (68) Heyne, B.; Kohnen, S.; Brault, D.; Mouithys-Mickalad, A.; Tfibel, F.; Hans, P.; Fontaine-Aupart, M.-P.; Hoebeke, M. *Photochem. Photobiol. Sci.* 2003, 2, 939-945.
- (69) ADF 2008.01; Scientific Computing and Modelling NV, Vrije Universiteit: Amsterdam, Netherlands, 2008.
- (70) te Velde, G.; Bickelhaupt, F. M.; Baerends, E. J.; Fonseca Guerra, C.; van Gisbergen, S. J. A.; Snijders, J. G.; Ziegler, T. *J. Comput. Chem.* 2001, 22, 931-967.
- (71) Vosko, S. H.; Wilk, L.; Nusair, M. *Can. J. Phys.* 1980, 58, 1200-1211.
- (72) Becke, A. D. *Phys. Rev.* 1988, A38, 3098-3100.
- (73) Perdew, J. P. *Phys. Rev.* 1986, B33, 8822-8824.
- (74) APEX II; Bruker Analytical X-ray Systems: Madison, WI, 2001.
- (75) An empirical correction for absorption anisotropy: Blessing, R. H. *Acta Crystallogr.* 1995, A51, 33-38.
- (76) SAINT+, V7.68; Bruker Analytical X-Ray Systems: Madison, WI, 2003
- (77) SHELXTL, V2008/4; Bruker Analytical X-Ray Systems: Madison, WI, 2008.
- (78) Mercury, 3.0; Cambridge Crystallographic Data Centre: Cambridge, UK, 2011.
- (79) Ruman, T.; Ciunik, Z.; Szklanny, E.; Wołowiec, S. *Polyhedron* 2002, 21, 2743-2753.
- (80) Kharasch, M. S.; Joshi, B. S. *J. Org. Chem.* 1957, 22, 1439-1443.
- (81) Yang, L.; Powell, D. R.; Houser, R. P. *Dalton Trans.* 2007, 955-964.
- (82) Desrochers, P. J.; LeLievre, S.; Johnson, R. J.; Lamb, B. T.; Phelps, A. L.; Cordes, A. W.; Gu, W.; Cramer, S. P. *Inorg. Chem.* 2003, 42, 7945-7950.

- (83) Northcutt, T. O.; Lachicotte, R. J.; Jones, W. D. *Organometallics* 1998, 17, 5148-5152.
- (84) Desrochers, P. J.; Telser, J.; Zvyagin, S. A.; Ozarowski, A.; Krzystek, J.; Vicic, D. A. *Inorg. Chem.* 2006, 45, 8930-8941.
- (85) Addison, A. W.; Rao, T. N.; Reedijk, J.; van Rijn, J.; Verschoor, G. C. *J. Chem. Soc., Dalton Trans.* 1984, 1349-1356.
- (86) Fujisawa, K.; Tada, N.; Nishida, Y.; Miyashita, Y.; Okamoto, K. *Inorg. Chem. Commun.* 2008, 11, 381-384.
- (87) Mehn, M. P.; Fujisawa, K.; Hegg, E. L.; Que, L., Jr. *J. Am. Chem. Soc.* 2003, 125, 7828-7842.
- (88) Higgs, T. C.; Carrano, C. J. *Inorg. Chem.* 1997, 36, 298-306.
- (89) Kitajima, N.; Hikichi, S.; Tanaka, M.; Moro-oka, Y. *J. Am. Chem. Soc.* 1993, 115, 5496-5508.
- (90) Trofimenko, S.; Rheingold, A. L.; Liable Sands, L. M. *Inorg. Chem.* 2002, 41, 1889-1896.
- (91) Janiak, C.; Temizdemir, S.; Dechert, S.; Deck, W.; Girgsdies, F.; Heinze, J.; Kolm, M. J.; Scharmann, T. G.; Zipffel, O. M. *Eur. J. Inorg. Chem.* 2000, 1229-1241.
- (92) Bandoli, G.; Clemente, D. A.; Paolucci, G.; Doretto, L. *Cryst. Struct. Commun.* 1979, 8, 965-970.
- (93) Cecchi, P.; Gioia Lobbia, G.; Marchetti, F.; Valle, G.; Calogero, S. *Polyhedron* 1994, 13, 2173-2178.
- (94) Desrochers, P. J.; Brown, J. R.; Arvin, M. E.; Jones, G. D.; Vicic, D. A. *Acta Crystallogr.* 2005, E51, m1455-m1458.

- (95) Calabrese, J. C.; Trofimenko, S. *Inorg. Chem.* 1992, 31, 4810-4814.
- (96) Santana, M. D.; López-Banet, L.; García, G.; García, L.; Pérez, J.; Liu, M. *Eur. J. Inorg. Chem.* 2008, 4012-4018.
- (97) Hammes, B. S.; Luo, X.; Chohan, B. S.; Carrano, M. W.; Carrano, C. J. *J. Chem. Soc., Dalton Trans.* 2002, 3374-3380.
- (98) Adams, H.; Batten, S. R.; Davies, G. M.; Duriska, M. B.; Jeffery, J. C.; Jensen, P.; Lu, J.; Motson, G. R.; Coles, S. J.; Hursthouse, M. B.; Ward, M. D. *Dalton Trans.* 2005, 1910-1923.
- (99) Batten, S. R.; Duriska, M. B.; Jensen, P.; Lu, J. *Aust. J. Chem.* 2007, 60, 72-74.
- (100) Jesson, J. P.; Trofimenko, S.; Eaton, D. R. *J. Am. Chem. Soc.* 1967, 89, 3148-3158.
- (101) Fulmer, G. R.; Miller, A. J. M.; Sherden, N. H.; Gottlieb, H. E.; Nudelman, A.; Stoltz, B. M.; Bercaw, J. E.; Goldberg, K. I. *Organometallics* 2010, 29, 2176-2179.

APPENDIX A: PERMISSIONS FOR FIGURES

Rightslink® by Copyright Clearance Center

Page 1 of 1



RightsLink®

Home

Create
Account

Help

ACS Publications **Title:**
High quality. High impact.2,4,5-Trihydroxyphenylalanine
Quinone Biogenesis in the
Copper Amine Oxidase from
Hansenula polymorpha with the
Alternate Metal Nickel†**Author:** Nicole M. Samuels and
Judith P. Klinman***Publication:** Biochemistry**Publisher:** American Chemical Society**Date:** Nov 1, 2005

Copyright © 2005, American Chemical Society

User ID
Password
<input type="checkbox"/> Enable Auto Login
LOGIN
Forgot Password/User ID?
If you're a copyright.com user, you can login to RightsLink using your copyright.com credentials. Already a RightsLink user or want to learn more?

PERMISSION/LICENSE IS GRANTED FOR YOUR ORDER AT NO CHARGE

This type of permission/license, instead of the standard Terms & Conditions, is sent to you because no fee is being charged for your order. Please note the following:

- Permission is granted for your request in both print and electronic formats, and translations.
- If figures and/or tables were requested, they may be adapted or used in part.
- Please print this page for your records and send a copy of it to your publisher/graduate school.
- Appropriate credit for the requested material should be given as follows: "Reprinted (adapted) with permission from (COMPLETE REFERENCE CITATION). Copyright (YEAR) American Chemical Society." Insert appropriate information in place of the capitalized words.
- One-time permission is granted only for the use specified in your request. No additional uses are granted (such as derivative works or other editions). For any other uses, please submit a new request

Rightslink® by Copyright Clearance Center



RightsLink®

Home

Create
Account

Help

ACS Publications
high quality | high impact.

Title: Nickel-Mediated Formation of Thio Esters from Bound Methyl, Thiols, and Carbon Monoxide: A Possible Reaction Pathway of Acetyl-Coenzyme A Synthase Activity in Nickel-Containing Carbon Monoxide Dehydrogenases

Author: Gregory C. Tucci and R. H. Holm

Publication: Journal of the American Chemical Society

Publisher: American Chemical Society

Date: Jun 1, 1995

Copyright © 1995, American Chemical Society

User ID
Password
<input type="checkbox"/> Enable Auto Login
LOGIN
Forgot Password/User ID?
If you're a copyright.com user, you can login to RightsLink using your copyright.com credentials.
Already a RightsLink user or want to learn more?

PERMISSION/LICENSE IS GRANTED FOR YOUR ORDER AT NO CHARGE

This type of permission/license, instead of the standard Terms & Conditions, is sent to you because no fee is being charged for your order. Please note the following:

- Permission is granted for your request in both print and electronic formats, and translations.
- If figures and/or tables were requested, they may be adapted or used in part.
- Please print this page for your records and send a copy of it to your publisher/graduate school.
- Appropriate credit for the requested material should be given as follows: "Reprinted (adapted) with permission from (COMPLETE REFERENCE CITATION). Copyright (YEAR) American Chemical Society." Insert appropriate information in place of the capitalized words.
- One-time permission is granted only for the use specified in your request. No additional uses are granted (such as derivative works or other editions). For any other uses, please submit a new request.

If credit is given to another source for the material you requested, permission must be obtained from that source.



RightsLink®

Home

Account
Info

Help

Structure

Title: Unusual ligand structure in Ni-Fe active center and an additional Mg site in hydrogenase revealed by high resolution X-ray structure analysis

Author: Yoshiki Higuchi, Tatsuhiko Yagi, Noritake Yasuoka

Publication: Structure

Publisher: Elsevier

Date: 15 December 1997

Copyright © 1997, Elsevier

Logged in as:
Tapash Deb

LOGOUT

Order Completed

Thank you very much for your order.

This is a License Agreement between Tapash Deb ("You") and Elsevier ("Elsevier"). The license consists of your order details, the terms and conditions provided by Elsevier, and the [payment terms and conditions](#).

[Get the printable license.](#)

License Number	3200970791791
License date	Aug 02, 2013
Licensed content publisher	Elsevier
Licensed content publication	Structure
Licensed content title	Unusual ligand structure in Ni-Fe active center and an additional Mg site in hydrogenase revealed by high resolution X-ray structure analysis
Licensed content author	Yoshiki Higuchi, Tatsuhiko Yagi, Noritake Yasuoka
Licensed content date	15 December 1997
Licensed content volume number	5

APPENDIX B: CRYSTAL DATA REFINEMENT AND BOND LENGTHS FOR

COMPLEX 2.1A

Table B1. Crystal data and structure refinement for $(C_{15}H_{22}N_6B)Ni(SPh)$ (**2.1a**).

Empirical formula	$C_{21}H_{27}BN_6Ni S$	
Formula weight	465.07	
Temperature	293(2) K	
Wavelength	0.71073 Å	
Crystal system	orthorhombic	
Space group	Pbca	
Unit cell dimensions	$a = 15.2586(16)$ Å	$\alpha = 90^\circ$
	$b = 14.4267(14)$ Å	$\beta = 90^\circ$
	$c = 21.182(2)$ Å	$\gamma = 90^\circ$
Volume	$4662.9(8)$ Å ³	
Z	8	
Density (calculated)	1.325 g/cm ³	
Absorption coefficient	9.41 cm ⁻¹	
F(000)	1952	
Crystal size	0.10 x 0.21 x 0.58 mm	
θ range for data collection	2.17 to 27.49°	
Index ranges	$-19 \leq h \leq 19, -18 \leq k \leq 16, -27 \leq l \leq 26$	
Reflections collected	30478	
Independent reflections	5327 [R(int) = 0.0528]	
Completeness to $\theta = 27.49^\circ$	99.4 %	
Refinement method	Full-matrix least-squares on F ²	
Data / restraints / parameters	5327 / 0 / 277	
Goodness-of-fit on F ²	1.043	
Final R indices [I > 2 σ (I)]	R1 = 0.0401, wR2 = 0.1061	
R indices (all data)	R1 = 0.0614, wR2 = 0.1246	
Largest diff. peak and hole	0.431 and -0.450 e/Å ³	

Table B2. Atomic coordinates ($\times 10^4$) and equivalent isotropic displacement parameters ($\text{\AA}^2 \times 10^3$) for $(\text{C}_{15}\text{H}_{22}\text{N}_6\text{B})\text{Ni}(\text{SPh})$ (**2.1a**). $U(\text{eq})$ is defined as one third of the trace of the orthogonalized U_{ij} tensor.

	x	y	z	U(eq)
Ni(1)	1496(1)	5008(1)	1637(1)	46(1)
S(1)	1099(1)	4697(1)	2621(1)	64(1)
N(1)	1196(1)	4490(1)	800(1)	53(1)
N(2)	1494(1)	4977(1)	286(1)	51(1)
N(3)	1129(1)	6264(1)	1350(1)	50(1)
N(4)	1521(1)	6554(1)	797(1)	49(1)
N(5)	2736(1)	5225(1)	1390(1)	45(1)
N(6)	2868(1)	5569(1)	794(1)	46(1)
C(1)	702(2)	3787(2)	584(1)	61(1)
C(2)	682(2)	3828(2)	-73(1)	69(1)
C(3)	1180(2)	4581(2)	-250(1)	60(1)
C(4)	705(2)	6993(2)	1590(1)	55(1)
C(5)	817(2)	7752(2)	1199(1)	60(1)
C(6)	1338(2)	7465(2)	707(1)	54(1)
C(7)	3520(2)	5118(2)	1658(1)	47(1)
C(8)	4170(2)	5391(2)	1231(1)	52(1)
C(9)	3738(2)	5671(2)	690(1)	49(1)
C(10)	278(2)	3128(2)	1025(2)	81(1)
C(11)	1385(3)	4944(2)	-891(1)	83(1)
C(12)	220(2)	6929(2)	2202(1)	71(1)
C(13)	1702(2)	8015(2)	172(2)	72(1)
C(14)	3616(2)	4759(2)	2312(1)	59(1)
C(15)	4107(2)	6009(2)	79(1)	69(1)
C(16)	1619(2)	3625(2)	2786(1)	51(1)
C(17)	1953(2)	3046(2)	2323(1)	60(1)
C(18)	2355(2)	2221(2)	2483(2)	78(1)
C(19)	2434(2)	1966(2)	3103(2)	95(1)
C(20)	2091(3)	2525(2)	3562(2)	104(1)
C(21)	1689(2)	3348(2)	3407(1)	76(1)
B(1)	2057(2)	5853(2)	401(1)	48(1)

Table B3. Complete interatomic distances [\AA] and bond angles [$^\circ$] for $(\text{C}_{15}\text{H}_{22}\text{N}_6\text{B})\text{Ni}(\text{SPh})$ (**2.1a**).

Ni(1)-N(1)	1.978(2)	C(18)-C(19)	1.369(5)
Ni(1)-N(5)	1.988(2)	C(19)-C(20)	1.367(5)
Ni(1)-N(3)	1.992(2)	C(20)-C(21)	1.376(5)
Ni(1)-S(1)	2.216(1)		
S(1)-C(16)	1.771(2)	N(1)-Ni(1)-N(5)	92.48(8)
N(1)-C(1)	1.344(3)	N(1)-Ni(1)-N(3)	90.25(8)
N(1)-N(2)	1.373(3)	N(5)-Ni(1)-N(3)	92.49(8)
N(2)-C(3)	1.357(3)	N(1)-Ni(1)-S(1)	134.69(6)
N(2)-B(1)	1.547(3)	N(5)-Ni(1)-S(1)	122.69(6)
N(3)-C(4)	1.336(3)	N(3)-Ni(1)-S(1)	113.26(6)
N(3)-N(4)	1.380(3)	C(16)-S(1)-Ni(1)	103.84(8)
N(4)-C(6)	1.357(3)	C(1)-N(1)-N(2)	107.5(2)
N(4)-B(1)	1.548(3)	C(1)-N(1)-Ni(1)	136.1(2)
N(5)-C(7)	1.333(3)	N(2)-N(1)-Ni(1)	116.2(1)
N(5)-N(6)	1.372(2)	C(3)-N(2)-N(1)	109.3(2)
N(6)-C(9)	1.354(3)	C(3)-N(2)-B(1)	132.2(2)
N(6)-B(1)	1.547(3)	N(1)-N(2)-B(1)	118.4(2)
C(1)-C(2)	1.393(4)	C(4)-N(3)-N(4)	107.2(2)
C(1)-C(10)	1.482(4)	C(4)-N(3)-Ni(1)	137.4(2)
C(2)-C(3)	1.378(4)	N(4)-N(3)-Ni(1)	114.4(1)
C(3)-C(11)	1.490(4)	C(6)-N(4)-N(3)	108.9(2)
C(4)-C(5)	1.384(4)	C(6)-N(4)-B(1)	131.7(2)
C(4)-C(12)	1.496(4)	N(3)-N(4)-B(1)	119.4(2)
C(5)-C(6)	1.375(4)	C(7)-N(5)-N(6)	107.6(2)
C(6)-C(13)	1.491(4)	C(7)-N(5)-Ni(1)	136.3(2)
C(7)-C(8)	1.399(3)	N(6)-N(5)-Ni(1)	116.1(1)
C(7)-C(14)	1.486(3)	C(9)-N(6)-N(5)	109.5(2)
C(8)-C(9)	1.383(3)	C(9)-N(6)-B(1)	132.0(2)
C(9)-C(15)	1.493(3)	N(5)-N(6)-B(1)	118.2(2)
C(16)-C(21)	1.381(4)	N(1)-C(1)-C(2)	108.7(2)
C(16)-C(17)	1.386(3)	N(1)-C(1)-C(10)	120.9(2)
C(17)-C(18)	1.380(4)	C(2)-C(1)-C(10)	130.3(2)

C(3)-C(2)-C(1)	107.0(2)	N(6)-C(9)-C(8)	107.5(2)
N(2)-C(3)-C(2)	107.4(2)	N(6)-C(9)-C(15)	123.1(2)
N(2)-C(3)-C(11)	122.7(3)	C(8)-C(9)-C(15)	129.4(2)
C(2)-C(3)-C(11)	129.8(2)	C(21)-C(16)-C(17)	118.1(2)
N(3)-C(4)-C(5)	109.5(2)	C(21)-C(16)-S(1)	118.4(2)
N(3)-C(4)-C(12)	121.5(2)	C(17)-C(16)-S(1)	123.5(2)
C(5)-C(4)-C(12)	128.9(2)	C(18)-C(17)-C(16)	120.7(3)
C(6)-C(5)-C(4)	106.7(2)	C(19)-C(18)-C(17)	120.4(3)
N(4)-C(6)-C(5)	107.7(2)	C(20)-C(19)-C(18)	119.4(3)
N(4)-C(6)-C(13)	123.1(2)	C(19)-C(20)-C(21)	120.6(3)
C(5)-C(6)-C(13)	129.2(2)	C(20)-C(21)-C(16)	120.8(3)
N(5)-C(7)-C(8)	109.2(2)	N(2)-B(1)-N(6)	108.3(2)
N(5)-C(7)-C(14)	121.8(2)	N(2)-B(1)-N(4)	109.0(2)
C(8)-C(7)-C(14)	129.1(2)	N(6)-B(1)-N(4)	107.7(2)
C(9)-C(8)-C(7)	106.3(2)		

APPENDIX C: CRYSTAL DATA REFINEMENT AND BOND LENGTHS 2.2C

Table C1. Crystal data and structure refinement for 2.2c.

Empirical formula	C ₄₂ H ₄₃ B N ₈ Ni S	
Formula weight	761.42	
Temperature	173(2) K	
Wavelength	0.71073 Å	
Crystal system	Monoclinic	
Space group	P2 ₁ /c	
Unit cell dimensions	$a = 10.8543(8) \text{ \AA}$	$\alpha = 90^\circ$
	$b = 39.977(3) \text{ \AA}$	$\beta = 114.972(1)^\circ$
	$c = 10.1747(8) \text{ \AA}$	$\gamma = 90^\circ$
Volume	4002.3(5) Å ³	
Z	4	
Density (calculated)	1.264 Mg/m ³	
Absorption coefficient	0.577 mm ⁻¹	
F(000)	1600	
Crystal color, morphology	Purple, Needle	
Crystal size	0.45 x 0.15 x 0.15 mm ³	
Theta range for data collection	2.04 to 27.51°	
Index ranges	$-14 \leq h \leq 12, 0 \leq k \leq 51, 0 \leq l \leq 13$	
Reflections collected	42917	
Independent reflections	9109 [$R(\text{int}) = 0.0438$]	
Observed reflections	7037	
Completeness to theta = 27.51°	99.0%	
Absorption correction	Multi-scan	
Max. and min. transmission	0.9184 and 0.7812	
Refinement method	Full-matrix least-squares on F^2	
Data / restraints / parameters	9109 / 0 / 488	
Goodness-of-fit on F^2	1.051	
Final R indices [$I > 2\sigma(I)$]	$R1 = 0.0402, wR2 = 0.0949$	
R indices (all data)	$R1 = 0.0579, wR2 = 0.1008$	
Largest diff. peak and hole	0.372 and -0.327 e.Å ⁻³	

Table C2. Atomic coordinates ($\times 10^4$) and equivalent isotropic displacement parameters ($\text{\AA}^2 \times 10^3$) for **2.2c**. U_{eq} is defined as one third of the trace of the orthogonalized U_{ij} tensor.

	x	y	z	U_{eq}
Ni1	1977(1)	1319(1)	3390(1)	20(1)
B1	681(2)	690(1)	1680(2)	22(1)
N1	70(2)	1004(1)	764(2)	22(1)
N2	379(2)	1313(1)	1406(2)	23(1)
C1	-1239(2)	743(1)	-1665(2)	34(1)
C2	-722(2)	1037(1)	-670(2)	24(1)
C3	-949(2)	1374(1)	-966(2)	26(1)
C4	-259(2)	1538(1)	353(2)	23(1)
C5	-276(2)	1898(1)	679(2)	26(1)
C6	-936(2)	2002(1)	1521(2)	35(1)
C7	-994(3)	2340(1)	1804(3)	47(1)
C8	-371(3)	2571(1)	1287(3)	50(1)
C9	276(3)	2472(1)	459(3)	51(1)
C10	309(3)	2135(1)	133(2)	38(1)
N3	474(2)	706(1)	3089(2)	23(1)
N4	1070(2)	959(1)	4063(2)	22(1)
C11	-918(2)	190(1)	2816(3)	38(1)
C12	-164(2)	492(1)	3630(2)	26(1)
C13	34(2)	605(1)	4979(2)	28(1)
C14	807(2)	898(1)	5216(2)	23(1)
C15	1337(2)	1112(1)	6513(2)	24(1)
C16	1272(2)	1459(1)	6411(2)	27(1)
C17	1854(2)	1656(1)	7643(2)	35(1)
C18	2481(3)	1508(1)	8991(3)	41(1)
C19	2521(3)	1164(1)	9112(2)	41(1)
C20	1960(2)	967(1)	7885(2)	32(1)
N5	2229(2)	691(1)	2099(2)	23(1)
N6	2968(2)	971(1)	2746(2)	22(1)
C21	2514(3)	134(1)	1136(3)	42(1)
C22	3033(2)	464(1)	1857(2)	28(1)

C23	4321(2)	595(1)	2370(2)	30(1)
C24	4245(2)	913(1)	2908(2)	24(1)
C25	5333(2)	1165(1)	3497(2)	26(1)
C26	5070(2)	1503(1)	3173(2)	31(1)
C27	6114(3)	1735(1)	3734(3)	40(1)
C28	7424(3)	1629(1)	4591(3)	48(1)
C29	7686(2)	1295(1)	4909(3)	45(1)
C30	6653(2)	1062(1)	4369(2)	35(1)
S1	2391(1)	1856(1)	3820(1)	28(1)
C31	3932(2)	1963(1)	5317(2)	23(1)
C32	4339(2)	2300(1)	5357(2)	31(1)
C33	5513(2)	2408(1)	6525(3)	43(1)
C34	6267(2)	2196(1)	7631(3)	47(1)
C35	5879(2)	1866(1)	7572(2)	37(1)
C36	4734(2)	1741(1)	6418(2)	26(1)
C37	3551(3)	2543(1)	4176(3)	44(1)
C38	4432(2)	1374(1)	6394(2)	31(1)
N7	5973(4)	604(1)	-324(4)	91(1)
C39	6346(3)	852(1)	220(3)	59(1)
C40	6847(4)	1170(1)	924(4)	79(1)
N8	2742(3)	-128(1)	4627(3)	71(1)
C41	3308(3)	106(1)	5185(3)	50(1)
C42	4043(3)	407(1)	5898(3)	60(1)

Table C3. Complete bond lengths [\AA] and angles [$^\circ$] for **2.2c**.

Ni(1)-N(4)	2.0187(16)	C(11)-H(11A)	0.9800
Ni(1)-N(6)	2.0301(16)	C(11)-H(11B)	0.9800
Ni(1)-N(2)	2.0319(16)	C(11)-H(11C)	0.9800
Ni(1)-S(1)	2.1978(5)	C(12)-C(13)	1.374(3)
B(1)-N(1)	1.540(3)	C(13)-C(14)	1.398(3)
B(1)-N(3)	1.543(3)	C(13)-H(13A)	0.9500
B(1)-N(5)	1.550(3)	C(14)-C(15)	1.472(3)
B(1)-H(1A)	1.09(2)	C(15)-C(16)	1.392(3)
N(1)-C(2)	1.351(2)	C(15)-C(20)	1.395(3)
N(1)-N(2)	1.370(2)	C(16)-C(17)	1.385(3)
N(2)-C(4)	1.345(2)	C(16)-H(16A)	0.9500
C(1)-C(2)	1.498(3)	C(17)-C(18)	1.381(3)
C(1)-H(1B)	0.9800	C(17)-H(17A)	0.9500
C(1)-H(1C)	0.9800	C(18)-C(19)	1.379(3)
C(1)-H(1D)	0.9800	C(18)-H(18A)	0.9500
C(2)-C(3)	1.380(3)	C(19)-C(20)	1.382(3)
C(3)-C(4)	1.394(3)	C(19)-H(19A)	0.9500
C(3)-H(3A)	0.9500	C(20)-H(20A)	0.9500
C(4)-C(5)	1.478(3)	N(5)-C(22)	1.351(3)
C(5)-C(10)	1.382(3)	N(5)-N(6)	1.372(2)
C(5)-C(6)	1.391(3)	N(6)-C(24)	1.344(2)
C(6)-C(7)	1.389(3)	C(21)-C(22)	1.497(3)
C(6)-H(6A)	0.9500	C(21)-H(21A)	0.9800
C(7)-C(8)	1.375(4)	C(21)-H(21B)	0.9800
C(7)-H(7A)	0.9500	C(21)-H(21C)	0.9800
C(8)-C(9)	1.364(4)	C(22)-C(23)	1.374(3)
C(8)-H(8A)	0.9500	C(23)-C(24)	1.401(3)
C(9)-C(10)	1.390(3)	C(23)-H(23A)	0.9500
C(9)-H(9A)	0.9500	C(24)-C(25)	1.473(3)
C(10)-H(10A)	0.9500	C(25)-C(26)	1.389(3)
N(3)-C(12)	1.356(2)	C(25)-C(30)	1.392(3)
N(3)-N(4)	1.371(2)	C(26)-C(27)	1.388(3)
N(4)-C(14)	1.342(2)	C(26)-H(26A)	0.9500
C(11)-C(12)	1.495(3)	C(27)-C(28)	1.384(4)

C(27)-H(27A)	0.9500	N(4)-Ni(1)-S(1)	135.73(5)
C(28)-C(29)	1.374(4)	N(6)-Ni(1)-S(1)	129.95(5)
C(28)-H(28A)	0.9500	N(2)-Ni(1)-S(1)	103.05(5)
C(29)-C(30)	1.381(3)	N(1)-B(1)-N(3)	109.36(16)
C(29)-H(29A)	0.9500	N(1)-B(1)-N(5)	107.71(15)
C(30)-H(30A)	0.9500	N(3)-B(1)-N(5)	108.14(16)
S(1)-C(31)	1.7753(19)	N(1)-B(1)-H(1A)	111.1(11)
C(31)-C(36)	1.407(3)	N(3)-B(1)-H(1A)	110.0(11)
C(31)-C(32)	1.412(3)	N(5)-B(1)-H(1A)	110.4(11)
C(32)-C(33)	1.394(3)	C(2)-N(1)-N(2)	110.12(15)
C(32)-C(37)	1.501(3)	C(2)-N(1)-B(1)	130.35(16)
C(33)-C(34)	1.371(4)	N(2)-N(1)-B(1)	119.45(15)
C(33)-H(33A)	0.9500	C(4)-N(2)-N(1)	106.37(15)
C(34)-C(35)	1.376(3)	C(4)-N(2)-Ni(1)	136.11(13)
C(34)-H(34A)	0.9500	N(1)-N(2)-Ni(1)	114.74(11)
C(35)-C(36)	1.393(3)	C(2)-C(1)-H(1B)	109.5
C(35)-H(35A)	0.9500	C(2)-C(1)-H(1C)	109.5
C(36)-C(38)	1.503(3)	H(1B)-C(1)-H(1C)	109.5
C(37)-H(37A)	0.9800	C(2)-C(1)-H(1D)	109.5
C(37)-H(37B)	0.9800	H(1B)-C(1)-H(1D)	109.5
C(37)-H(37C)	0.9800	H(1C)-C(1)-H(1D)	109.5
C(38)-H(38A)	0.9800	N(1)-C(2)-C(3)	107.68(17)
C(38)-H(38B)	0.9800	N(1)-C(2)-C(1)	122.70(18)
C(38)-H(38C)	0.9800	C(3)-C(2)-C(1)	129.60(18)
N(7)-C(39)	1.125(4)	C(2)-C(3)-C(4)	105.91(17)
C(39)-C(40)	1.445(5)	C(2)-C(3)-H(3A)	127.0
C(40)-H(40A)	0.9800	C(4)-C(3)-H(3A)	127.0
C(40)-H(40B)	0.9800	N(2)-C(4)-C(3)	109.89(17)
C(40)-H(40C)	0.9800	N(2)-C(4)-C(5)	121.49(17)
N(8)-C(41)	1.129(4)	C(3)-C(4)-C(5)	128.37(17)
C(41)-C(42)	1.458(4)	C(10)-C(5)-C(6)	119.1(2)
C(42)-H(42A)	0.9800	C(10)-C(5)-C(4)	121.77(19)
C(42)-H(42B)	0.9800	C(6)-C(5)-C(4)	119.14(19)
C(42)-H(42C)	0.9800	C(7)-C(6)-C(5)	119.9(2)
N(4)-Ni(1)-N(6)	91.23(6)	C(7)-C(6)-H(6A)	120.1
N(4)-Ni(1)-N(2)	89.70(6)	C(5)-C(6)-H(6A)	120.1
N(6)-Ni(1)-N(2)	91.02(6)	C(8)-C(7)-C(6)	120.2(2)

C(8)-C(7)-H(7A)	119.9	C(15)-C(16)-H(16A)	119.7
C(6)-C(7)-H(7A)	119.9	C(18)-C(17)-C(16)	120.0(2)
C(9)-C(8)-C(7)	120.3(2)	C(18)-C(17)-H(17A)	120.0
C(9)-C(8)-H(8A)	119.8	C(16)-C(17)-H(17A)	120.0
C(7)-C(8)-H(8A)	119.8	C(19)-C(18)-C(17)	120.0(2)
C(8)-C(9)-C(10)	120.1(3)	C(19)-C(18)-H(18A)	120.0
C(8)-C(9)-H(9A)	120.0	C(17)-C(18)-H(18A)	120.0
C(10)-C(9)-H(9A)	120.0	C(18)-C(19)-C(20)	120.2(2)
C(5)-C(10)-C(9)	120.4(2)	C(18)-C(19)-H(19A)	119.9
C(5)-C(10)-H(10A)	119.8	C(20)-C(19)-H(19A)	119.9
C(9)-C(10)-H(10A)	119.8	C(19)-C(20)-C(15)	120.6(2)
C(12)-N(3)-N(4)	109.81(15)	C(19)-C(20)-H(20A)	119.7
C(12)-N(3)-B(1)	130.43(16)	C(15)-C(20)-H(20A)	119.7
N(4)-N(3)-B(1)	119.61(15)	C(22)-N(5)-N(6)	110.11(16)
C(14)-N(4)-N(3)	106.66(15)	C(22)-N(5)-B(1)	131.02(16)
C(14)-N(4)-Ni(1)	137.85(13)	N(6)-N(5)-B(1)	118.72(15)
N(3)-N(4)-Ni(1)	115.39(12)	C(24)-N(6)-N(5)	106.44(15)
C(12)-C(11)-H(11A)	109.5	C(24)-N(6)-Ni(1)	137.45(13)
C(12)-C(11)-H(11B)	109.5	N(5)-N(6)-Ni(1)	115.62(12)
H(11A)-C(11)-H(11B)	109.5	C(22)-C(21)-H(21A)	109.5
C(12)-C(11)-H(11C)	109.5	C(22)-C(21)-H(21B)	109.5
H(11A)-C(11)-H(11C)	109.5	H(21A)-C(21)-H(21B)	109.5
H(11B)-C(11)-H(11C)	109.5	C(22)-C(21)-H(21C)	109.5
N(3)-C(12)-C(13)	107.76(17)	H(21A)-C(21)-H(21C)	109.5
N(3)-C(12)-C(11)	122.60(18)	H(21B)-C(21)-H(21C)	109.5
C(13)-C(12)-C(11)	129.64(19)	N(5)-C(22)-C(23)	107.79(17)
C(12)-C(13)-C(14)	106.14(18)	N(5)-C(22)-C(21)	122.81(19)
C(12)-C(13)-H(13A)	126.9	C(23)-C(22)-C(21)	129.4(2)
C(14)-C(13)-H(13A)	126.9	C(22)-C(23)-C(24)	106.10(18)
N(4)-C(14)-C(13)	109.62(17)	C(22)-C(23)-H(23A)	127.0
N(4)-C(14)-C(15)	122.00(17)	C(24)-C(23)-H(23A)	127.0
C(13)-C(14)-C(15)	128.33(18)	N(6)-C(24)-C(23)	109.56(17)
C(16)-C(15)-C(20)	118.56(19)	N(6)-C(24)-C(25)	122.77(17)
C(16)-C(15)-C(14)	121.71(18)	C(23)-C(24)-C(25)	127.59(18)
C(20)-C(15)-C(14)	119.70(18)	C(26)-C(25)-C(30)	119.5(2)
C(17)-C(16)-C(15)	120.6(2)	C(26)-C(25)-C(24)	121.19(18)
C(17)-C(16)-H(16A)	119.7	C(30)-C(25)-C(24)	119.31(19)

C(27)-C(26)-C(25)	120.1(2)	C(32)-C(37)-H(37C)	109.5
C(27)-C(26)-H(26A)	119.9	H(37A)-C(37)-H(37C)	109.5
C(25)-C(26)-H(26A)	119.9	H(37B)-C(37)-H(37C)	109.5
C(28)-C(27)-C(26)	119.8(2)	C(36)-C(38)-H(38A)	109.5
C(28)-C(27)-H(27A)	120.1	C(36)-C(38)-H(38B)	109.5
C(26)-C(27)-H(27A)	120.1	H(38A)-C(38)-H(38B)	109.5
C(29)-C(28)-C(27)	120.1(2)	C(36)-C(38)-H(38C)	109.5
C(29)-C(28)-H(28A)	119.9	H(38A)-C(38)-H(38C)	109.5
C(27)-C(28)-H(28A)	119.9	H(38B)-C(38)-H(38C)	109.5
C(28)-C(29)-C(30)	120.6(2)	N(7)-C(39)-C(40)	179.1(4)
C(28)-C(29)-H(29A)	119.7	C(39)-C(40)-H(40A)	109.5
C(30)-C(29)-H(29A)	119.7	C(39)-C(40)-H(40B)	109.5
C(29)-C(30)-C(25)	119.8(2)	H(40A)-C(40)-H(40B)	109.5
C(29)-C(30)-H(30A)	120.1	C(39)-C(40)-H(40C)	109.5
C(25)-C(30)-H(30A)	120.1	H(40A)-C(40)-H(40C)	109.5
C(31)-S(1)-Ni(1)	116.51(7)	H(40B)-C(40)-H(40C)	109.5
C(36)-C(31)-C(32)	119.86(18)	N(8)-C(41)-C(42)	179.5(3)
C(36)-C(31)-S(1)	124.94(15)	C(41)-C(42)-H(42A)	109.5
C(32)-C(31)-S(1)	115.19(15)	C(41)-C(42)-H(42B)	109.5
C(33)-C(32)-C(31)	118.8(2)	H(42A)-C(42)-H(42B)	109.5
C(33)-C(32)-C(37)	119.2(2)	C(41)-C(42)-H(42C)	109.5
C(31)-C(32)-C(37)	121.92(19)	H(42A)-C(42)-H(42C)	109.5
C(34)-C(33)-C(32)	121.4(2)	H(42B)-C(42)-H(42C)	109.5
C(34)-C(33)-H(33A)	119.3		
C(32)-C(33)-H(33A)	119.3		
C(33)-C(34)-C(35)	119.4(2)		
C(33)-C(34)-H(34A)	120.3		
C(35)-C(34)-H(34A)	120.3		
C(34)-C(35)-C(36)	121.9(2)		
C(34)-C(35)-H(35A)	119.1		
C(36)-C(35)-H(35A)	119.1		
C(35)-C(36)-C(31)	118.46(19)		
C(35)-C(36)-C(38)	118.41(19)		
C(31)-C(36)-C(38)	123.12(18)		
C(32)-C(37)-H(37A)	109.5		
C(32)-C(37)-H(37B)	109.5		
H(37A)-C(37)-H(37B)	109.5		

APPENDIX D: ELECTRONIC SPECTRA AND CONFIGURATIONAL DATA

FOR CHAPTER 3

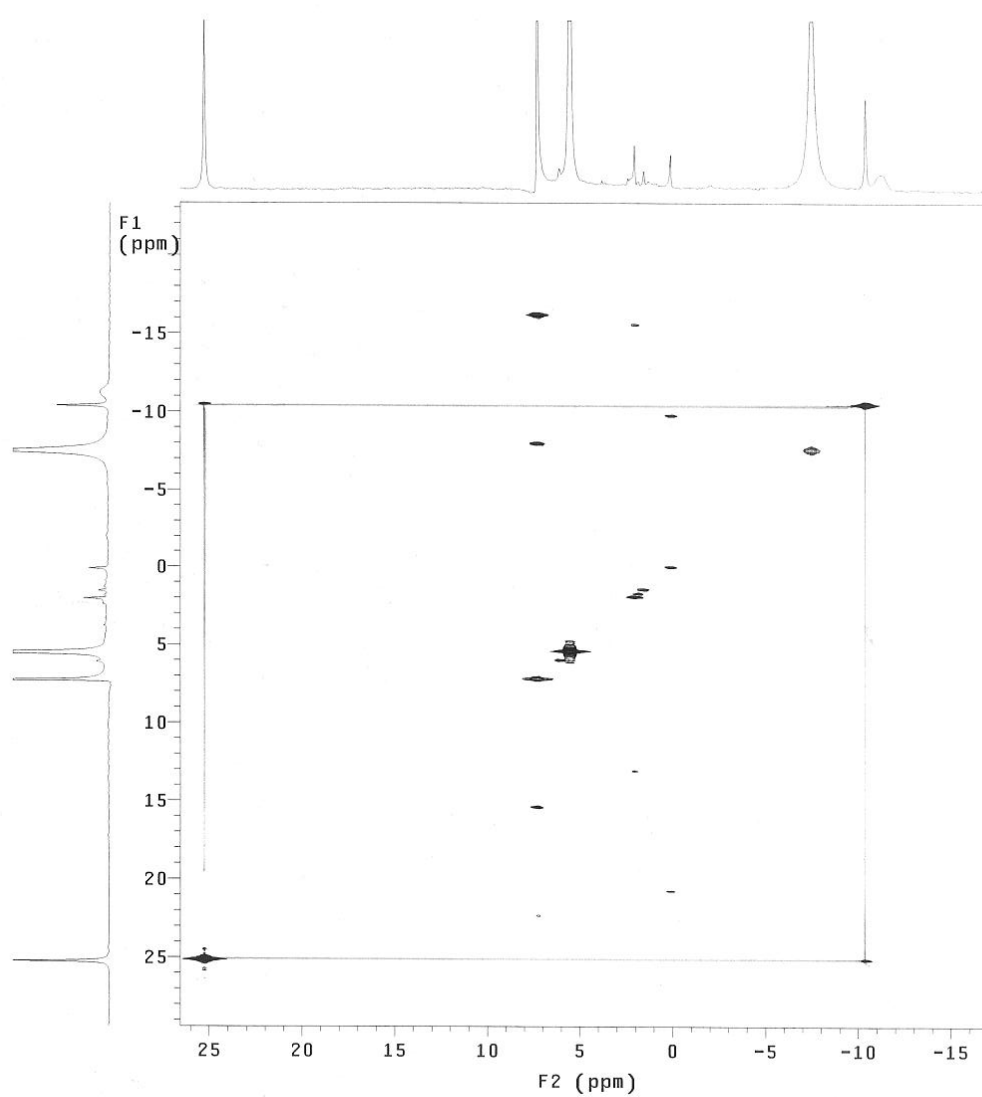


Figure 3-S1. Excerpt of COSY for **3.2** in CDCl₃, demonstrating J-coupling between assigned *meta* and *para* arylthiolate proton resonances.

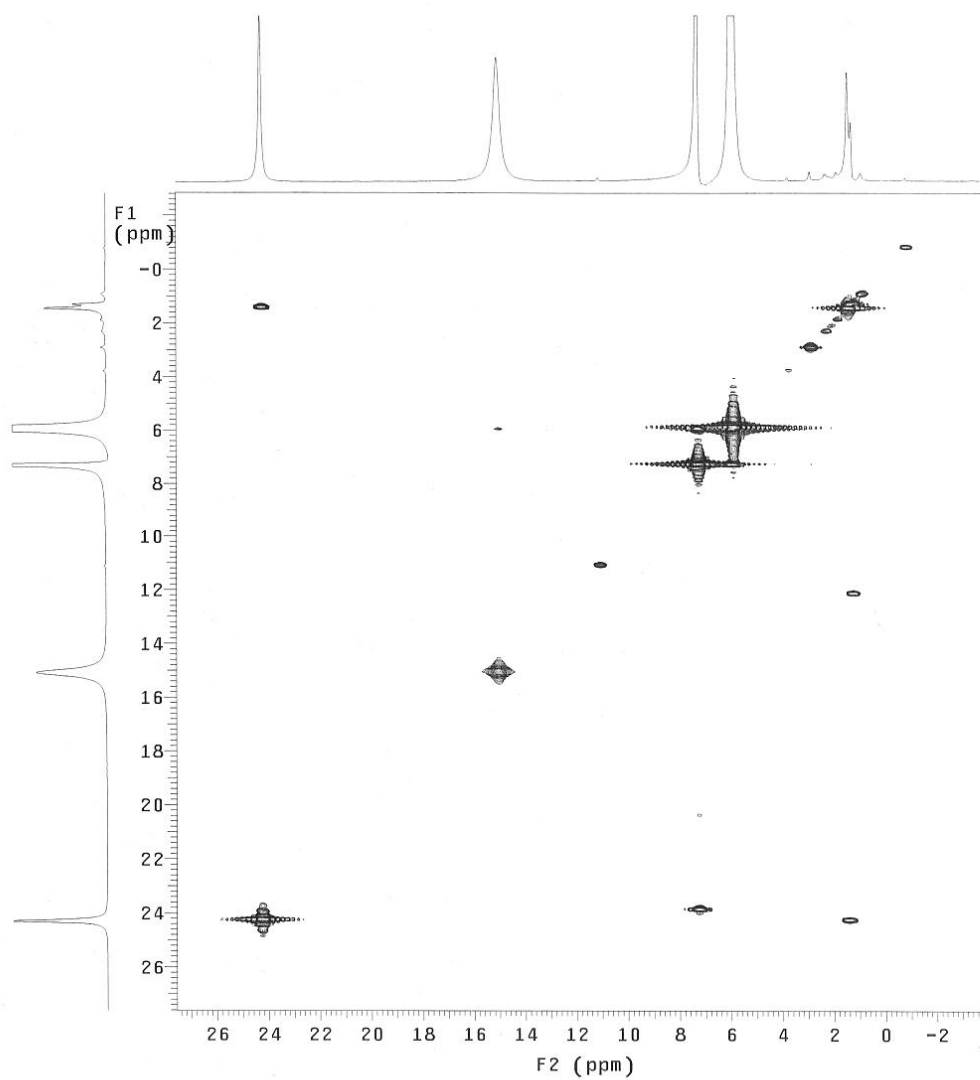


Figure 3-S2. Excerpt of COSY for **3.5** in CDCl_3 , demonstrating J-coupling between assigned *meta* and *para* arylthiolate proton resonances.

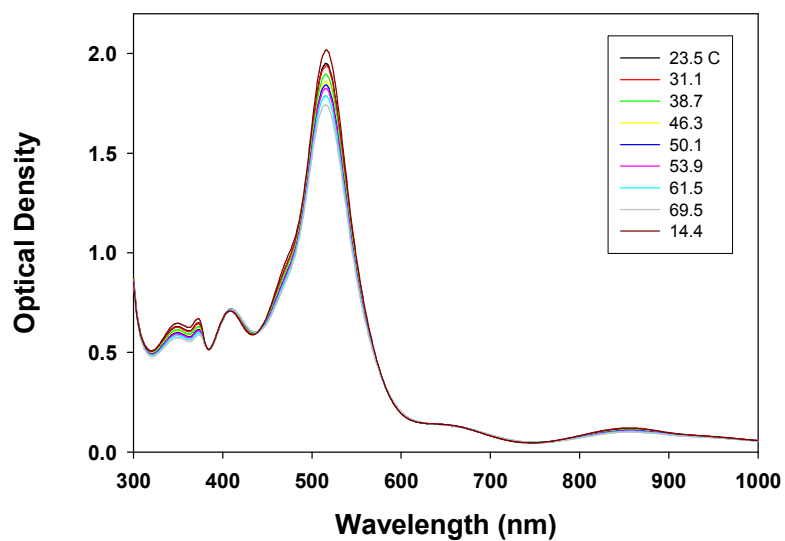


Figure 3-S3. Raw absorption data (uncorrected for changes in solvent density) for **3.3** in toluene as a function of temperature.

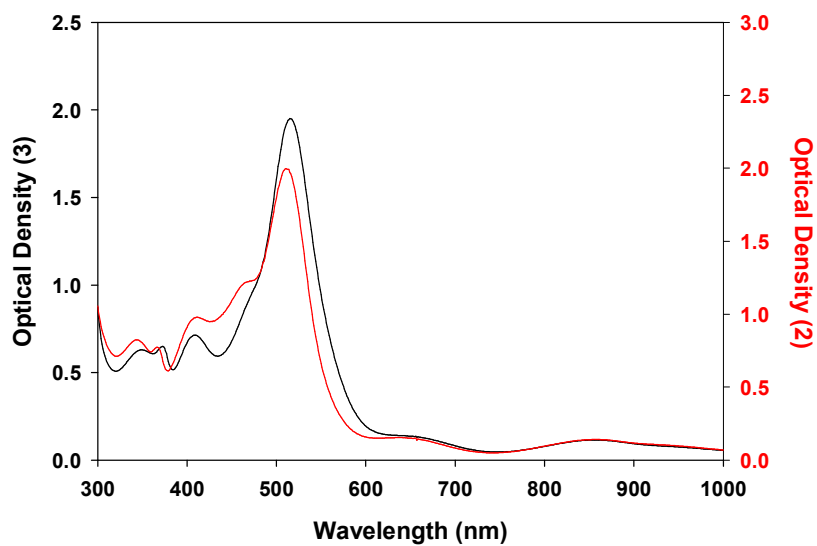
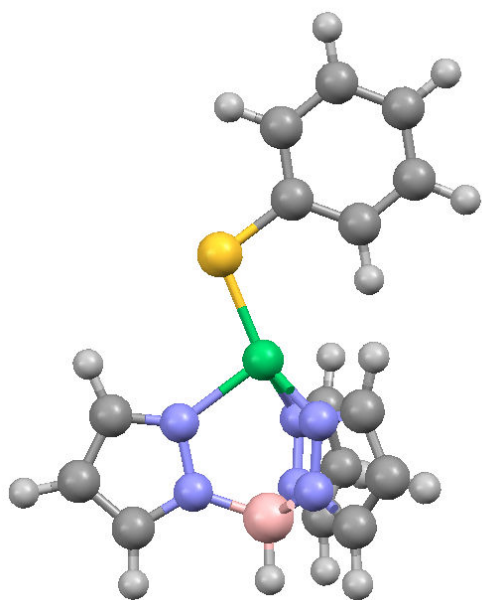
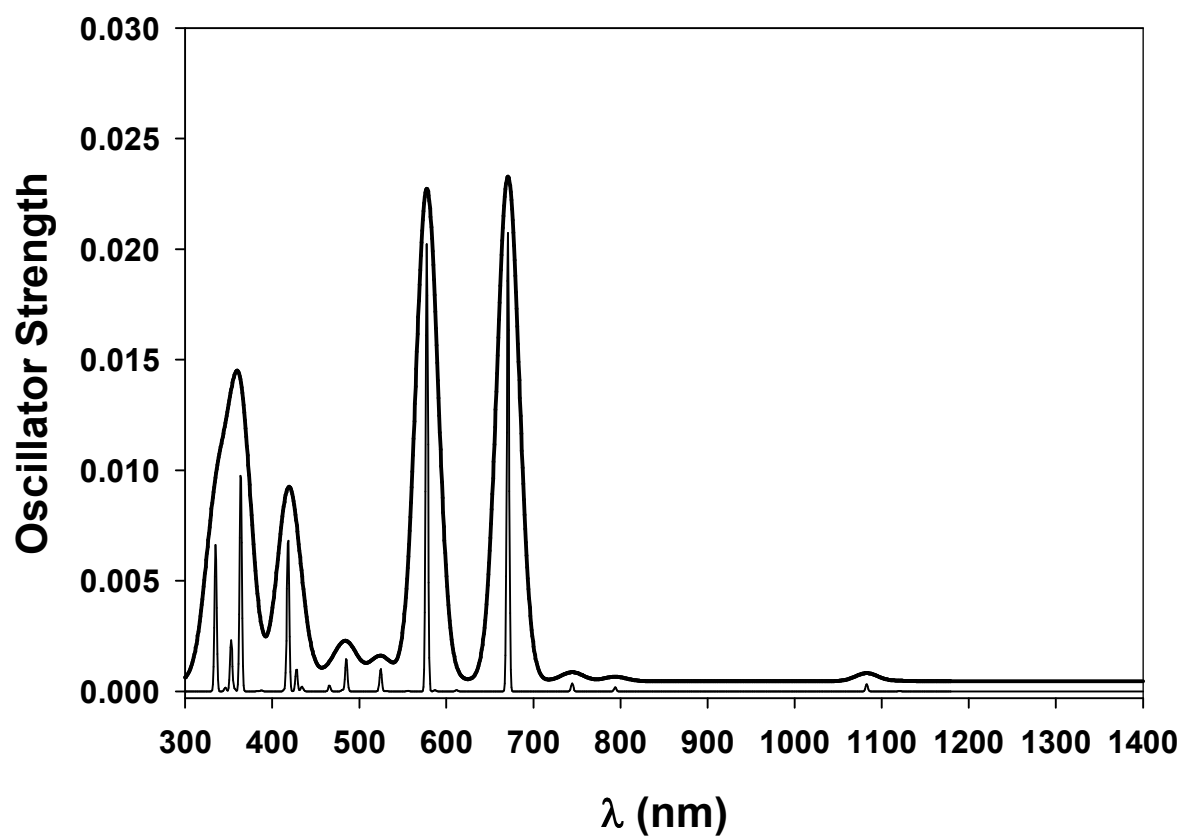


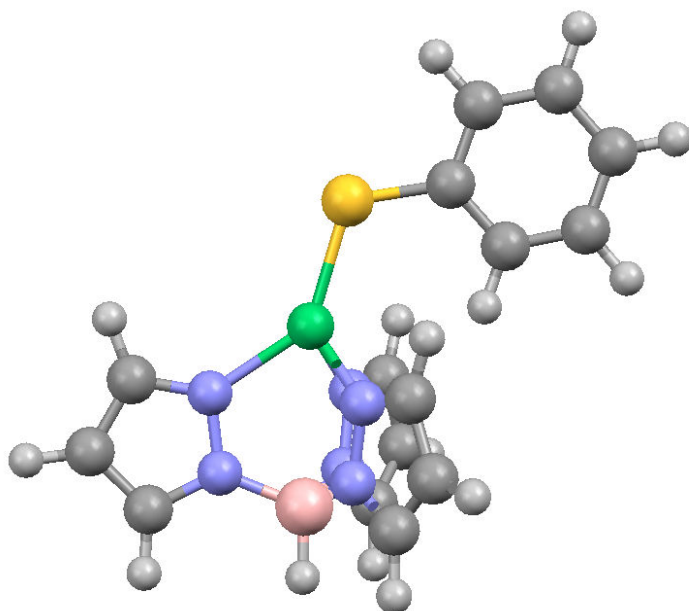
Figure 3-S4. UV-Vis-NIR spectra of **3.2** (red) and **3.3** (black) in toluene at 297 K.



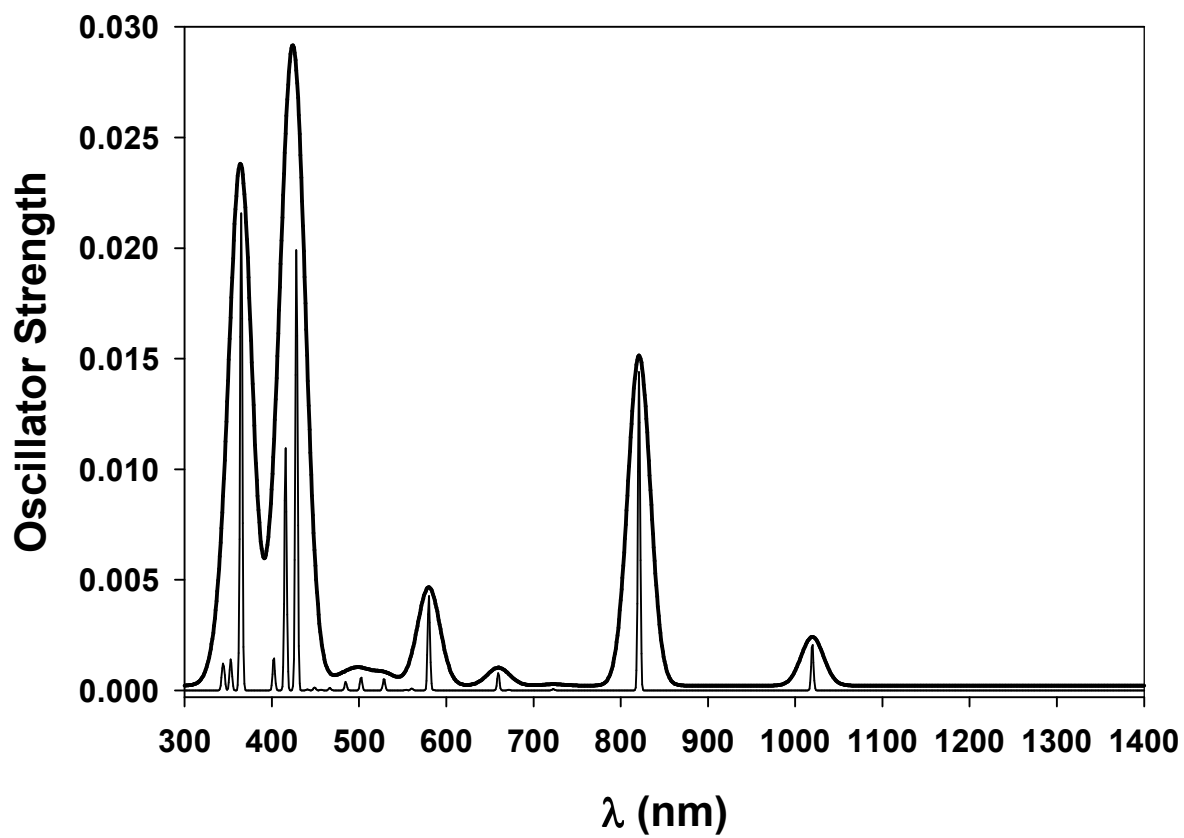
Configuration 1 (up) and calculated spectra (below): Equatorial/Vertical/ 0°



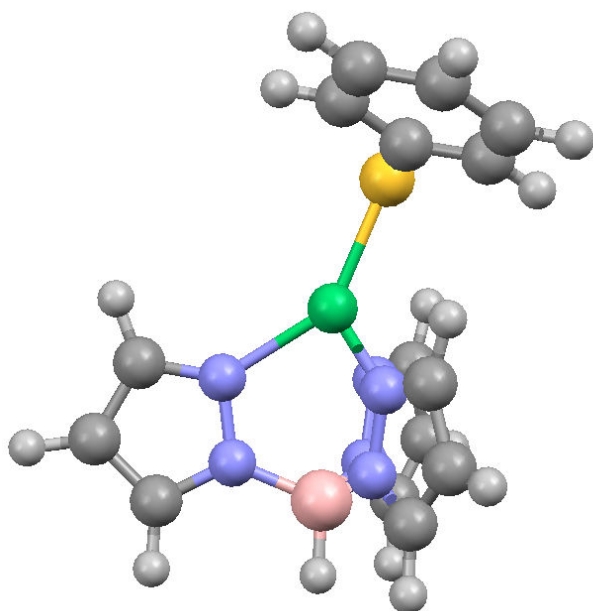
# Atom	X	Y	Z
1 Ni	0.154079348842	-0.101724107947	0.000000000000
2 B	0.808722295181	-3.091789149340	0.000000000000
3 H	1.082232254720	-4.261310894140	0.000000000000
4 N	2.104686755050	-2.237213853180	0.000000000000
5 N	2.033989165960	-0.873879375899	0.000000000000
6 H	3.672896325730	-3.670880943240	0.000000000000
7 C	3.407379641970	-2.619137105050	0.000000000000
8 C	4.201682389100	-1.476840053840	0.000000000000
9 H	5.285191513720	-1.426328052710	0.000000000000
10 C	3.290424114690	-0.406242772265	0.000000000000
11 H	3.470537455560	0.663503557646	0.000000000000
12 N	-0.027670392584	-2.733993480140	-1.255725965080
13 N	-0.421465403611	-1.442709462960	-1.451938421360
14 H	-0.277245119925	-4.575522648500	-2.286343854440
15 C	-0.492998901122	-3.512395400830	-2.264184760720
16 C	-1.212959509930	-2.707575842510	-3.142519539820
17 H	-1.714402490890	-3.010339582550	-4.055340149960
18 C	-1.135615617990	-1.417399010810	-2.589750007700
19 H	-1.542194256580	-0.479883836657	-2.955486294000
20 N	-0.027670392584	-2.733993480140	1.255725965080
21 N	-0.421465403611	-1.442709462960	1.451938421360
22 H	-0.277245119925	-4.575522648500	2.286343854440
23 C	-0.492998901122	-3.512395400830	2.264184760720
24 C	-1.212959509930	-2.707575842510	3.142519539820
25 H	-1.714402490890	-3.010339582550	4.055340149960
26 C	-1.135615617990	-1.417399010810	2.589750007700
27 H	-1.542194256580	-0.479883836657	2.955486294000
28 S	0.464997081127	2.088207823170	0.000000000000
29 C	-1.170628886890	2.784143511160	0.000000000000
30 C	-1.315540088770	4.185279454350	0.000000000000
31 C	-2.583812489100	4.768032984640	0.000000000000
32 H	-2.674215966570	5.855347478770	0.000000000000
33 C	-3.733479359270	3.969813831250	0.000000000000
34 H	-4.723138470580	4.428269124610	0.000000000000
35 C	-3.602124096090	2.575808334990	0.000000000000
36 H	-4.487904110600	1.938936526920	0.000000000000
37 C	-2.336438619170	1.991178128330	0.000000000000
38 H	-0.420727253213	4.809263420280	0.000000000000
39 H	-2.252166356390	0.899244370229	0.000000000000



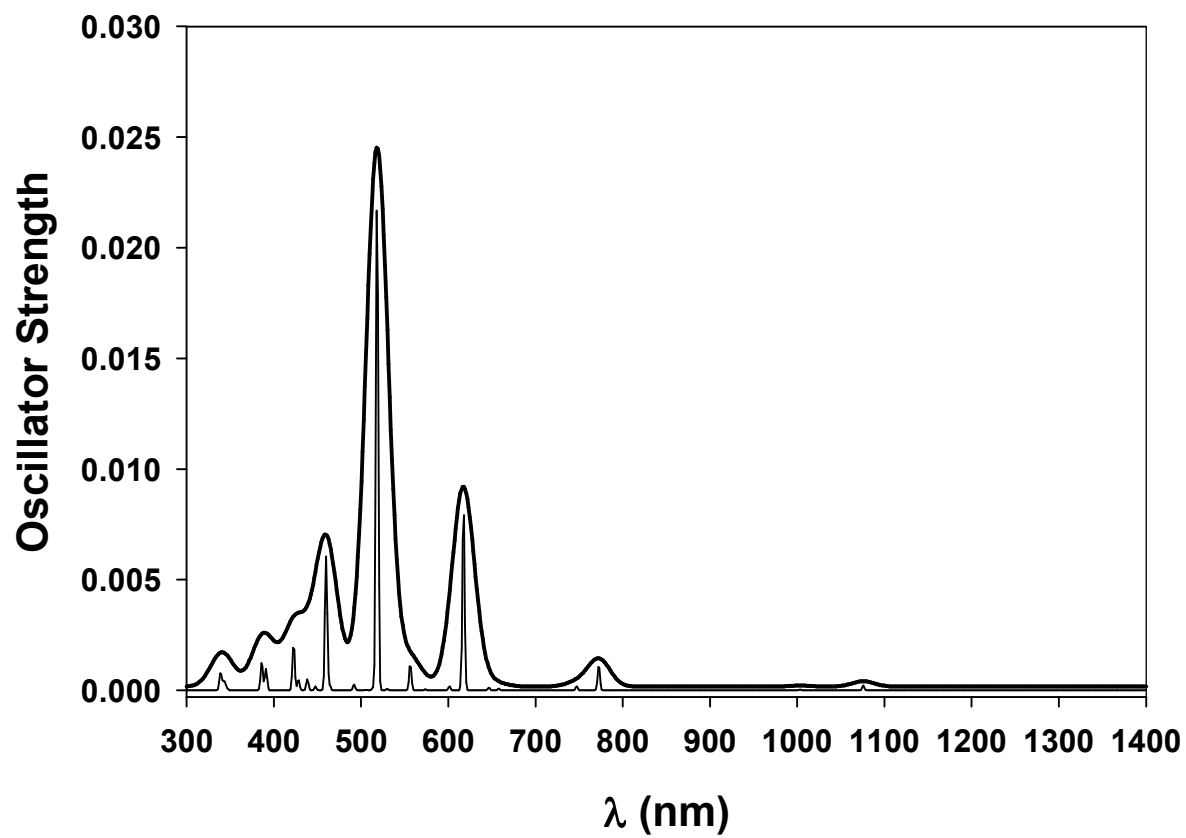
Configuration 2 (up) and calculated spectra (below): Axial/Vertical/180°



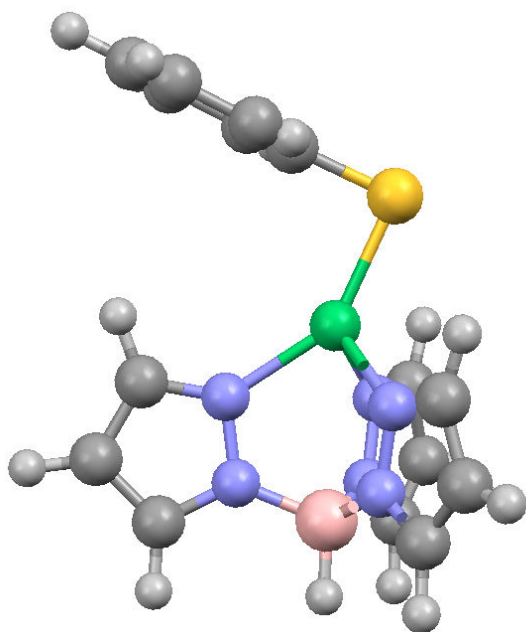
# Atom	X	Y	Z
1 Ni	0.132505557992	-0.098893462668	0.000000000000
2 B	-1.076553003860	-2.915137213780	0.000000000000
3 H	-1.560645999630	-4.014515576480	0.000000000000
4 N	0.468974566989	-3.000362651800	0.000000000000
5 N	1.195583047370	-1.846809105040	0.000000000000
6 H	0.910840342890	-5.079496072840	0.000000000000
7 C	1.305311850070	-4.068643497190	0.000000000000
8 C	2.615404687930	-3.598825355830	0.000000000000
9 H	3.527662016950	-4.185584752540	0.000000000000
10 C	2.492400036870	-2.198108273790	0.000000000000
11 H	3.263471314030	-1.434270058010	0.000000000000
12 N	-1.526098570590	-2.131506503400	-1.260457245070
13 N	-1.083554124450	-0.855825665258	-1.469508694400
14 H	-2.832777045380	-3.470340033300	-2.266269988480
15 C	-2.372487123230	-2.487881050120	-2.258952008490
16 C	-2.483481366330	-1.419425503440	-3.143605599470
17 H	-3.078072603190	-1.372356405610	-4.049499605000
18 C	-1.655975408980	-0.419469985709	-2.603052715820
19 H	-1.446542183960	0.582615273516	-2.962473289860
20 N	-1.526098570590	-2.131506503400	1.260457245070
21 N	-1.083554124450	-0.855825665258	1.469508694400
22 H	-2.832777045380	-3.470340033300	2.266269988480
23 C	-2.372487123230	-2.487881050120	2.258952008490
24 C	-2.483481366330	-1.419425503440	3.143605599470
25 H	-3.078072603190	-1.372356405610	4.049499605000
26 C	-1.655975408980	-0.419469985709	2.603052715820
27 H	-1.446542183960	0.582615273516	2.962473289860
28 S	0.468192736061	2.084308419880	0.000000000000
29 C	-0.999183421276	3.083205075850	0.000000000000
30 C	-0.855615128369	4.485975382660	0.000000000000
31 C	-1.981384834010	5.310483194400	0.000000000000
32 H	-1.852809326210	6.394127261760	0.000000000000
33 C	-3.266902295520	4.755830683290	0.000000000000
34 H	-4.145288598720	5.403005087320	0.000000000000
35 C	-3.414916256370	3.363613311010	0.000000000000
36 H	-4.411138695550	2.918215340700	0.000000000000
37 C	-2.295125506380	2.531124559980	0.000000000000
38 H	0.145729104962	4.919177357420	0.000000000000
39 H	-2.412430119200	1.447131193160	0.000000000000



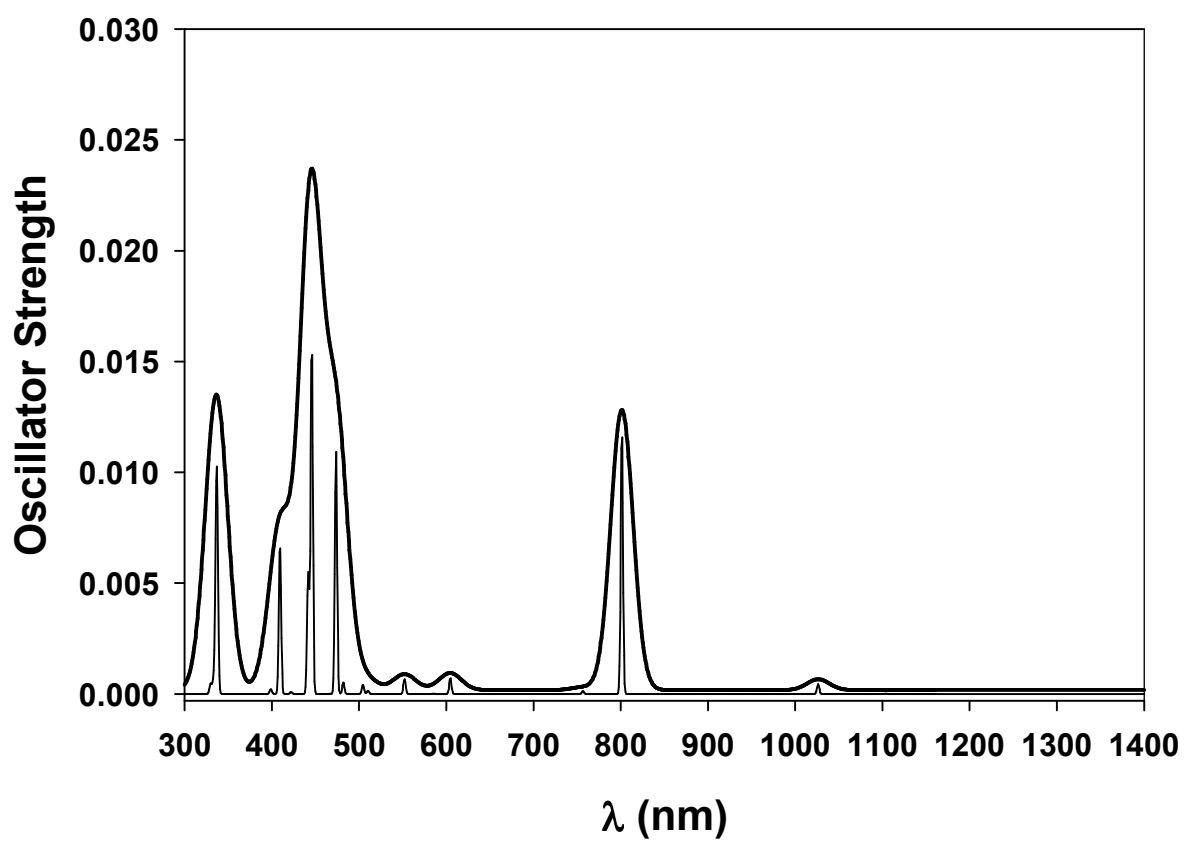
Configuration 3 (up) and calculated spectra (below): Axial/Horizontal/90°



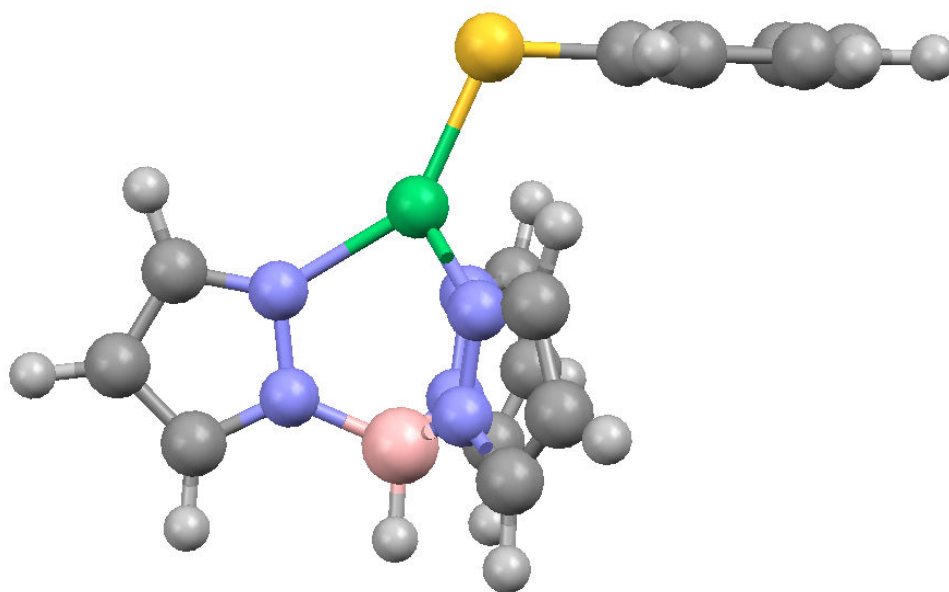
# Atom	X	Y	Z
1 Ni	0.020483533547	0.079811097330	0.078631825824
2 B	-2.147149670310	-2.091857219680	-0.018034278434
3 H	-2.985466882190	-2.950925888200	-0.056079900001
4 N	-2.809756716540	-0.690112121248	-0.002589721149
5 N	-2.026529468770	0.427763297380	0.019539950034
6 H	-4.895675138480	-1.090272545660	-0.042641370284
7 C	-4.117661253210	-0.334112782756	-0.024117844882
8 C	-4.194279356010	1.055965181730	-0.017249885260
9 H	-5.090093828160	1.667184369120	-0.030586420803
10 C	-2.856376138720	1.485181274190	0.009772334843
11 H	-2.451936635250	2.492110696920	0.017253367705
12 N	-1.224594035170	-2.181923919400	-1.261073957140
13 N	-0.188355627209	-1.305395736030	-1.403863872810
14 H	-2.003286828350	-3.807714993700	-2.383801640290
15 C	-1.247732566010	-3.031903194450	-2.317622613280
16 C	-0.199422698886	-2.701657790340	-3.171122548720
17 H	0.065947642042	-3.183810386720	-4.105724812020
18 C	0.438182409541	-1.613100731950	-2.550861353650
19 H	1.307195366470	-1.044519746750	-2.864481037540
20 S	2.047124736010	1.031348688340	-0.050433665163
21 C	2.529497421840	1.263461628030	1.663314238760
22 C	2.203228573040	2.435486883190	2.371112851750
23 C	2.626017796930	2.607912043280	3.692107428860
24 H	2.368037697620	3.525824019730	4.223280588640
25 C	3.371349130770	1.613983103980	4.335766087740
26 H	3.692583574950	1.748078464470	5.369701555120
27 H	1.621227125130	3.213000848020	1.874519935050
28 N	-1.275978794620	-2.239908328510	1.252836652920
29 N	-0.259290730673	-1.358575345090	1.477738358840
30 H	-2.086138788660	-3.912603828160	2.282152050580
31 C	-1.338451629300	-3.126838430930	2.278311200090
32 C	-0.337525850939	-2.812421966650	3.192130268110
33 H	-0.108916472388	-3.319595614490	4.123294428800
34 C	0.314010420303	-1.694305782150	2.643629840580
35 H	1.154623405890	-1.118134109550	3.017776067260
36 C	3.302627956750	0.279191568296	2.309645844680
37 C	3.708433575620	0.450060806164	3.635429772760
38 H	4.297829381960	-0.329523698154	4.121787599970
39 H	3.578566295680	-0.621541012494	1.760194257840



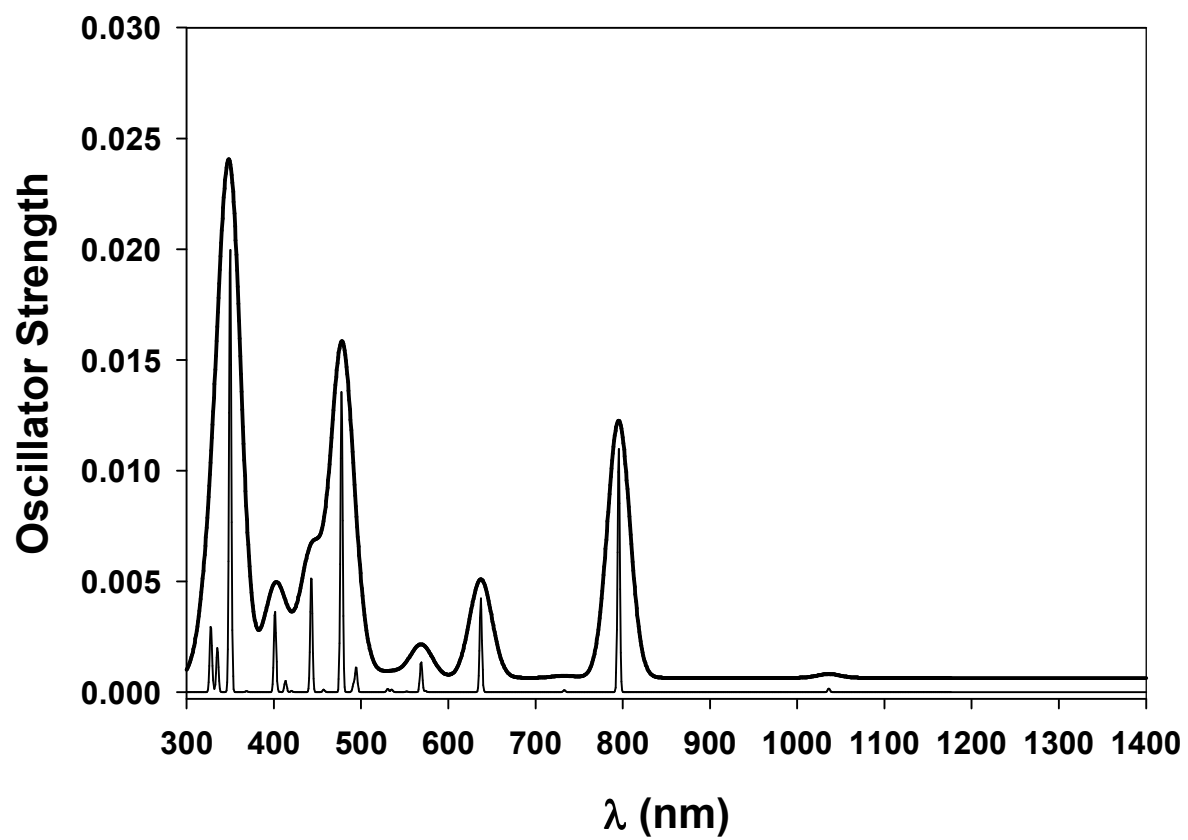
Configuration 4 (up) and calculated spectra (below): Axial/Horizontal/0°



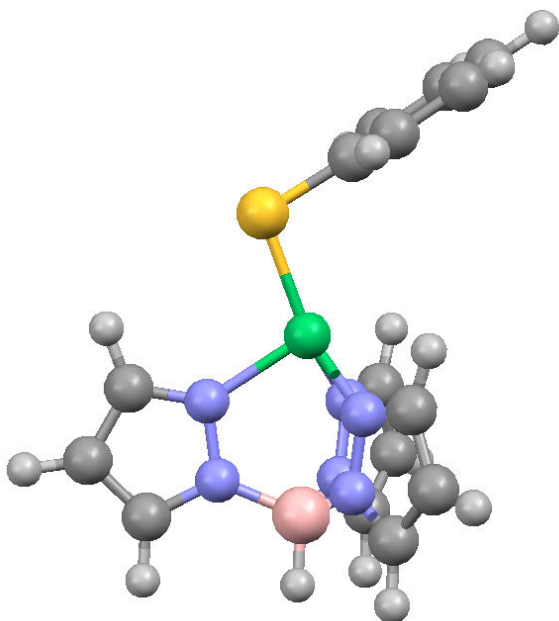
# Atom	X	Y	Z
1 Ni	-0.002905703705	0.112994623355	0.000000000000
2 B	-2.125368579790	-2.094754336110	0.000000000000
3 H	-2.946505318410	-2.970915978480	0.000000000000
4 N	-2.809027510690	-0.706741845135	0.000000000000
5 N	-2.035749292600	0.416887808042	0.000000000000
6 H	-4.894586503640	-1.117512917280	0.000000000000
7 C	-4.121226008810	-0.357672236151	0.000000000000
8 C	-4.203979223680	1.032024902170	0.000000000000
9 H	-5.102083957710	1.639514803950	0.000000000000
10 C	-2.867635357030	1.469921800520	0.000000000000
11 H	-2.466043884920	2.479019535330	0.000000000000
12 N	-1.228751150710	-2.199720698650	-1.261687844110
13 N	-0.220185851883	-1.301823176940	-1.460320988970
14 H	-1.997967394790	-3.877859804330	-2.313323715900
15 C	-1.261325218210	-3.081278468120	-2.292194463340
16 C	-0.248207302354	-2.749912689550	-3.186673883080
17 H	0.000944161982	-3.251130475040	-4.115885576870
18 C	0.378211787889	-1.626446367680	-2.617886544140
19 H	1.222410959960	-1.044150318130	-2.971162196690
20 S	2.045188984670	1.015342584610	0.000000000000
21 C	1.332528395030	2.664013337590	0.000000000000
22 C	1.072629376190	3.338435847350	-1.212359381390
23 C	0.561807701173	4.637956636500	-1.208769148950
24 H	0.369772711033	5.142381477680	-2.157228304540
25 C	0.301707146286	5.294460776210	0.000000000000
26 H	-0.091649395186	6.311858084960	0.000000000000
27 H	1.281256774300	2.831723044150	-2.155647154280
28 N	-1.228751150710	-2.199720698650	1.261687844110
29 N	-0.220185851883	-1.301823176940	1.460320988970
30 H	-1.997967394790	-3.877859804330	2.313323715900
31 C	-1.261325218210	-3.081278468120	2.292194463340
32 C	-0.248207302354	-2.749912689550	3.186673883080
33 H	0.000944161982	-3.251130475040	4.115885576870
34 C	0.378211787889	-1.626446367680	2.617886544140
35 H	1.222410959960	-1.044150318130	2.971162196690
36 C	1.072629376190	3.338435847350	1.212359381390
37 C	0.561807701173	4.637956636500	1.208769148950
38 H	0.369772711033	5.142381477680	2.157228304540
39 H	1.281256774300	2.831723044150	2.155647154280



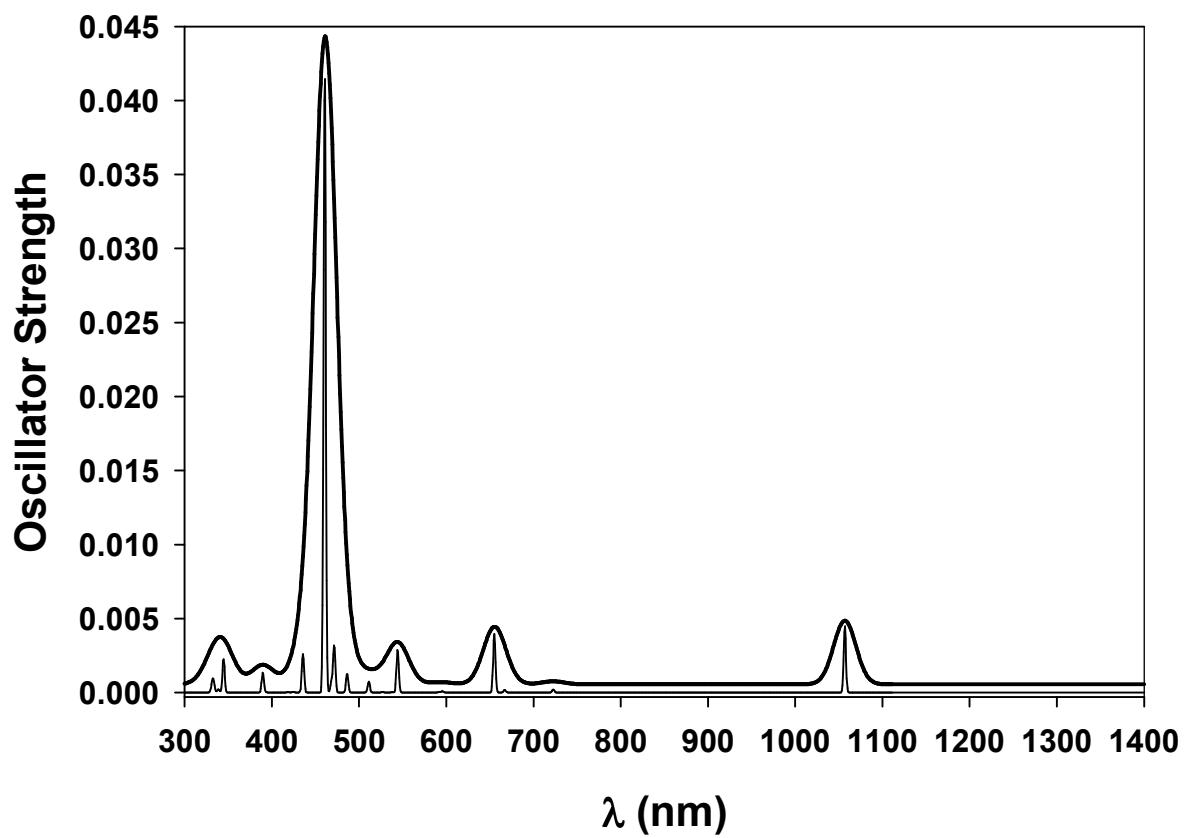
Configuration 5 (up) and calculated spectra (below): Axial/Horizontal/180°



# Atom	X	Y	Z
1 Ni	0.011546939012	-0.040867351879	0.000000000000
2 B	-2.804932501690	-1.219720067060	0.000000000000
3 H	-3.905926711000	-1.700089603200	0.000000000000
4 N	-2.888726587610	0.327858495674	0.000000000000
5 N	-1.739240744370	1.064041570680	0.000000000000
6 H	-4.970840664420	0.747721937786	0.000000000000
7 C	-3.964347414700	1.152974462860	0.000000000000
8 C	-3.508014306080	2.467392708330	0.000000000000
9 H	-4.105409837400	3.372604699370	0.000000000000
10 C	-2.106479656370	2.357363537470	0.000000000000
11 H	-1.353207200270	3.138529344360	0.000000000000
12 N	-2.025260889450	-1.664004249180	-1.263338738930
13 N	-0.750974396533	-1.221085663030	-1.469343739470
14 H	-3.383157123400	-2.921879157750	-2.307122745830
15 C	-2.398291256310	-2.467060406210	-2.291887835070
16 C	-1.340949342170	-2.546450416200	-3.192645555350
17 H	-1.305368816710	-3.105023087890	-4.121659059010
18 C	-0.330550184336	-1.748210470400	-2.629185040760
19 H	0.667374004798	-1.528589246180	-2.991168934140
20 S	2.229692345320	0.050823837132	0.000000000000
21 C	2.968263974770	-1.577740901180	0.000000000000
22 C	3.292536071350	-2.215143153640	1.209958487570
23 C	3.904774739200	-3.470791918570	1.207785574900
24 H	4.143889962480	-3.954786854000	2.156269259360
25 C	4.211576657660	-4.106056253640	0.000000000000
26 H	4.688232505130	-5.087341232230	0.000000000000
27 H	3.069364223340	-1.714656063490	2.152486243460
28 N	-2.025260889450	-1.664004249180	1.263338738930
29 N	-0.750974396533	-1.221085663030	1.469343739470
30 H	-3.383157123400	-2.921879157750	2.307122745830
31 C	-2.398291256310	-2.467060406210	2.291887835070
32 C	-1.340949342170	-2.546450416200	3.192645555350
33 H	-1.305368816710	-3.105023087890	4.121659059010
34 C	-0.330550184336	-1.748210470400	2.629185040760
35 H	0.667374004798	-1.528589246180	2.991168934140
36 C	3.292536071350	-2.215143153640	-1.209958487570
37 C	3.904774739200	-3.470791918570	-1.207785574900
38 H	4.143889962480	-3.954786854000	-2.156269259360
39 H	3.069364223340	-1.714656063490	-2.152486243460



Configuration 6 (up) and calculated spectra (below): Equatorial/Horizontal/0°



# Atom	X	Y	Z
1 Ni	-0.018596571106	0.011546786940	0.000000000000
2 B	0.651509222544	-2.986556356830	0.000000000000
3 H	0.932176623261	-4.154522896410	0.000000000000
4 N	1.942416577490	-2.126867205490	0.000000000000
5 N	1.868897288030	-0.762954928249	0.000000000000
6 H	3.509139843830	-3.561499090440	0.000000000000
7 C	3.244471900240	-2.509364738790	0.000000000000
8 C	4.039095227210	-1.367471681170	0.000000000000
9 H	5.122663700970	-1.317817787750	0.000000000000
10 C	3.127330740220	-0.297274099828	0.000000000000
11 H	3.310075516390	0.772004344540	0.000000000000
12 N	-0.184481431615	-2.630312270620	-1.253958234260
13 N	-0.589361521731	-1.341694492460	-1.445788303070
14 H	-0.412604277590	-4.469803326490	-2.292327683490
15 C	-0.636257817635	-3.408353001370	-2.268727847810
16 C	-1.356156688650	-2.606015211810	-3.148864953830
17 H	-1.851763320210	-2.910145545410	-4.064365870270
18 C	-1.296200861310	-1.318468363290	-2.587541321830
19 H	-1.716801294680	-0.385096383649	-2.946423050320
20 N	-0.184481431615	-2.630312270620	1.253958234260
21 N	-0.589361521731	-1.341694492460	1.445788303070
22 H	-0.412604277590	-4.469803326490	2.292327683490
23 C	-0.636257817635	-3.408353001370	2.268727847810
24 C	-1.356156688650	-2.606015211810	3.148864953830
25 H	-1.851763320210	-2.910145545410	4.064365870270
26 C	-1.296200861310	-1.318468363290	2.587541321830
27 H	-1.716801294680	-0.385096383649	2.946423050320
28 S	0.346396279791	2.196911968560	0.000000000000
29 C	-1.326751265450	2.847239775790	0.000000000000
30 C	-1.981324440530	3.142694725710	1.211890507620
31 C	-3.261068163800	3.703182331720	1.207986625720
32 H	-3.753288134450	3.926039481420	2.156418491330
33 C	-3.910010599890	3.982437533370	0.000000000000
34 H	-4.910635467650	4.417766931590	0.000000000000
35 C	-3.261068163800	3.703182331720	-1.207986625720
36 H	-3.753288134450	3.926039481420	-2.156418491330
37 C	-1.981324440530	3.142694725710	-1.211890507620
38 H	-1.471784435400	2.938119382710	2.154379853750
39 H	-1.471784435400	2.938119382710	-2.154379853750

APPENDIX E: CRYSTAL STRUCTURE AND DATA REFINEMENT FOR
COMPLEX 3.5

Table E1. Crystal data and structure refinement for $\text{Tp}^{\text{Me,Me}}\text{Ni-S-2,6-Ph}_2\text{C}_6\text{H}_3$ (**3.5**).

Empirical formula	$\text{C}_{41} \text{H}_{51} \text{B N}_6 \text{Ni O}_2 \text{S}$	
Formula weight	761.46	
Temperature	123(2) K	
Wavelength	0.71073 Å	
Crystal system	Orthorhombic	
Space group	Pnma	
Unit cell dimensions	$a = 15.9841(19)$ Å	$\alpha = 90^\circ$
	$b = 23.499(3)$ Å	$\beta = 90^\circ$
	$c = 10.6851(13)$ Å	$\gamma = 90^\circ$
Volume	4013.4(8) Å ³	
Z	4	
Density (calculated)	1.260 Mg/m ³	
Absorption coefficient	0.578 mm ⁻¹	
$F(000)$	1616	
Crystal color, morphology	Orange, Block	
Crystal size	0.35 x 0.30 x 0.30 mm ³	
Theta range for data collection	1.73 to 27.51°	
Index ranges	$0 \leq h \leq 20, 0 \leq k \leq 30, 0 \leq l \leq 13$	
Reflections collected	46783	
Independent reflections	4718 [$R(\text{int}) = 0.0323$]	
Observed reflections	4062	
Completeness to $\theta = 27.51^\circ$	99.8%	
Absorption correction	Multi-scan	
Max. and min. transmission	0.8458 and 0.8234	
Refinement method	Full-matrix least-squares on F^2	
Data / restraints / parameters	4718 / 42 / 291	
Goodness-of-fit on F^2	1.122	
Final R indices [$I > 2\sigma(I)$]	$R1 = 0.0352, wR2 = 0.1002$	
R indices (all data)	$R1 = 0.0411, wR2 = 0.1042$	
Largest diff. peak and hole	0.492 and -0.430 e.Å ⁻³	

Table E2. Atomic coordinates($\times 10^4$) and equivalent isotropic displacement parameters ($\text{\AA}^2 \times 10^3$) for $\text{Tp}^{\text{Me,Me}}\text{Ni-S-2,6-Ph}_2\text{C}_6\text{H}_3$ (**3.5**). U_{eq} is defined as one third of the trace of the orthogonalized U_{ij} tensor.

	x	y	z	U_{eq}
Ni1	4296(1)	2500	4432(1)	17(1)
B1	2956(2)	2500	2431(2)	21(1)
N1	2554(1)	2500	3742(2)	21(1)
N2	3066(1)	2500	4780(2)	21(1)
C1	1031(2)	2500	3200(2)	33(1)
C2	1747(1)	2500	4100(2)	23(1)
C3	1732(2)	2500	5397(2)	26(1)
C4	2564(1)	2500	5781(2)	22(1)
C5	2899(2)	2500	7085(2)	33(1)
N3	3512(1)	3037(1)	2326(1)	21(1)
N4	4161(1)	3111(1)	3152(1)	20(1)
C6	2819(1)	3544(1)	545(2)	33(1)
C7	3468(1)	3491(1)	1548(2)	24(1)
C8	4102(1)	3859(1)	1871(2)	27(1)
C9	4523(1)	3608(1)	2878(2)	22(1)
C10	5258(1)	3823(1)	3602(2)	28(1)
S1	5529(1)	2500	5466(1)	18(1)
C11	5162(1)	2500	7044(2)	18(1)
C12	5006(1)	3018(1)	7683(1)	20(1)
C13	4654(1)	3008(1)	8881(2)	24(1)
C14	4465(2)	2500	9470(2)	26(1)
C15	5218(1)	3587(1)	7161(2)	22(1)
C16	4614(1)	4016(1)	7120(2)	32(1)
C17	4821(1)	4566(1)	6750(2)	40(1)
C18	5635(1)	4697(1)	6437(2)	36(1)
C19	6246(1)	4277(1)	6470(2)	30(1)
C20	6035(1)	3726(1)	6822(2)	25(1)
O1	3086(2)	5019(1)	-60(6)	97(2)
C21	2501(3)	5322(2)	598(4)	78(2)

C22	2536(5)	5910(3)	141(7)	105(3)
C23	3328(7)	5933(3)	-587(15)	181(5)
C24	3735(5)	5389(4)	-267(15)	115(2)
O1'	3247(7)	5158(6)	-1198(11)	131(4)
C21'	2721(7)	5506(4)	-1629(11)	86(4)
C22'	2607(14)	5922(7)	-626(19)	132(9)
C23'	3502(16)	5968(8)	-290(30)	181(5)
C24'	3747(13)	5347(9)	-260(30)	115(2)

Table E3. Bond lengths [\AA] and angles [$^\circ$] for $\text{Tp}^{\text{Me,Me}}\text{Ni-S-2,6-Ph}_2\text{C}_6\text{H}_3$ (**3.5**).

Ni(1)-N(4)	1.9946(13)	C(10)-H(10A)	0.9800
Ni(1)-N(4)#1	1.9947(13)	C(10)-H(10B)	0.9800
Ni(1)-N(2)	2.0014(19)	C(10)-H(10C)	0.9800
Ni(1)-S(1)	2.2589(6)	S(1)-C(11)	1.785(2)
B(1)-N(1)	1.541(3)	C(11)-C(12)	1.4180(18)
B(1)-N(3)	1.547(2)	C(11)-C(12)#1	1.4180(18)
B(1)-N(3)#1	1.547(2)	C(12)-C(13)	1.399(2)
B(1)-H(1A)	1.1200	C(12)-C(15)	1.488(2)
N(1)-C(2)	1.346(3)	C(13)-C(14)	1.382(2)
N(1)-N(2)	1.378(3)	C(13)-H(13A)	0.9500
N(2)-C(4)	1.336(3)	C(14)-C(13)#1	1.382(2)
C(1)-C(2)	1.494(3)	C(14)-H(14A)	0.9500
C(1)-H(1B)	0.9800	C(15)-C(20)	1.394(2)
C(1)-H(1C)	0.9800	C(15)-C(16)	1.397(2)
C(1)-H(1D)	0.9800	C(16)-C(17)	1.391(3)
C(2)-C(3)	1.387(3)	C(16)-H(16A)	0.9500
C(3)-C(4)	1.393(3)	C(17)-C(18)	1.378(3)
C(3)-H(3A)	0.9500	C(17)-H(17A)	0.9500
C(4)-C(5)	1.493(3)	C(18)-C(19)	1.390(3)
C(5)-H(5A)	0.9800	C(18)-H(18A)	0.9500
C(5)-H(5B)	0.9800	C(19)-C(20)	1.389(2)
C(5)-H(5C)	0.9800	C(19)-H(19A)	0.9500
N(3)-C(7)	1.354(2)	C(20)-H(20A)	0.9500
N(3)-N(4)	1.3738(18)	O(1)-C(21)	1.370(6)
N(4)-C(9)	1.336(2)	O(1)-C(24)	1.371(7)
C(6)-C(7)	1.497(2)	C(21)-C(22)	1.467(7)
C(6)-H(6A)	0.9800	C(21)-H(21A)	0.9900
C(6)-H(6B)	0.9800	C(21)-H(21B)	0.9900
C(6)-H(6C)	0.9800	C(22)-C(23)	1.487(13)
C(7)-C(8)	1.378(2)	C(22)-H(22A)	0.9900
C(8)-C(9)	1.400(2)	C(22)-H(22B)	0.9900
C(8)-H(8A)	0.9500	C(23)-C(24)	1.474(7)
C(9)-C(10)	1.494(2)	C(23)-H(23A)	0.9900

C(23)-H(23B)	0.9900	C(2)-C(1)-H(1C)	109.5
C(24)-H(24A)	0.9900	H(1B)-C(1)-H(1C)	109.5
C(24)-H(24B)	0.9900	C(2)-C(1)-H(1D)	109.5
O(1')-C(21')	1.260(11)	H(1B)-C(1)-H(1D)	109.5
O(1')-C(24')	1.359(17)	H(1C)-C(1)-H(1D)	109.5
C(21')-C(22')	1.461(14)	N(1)-C(2)-C(3)	107.5(2)
C(21')-H(21C)	0.9900	N(1)-C(2)-C(1)	123.5(2)
C(21')-H(21D)	0.9900	C(3)-C(2)-C(1)	129.0(2)
C(22')-C(23')	1.479(18)	C(2)-C(3)-C(4)	106.1(2)
C(22')-H(22C)	0.9900	C(2)-C(3)-H(3A)	126.9
C(22')-H(22D)	0.9900	C(4)-C(3)-H(3A)	126.9
C(23')-C(24')	1.511(14)	N(2)-C(4)-C(3)	109.8(2)
C(23')-H(23C)	0.9900	N(2)-C(4)-C(5)	122.2(2)
C(23')-H(23E)	0.9900	C(3)-C(4)-C(5)	128.1(2)
C(24')-H(24E)	0.9900	C(4)-C(5)-H(5A)	109.5
C(24')-H(24C)	0.9900	C(4)-C(5)-H(5B)	109.5
		H(5A)-C(5)-H(5B)	109.5
N(4)-Ni(1)-N(4)#1	92.06(8)	C(4)-C(5)-H(5C)	109.5
N(4)-Ni(1)-N(2)	91.20(5)	H(5A)-C(5)-H(5C)	109.5
N(4)#1-Ni(1)-N(2)	91.20(5)	H(5B)-C(5)-H(5C)	109.5
N(4)-Ni(1)-S(1)	115.47(4)	C(7)-N(3)-N(4)	109.52(13)
N(4)#1-Ni(1)-S(1)	115.46(4)	C(7)-N(3)-B(1)	131.08(15)
N(2)-Ni(1)-S(1)	140.01(6)	N(4)-N(3)-B(1)	119.37(14)
N(1)-B(1)-N(3)	107.76(12)	C(9)-N(4)-N(3)	107.28(13)
N(1)-B(1)-N(3)#1	107.76(12)	C(9)-N(4)-Ni(1)	137.11(11)
N(3)-B(1)-N(3)#1	109.29(18)	N(3)-N(4)-Ni(1)	115.56(10)
N(1)-B(1)-H(1A)	110.6	C(7)-C(6)-H(6A)	109.5
N(3)-B(1)-H(1A)	110.6	C(7)-C(6)-H(6B)	109.5
N(3)#1-B(1)-H(1A)	110.6	H(6A)-C(6)-H(6B)	109.5
C(2)-N(1)-N(2)	109.88(18)	C(7)-C(6)-H(6C)	109.5
C(2)-N(1)-B(1)	131.12(19)	H(6A)-C(6)-H(6C)	109.5
N(2)-N(1)-B(1)	119.00(17)	H(6B)-C(6)-H(6C)	109.5
C(4)-N(2)-N(1)	106.76(18)	N(3)-C(7)-C(8)	107.66(14)
C(4)-N(2)-Ni(1)	137.57(16)	N(3)-C(7)-C(6)	122.83(16)
N(1)-N(2)-Ni(1)	115.67(14)	C(8)-C(7)-C(6)	129.51(16)
C(2)-C(1)-H(1B)	109.5	C(7)-C(8)-C(9)	106.30(15)

C(7)-C(8)-H(8A)	126.8	C(20)-C(19)-C(18)	119.99(17)
C(9)-C(8)-H(8A)	126.8	C(20)-C(19)-H(19A)	120.0
N(4)-C(9)-C(8)	109.24(15)	C(18)-C(19)-H(19A)	120.0
N(4)-C(9)-C(10)	121.48(14)	C(19)-C(20)-C(15)	120.97(16)
C(8)-C(9)-C(10)	129.29(15)	C(19)-C(20)-H(20A)	119.5
C(9)-C(10)-H(10A)	109.5	C(15)-C(20)-H(20A)	119.5
C(9)-C(10)-H(10B)	109.5	C(21)-O(1)-C(24)	105.6(6)
H(10A)-C(10)-H(10B)	109.5	O(1)-C(21)-C(22)	107.1(4)
C(9)-C(10)-H(10C)	109.5	O(1)-C(21)-H(21A)	110.3
H(10A)-C(10)-H(10C)	109.5	C(22)-C(21)-H(21A)	110.3
H(10B)-C(10)-H(10C)	109.5	O(1)-C(21)-H(21B)	110.3
C(11)-S(1)-Ni(1)	100.11(7)	C(22)-C(21)-H(21B)	110.3
C(12)-C(11)-C(12)#1	118.34(19)	H(21A)-C(21)-H(21B)	108.5
C(12)-C(11)-S(1)	120.82(10)	C(21)-C(22)-C(23)	103.9(4)
C(12)#1-C(11)-S(1)	120.82(10)	C(21)-C(22)-H(22A)	111.0
C(13)-C(12)-C(11)	119.75(15)	C(23)-C(22)-H(22A)	111.0
C(13)-C(12)-C(15)	116.76(14)	C(21)-C(22)-H(22B)	111.0
C(11)-C(12)-C(15)	123.47(14)	C(23)-C(22)-H(22B)	111.0
C(14)-C(13)-C(12)	121.33(16)	H(22A)-C(22)-H(22B)	109.0
C(14)-C(13)-H(13A)	119.3	C(24)-C(23)-C(22)	102.9(5)
C(12)-C(13)-H(13A)	119.3	C(24)-C(23)-H(23A)	111.2
C(13)#1-C(14)-C(13)	119.3(2)	C(22)-C(23)-H(23A)	111.2
C(13)#1-C(14)-H(14A)	120.3	C(24)-C(23)-H(23B)	111.2
C(13)-C(14)-H(14A)	120.3	C(22)-C(23)-H(23B)	111.2
C(20)-C(15)-C(16)	118.14(15)	H(23A)-C(23)-H(23B)	109.1
C(20)-C(15)-C(12)	121.39(14)	O(1)-C(24)-C(23)	104.8(5)
C(16)-C(15)-C(12)	120.16(15)	O(1)-C(24)-H(24A)	110.8
C(17)-C(16)-C(15)	120.93(17)	C(23)-C(24)-H(24A)	110.8
C(17)-C(16)-H(16A)	119.5	O(1)-C(24)-H(24B)	110.8
C(15)-C(16)-H(16A)	119.5	C(23)-C(24)-H(24B)	110.8
C(18)-C(17)-C(16)	120.16(18)	H(24A)-C(24)-H(24B)	108.9
C(18)-C(17)-H(17A)	119.9	C(21')-O(1')-C(24')	116.9(13)
C(16)-C(17)-H(17A)	119.9	O(1')-C(21')-C(22')	104.4(9)
C(17)-C(18)-C(19)	119.79(17)	O(1')-C(21')-H(21C)	110.9
C(17)-C(18)-H(18A)	120.1	C(22')-C(21')-H(21C)	110.9
C(19)-C(18)-H(18A)	120.1	O(1')-C(21')-H(21D)	110.9

C(22')-C(21')-H(21D)	110.9	C(24')-C(23')-H(23C)	111.6
H(21C)-C(21')-H(21D)	108.9	C(22')-C(23')-H(23E)	111.6
C(21')-C(22')-C(23')	96.1(14)	C(24')-C(23')-H(23E)	111.6
C(21')-C(22')-H(22C)	112.5	H(23C)-C(23')-H(23E)	109.4
C(23')-C(22')-H(22C)	112.5	O(1')-C(24')-C(23')	98.3(15)
C(21')-C(22')-H(22D)	112.5	O(1')-C(24')-H(24E)	112.1
C(23')-C(22')-H(22D)	112.5	C(23')-C(24')-H(24E)	112.1
H(22C)-C(22')-H(22D)	110.0	O(1')-C(24')-H(24C)	112.1
C(22')-C(23')-C(24')	100.7(12)	C(23')-C(24')-H(24C)	112.1
C(22')-C(23')-H(23C)	111.6	H(24E)-C(24')-H(24C)	109.7

Symmetry transformations used to generate equivalent atoms:

#1 x,-y+1/2,z

APPENDIX F: DETAILED SPECTRA OF OXIDATION OF
NICKEL(II)PHENOLATES

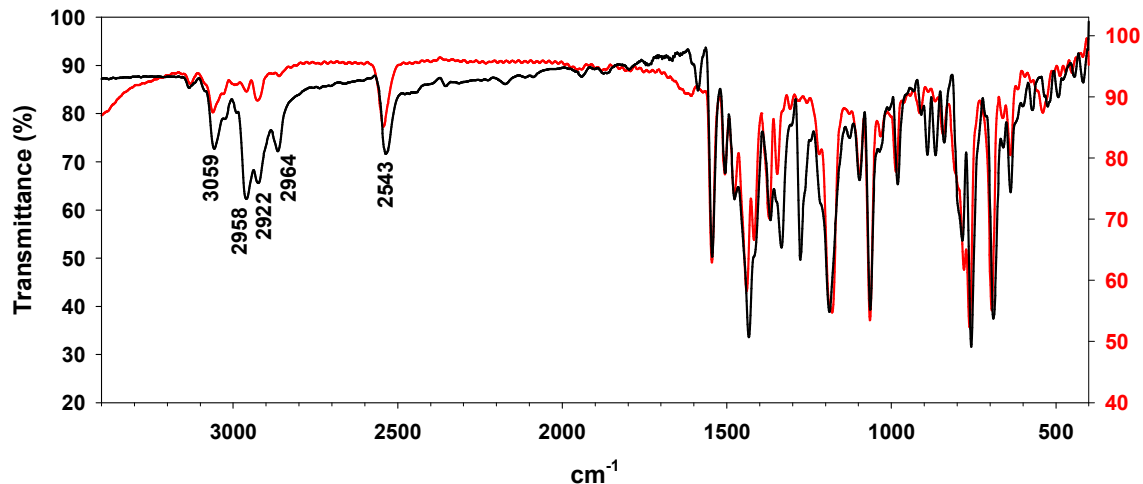


Figure 4-S1. Comparison of FTIR spectra (KBr pellets) of $\text{Tp}^{\text{Ph,Me}}\text{Ni-O-2,6-}i\text{-Pr}_2\text{C}_6\text{H}_3$ (4.1a, black) and $\text{Tp}^{\text{Ph,Me}}\text{NiCl}$ (red).

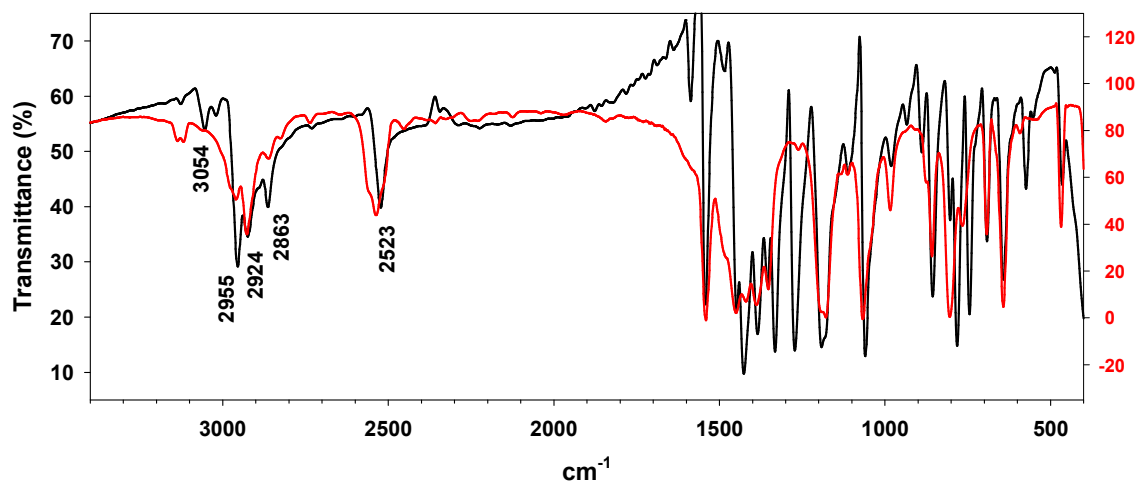


Figure 4-S2. Comparison of FTIR spectra (KBr pellets) of $\text{Tp}^{\text{Me,Me}}\text{Ni-O-2,6-}i\text{-Pr}_2\text{C}_6\text{H}_3$ (4.1b, black) and $\text{Tp}^{\text{Me,Me}}\text{NiCl}$ (red).

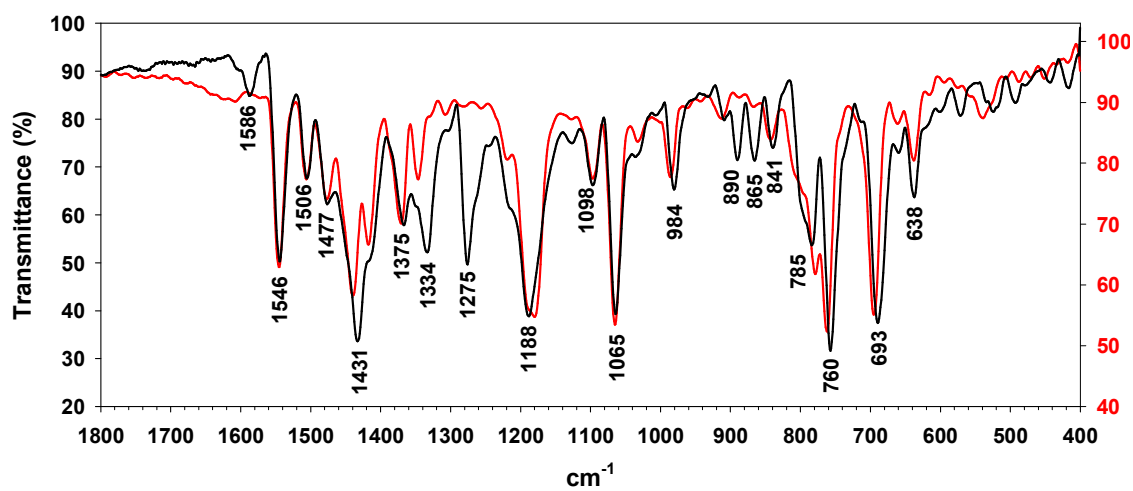


Figure 4-S3. Detail of FTIR spectra of **4.1a** (black) and $\text{Tp}^{\text{Ph,Me}}\text{NiCl}$ (red).

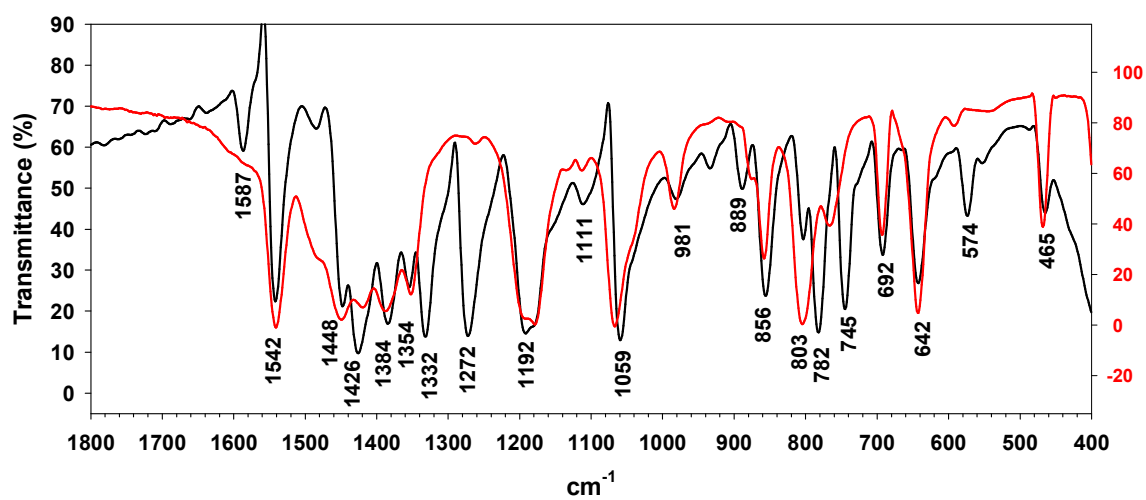


Figure 4-S4. Detail of FTIR spectra of **4.1b** (black) and $\text{Tp}^{\text{Me,Me}}\text{NiCl}$ (red).

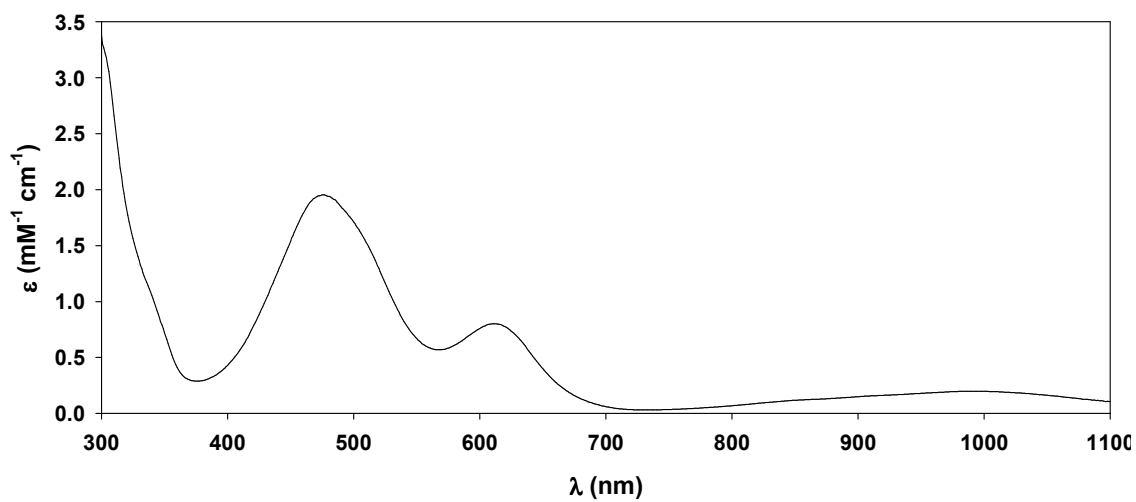


Figure 4-S5. UV-Vis-NIR spectrum (CH_2Cl_2 , 293 K) of $\text{Tp}^{\text{Ph,Me}}\text{Ni-O-2,6-}i\text{Pr}_2\text{C}_6\text{H}_3$ (4.1a).

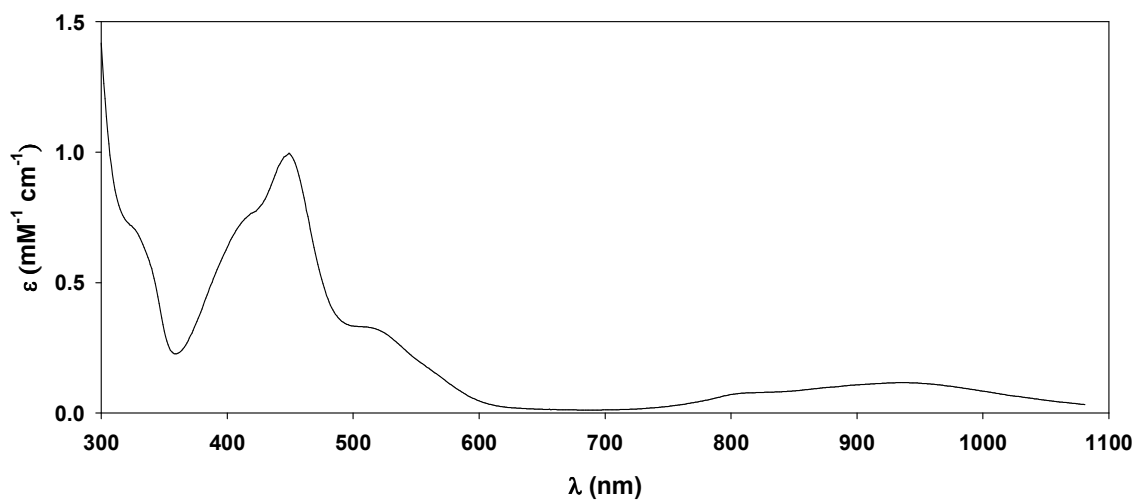


Figure 4-S6. UV-Vis-NIR spectrum (CH_2Cl_2 , 293 K) of $\text{Tp}^{\text{Me,Me}}\text{Ni-O-2,6-}i\text{Pr}_2\text{C}_6\text{H}_3$ (4.1b).

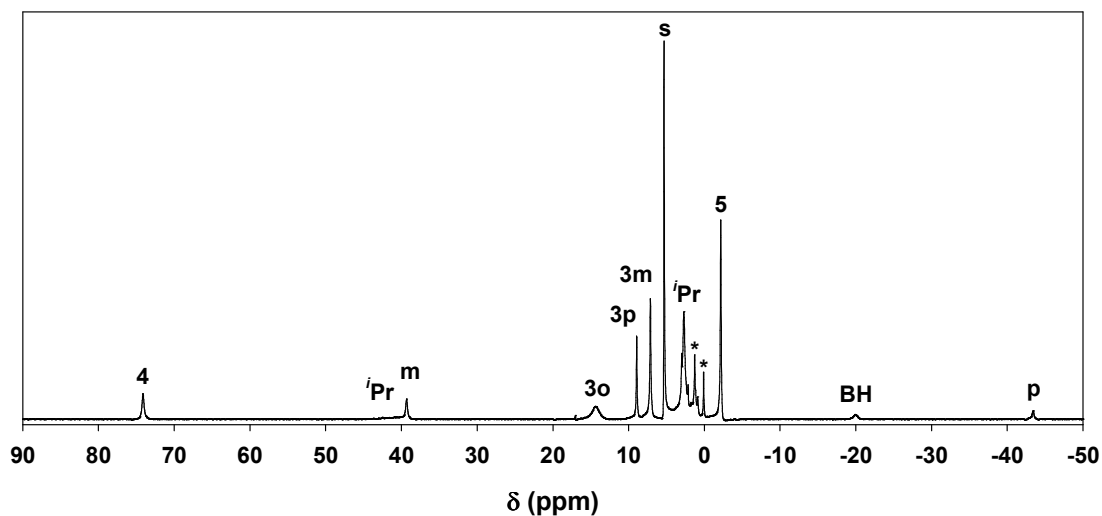


Figure 4-S7. ^1H NMR spectrum (500 MHz, CD_2Cl_2 , 293 K) of $\text{Tp}^{\text{Ph,Me}}\text{Ni-O-2,6-}i\text{Pr}_2\text{C}_6\text{H}_3$ (**4.1a**). Peak due to residual solvent is labeled (s), peaks labeled (*) are assigned to hexane and silicone grease.¹⁰¹

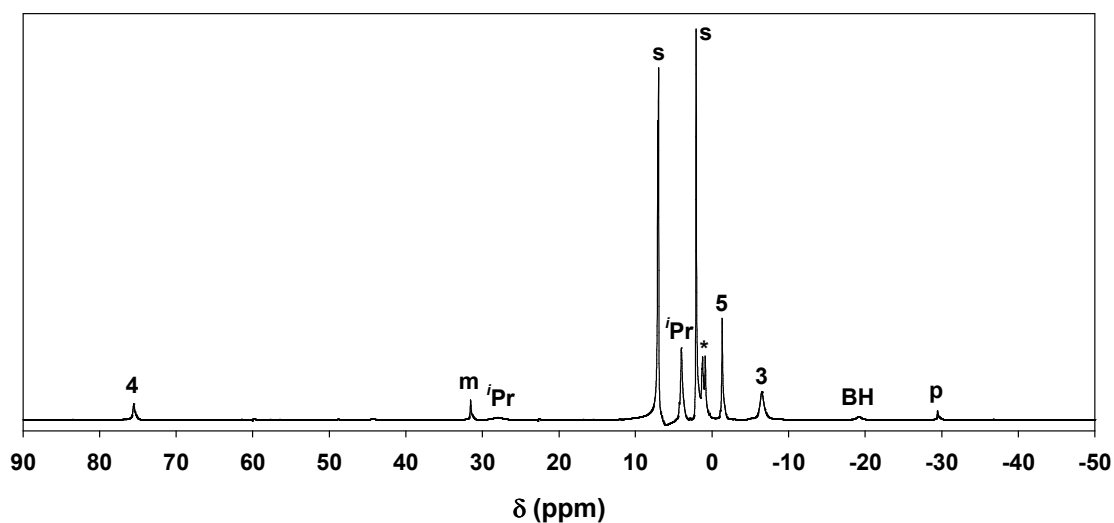


Figure 4-S8. ^1H NMR spectrum (500 MHz, $\text{C}_6\text{D}_5\text{CD}_3$, 293 K) of $\text{Tp}^{\text{Me,Me}}\text{Ni-O-2,6-}i\text{Pr}_2\text{C}_6\text{H}_3$ (**4.1b**). Peaks labeled (*) and (s) are assigned as hexane and residual solvent, respectively.¹⁰¹

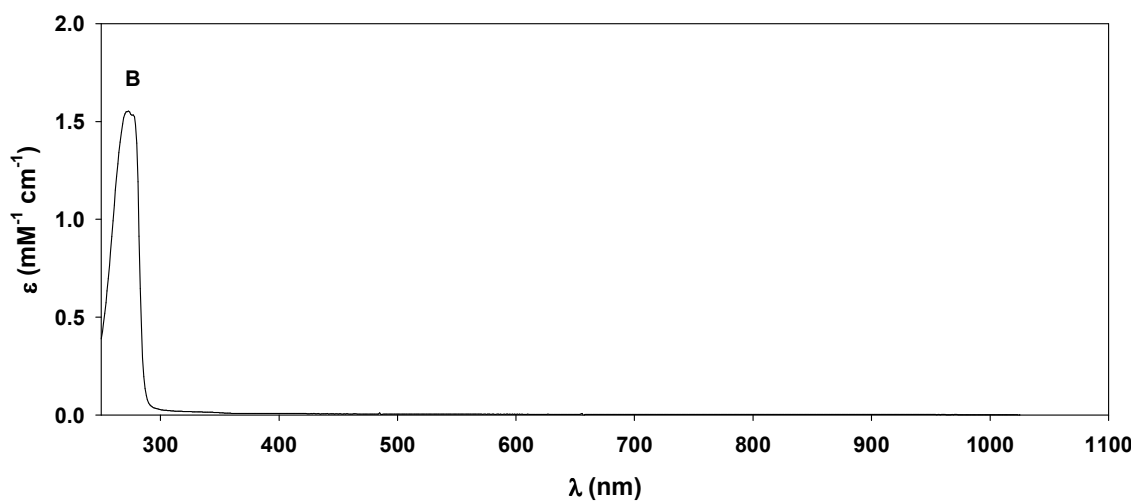


Figure 4-S9. UV-Vis-NIR spectrum of 2,6-diisopropylphenol (B) in CH_2Cl_2 (293 K).

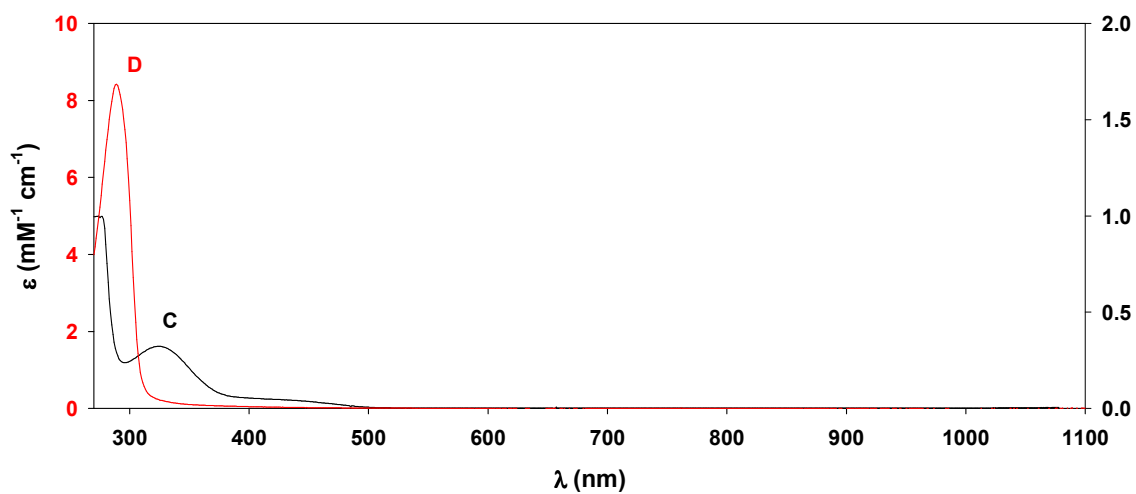


Figure 4-S10. UV-Vis-NIR spectra of 2,6-diisopropyl-1,4-benzoquinone (C, black, right axis) and 2,6-diisopropyl-1,4-benzodihydroquinone (D, red, left axis) in CH_2Cl_2 (293 K).

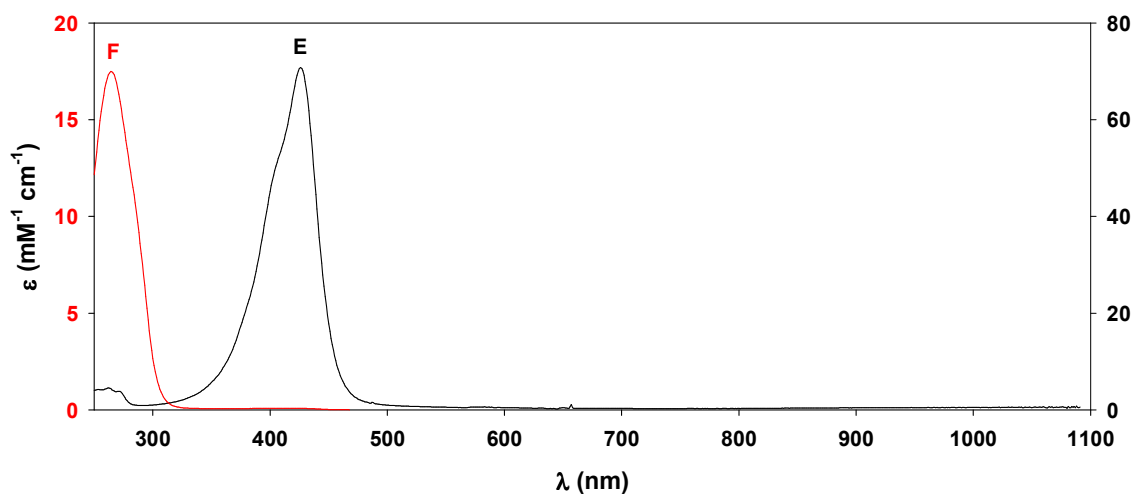


Figure 4-S11. UV-Vis-NIR spectra of 3,5,3',5'-tetraisopropyl-4,4'-diphenoquinone (E, black, right axis) and 3,5,3',5'-tetraisopropyl-4,4'-diphenodihydroquinone (F, red, left axis) in CH_2Cl_2 (293 K).

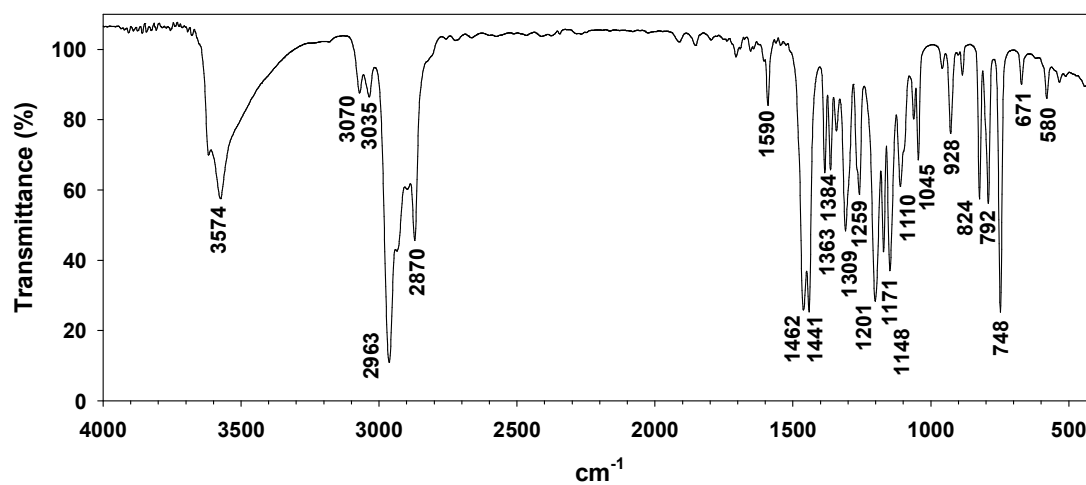


Figure 4-S12. FTIR spectrum (thin film) of 2,6-diisopropylphenol (B).

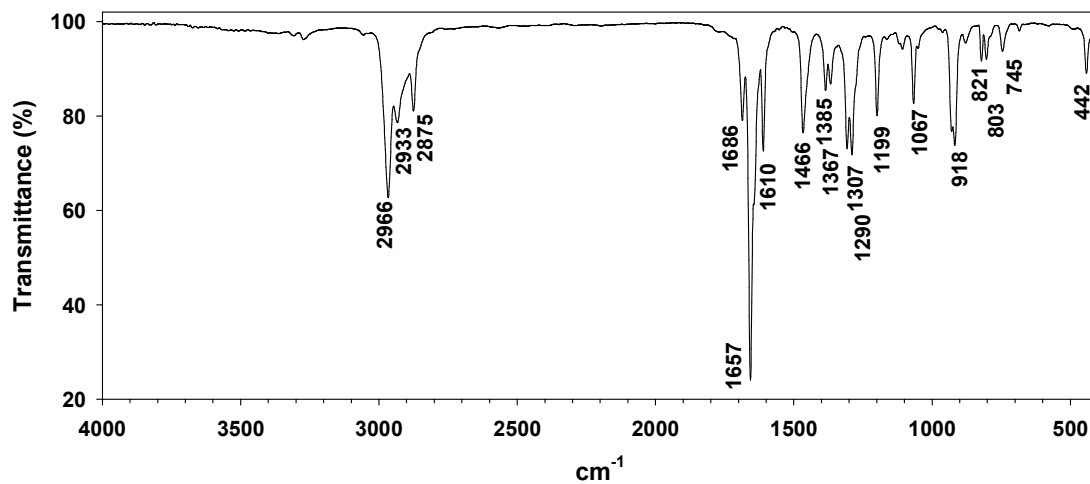


Figure 4-S13. FTIR spectrum (thin film) of 2,6-diisopropyl-1,4-benzoquinone (C).

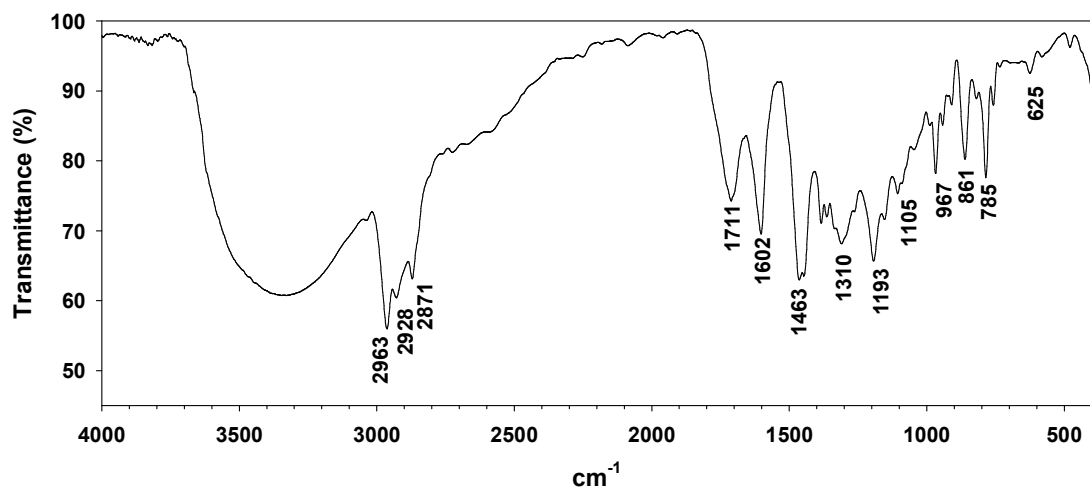


Figure 4-S14. FTIR spectrum (thin film) of 2,6-diisopropyl-1,4-benzodihydroquinone (D).

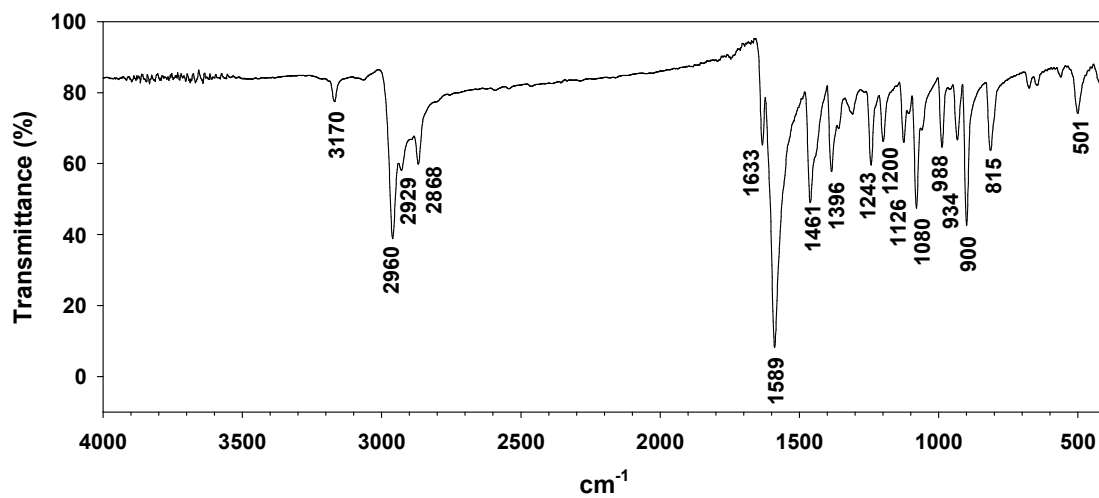


Figure 4-S15. FTIR spectrum (KBr pellet) of 3,5,3',5'-tetraisopropyl-4,4'-diphenylquinone (E).

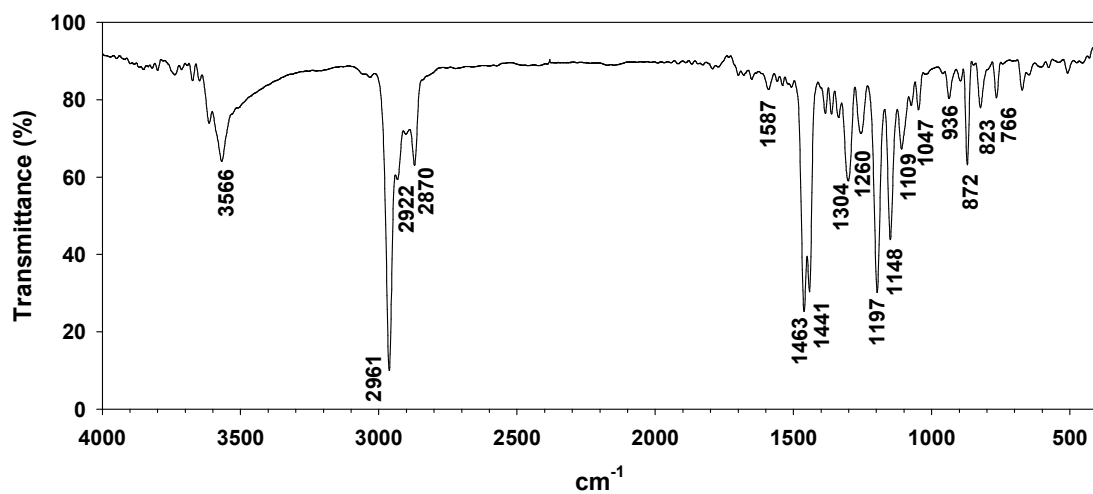


Figure 4-S16. FTIR spectrum (KBr pellet) of 3,5,3',5'-tetraisopropyl-4,4'-diphenylhydroquinone (F).

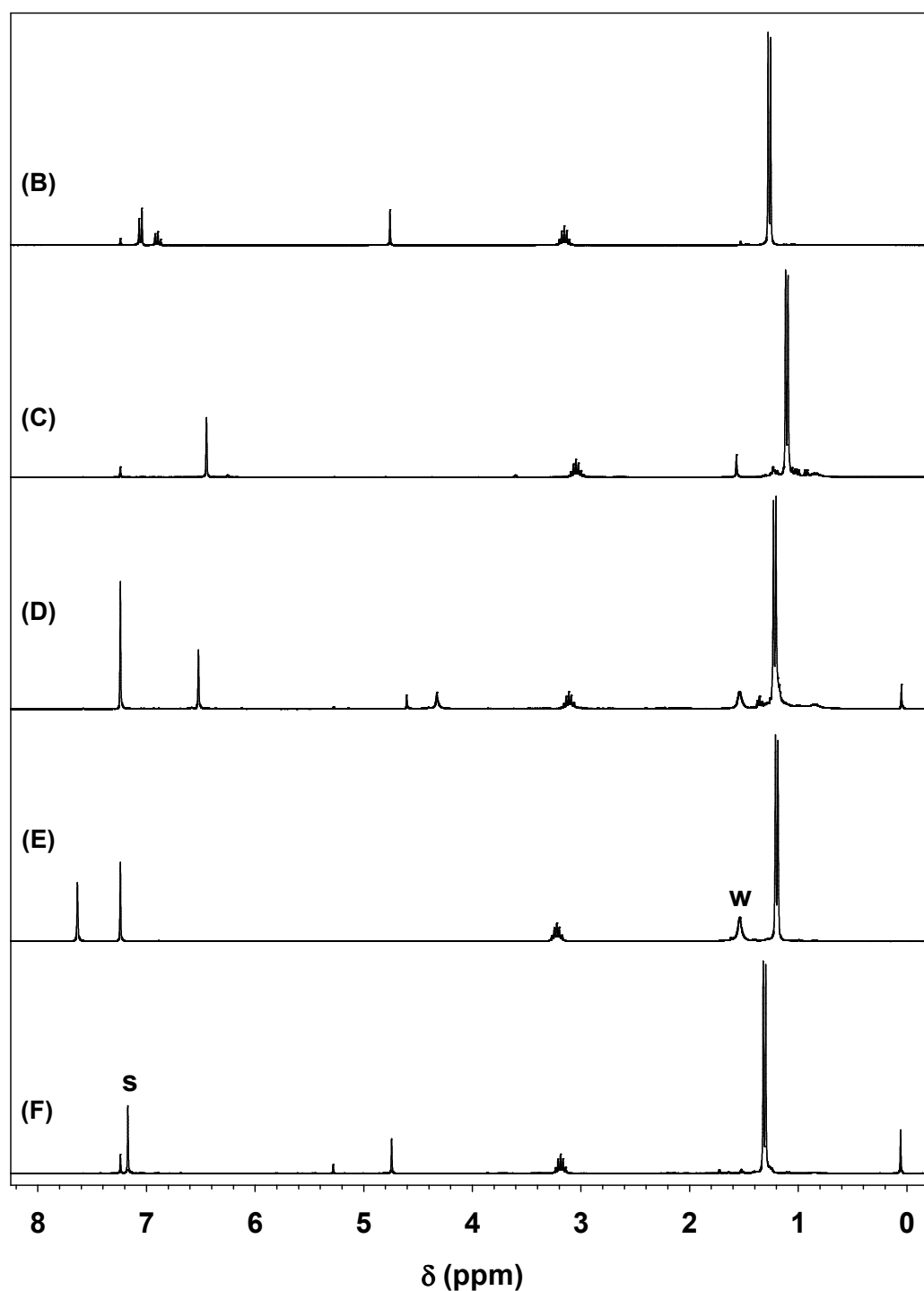


Figure 4-S17. ¹H NMR spectra (300 MHz, CDCl₃, 293 K) of authentic samples of 2,6-diisopropyl phenol (B), 2,6-diisopropyl-1,4-benzoquinone (C), 2,6-diisopropyl-1,4-benzodihydroquinone (D), 3,5,3',5'-tetraisopropyl-4,4'-diphenoquinone (E), and 3,5,3',5'-tetraisopropyl-4,4'-diphenodihydroquinone (F). Peaks marked (s) and (w) are residual solvent and water, respectively.¹⁰¹

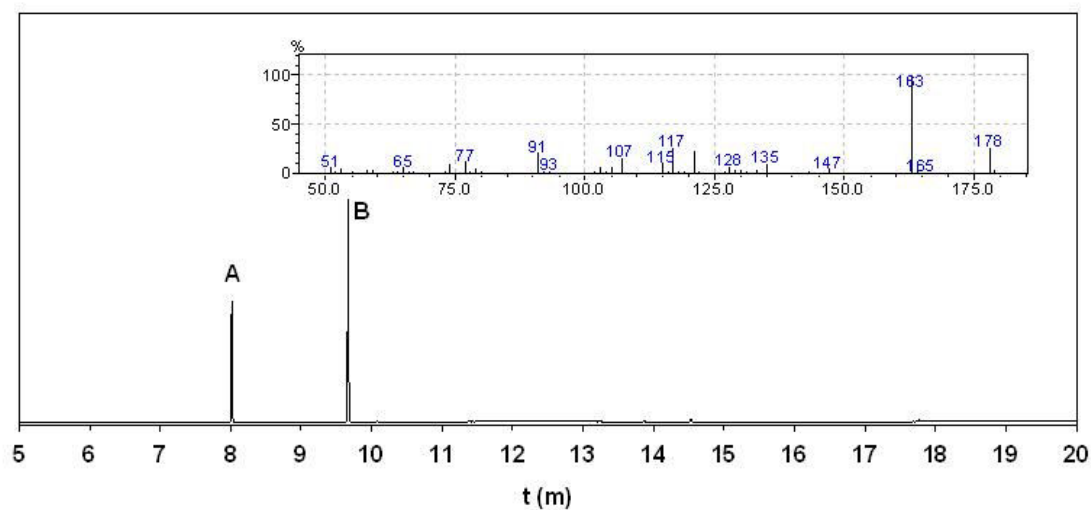


Figure 4-S18. GC-MS data for authentic 2,6-diisopropylphenol (B and inset) against naphthalene standard (A).

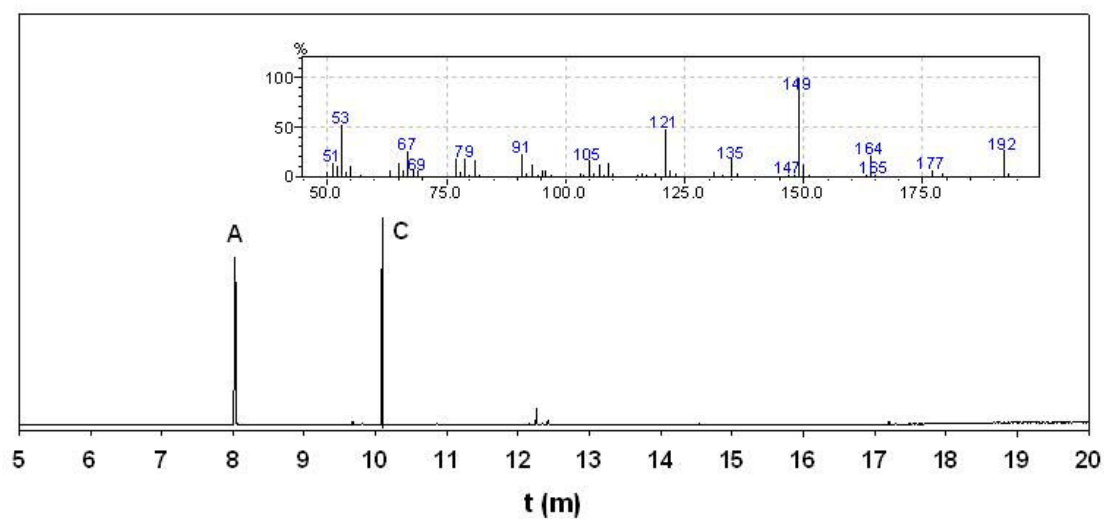


Figure 4-S19. GC-MS data for authentic 2,6-diisopropyl-1,4-benzoquinone (C and inset) against naphthalene standard (A).

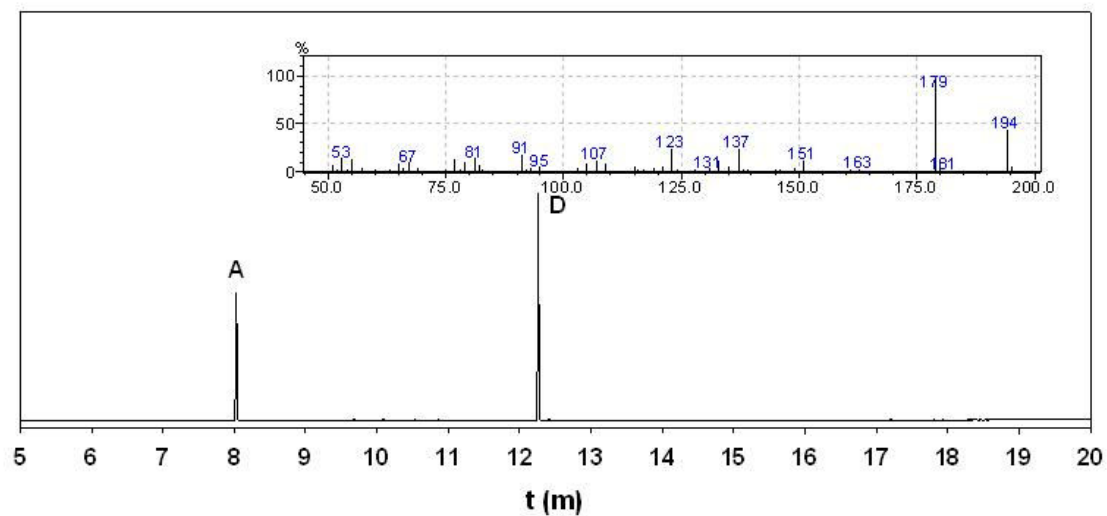


Figure 4-S20. GC-MS data for authentic 2,6-diisopropyl-1,4-benzodihydroquinone (D and inset) against naphthalene standard (A).

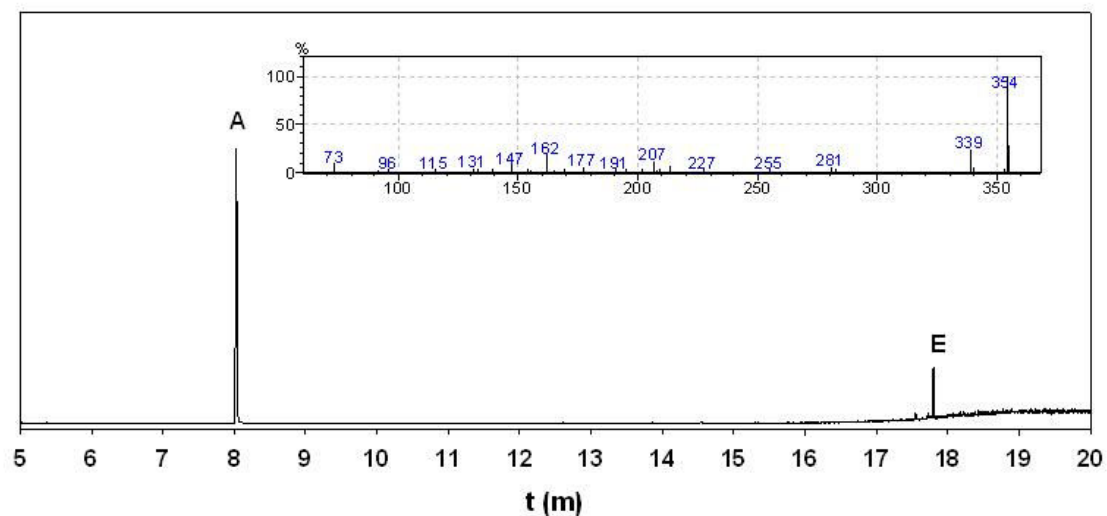


Figure 4-S21. GC-MS data for authentic 3,5,3',5'-tetraisopropyl-4,4'-diphenquinone (E and inset) against naphthalene standard (A).

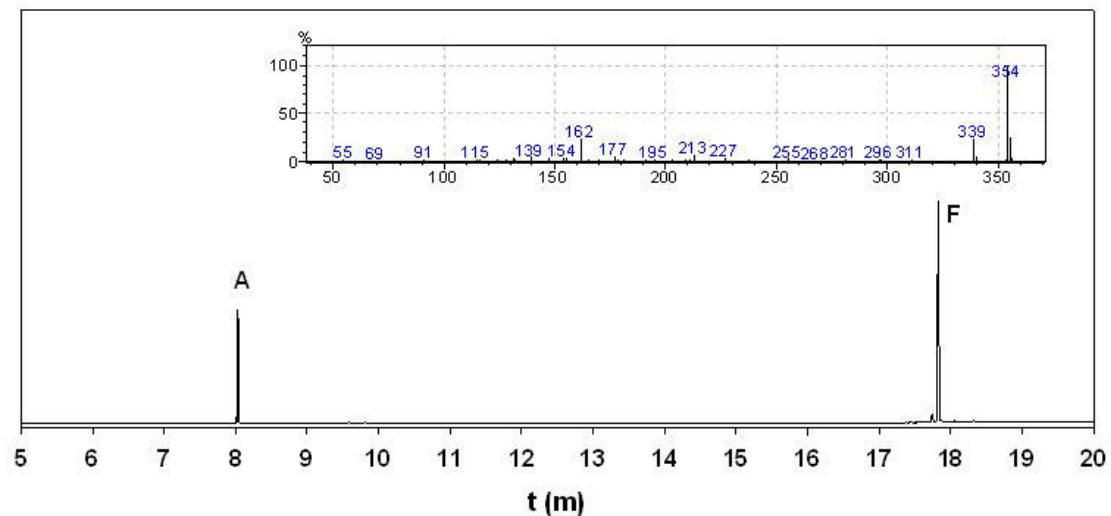


Figure 4-S22. GC-MS data for authentic 3,5,3',5'-tetraisopropyl-4,4'-diphenodihydroquinone (F and inset) against naphthalene standard (A).

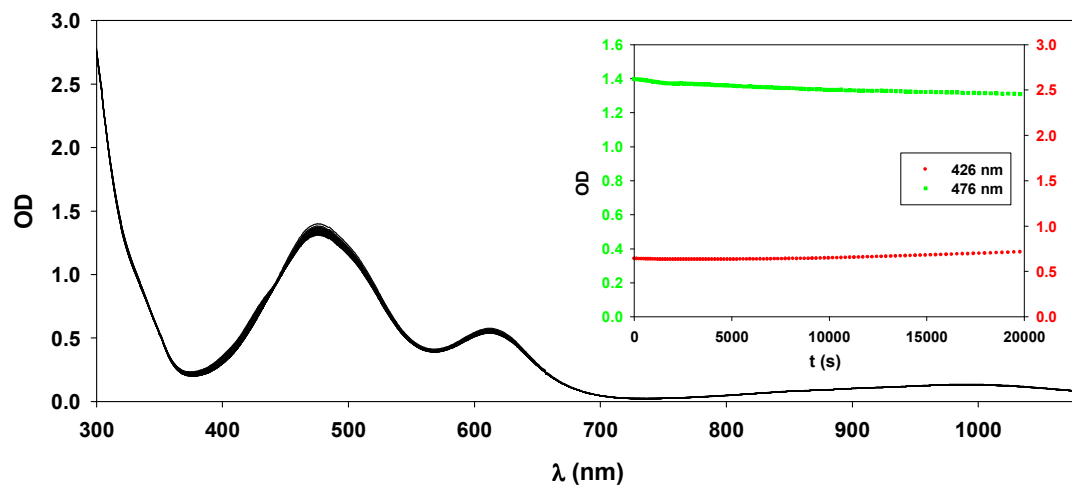


Figure 4-S23. UV-Vis-NIR spectra demonstrating thermal and photolytic stability of 4.1a in dry anaerobic solution (CH_2Cl_2 , 306 K).

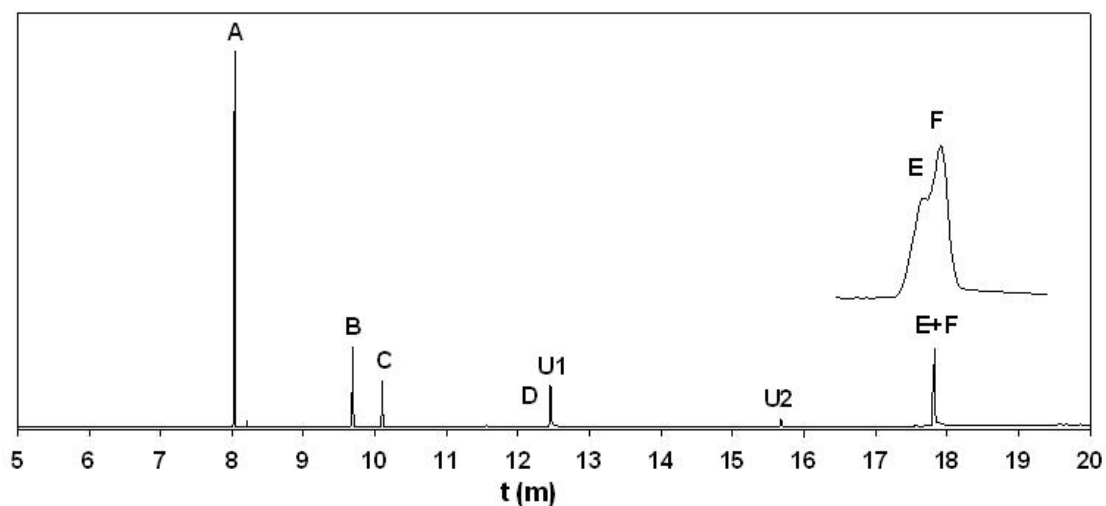


Figure 4-S24. GC trace of organic products obtained following decomposition of **1a** under O_2 in CH_2Cl_2 solution, with peaks assigned as follows: naphthalene (A), 2,6-diisopropyl phenol (B), 2,6-diisopropyl-1,4-benzoquinone (C), 2,6-diisopropyl-1,4-benzodihydroquinone (D), 3,5,3',5'-tetraisopropyl-4,4'-diphenodihydroquinone (E), and 3,5,3',5'-tetraisopropyl-4,4'-diphenodihydroquinone (F). Inset shows horizontal expansion of E+F.

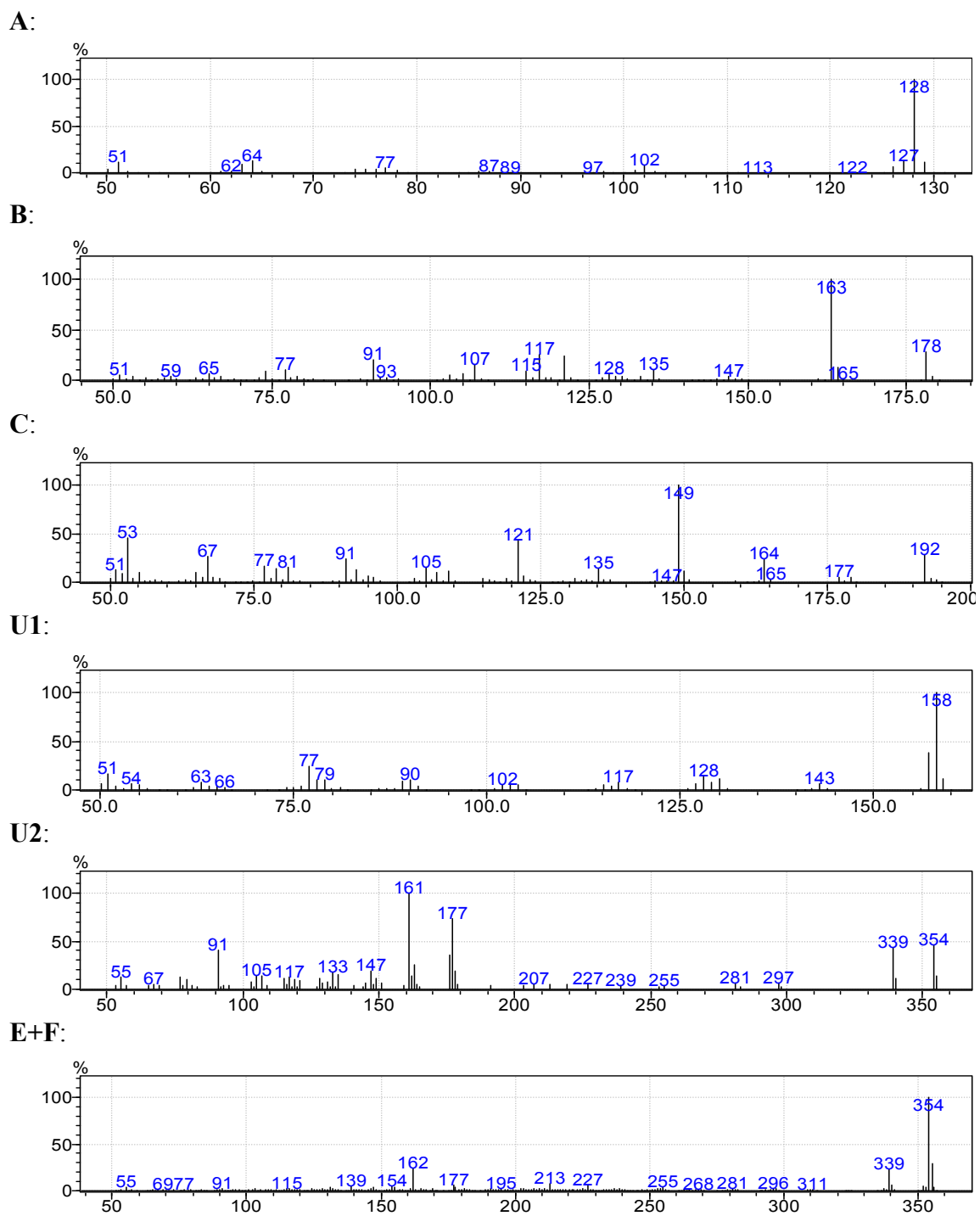


Figure 4-S25. Mass spectra of peaks from GC trace in Figure 4-S24.

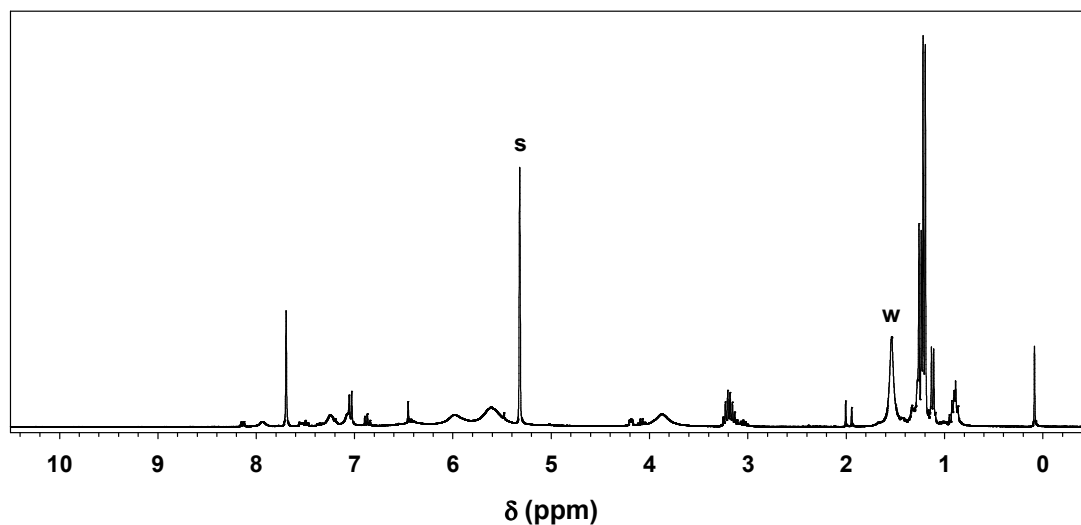


Figure 4-S26. ^1H NMR spectrum (300 MHz, 293 K) of residue from decomposition of **4.1a** under O_2 in CH_2Cl_2 , extracted into CD_2Cl_2 . Residual solvent (s) and water (w) peaks are labeled.¹⁰¹

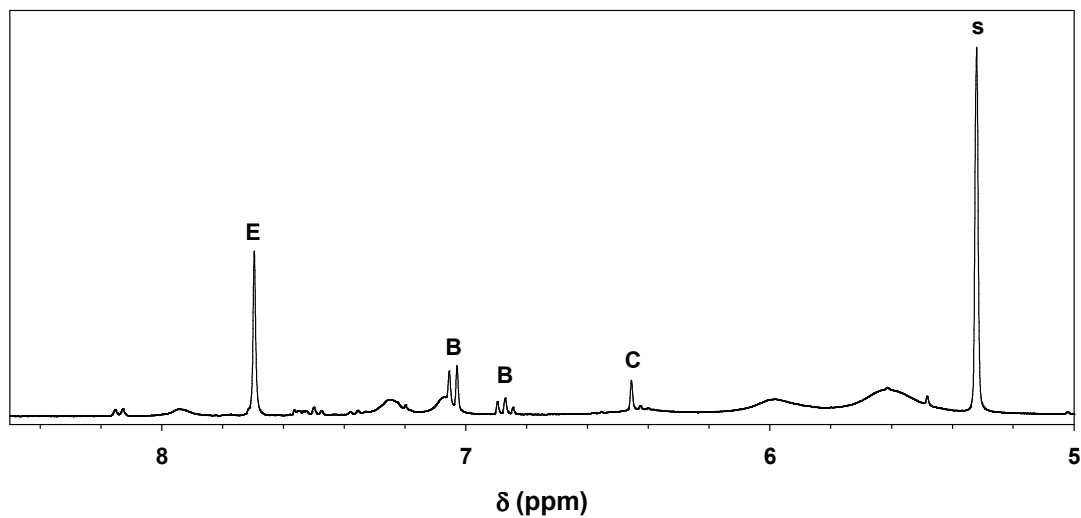


Figure 4-S27. Detail of Figure S26, showing assignment of aromatic proton resonances to 2,6-diisopropylphenol (B), 2,6-diisopropyl-1,4-benzoquinone (C) and 3,5,3',5'-tetraisopropyl-4,4'-diphenylquinone (E).

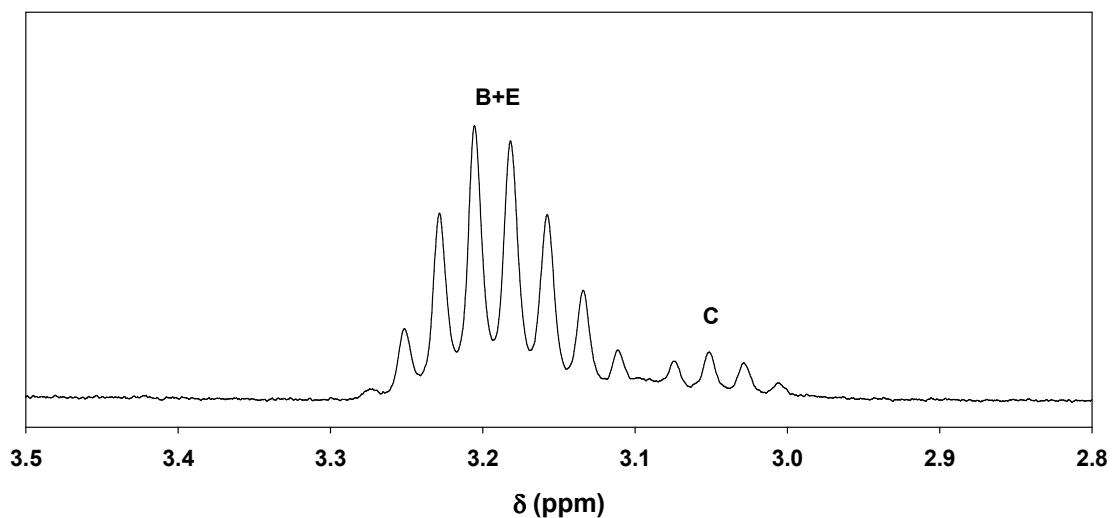


Figure 4-S28. Detail of Figure S26, showing assignment of isopropyl methine resonances to 2,6-diisopropyl phenol (B), 2,6-diisopropyl-1,4-benzoquinone (C) and 3,5,3',5'-tetraisopropyl-4,4'-diphenyl-1,4-benzoquinone (E).

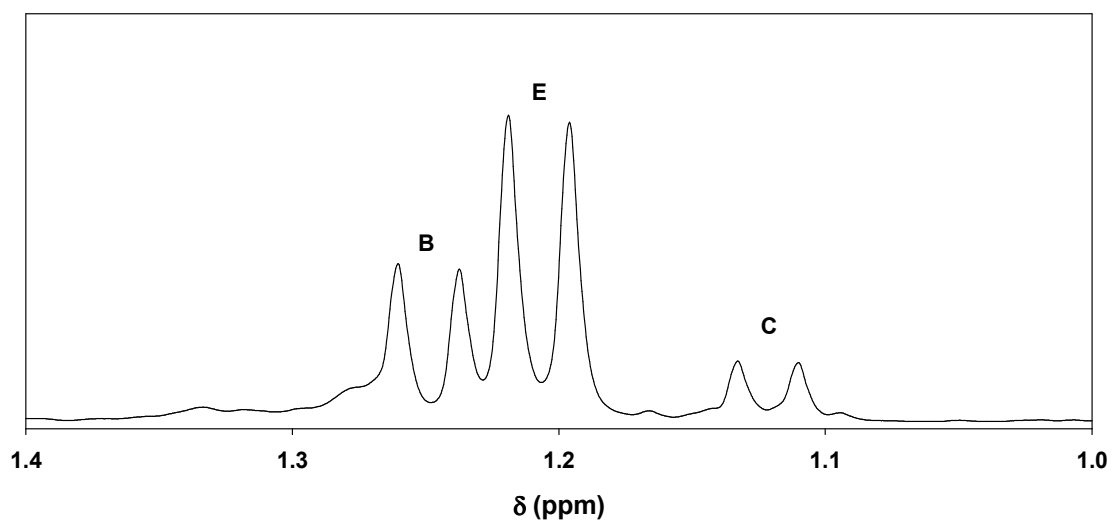


Figure 4-S29. Detail of Figure S26, showing assignment of isopropyl methyl resonances to 2,6-diisopropyl phenol (B), 2,6-diisopropyl-1,4-benzoquinone (C) and 3,5,3',5'-tetraisopropyl-4,4'-diphenyl-1,4-benzoquinone (E).

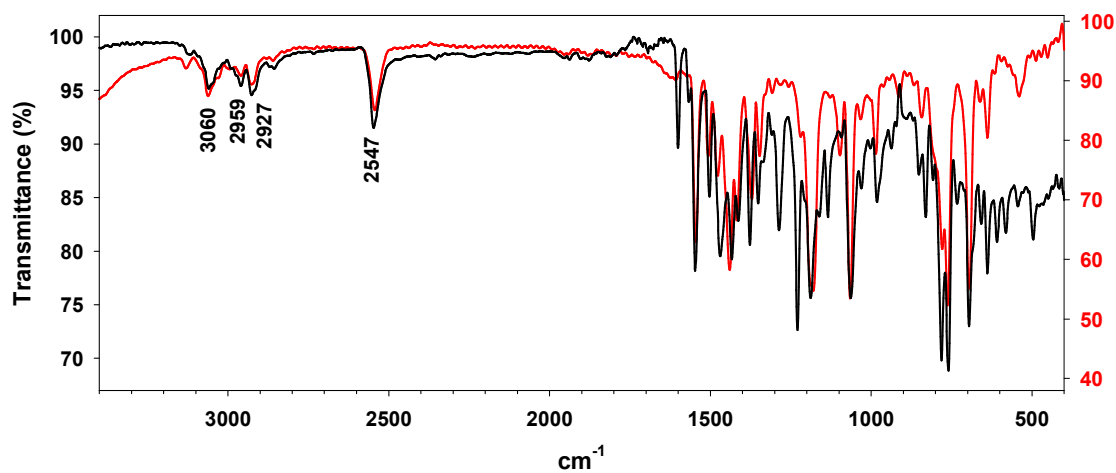


Figure 4-S30. Comparison of FTIR spectra (KBr pellets) of $[(\text{Tp}^{\text{Ph,Me}^*})\text{Ni}]_2$ (4.2) (black) and $\text{Tp}^{\text{Ph,Me}}\text{NiCl}$ (red).

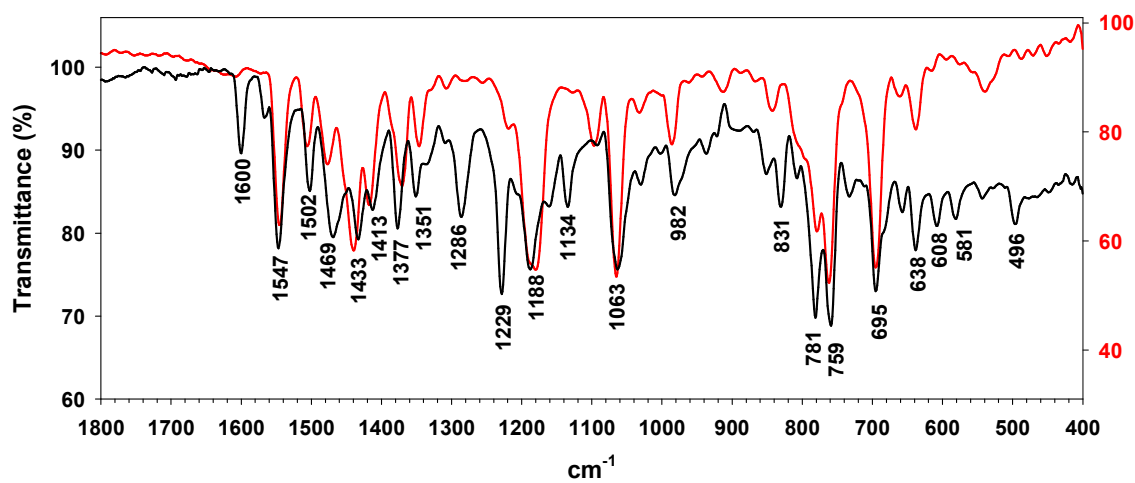


Figure 4-S31. Detail of FTIR spectra of $[(\text{Tp}^{\text{Ph,Me}^*})\text{Ni}]_2$ (4.2) (black) and $\text{Tp}^{\text{Ph,Me}}\text{NiCl}$ (red).

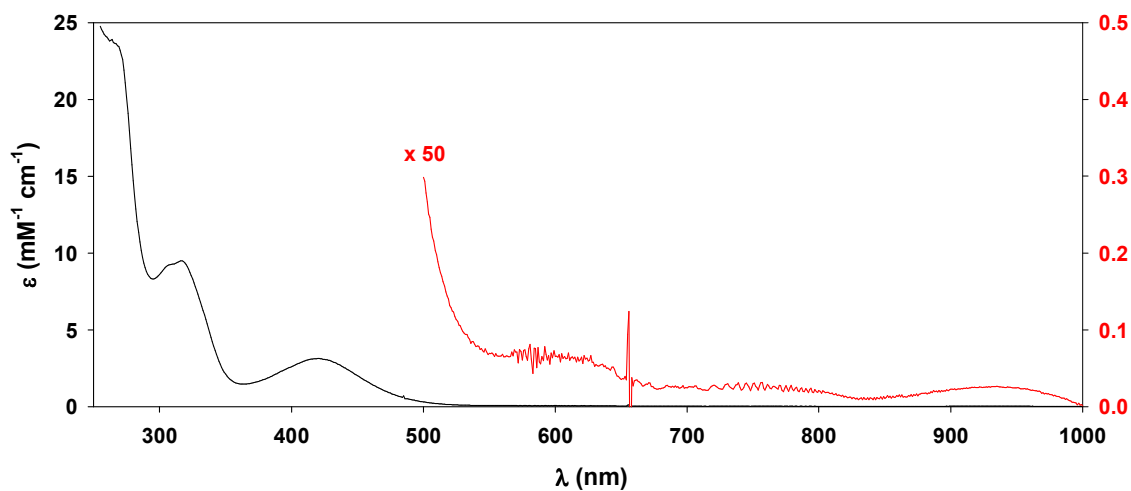


Figure 4-S32. UV-Vis-NIR spectrum (CH_2Cl_2 , 293 K) of $[(\text{Tp}^{\text{Ph,Me}^*})\text{Ni}]_2$ (**4.2**). Data in red are shown as a 50-fold vertical expansion (right axis).

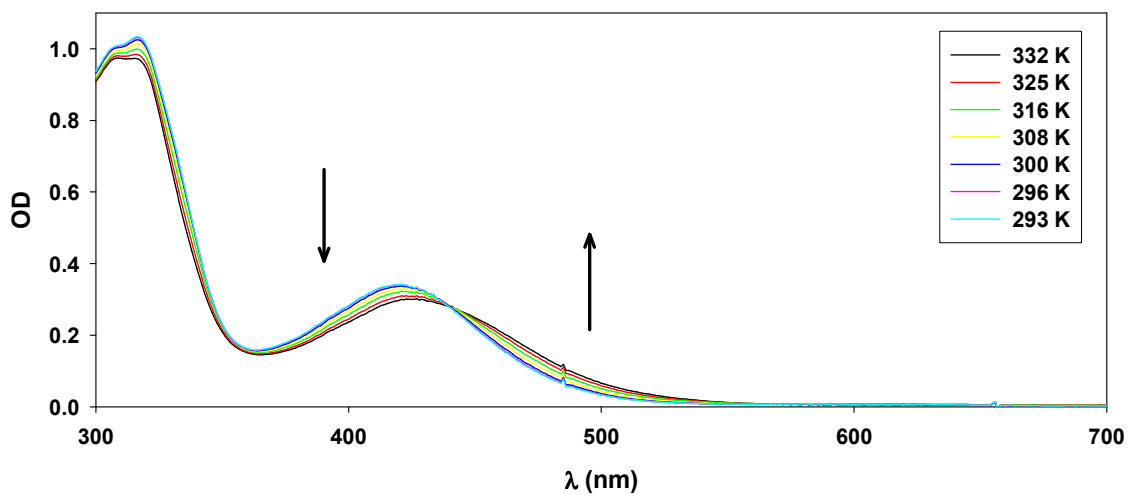


Figure 4-S33. UV-Vis spectra of $[(\text{Tp}^{\text{Ph,Me}^*})\text{Ni}]_2$ (**4.2**) observed on cooling a CH_2Cl_2 solution from 332 to 293 K (raw data, not corrected for changes in solvent volume).

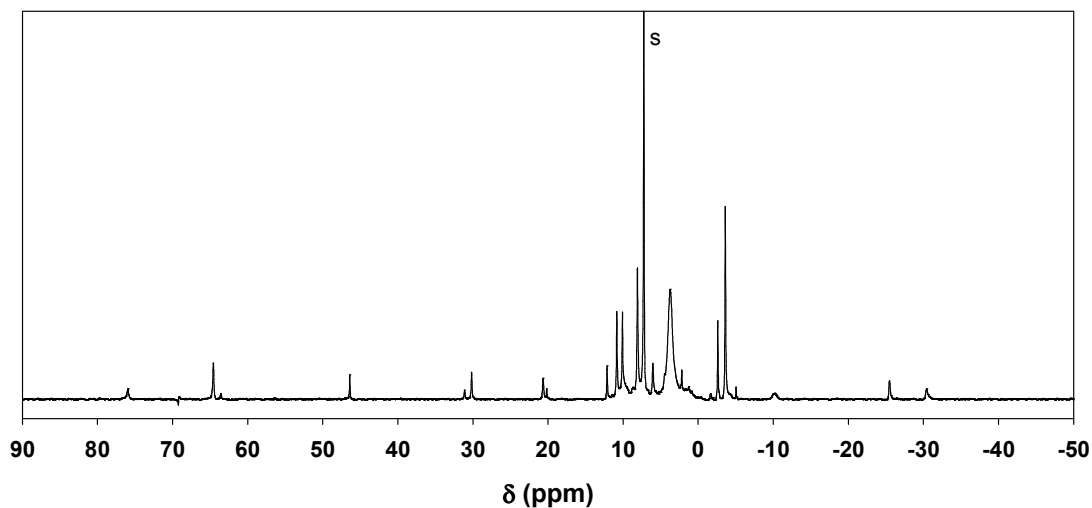


Figure 4-S34. ^1H NMR spectrum (500 MHz, CDCl_3 , 293 K) of $[(\text{Tp}^{\text{Ph,Me}^*})\text{Ni}]_2$ (**4.2**), derived from reaction of **4.1a** with O_2 . Residual solvent peak marked (s).¹⁰¹

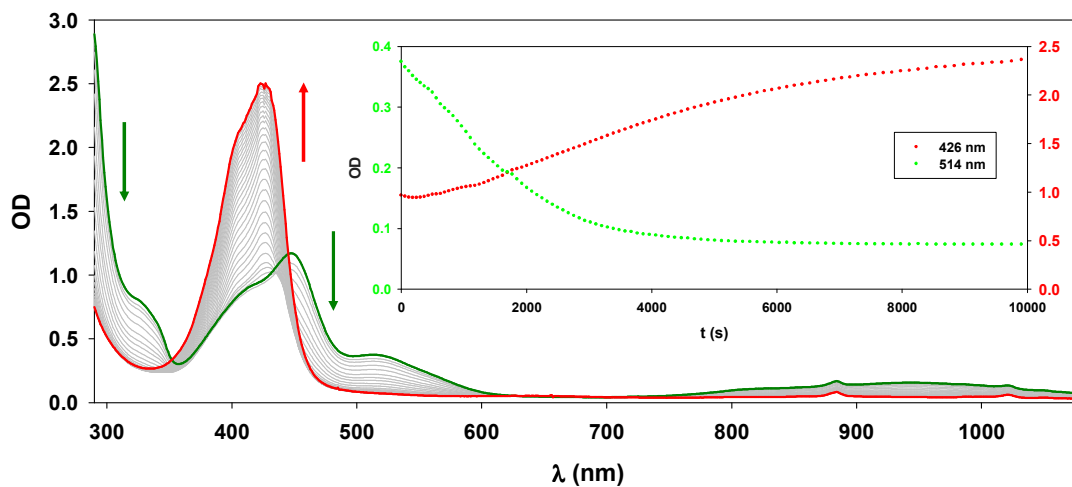


Figure 4-S35. Monitoring of decomposition of **4.1b** (1.1 mM) in O_2 -saturated CH_2Cl_2 (293 K) by UV-Vis-NIR spectroscopy. Inset shows time-dependent decay of **4.1b** (at 514 nm, green) and growth of the chromophore assigned to 3,5,3',5'-tetraisopropyl-4,4'-diphenoquinone (at 426 nm, red).

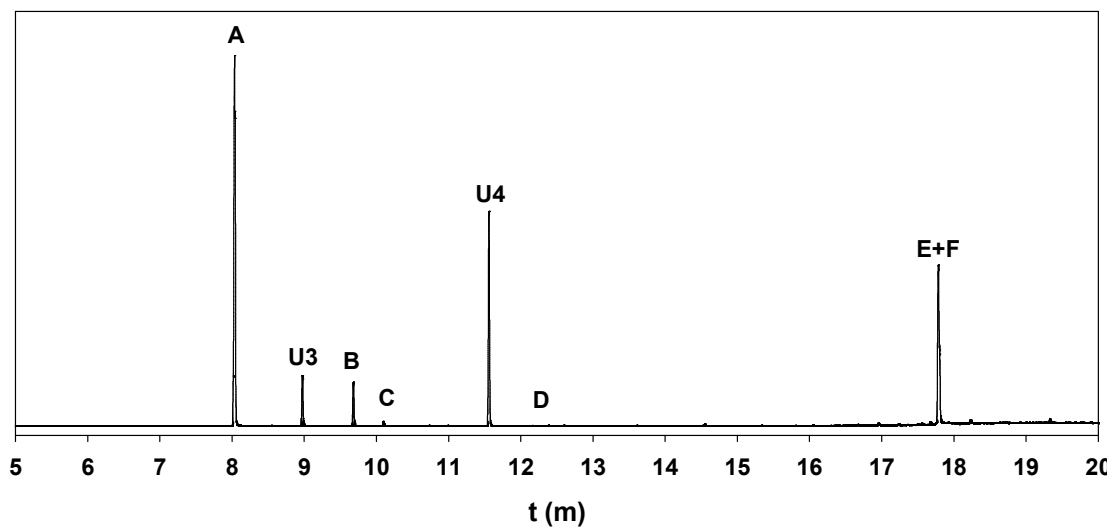


Figure 4-S36. GC trace of organic products obtained following decomposition of **4.1b** under O_2 in CH_2Cl_2 solution, with peaks assigned as follows: naphthalene (A), 2,6-diisopropyl phenol (B), 2,6-diisopropyl-1,4-benzoquinone (C), 2,6-diisopropyl-1,4-benzodihydroquinone (D), 3,5,3',5'-tetraisopropyl-4,4'-diphenodihydroquinone (E), and 3,5,3',5'-tetraisopropyl-4,4'-diphenodihydroquinone (F).

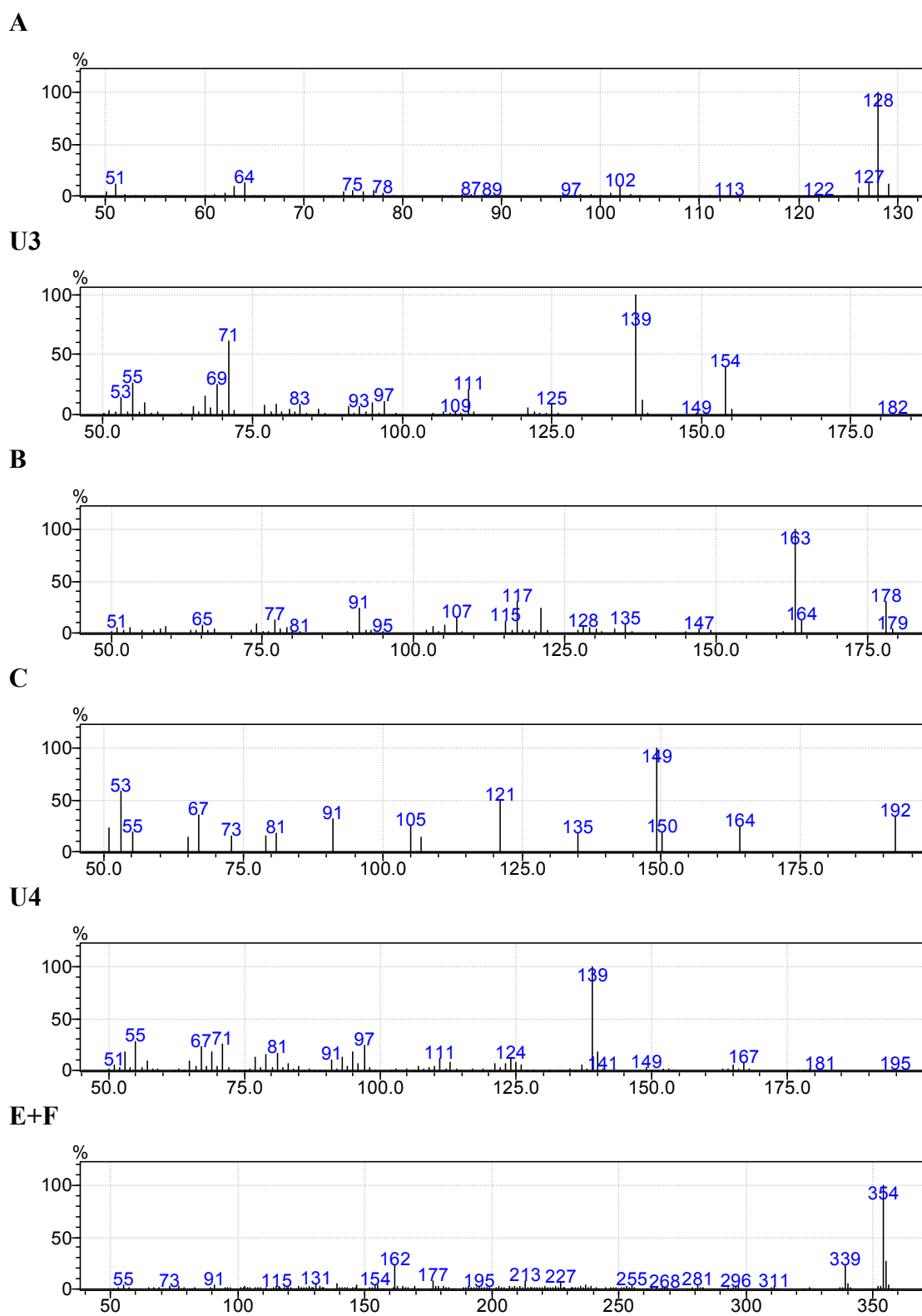


Figure 4-S37. Mass spectra of peaks from GC trace in Figure 4-S36.

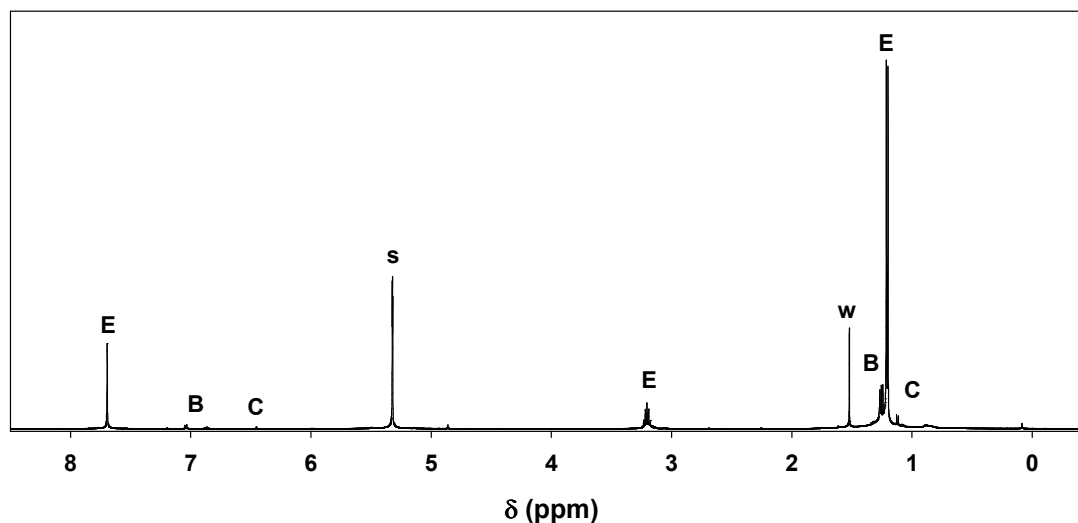


Figure 4-S38. ^1H NMR spectrum (CD_2Cl_2) of extracted organic products from aerobic decomposition of **4.1b**, following chromatographic separation of unknowns **U3** and **U4**, showing assignment of resonances to 2,6-diisopropylphenol (**B**), 2,6-diisopropyl-1,4-benzoquinone (**C**) and 3,5,3',5'-tetraisopropyl-4,4'-diphenylquinone (**E**). Peaks due to residual solvent (**s**) and water (**w**) are marked.¹⁰¹

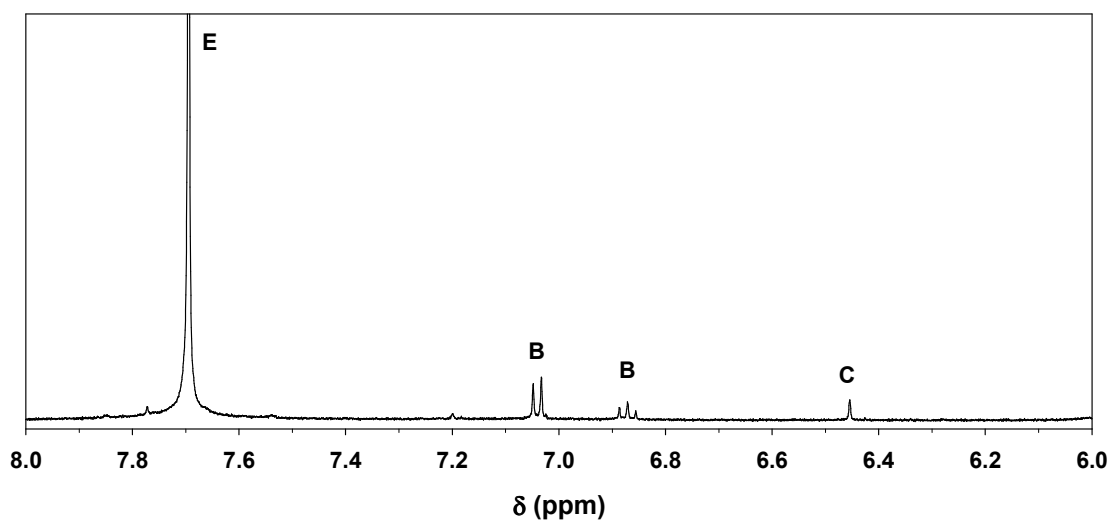


Figure 4-S39. Detail of Figure S38, showing assignment of aromatic proton resonances to 2,6-diisopropylphenol (**B**), 2,6-diisopropyl-1,4-benzoquinone (**C**) and 3,5,3',5'-tetraisopropyl-4,4'-diphenylquinone (**E**).

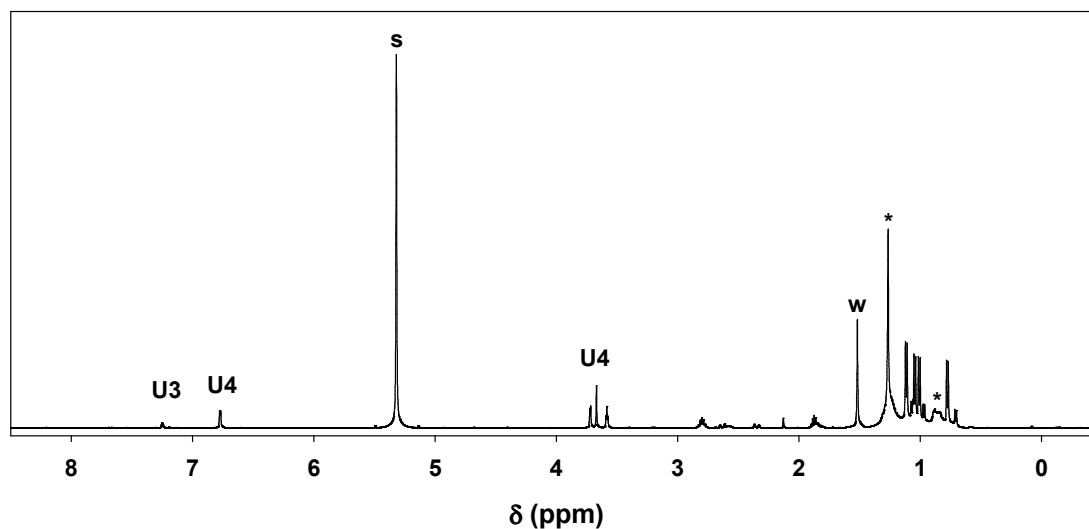


Figure 4-S40. ¹H NMR spectrum (CD₂Cl₂) of chromatographic extracts containing unknown organic products **U3** and **U4** from aerobic decomposition of **4.1b**. Peaks due to residual solvent (s), water (w) and Apiezon H grease (*) are marked.¹⁰¹

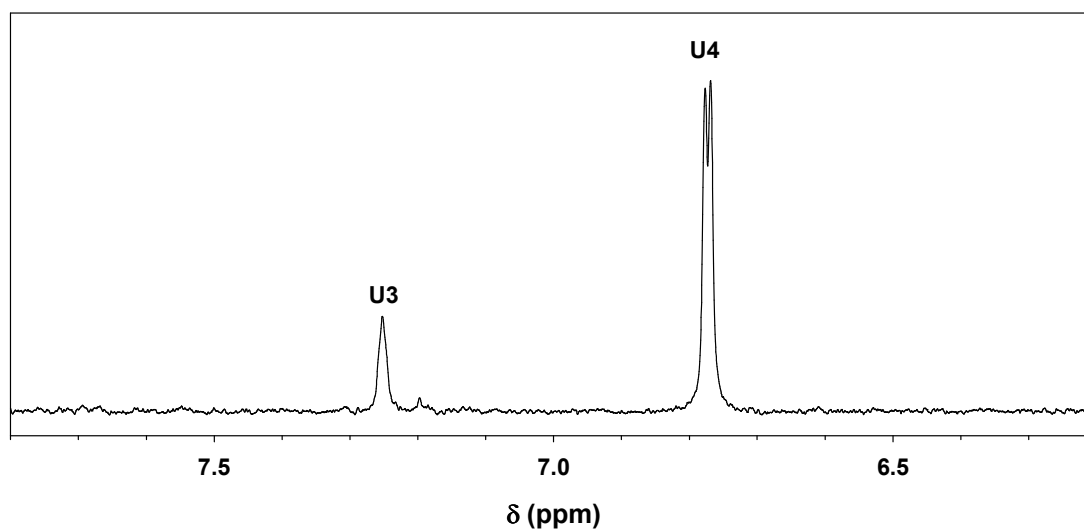


Figure 4-S41. Detail of Figure 4-S40, showing assignment of resonances.

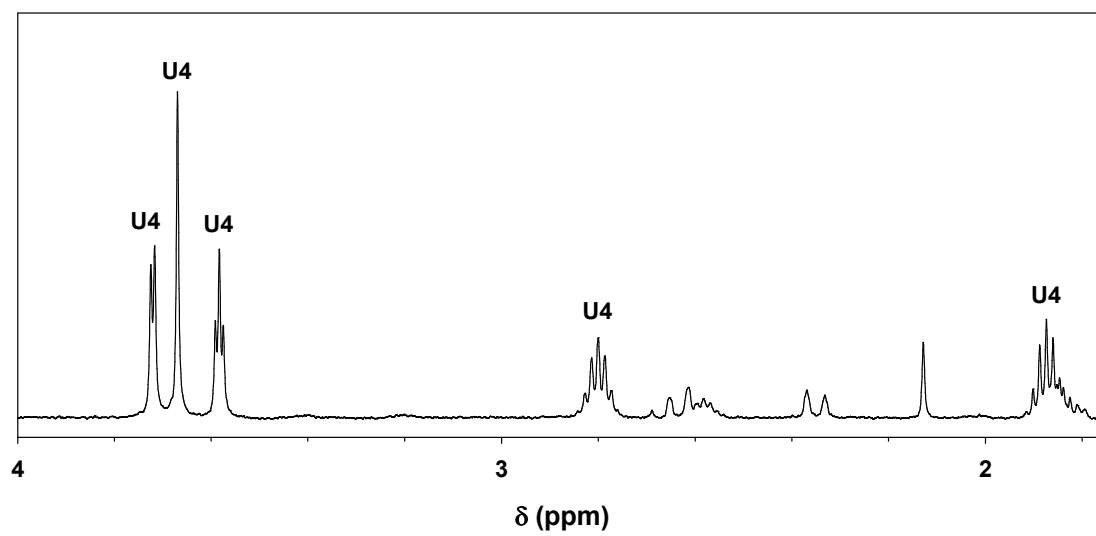


Figure 4-S42. Detail of Figure 4-S38, showing assignment of resonances.

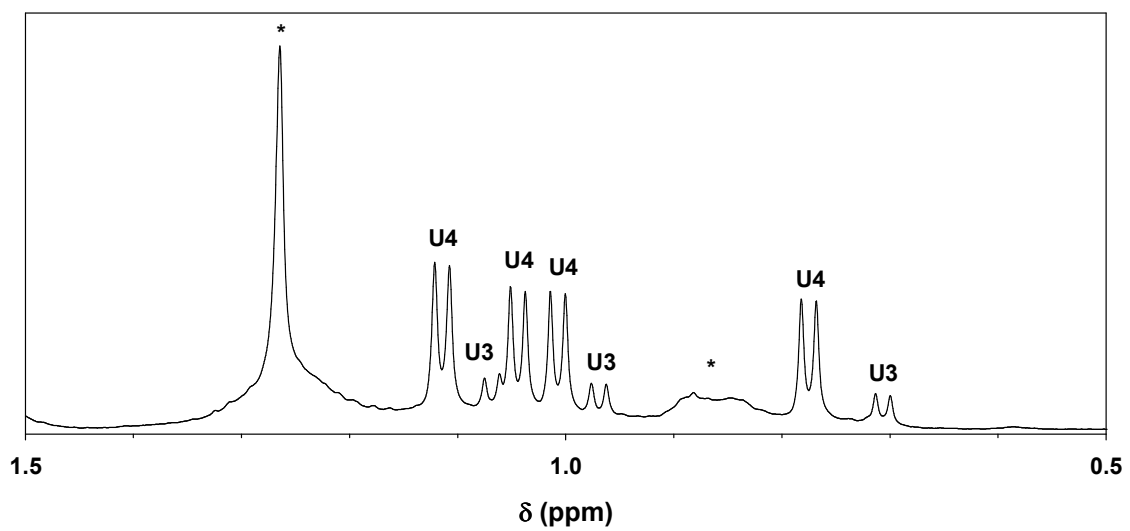


Figure 4-S43. Detail of Figure 4-S38, showing assignment of resonances.

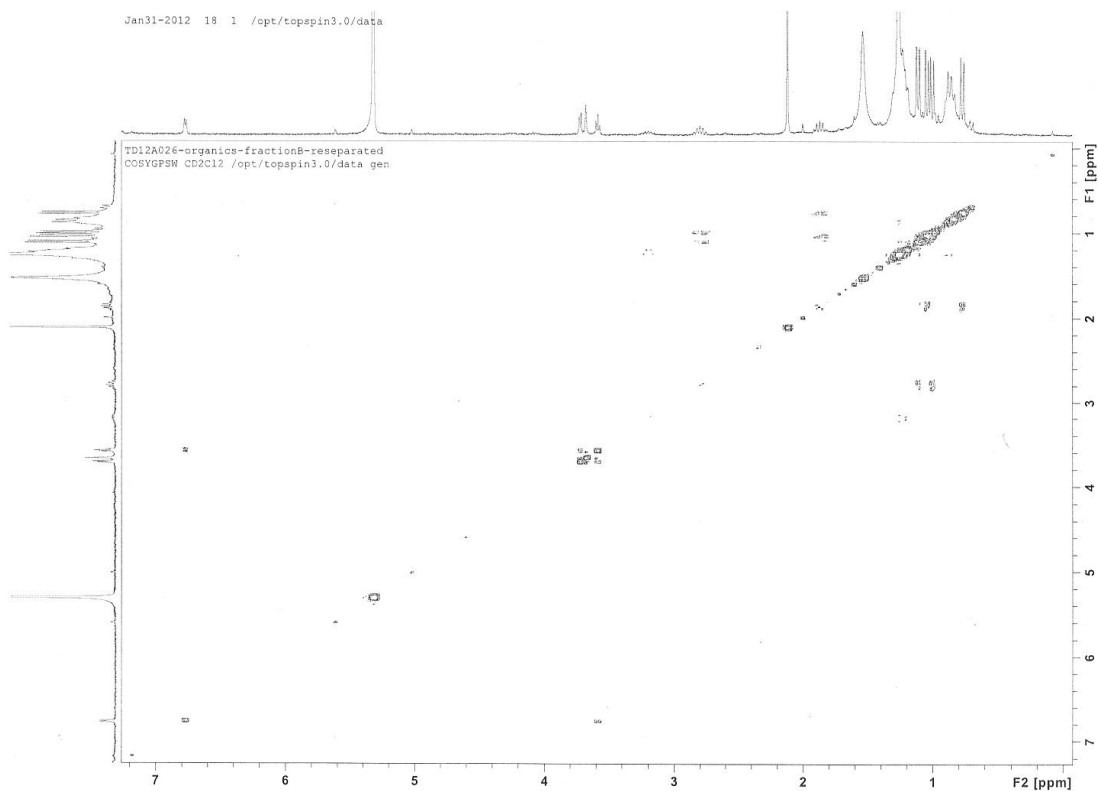


Figure 4-S44. COSY contour plot of U4 from aerobic decomposition of **4.1b** in CD_2Cl_2 .

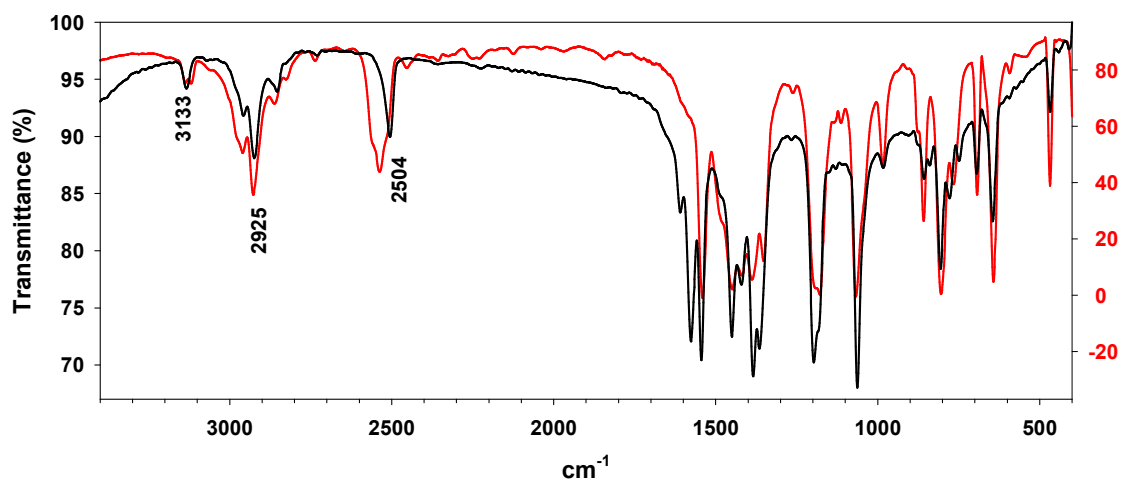


Figure 4-S45. Comparison of FTIR spectra (KBr pellets) of $[\text{Tp}^{\text{Me,Me}}\text{Ni}]_2(\mu\text{-CO}_3)$ (**4.3**, black) and $\text{Tp}^{\text{Me,Me}}\text{NiCl}$ (red).

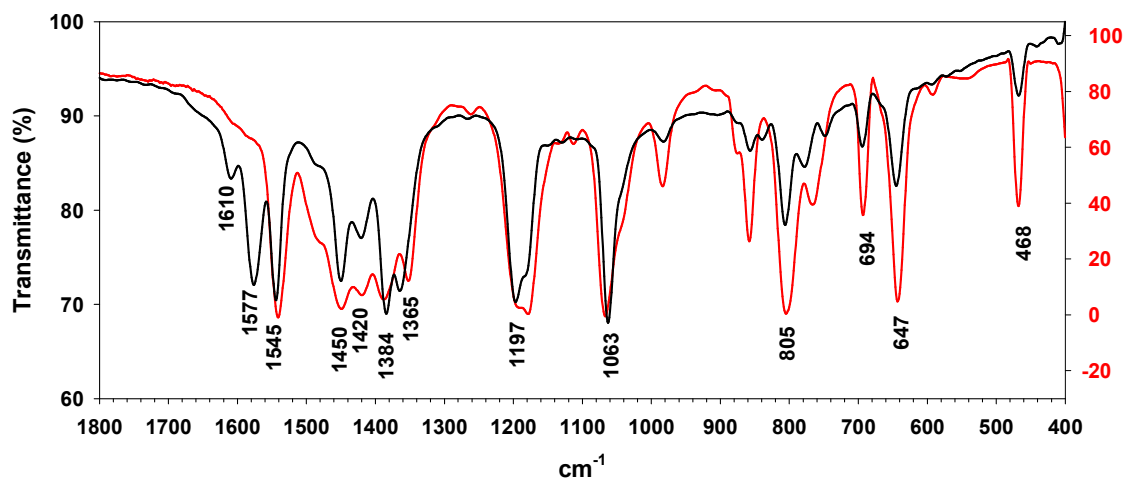


Figure 4-S46. Detail of FTIR spectra of $[\text{Tp}^{\text{Me,Me}}\text{Ni}]_2(\mu\text{-CO}_3)$ (4.3, black) and $\text{Tp}^{\text{Me,Me}}\text{NiCl}$ (red).

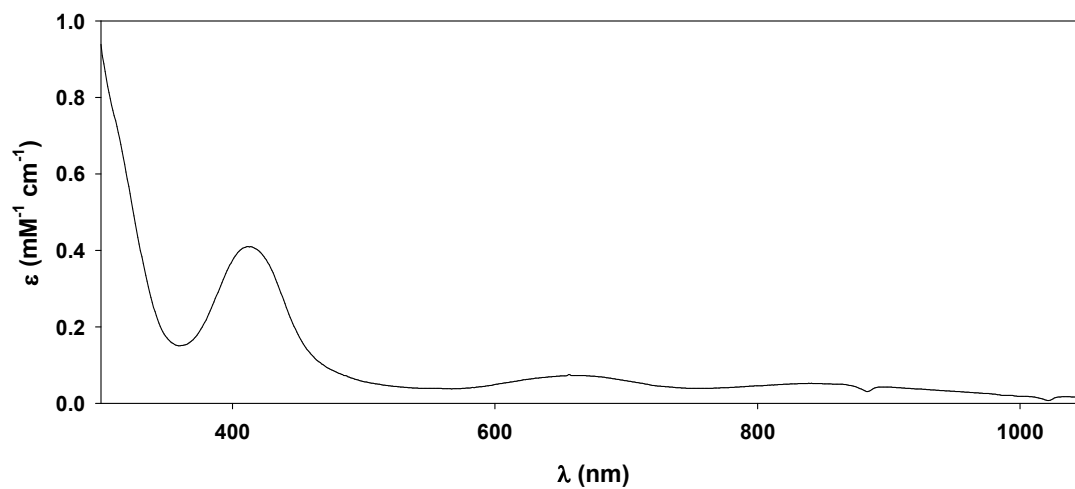


Figure 4-S47. UV-Vis-NIR spectrum (CH_2Cl_2 , 293 K) of $[\text{Tp}^{\text{Me,Me}}\text{Ni}]_2(\mu\text{-CO}_3)$ (4.3).

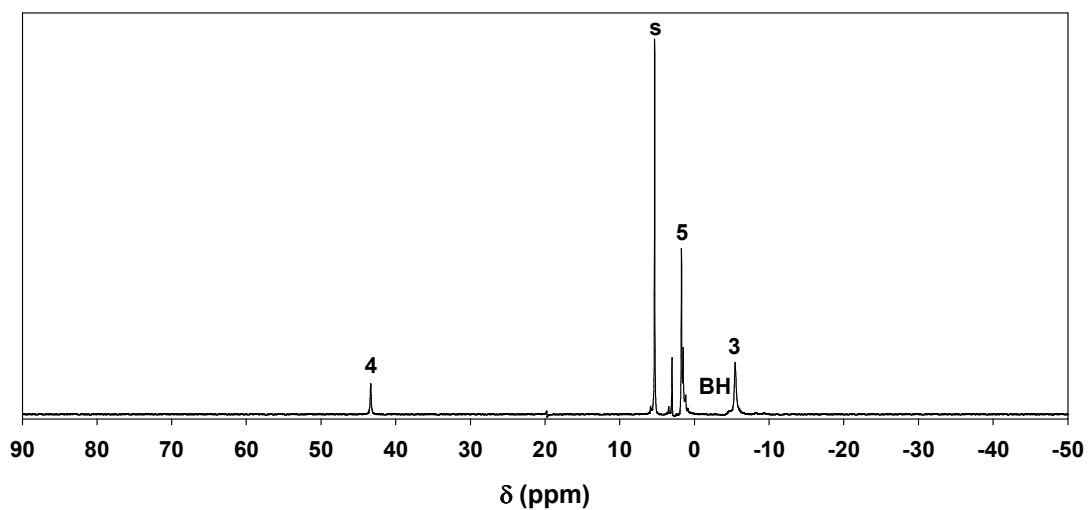


Figure 4-S48. ¹H NMR spectrum (500 MHz, CD₂Cl₂, 293 K) of [Tp^{Me,Me}Ni]₂(μ-CO₃) (4.3).

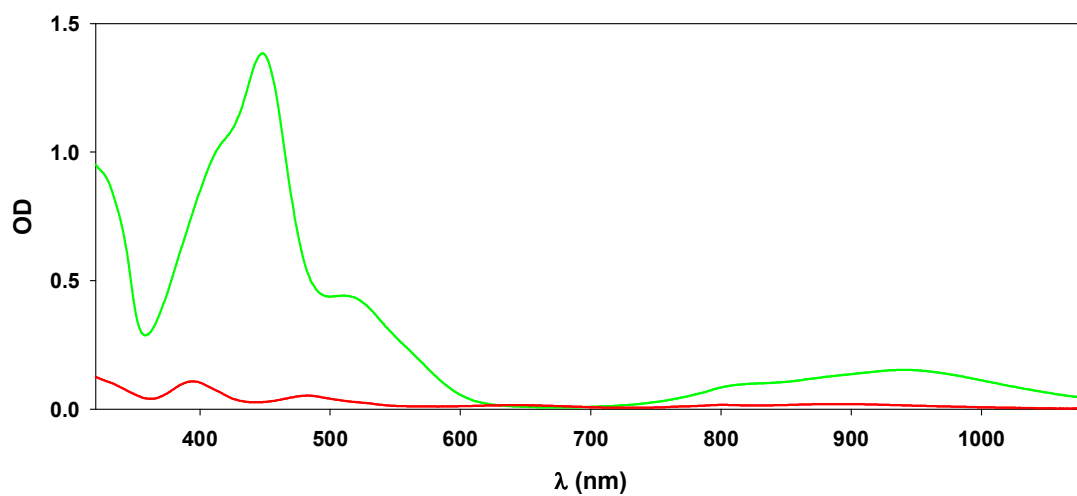


Figure 4-S49. UV-Vis-NIR spectra of **4.1b** (1.4 mM, CH₂Cl₂, 293 K), before (green) and after addition of H₂O (220 mM, red).

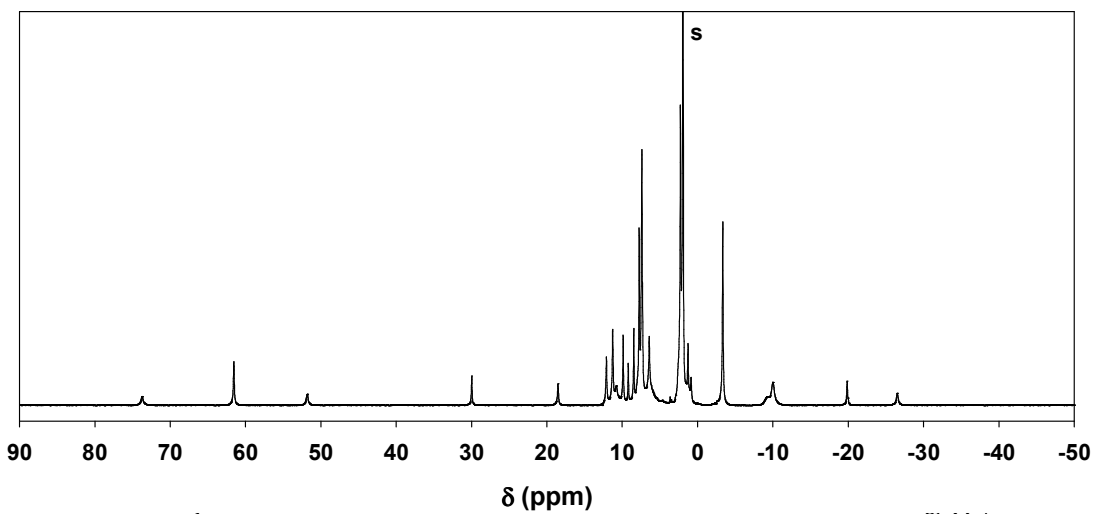


Figure 4-S50. ¹H NMR spectrum (500 MHz, CD₃CN, 293 K) of [(Tp^{Ph,Me*})Ni]₂ (**4.2**), derived from reaction of **4.1a** with aqueous H₂O₂.

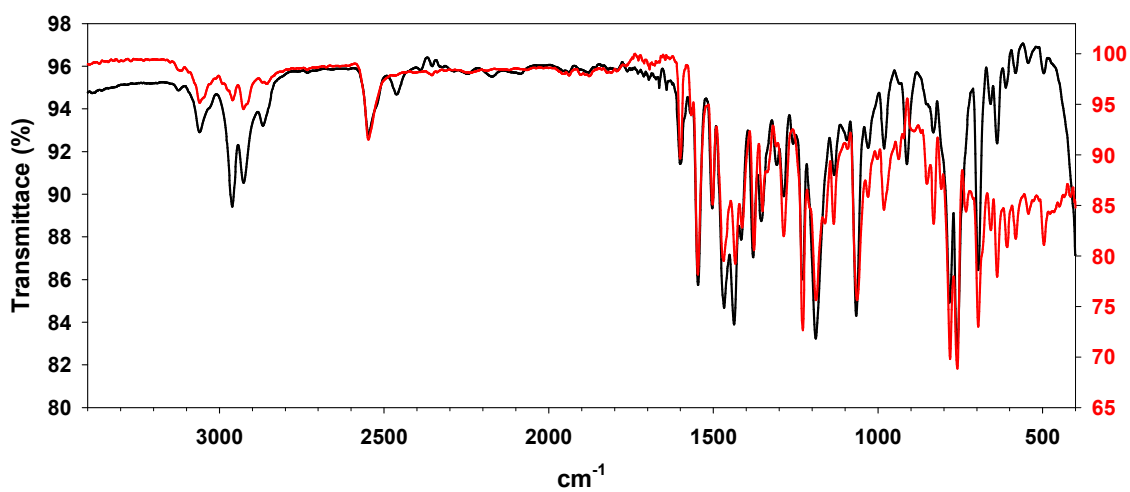


Figure 4-S51. Comparison of FTIR spectra (KBr pellets) of [(Tp^{Ph,Me*})Ni]₂ (**4.2**) derived from oxidation of **4.1a** with aqueous H₂O₂ (black) and O₂ (red).

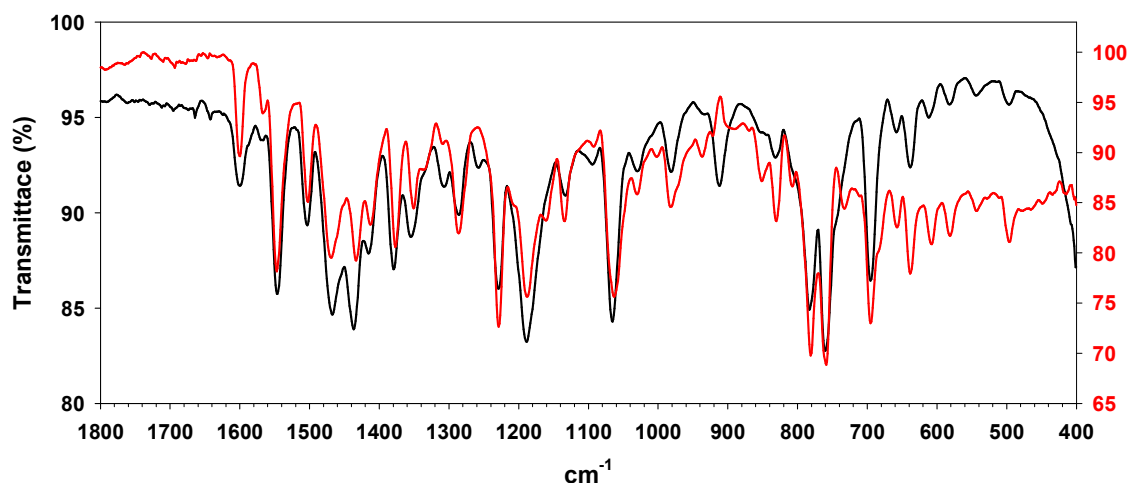


Figure 4-S52. Detail of FTIR spectra (KBr pellets) of $[(\text{Tp}^{\text{Ph,Me}^*})\text{Ni}]_2$ (**4.2**) derived from oxidation of **1a** with aqueous H_2O_2 (black) and O_2 (red).

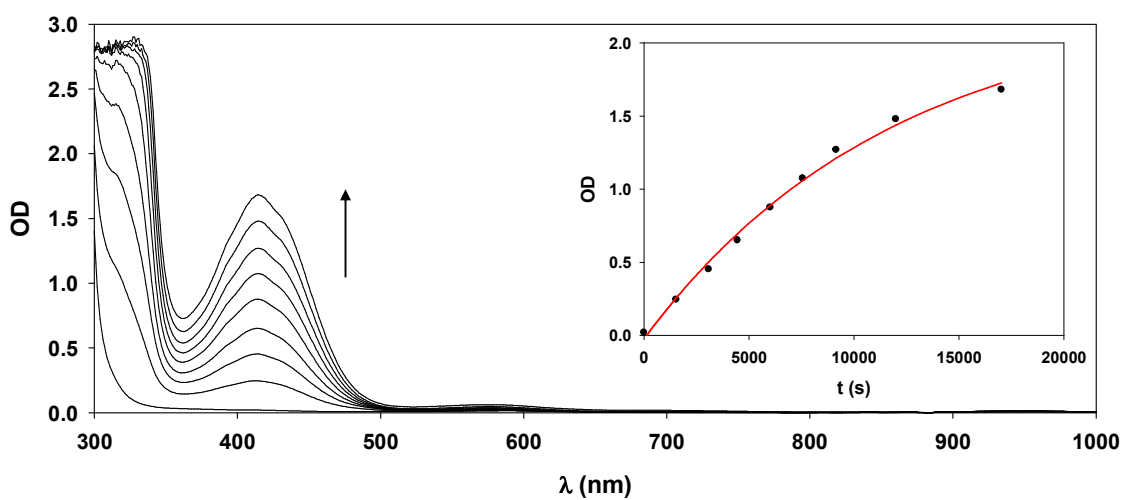


Figure 4-S53. Time-dependent UV-Vis-NIR spectra for oxidation of $[(\text{Tp}^{\text{Ph,Me}})_2\text{Ni}]$ (**4.4**) (1.2 mM) with aqueous H_2O_2 (140 mM, added as a 30 wt% aqueous solution) at 298 K. Inset shows optical density and fit to pseudo-first-order exponential growth at 415 nm ($k_{\text{obs}} = 8(1) \times 10^{-5} \text{ s}^{-1}$; $R^2 = 0.995$).

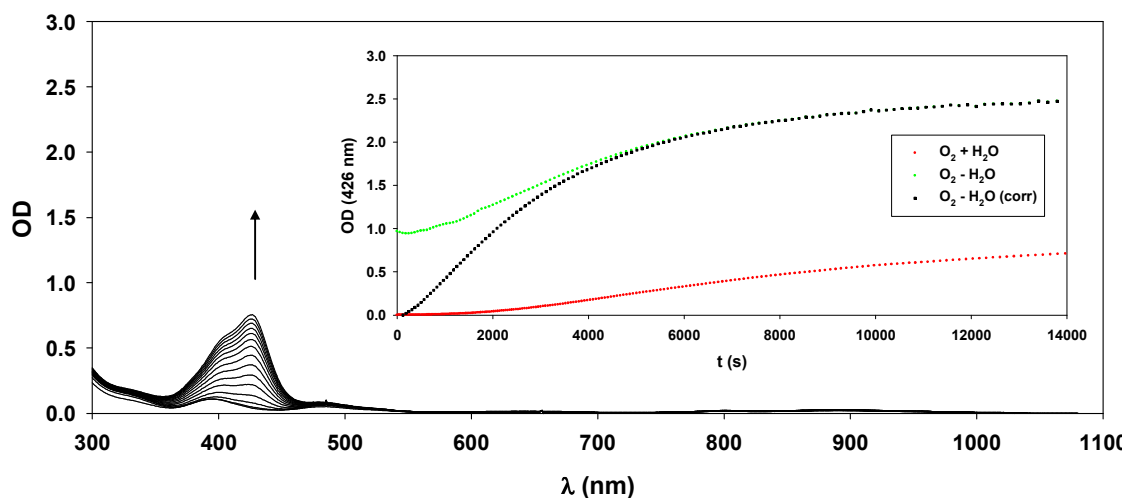


Figure 4-S54. UV-Vis-NIR absorption vs. time ($\Delta t = 1000$ s) following addition of O_2 to a hydrolyzed solution of **4.1b** (from Figure S49, 1.4 mM in CH_2Cl_2 , 293 K). Inset shows trace at 426 nm (red), corresponding to accumulation of 3,5,3',5'-tetraisopropyl-4,4'-diphenoquinone, compared to oxygenation of intact **4.1b** without added H_2O (Figure S35, 1.1 mM, green), and corrected to remove the overlapping absorption of **4.1b** (black).

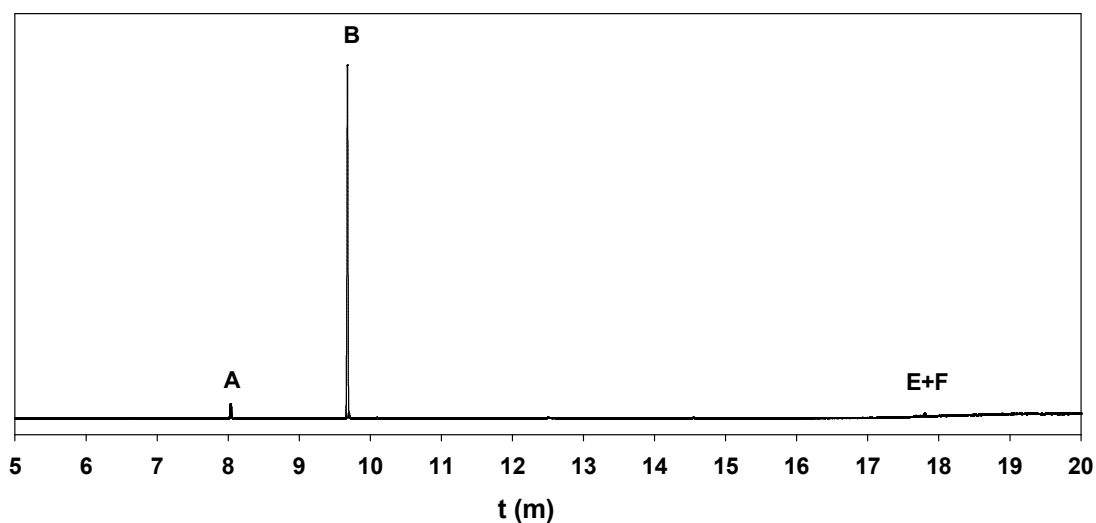


Figure 4-S55. GC trace of organic products obtained following decomposition of **4.1a** under H_2O and O_2 in CH_2Cl_2 solution, with peaks assigned as follows: naphthalene (A), 2,6-diisopropyl phenol (B), 3,5,3',5'-tetraisopropyl-4,4'-diphenoquinone (E), and 3,5,3',5'-tetraisopropyl-4,4'-diphenodihydroquinone (F).

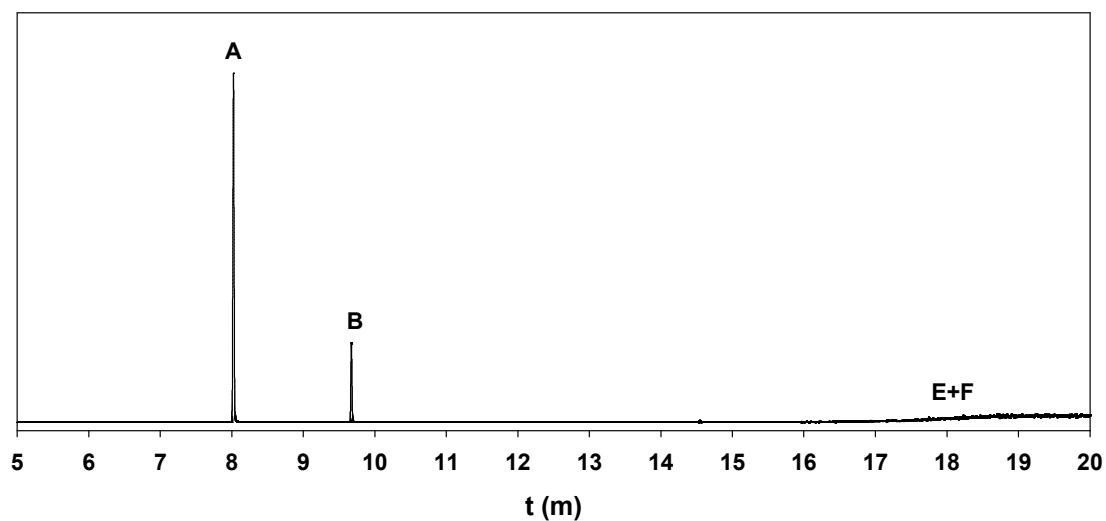


Figure 4-S56. GC trace of organic products obtained following decomposition of **4.1b** under H_2O and O_2 in CH_2Cl_2 solution, with peaks assigned as follows: naphthalene (A), 2,6-diisopropyl phenol (B), 3,5,3',5'-tetraisopropyl-4,4'-diphenoquinone (E), and 3,5,3',5'-tetraisopropyl-4,4'-diphenodihydroquinone (F).

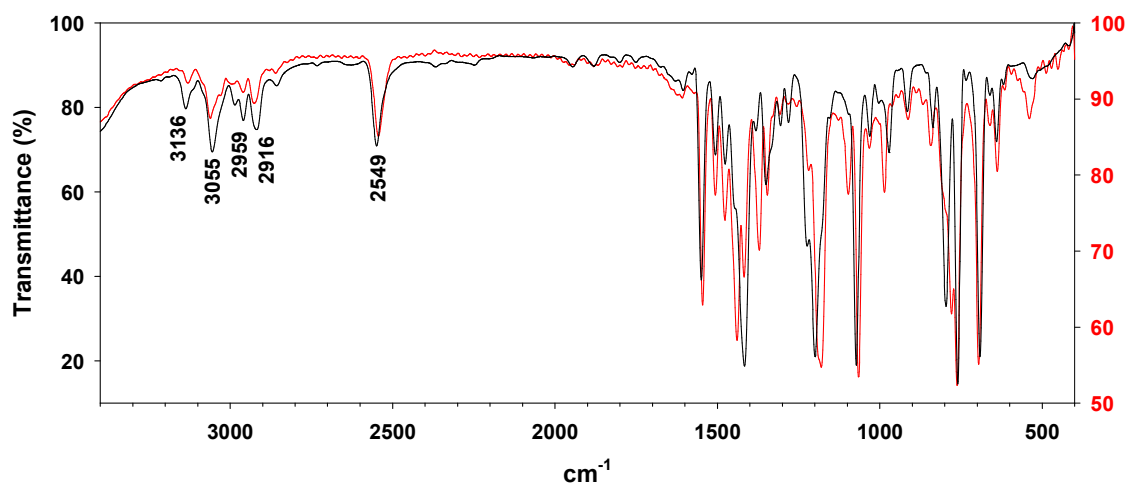


Figure 4-S57. FTIR spectra (KBr pellets) of $[(\text{Tp}^{\text{Ph,Me}})_2\text{Ni}]$ (**4.4**, black) and $\text{Tp}^{\text{Ph,Me}}\text{NiCl}$ (red).

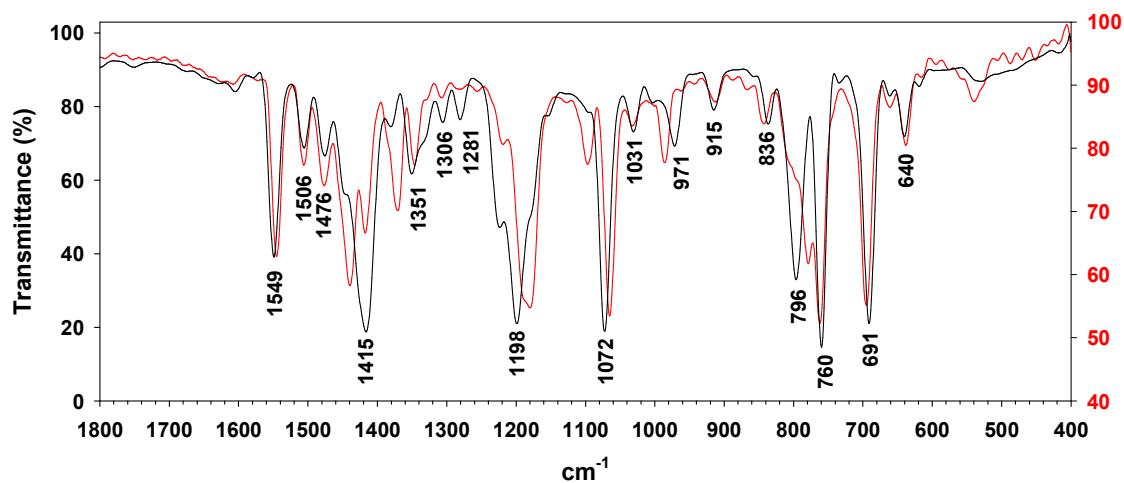


Figure 4-S58. Detail of FTIR spectra (KBr pellets) of $[(\text{Tp}^{\text{Ph,Me}})_2\text{Ni}]$ (4.4, black) and $\text{Tp}^{\text{Ph,Me}}\text{NiCl}$ (red).

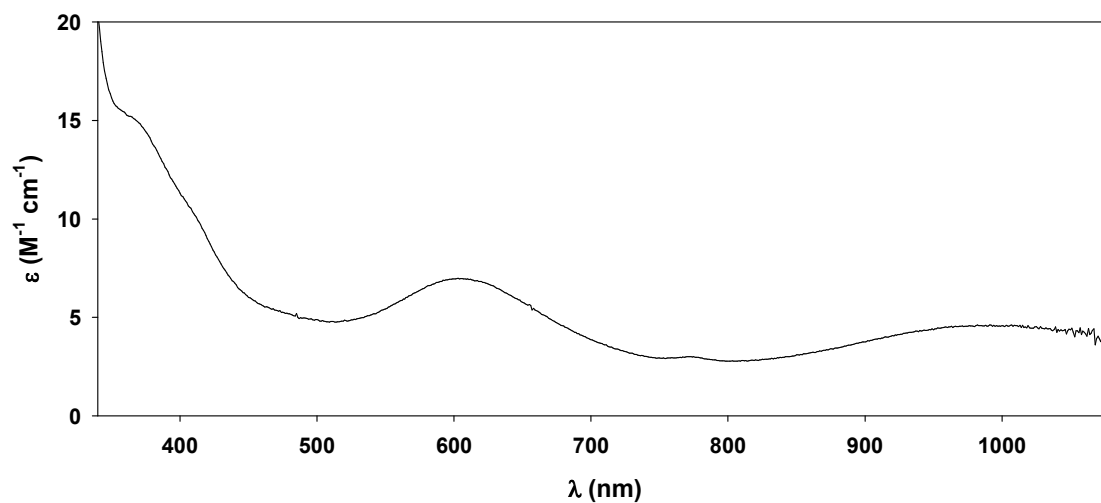


Figure 4-S59. UV-Vis-NIR spectrum (CH_2Cl_2 , 293 K) of $[(\text{Tp}^{\text{Ph,Me}})_2\text{Ni}]$ (4.4).

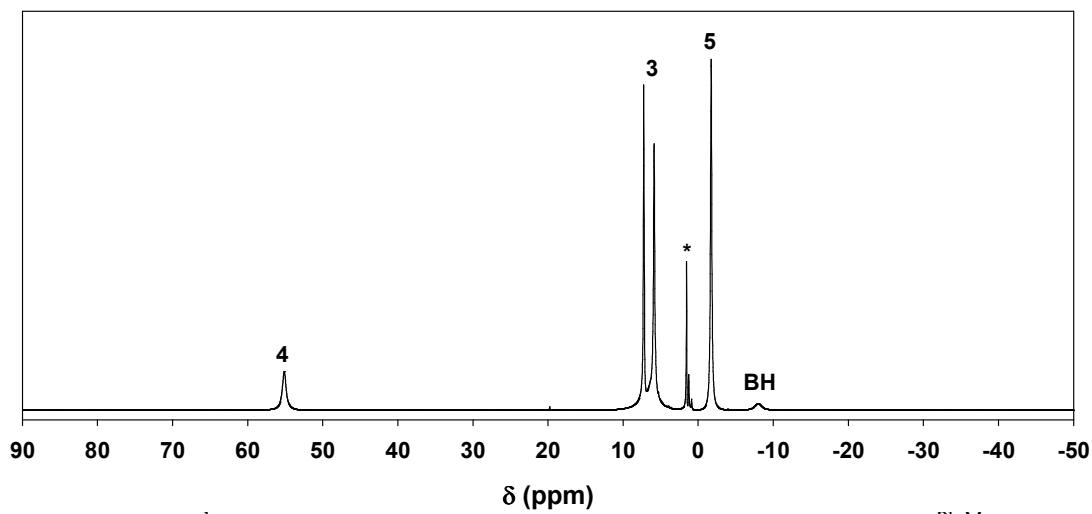


Figure 4-S60. ¹H NMR spectrum (500 MHz, CDCl₃, 293 K) of [(Tp^{Ph,Me})₂Ni] (**4.4**). Peaks labeled (*) are assigned to residual hexane and water.¹⁰¹

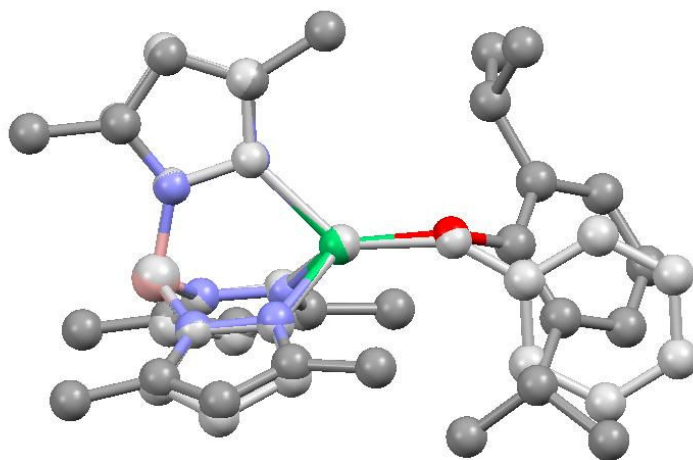


Figure 4-S61. Least-squares overlay of computational TpNi-OPh model (grayscale) and the experimental structure of Tp^{Me,Me}Ni-O-2,6-*i*-Pr₂C₆H₃ (**4.1b**, color).

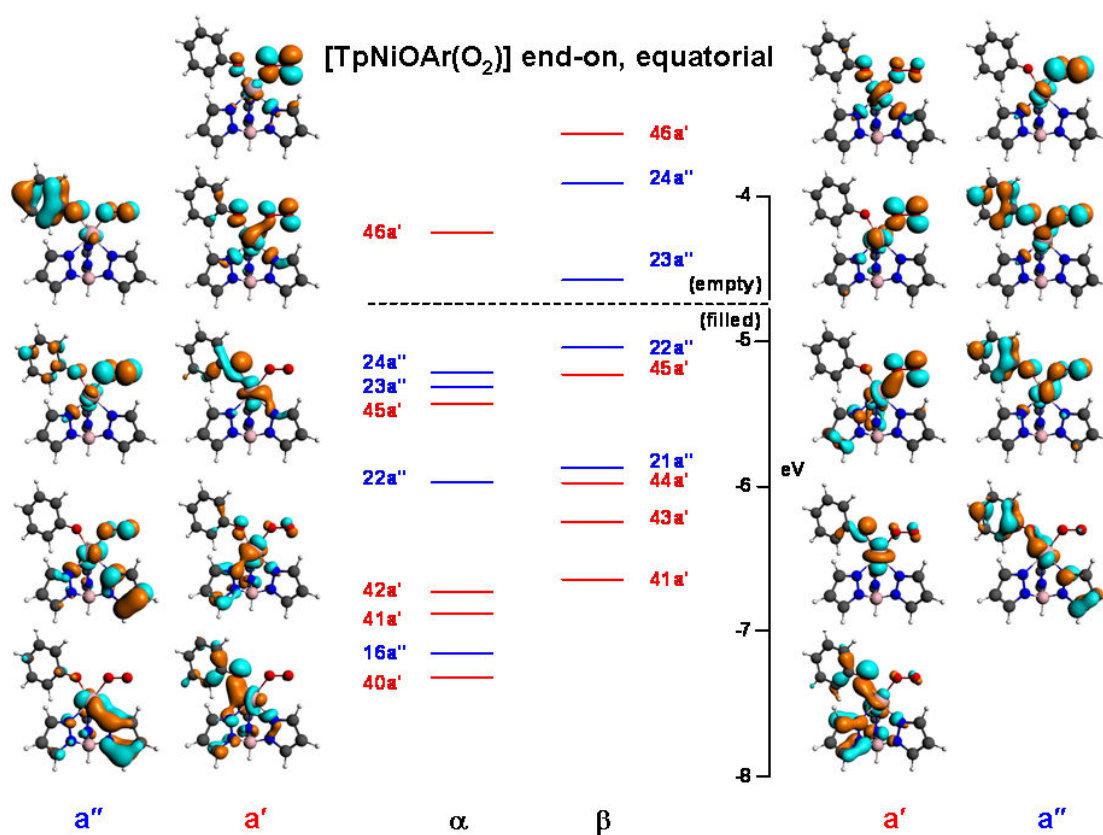


Figure 4-S62. Spin-unrestricted frontier orbitals relevant to Ni-OPh and Ni-O₂ bonding in the TpNiOPh(O₂) model (Figure 32C). Red and blue respectively indicate symmetry (a') and antisymmetry (a'') with respect to the mirror plane.

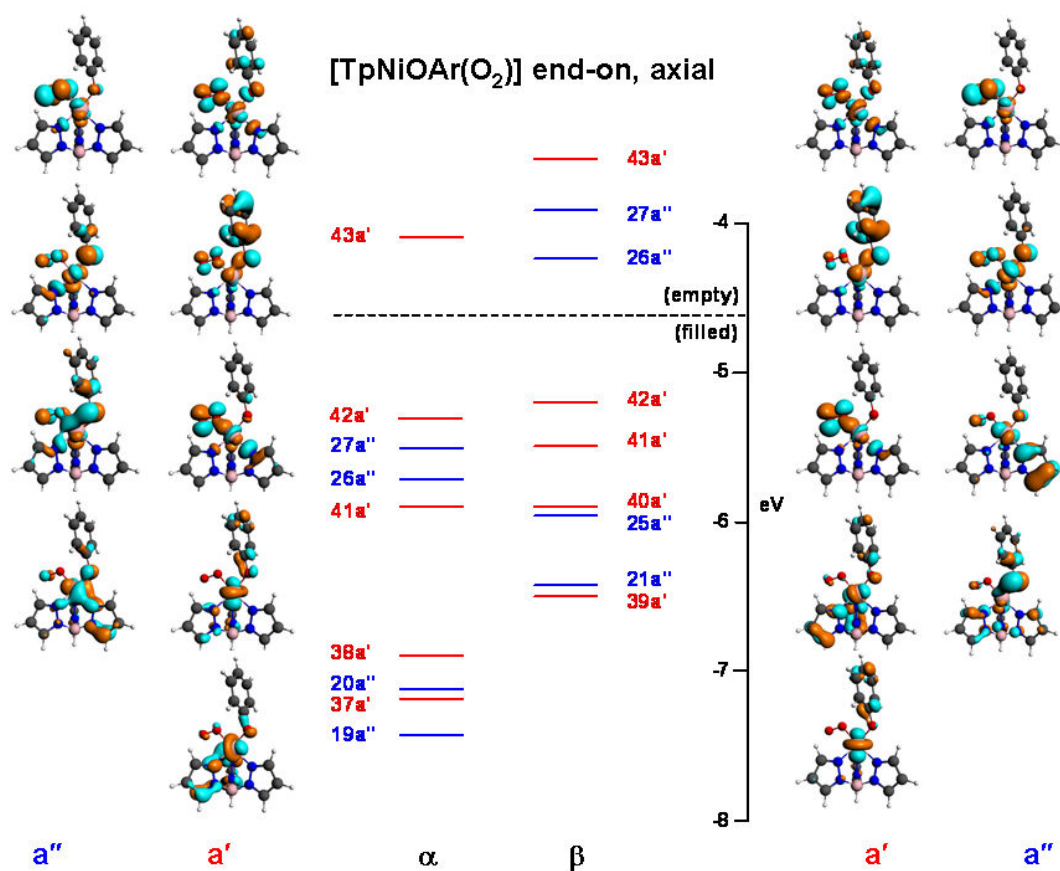


Figure 4-S63. Spin-unrestricted molecular orbitals relevant to Ni-O_{Ph} and Ni-O₂ bonding in the TpNiOPh(O₂) model (Figure 32D). Red and blue respectively indicate symmetry (a') and antisymmetry (a'') with respect to the mirror plane.

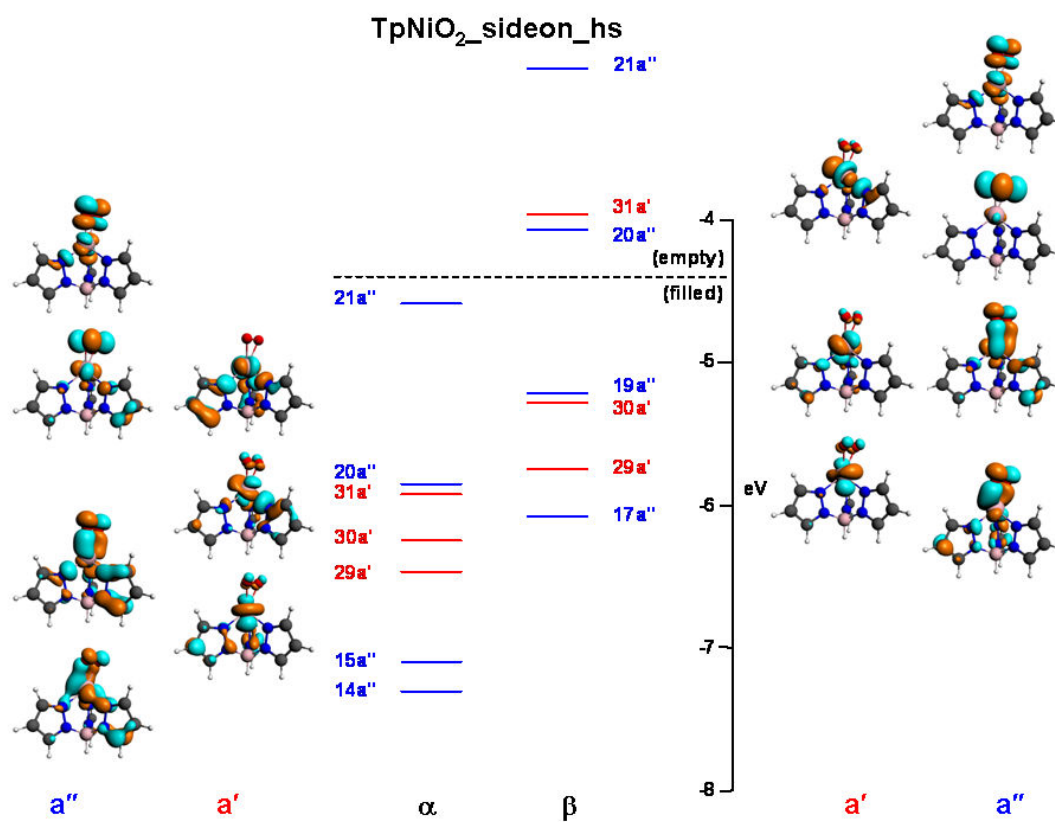


Figure 4-S65. Spin-unrestricted molecular orbitals relevant to Ni-O₂ bonding in the TpNiO₂ model (Figure 32F). Red and blue respectively indicate symmetry (a') and antisymmetry (a'') with respect to the mirror plane.

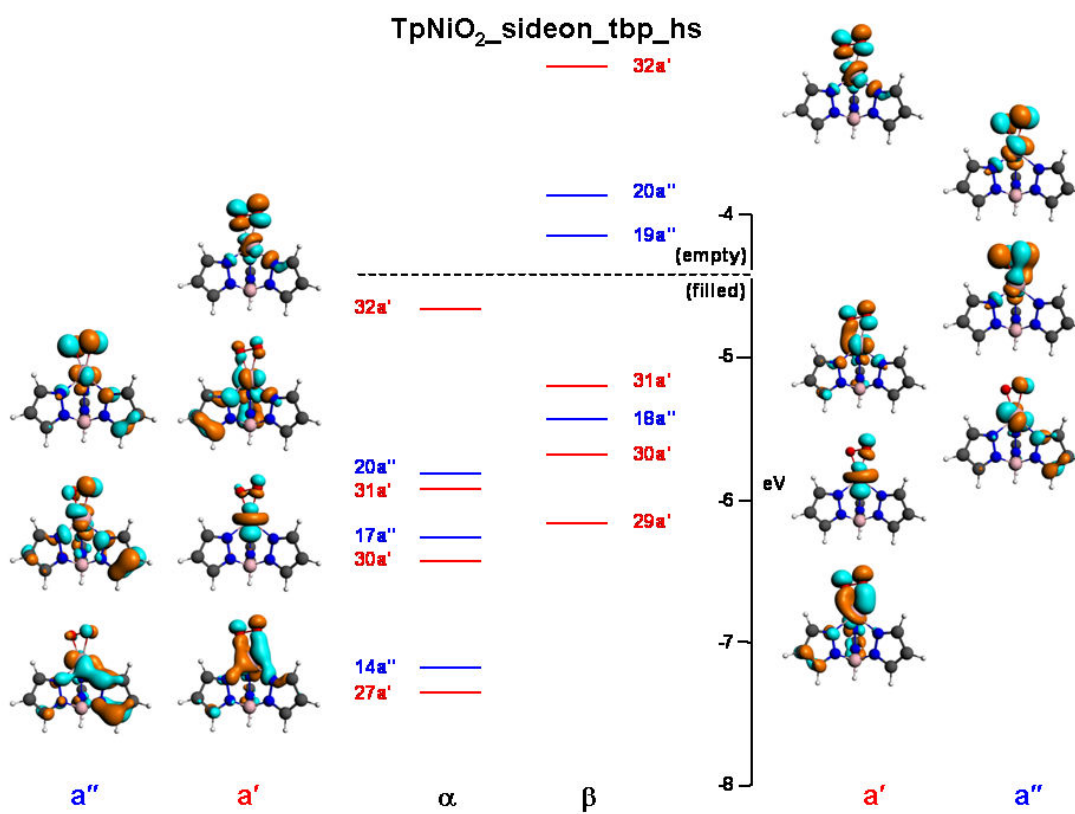


Figure 4-S66. Spin-unrestricted frontier orbitals relevant to Ni-O₂ bonding in the TpNiO₂ model (Figure 32G). Red and blue respectively indicate symmetry (a') and antisymmetry (a'') with respect to the mirror plane.

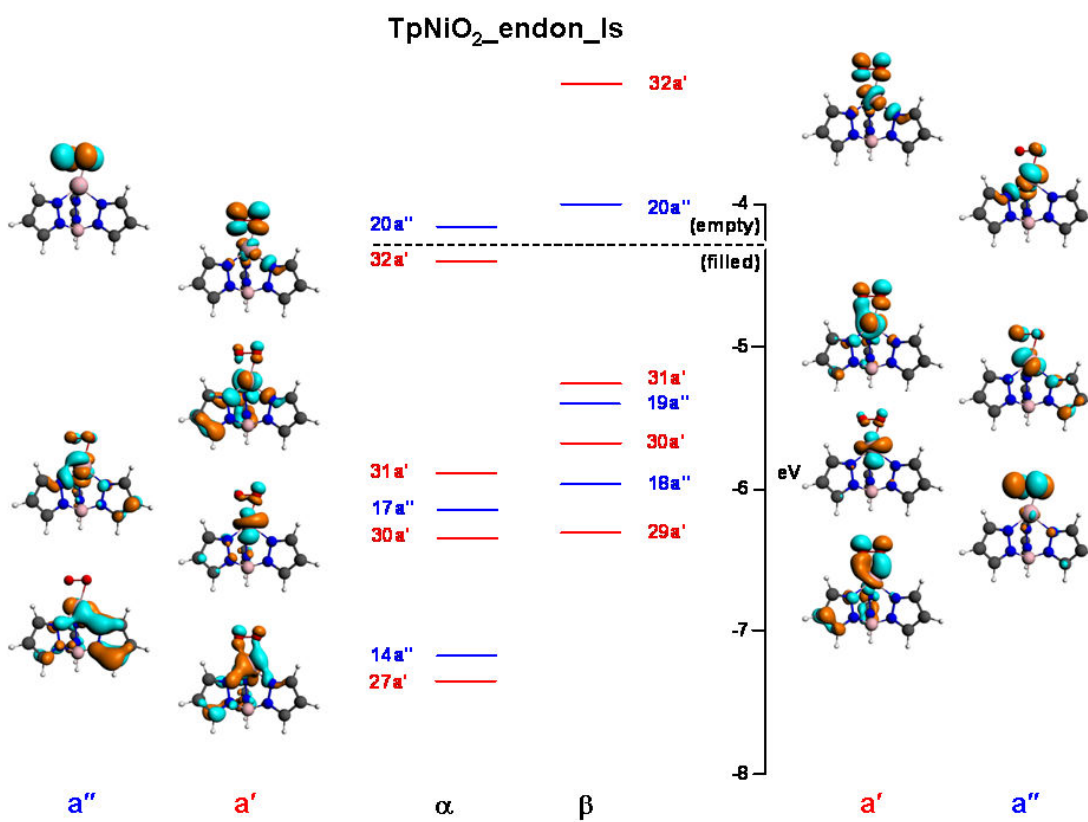


Figure 4-S67. Spin-unrestricted molecular orbitals relevant to Ni-O₂ bonding in the TpNiO₂ model (Figure 32H). Red and blue respectively indicate symmetry (a') and antisymmetry (a'') with respect to the mirror plane.

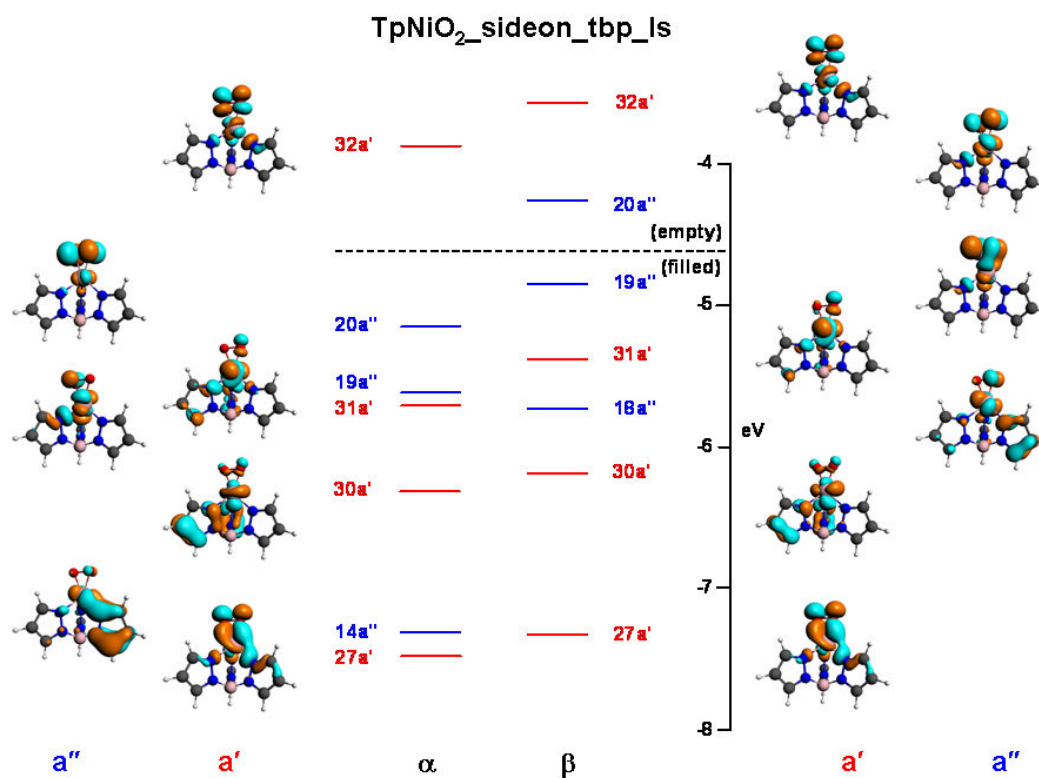


Figure 4-S68. Spin-unrestricted frontier orbitals relevant to Ni-O₂ bonding in the TpNiO₂ model (Figure 32). Red and blue respectively indicate symmetry (a') and antisymmetry (a'') with respect to the mirror plane.

Table 4-S1. Positional parameters for computational TpNiOPh model (Figure 32A).

	<u>X</u>	<u>Y</u>	<u>Z</u>
Ni	0.00000000	0.00000000	0.00000000
B	-1.23099338	-2.82501222	0.00000000
H	-1.71092825	-3.92578103	0.00000000
N	0.31709078	-2.90975675	0.00000000
N	1.04719776	-1.75667461	0.00000000
H	0.75329614	-4.98930637	0.00000000
C	1.15070218	-3.97925599	0.00000000
C	2.46332282	-3.51258077	0.00000000
H	3.37332192	-4.10288559	0.00000000
C	2.34396468	-2.11181141	0.00000000
H	3.11731069	-1.35003503	0.00000000
N	-1.67318225	-2.04241531	-1.26290512
N	-1.24196111	-0.76086619	-1.45473346
H	-2.91939670	-3.40241462	-2.31892061
C	-2.47596811	-2.41201347	-2.29336252
C	-2.57517539	-1.34161742	-3.17723140
H	-3.14196671	-1.29968325	-4.10082205
C	-1.78143293	-0.32969078	-2.60601089
H	-1.57205550	0.67460691	-2.96096584
N	-1.67318225	-2.04241531	1.26290512
N	-1.24196111	-0.76086619	1.45473346
H	-2.91939670	-3.40241462	2.31892061
C	-2.47596811	-2.41201347	2.29336252
C	-2.57517539	-1.34161742	3.17723140
H	-3.14196671	-1.29968325	4.10082205
C	-1.78143293	-0.32969078	2.60601089
H	-1.57205550	0.67460691	2.96096584
O	0.47236804	1.77780633	0.00000000
C	0.09315379	3.05437202	0.00000000
C	1.08611179	4.06516981	0.00000000
C	0.72735865	5.41033114	0.00000000
H	1.50872830	6.17258526	0.00000000
C	-0.62231919	5.78814448	0.00000000
H	-0.89786976	6.84305645	0.00000000
C	-1.61254705	4.79576077	0.00000000
H	-2.66627039	5.08389398	0.00000000
C	-1.26987561	3.44308970	0.00000000
H	2.13282280	3.75466235	0.00000000
H	-2.03888358	2.66702640	0.00000000

Table 4-S2. Positional parameters for computational TpNiOPh(O₂) model (Figure 32B).

	<u>X</u>	<u>Y</u>	<u>Z</u>
Ni	0.00000000	0.00000000	0.00000000
B	-1.25933829	-2.82494826	0.00000000
H	-1.81471634	-3.88926805	0.00000000
N	0.27249836	-2.99664200	0.00000000
N	1.03782642	-1.87366166	0.00000000
H	0.64272408	-5.09391626	0.00000000
C	1.07032344	-4.09676312	0.00000000
C	2.39505159	-3.66966227	0.00000000
H	3.28778537	-4.28610810	0.00000000
C	2.32022375	-2.26374932	0.00000000
H	3.11076011	-1.52070319	0.00000000
N	-1.66230419	-1.99914949	-1.25143501
N	-1.21008491	-0.72012129	-1.40472813
H	-2.87605474	-3.31916383	-2.38528326
C	-2.42387017	-2.33480708	-2.32139528
C	-2.46948213	-1.24818951	-3.19012341
H	-2.99428790	-1.18318858	-4.13690345
C	-1.69195714	-0.25591581	-2.56877379
H	-1.46385733	0.75587142	-2.88573360
N	-1.66230419	-1.99914949	1.25143501
N	-1.21008491	-0.72012129	1.40472813
H	-2.87605474	-3.31916383	2.38528326
C	-2.42387017	-2.33480708	2.32139528
C	-2.46948213	-1.24818951	3.19012341
H	-2.99428790	-1.18318858	4.13690345
C	-1.69195714	-0.25591581	2.56877379
H	-1.46385733	0.75587142	2.88573360
O	-0.53820279	2.04048879	0.00000000
C	-1.53322906	2.88355342	0.00000000
C	-1.21379855	4.28379835	0.00000000
C	-2.21100716	5.24530812	0.00000000
H	-1.94024280	6.30312634	0.00000000
C	-3.56510415	4.86649121	0.00000000
H	-4.34713579	5.62685555	0.00000000
C	-3.90143356	3.50254124	0.00000000
H	-4.95356583	3.21090282	0.00000000
C	-2.91629714	2.51950664	0.00000000
H	-0.15646954	4.55227621	0.00000000
H	-3.17773342	1.46057271	0.00000000
O	1.61465026	0.83746711	-0.66289861
O	1.61465026	0.83746711	0.66289861

Table 4-S3. Positional parameters for computational TpNiOPh(O₂) model (Figure 32C).

	<u>X</u>	<u>Y</u>	<u>Z</u>
Ni	0.00000000	0.00000000	0.00000000
B	1.23492715	-2.86309984	0.00000000
H	1.68654635	-3.97580248	0.00000000
N	-0.30821673	-2.90194206	0.00000000
N	-1.02662016	-1.74033821	0.00000000
H	-0.77328486	-4.97300894	0.00000000
C	-1.15799644	-3.95868662	0.00000000
C	-2.46073297	-3.47354467	0.00000000
H	-3.38146307	-4.04657029	0.00000000
C	-2.32477438	-2.07553182	0.00000000
H	-3.07990790	-1.29621881	0.00000000
N	1.69436725	-2.09001843	1.25813742
N	1.26537215	-0.81125154	1.45595052
H	2.90957322	-3.47098573	2.32069741
C	2.47674935	-2.47619263	2.29690237
C	2.56268537	-1.41796414	3.19618619
H	3.10737070	-1.39239589	4.13372587
C	1.78427075	-0.39649948	2.62279467
H	1.57699168	0.60489971	2.98514764
N	1.69436725	-2.09001843	-1.25813742
N	1.26537215	-0.81125154	-1.45595052
H	2.90957322	-3.47098573	-2.32069741
C	2.47674935	-2.47619263	-2.29690237
C	2.56268537	-1.41796414	-3.19618619
H	3.10737070	-1.39239589	-4.13372587
C	1.78427075	-0.39649948	-2.62279467
H	1.57699168	0.60489971	-2.98514764
O	0.49553344	1.84168651	0.00000000
C	1.59606237	2.57355486	0.00000000
C	1.42518917	3.98975113	0.00000000
C	2.52623227	4.83456290	0.00000000
H	2.37628140	5.91570346	0.00000000
C	3.82640554	4.30449472	0.00000000
H	4.68943023	4.97158088	0.00000000
C	4.00742055	2.91243117	0.00000000
H	5.01797145	2.50039657	0.00000000
C	2.91598069	2.04779974	0.00000000
H	0.40535133	4.37598716	0.00000000
H	3.05074150	0.96660386	0.00000000
O	-1.75263666	1.13000036	0.00000000
O	-2.97893522	0.77034680	0.00000000

Table 4-S4. Positional parameters for computational TpNiOPh(O₂) model (Figure 32D).

	<u>X</u>	<u>Y</u>	<u>Z</u>
Ni	0.00000000	0.00000000	0.00000000
B	-0.94310351	-2.98269715	0.00000000
H	-1.31165426	-4.12552955	0.00000000
N	0.60096084	-2.90078183	0.00000000
N	1.19194905	-1.67508818	0.00000000
H	1.28226732	-4.91403749	0.00000000
C	1.55635552	-3.86405582	0.00000000
C	2.80244875	-3.24246158	0.00000000
H	3.77664065	-3.71969557	0.00000000
C	2.51964868	-1.86485040	0.00000000
H	3.18014533	-1.00487336	0.00000000
N	-1.46547223	-2.23852758	-1.25515220
N	-1.17580793	-0.91833505	-1.42643313
H	-2.55975910	-3.70541385	-2.33390887
C	-2.22556142	-2.67406431	-2.29110054
C	-2.43604461	-1.60737109	-3.15984167
H	-3.00100694	-1.61141253	-4.08564061
C	-1.75723773	-0.52637968	-2.57098576
H	-1.66586681	0.50197897	-2.90410514
N	-1.46547223	-2.23852758	1.25515220
N	-1.17580793	-0.91833505	1.42643313
H	-2.55975910	-3.70541385	2.33390887
C	-2.22556142	-2.67406431	2.29110054
C	-2.43604461	-1.60737109	3.15984167
H	-3.00100694	-1.61141253	4.08564061
C	-1.75723773	-0.52637968	2.57098576
H	-1.66586681	0.50197897	2.90410514
O	1.60038502	1.00797713	0.00000000
C	1.66286505	2.34618273	0.00000000
C	1.73154478	3.06211722	1.21881810
C	1.90067698	4.44527782	1.21127812
H	1.96317662	4.98558594	2.15769391
C	1.98989496	5.14479813	0.00000000
H	2.12363142	6.22777603	0.00000000
C	1.90067698	4.44527782	-1.21127812
H	1.96317662	4.98558594	-2.15769391
C	1.73154478	3.06211722	-1.21881810
H	1.66760270	2.50183441	2.15290855
H	1.66760270	2.50183441	-2.15290855
O	-0.94088956	1.66242956	0.00000000
O	-2.22279727	1.66095794	0.00000000

Table 4-S5. Positional parameters for computational TpNiO₂ model (Figure 32E).

	<u>X</u>	<u>Y</u>	<u>Z</u>
Ni	0.00000000	0.00000000	0.00000000
B	-1.56363866	-2.56712269	0.00000000
H	-2.18140757	-3.59710123	0.00000000
N	-0.03852110	-2.85750365	0.00000000
N	0.84661246	-1.81866628	0.00000000
H	0.11338016	-4.97652972	0.00000000
C	0.64376124	-4.03027526	0.00000000
C	2.00624604	-3.74686437	0.00000000
H	2.82749709	-4.45532183	0.00000000
C	2.08219091	-2.34308897	0.00000000
H	2.94967826	-1.69148488	0.00000000
N	-1.90842961	-1.74344153	-1.27127751
N	-1.28680919	-0.54909441	-1.51403735
H	-3.35513954	-2.93448649	-2.27303299
C	-2.76586105	-2.02358589	-2.28492955
C	-2.70587860	-0.98753141	-3.21217822
H	-3.26300966	-0.89795441	-4.13850593
C	-1.76297120	-0.08979711	-2.68281069
H	-1.40436384	0.85446724	-3.08011683
N	-1.90842961	-1.74344153	1.27127751
N	-1.28680919	-0.54909441	1.51403735
H	-3.35513954	-2.93448649	2.27303299
C	-2.76586105	-2.02358589	2.28492955
C	-2.70587860	-0.98753141	3.21217822
H	-3.26300966	-0.89795441	4.13850593
C	-1.76297120	-0.08979711	2.68281069
H	-1.40436384	0.85446724	3.08011683
O	1.29382607	1.35429697	0.00000000
O	0.97134814	2.62438044	0.00000000

Table 4-S6. Positional parameters for computational TpNiO₂ model (Figure 32F).

	<u>X</u>	<u>Y</u>	<u>Z</u>
Ni	0.00000000	0.00000000	0.00000000
B	-1.43798764	-2.68845112	0.00000000
H	-1.98984476	-3.75534769	0.00000000
N	0.10154841	-2.88514553	0.00000000
N	0.92718723	-1.79996664	0.00000000
H	0.36953085	-4.99290064	0.00000000
C	0.84711444	-4.01899525	0.00000000
C	2.19154332	-3.66079124	0.00000000
H	3.05064702	-4.32269993	0.00000000
C	2.18916710	-2.25492132	0.00000000
H	3.01862147	-1.55584972	0.00000000
N	-1.83280551	-1.87991894	-1.26196197
N	-1.30061034	-0.63987380	-1.47014106
H	-3.15814263	-3.16383668	-2.31518511
C	-2.64824647	-2.20652424	-2.29572384
C	-2.65964843	-1.14722836	-3.19774955
H	-3.20970214	-1.08044644	-4.13002109
C	-1.79857416	-0.19000986	-2.63382774
H	-1.51298572	0.78907173	-3.00467203
N	-1.83280551	-1.87991894	1.26196197
N	-1.30061034	-0.63987380	1.47014106
H	-3.15814263	-3.16383668	2.31518511
C	-2.64824647	-2.20652424	2.29572384
C	-2.65964843	-1.14722836	3.19774955
H	-3.20970214	-1.08044644	4.13002109
C	-1.79857416	-0.19000986	2.63382774
H	-1.51298572	0.78907173	3.00467203
O	1.33469422	1.38090236	-0.67259214
O	1.33469422	1.38090236	0.67259214

Table 4-S7. Positional parameters for computational TpNiO₂ model (Figure 32G).

	<u>X</u>	<u>Y</u>	<u>Z</u>
Ni	0.00000000	0.00000000	0.00000000
B	-1.50757537	-2.66012380	0.00000000
H	-2.10985821	-3.69929834	0.00000000
N	0.02266800	-2.92593701	0.00000000
N	0.89559318	-1.87531524	0.00000000
H	0.18960889	-5.04434777	0.00000000
C	0.71250854	-4.09368566	0.00000000
C	2.07263177	-3.80038409	0.00000000
H	2.89861814	-4.50322910	0.00000000
C	2.13325803	-2.39651784	0.00000000
H	2.99656219	-1.73873876	0.00000000
N	-1.87180660	-1.82630909	-1.25598216
N	-1.32987952	-0.58585335	-1.42791964
H	-3.22415420	-3.05631557	-2.33914874
C	-2.69627399	-2.10935898	-2.29544884
C	-2.69060721	-1.02587473	-3.16811347
H	-3.24132464	-0.92426413	-4.09697115
C	-1.81968230	-0.09418528	-2.57751774
H	-1.52749167	0.89468622	-2.91522536
N	-1.87180660	-1.82630909	1.25598216
N	-1.32987952	-0.58585335	1.42791964
H	-3.22415420	-3.05631557	2.33914874
C	-2.69627399	-2.10935898	2.29544884
C	-2.69060721	-1.02587473	3.16811347
H	-3.24132464	-0.92426413	4.09697115
C	-1.81968230	-0.09418528	2.57751774
H	-1.52749167	0.89468622	2.91522536
O	1.46251242	1.51970554	0.00000000
O	0.19700549	1.97023203	0.00000000

Table 4-S8. Positional parameters for computational TpNiO_2 model (Figure 32H).

	<u>X</u>	<u>Y</u>	<u>Z</u>
Ni	0.00000000	0.00000000	0.00000000
B	-1.57094731	-2.60958063	0.00000000
H	-2.20035116	-3.63213995	0.00000000
N	-0.04955718	-2.90912856	0.00000000
N	0.84410249	-1.87556888	0.00000000
H	0.07833403	-5.03059104	0.00000000
C	0.61907280	-4.08993174	0.00000000
C	1.98445967	-3.82188227	0.00000000
H	2.79731859	-4.53994787	0.00000000
C	2.07258521	-2.41919562	0.00000000
H	2.94849689	-1.77845103	0.00000000
N	-1.91395335	-1.76642303	-1.25605308
N	-1.33980263	-0.54026681	-1.42524429
H	-3.28632214	-2.96499929	-2.34961008
C	-2.73382593	-2.03243515	-2.30348011
C	-2.69449505	-0.95007076	-3.17779062
H	-3.23396021	-0.83615922	-4.11174284
C	-1.80493293	-0.03944871	-2.58139168
H	-1.48337977	0.94020505	-2.91928557
N	-1.91395335	-1.76642303	1.25605308
N	-1.33980263	-0.54026681	1.42524429
H	-3.28632214	-2.96499929	2.34961008
C	-2.73382593	-2.03243515	2.30348011
C	-2.69449505	-0.95007076	3.17779062
H	-3.23396021	-0.83615922	4.11174284
C	-1.80493293	-0.03944871	2.58139168
H	-1.48337977	0.94020505	2.91928557
O	1.44687854	1.39021202	0.00000000
O	0.29270426	2.08394204	0.00000000

Table 4-S9. Positional parameters for computational TpNiO_2 model (Figure 32I).

	<u>X</u>	<u>Y</u>	<u>Z</u>
Ni	0.00000000	0.00000000	0.00000000
B	-1.62243125	-2.62084041	0.00000000
H	-2.20455876	-3.67120205	0.00000000
N	-0.08506456	-2.86068847	0.00000000
N	0.77567933	-1.80156754	0.00000000
H	0.11761522	-4.97270774	0.00000000
C	0.62614129	-4.01427591	0.00000000
C	1.98269216	-3.69995542	0.00000000
H	2.82013491	-4.38905300	0.00000000
C	2.02612277	-2.29683188	0.00000000
H	2.87791841	-1.62544119	0.00000000
N	-1.98292139	-1.79127369	-1.25471007
N	-1.40905309	-0.56645633	-1.42761065
H	-3.38008027	-2.98336356	-2.32665445
C	-2.82611078	-2.05130178	-2.28640670
C	-2.80279935	-0.96356899	-3.15350164
H	-3.36190601	-0.84287368	-4.07523882
C	-1.89830956	-0.05812884	-2.56852509
H	-1.58014246	0.92309680	-2.90498311
N	-1.98292139	-1.79127369	1.25471007
N	-1.40905309	-0.56645633	1.42761065
H	-3.38008027	-2.98336356	2.32665445
C	-2.82611078	-2.05130178	2.28640670
C	-2.80279935	-0.96356899	3.15350164
H	-3.36190601	-0.84287368	4.07523882
C	-1.89830956	-0.05812884	2.56852509
H	-1.58014246	0.92309680	2.90498311
O	1.27633027	1.32035261	0.00000000
O	0.03456332	1.88731426	0.00000000

APPENDIX G: CRYSTAL STRUCTURE AND DATA REFINEMENT FOR
COMPLEX 4.1B

Table G1. Crystal data and structure refinement for **4.1b**

Empirical formula	C ₂₇ H ₃₉ B N ₆ O Ni	
Formula weight	533.16	
Temperature	123(2) K	
Wavelength	0.71073 Å	
Crystal system	Monoclinic	
Space group	P2 ₁ /n	
Unit cell dimensions	$a = 8.8030(10) \text{ \AA}$	$\alpha = 90^\circ$
	$b = 29.373(3) \text{ \AA}$	$\beta = 91.8320(10)^\circ$
	$c = 10.6299(12) \text{ \AA}$	$\gamma = 90^\circ$
Volume	2747.2(5) Å ³	
Z	4	
Density (calculated)	1.289 Mg/m ³	
Absorption coefficient	0.737 mm ⁻¹	
$F(000)$	1136	
Crystal color, morphology	green, block	
Crystal size	0.22 x 0.12 x 0.10 mm ³	
Theta range for data collection	2.04 to 27.48°	
Index ranges	$-11 \leq h \leq 11, -37 \leq k \leq 37, -13 \leq l \leq 13$	
Reflections collected	30891	
Independent reflections	6280 [$R(\text{int}) = 0.0751$]	
Observed reflections	4388	
Completeness to theta = 27.48°	99.6%	
Absorption correction	Multi-scan	
Max. and min. transmission	0.9319 and 0.8559	
Refinement method	Full-matrix least-squares on F^2	
Data / restraints / parameters	6280 / 0 / 339	
Goodness-of-fit on F^2	1.037	
Final R indices [$I > 2\sigma(I)$]	$R1 = 0.0476, wR2 = 0.1056$	
R indices (all data)	$R1 = 0.0803, wR2 = 0.1190$	
Largest diff. peak and hole	0.661 and -0.503 e.Å ⁻³	

Table G2. Atomic coordinates ($\times 10^4$) and equivalent isotropic displacement parameters ($\text{\AA}^2 \times 10^3$) for **4.1b**. U_{eq} is defined as one third of the trace of the orthogonalized U_{ij} tensor.

	x	y	z	U_{eq}
Ni1	6402(1)	1403(1)	5066(1)	19(1)
O1	7268(2)	1711(1)	6416(2)	22(1)
N1	4840(2)	923(1)	5379(2)	21(1)
N2	4240(2)	714(1)	4315(2)	22(1)
N3	5091(2)	1689(1)	3736(2)	21(1)
N4	4353(3)	1402(1)	2897(2)	23(1)
N5	7378(3)	1013(1)	3760(2)	21(1)
N6	6408(3)	816(1)	2878(2)	21(1)
C1	2524(3)	60(1)	3730(3)	29(1)
C2	3340(3)	365(1)	4649(3)	23(1)
C3	3336(3)	353(1)	5948(3)	24(1)
C4	4281(3)	704(1)	6369(3)	23(1)
C5	4688(3)	839(1)	7699(3)	26(1)
C6	2671(4)	1444(1)	953(3)	36(1)
C7	3581(3)	1654(1)	2018(3)	24(1)
C8	3822(3)	2106(1)	2298(3)	26(1)
C9	4763(3)	2117(1)	3381(3)	23(1)
C10	5376(3)	2515(1)	4103(3)	27(1)
C11	6502(4)	350(1)	925(3)	31(1)
C12	7222(3)	592(1)	2024(3)	23(1)
C13	8739(3)	639(1)	2357(3)	24(1)
C14	8793(3)	907(1)	3449(3)	22(1)
C15	10132(3)	1066(1)	4229(3)	27(1)
C16	7252(3)	1702(1)	7686(2)	20(1)
C17	8187(3)	1394(1)	8360(2)	21(1)
C18	8131(3)	1388(1)	9673(3)	26(1)
C19	7182(3)	1677(1)	10308(3)	29(1)
C20	6282(3)	1984(1)	9632(3)	28(1)
C21	6296(3)	2005(1)	8324(3)	22(1)
C22	5298(3)	2339(1)	7583(3)	26(1)
C23	3837(3)	2107(1)	7091(3)	33(1)

C24	4917(4)	2769(1)	8316(3)	39(1)
C25	9275(3)	1092(1)	7666(3)	25(1)
C26	9722(4)	651(1)	8358(3)	37(1)
C27	10714(3)	1358(1)	7361(3)	29(1)
B1	4669(4)	887(1)	2992(3)	23(1)

Table G3. Bond lengths [\AA] and angles [$^\circ$] for **4.1b**.

Ni(1)-O(1)	1.8412(18)	C(8)-C(9)	1.398(4)
Ni(1)-N(3)	1.982(2)	C(8)-H(8A)	0.9500
Ni(1)-N(1)	2.005(2)	C(9)-C(10)	1.489(4)
Ni(1)-N(5)	2.014(2)	C(10)-H(10A)	0.9800
O(1)-C(16)	1.350(3)	C(10)-H(10B)	0.9800
N(1)-C(4)	1.341(3)	C(10)-H(10C)	0.9800
N(1)-N(2)	1.379(3)	C(11)-C(12)	1.492(4)
N(2)-C(2)	1.350(3)	C(11)-H(11A)	0.9800
N(2)-B(1)	1.553(4)	C(11)-H(11B)	0.9800
N(3)-C(9)	1.341(3)	C(11)-H(11C)	0.9800
N(3)-N(4)	1.376(3)	C(12)-C(13)	1.377(4)
N(4)-C(7)	1.358(3)	C(13)-C(14)	1.401(4)
N(4)-B(1)	1.539(4)	C(13)-H(13A)	0.9500
N(5)-C(14)	1.336(3)	C(14)-C(15)	1.495(4)
N(5)-N(6)	1.374(3)	C(15)-H(15A)	0.9800
N(6)-C(12)	1.347(3)	C(15)-H(15B)	0.9800
N(6)-B(1)	1.553(4)	C(15)-H(15C)	0.9800
C(1)-C(2)	1.492(4)	C(16)-C(17)	1.405(4)
C(1)-H(1A)	0.9800	C(16)-C(21)	1.413(4)
C(1)-H(1B)	0.9800	C(17)-C(18)	1.398(4)
C(1)-H(1C)	0.9800	C(17)-C(25)	1.515(4)
C(2)-C(3)	1.381(4)	C(18)-C(19)	1.381(4)
C(3)-C(4)	1.389(4)	C(18)-H(18A)	0.9500
C(3)-H(3A)	0.9500	C(19)-C(20)	1.387(4)
C(4)-C(5)	1.501(4)	C(19)-H(19A)	0.9500
C(5)-H(5A)	0.9800	C(20)-C(21)	1.392(4)
C(5)-H(5B)	0.9800	C(20)-H(20A)	0.9500
C(5)-H(5C)	0.9800	C(21)-C(22)	1.519(4)
C(6)-C(7)	1.499(4)	C(22)-C(24)	1.528(4)
C(6)-H(6A)	0.9800	C(22)-C(23)	1.533(4)
C(6)-H(6B)	0.9800	C(22)-H(22A)	1.0000
C(6)-H(6C)	0.9800	C(23)-H(23A)	0.9800
C(7)-C(8)	1.375(4)	C(23)-H(23B)	0.9800

C(23)-H(23C)	0.9800	C(14)-N(5)-Ni(1)	136.47(19)
C(24)-H(24A)	0.9800	N(6)-N(5)-Ni(1)	116.07(16)
C(24)-H(24B)	0.9800	C(12)-N(6)-N(5)	109.4(2)
C(24)-H(24C)	0.9800	C(12)-N(6)-B(1)	131.7(2)
C(25)-C(26)	1.533(4)	N(5)-N(6)-B(1)	118.9(2)
C(25)-C(27)	1.533(4)	C(2)-C(1)-H(1A)	109.5
C(25)-H(25A)	1.0000	C(2)-C(1)-H(1B)	109.5
C(26)-H(26A)	0.9800	H(1A)-C(1)-H(1B)	109.5
C(26)-H(26B)	0.9800	C(2)-C(1)-H(1C)	109.5
C(26)-H(26C)	0.9800	H(1A)-C(1)-H(1C)	109.5
C(27)-H(27A)	0.9800	H(1B)-C(1)-H(1C)	109.5
C(27)-H(27B)	0.9800	N(2)-C(2)-C(3)	107.6(2)
C(27)-H(27C)	0.9800	N(2)-C(2)-C(1)	123.8(3)
B(1)-H(1)	1.09(3)	C(3)-C(2)-C(1)	128.5(3)
		C(2)-C(3)-C(4)	106.5(2)
O(1)-Ni(1)-N(3)	124.41(9)	C(2)-C(3)-H(3A)	126.8
O(1)-Ni(1)-N(1)	118.99(9)	C(4)-C(3)-H(3A)	126.8
N(3)-Ni(1)-N(1)	91.71(9)	N(1)-C(4)-C(3)	109.5(2)
O(1)-Ni(1)-N(5)	129.92(9)	N(1)-C(4)-C(5)	121.9(2)
N(3)-Ni(1)-N(5)	90.09(9)	C(3)-C(4)-C(5)	128.5(3)
N(1)-Ni(1)-N(5)	91.37(9)	C(4)-C(5)-H(5A)	109.5
C(16)-O(1)-Ni(1)	138.85(17)	C(4)-C(5)-H(5B)	109.5
C(4)-N(1)-N(2)	106.8(2)	H(5A)-C(5)-H(5B)	109.5
C(4)-N(1)-Ni(1)	137.69(19)	C(4)-C(5)-H(5C)	109.5
N(2)-N(1)-Ni(1)	115.10(16)	H(5A)-C(5)-H(5C)	109.5
C(2)-N(2)-N(1)	109.6(2)	H(5B)-C(5)-H(5C)	109.5
C(2)-N(2)-B(1)	130.5(2)	C(7)-C(6)-H(6A)	109.5
N(1)-N(2)-B(1)	119.9(2)	C(7)-C(6)-H(6B)	109.5
C(9)-N(3)-N(4)	107.5(2)	H(6A)-C(6)-H(6B)	109.5
C(9)-N(3)-Ni(1)	135.45(19)	C(7)-C(6)-H(6C)	109.5
N(4)-N(3)-Ni(1)	117.01(16)	H(6A)-C(6)-H(6C)	109.5
C(7)-N(4)-N(3)	109.1(2)	H(6B)-C(6)-H(6C)	109.5
C(7)-N(4)-B(1)	131.8(2)	N(4)-C(7)-C(8)	107.9(2)
N(3)-N(4)-B(1)	118.6(2)	N(4)-C(7)-C(6)	122.6(3)
C(14)-N(5)-N(6)	107.3(2)	C(8)-C(7)-C(6)	129.4(3)

C(7)-C(8)-C(9)	106.5(2)	C(17)-C(16)-C(21)	120.6(2)
C(7)-C(8)-H(8A)	126.8	C(18)-C(17)-C(16)	118.5(3)
C(9)-C(8)-H(8A)	126.8	C(18)-C(17)-C(25)	121.5(3)
N(3)-C(9)-C(8)	109.1(2)	C(16)-C(17)-C(25)	119.9(2)
N(3)-C(9)-C(10)	121.3(3)	C(19)-C(18)-C(17)	121.5(3)
C(8)-C(9)-C(10)	129.7(3)	C(19)-C(18)-H(18A)	119.3
C(9)-C(10)-H(10A)	109.5	C(17)-C(18)-H(18A)	119.3
C(9)-C(10)-H(10B)	109.5	C(18)-C(19)-C(20)	119.4(3)
H(10A)-C(10)-H(10B)	109.5	C(18)-C(19)-H(19A)	120.3
C(9)-C(10)-H(10C)	109.5	C(20)-C(19)-H(19A)	120.3
H(10A)-C(10)-H(10C)	109.5	C(19)-C(20)-C(21)	121.6(3)
H(10B)-C(10)-H(10C)	109.5	C(19)-C(20)-H(20A)	119.2
C(12)-C(11)-H(11A)	109.5	C(21)-C(20)-H(20A)	119.2
C(12)-C(11)-H(11B)	109.5	C(20)-C(21)-C(16)	118.4(3)
H(11A)-C(11)-H(11B)	109.5	C(20)-C(21)-C(22)	121.5(2)
C(12)-C(11)-H(11C)	109.5	C(16)-C(21)-C(22)	120.0(2)
H(11A)-C(11)-H(11C)	109.5	C(21)-C(22)-C(24)	113.7(2)
H(11B)-C(11)-H(11C)	109.5	C(21)-C(22)-C(23)	110.8(2)
N(6)-C(12)-C(13)	108.1(2)	C(24)-C(22)-C(23)	110.2(2)
N(6)-C(12)-C(11)	122.6(3)	C(21)-C(22)-H(22A)	107.3
C(13)-C(12)-C(11)	129.3(3)	C(24)-C(22)-H(22A)	107.3
C(12)-C(13)-C(14)	106.0(2)	C(23)-C(22)-H(22A)	107.3
C(12)-C(13)-H(13A)	127.0	C(22)-C(23)-H(23A)	109.5
C(14)-C(13)-H(13A)	127.0	C(22)-C(23)-H(23B)	109.5
N(5)-C(14)-C(13)	109.2(2)	H(23A)-C(23)-H(23B)	109.5
N(5)-C(14)-C(15)	121.0(2)	C(22)-C(23)-H(23C)	109.5
C(13)-C(14)-C(15)	129.9(3)	H(23A)-C(23)-H(23C)	109.5
C(14)-C(15)-H(15A)	109.5	H(23B)-C(23)-H(23C)	109.5
C(14)-C(15)-H(15B)	109.5	C(22)-C(24)-H(24A)	109.5
H(15A)-C(15)-H(15B)	109.5	C(22)-C(24)-H(24B)	109.5
C(14)-C(15)-H(15C)	109.5	H(24A)-C(24)-H(24B)	109.5
H(15A)-C(15)-H(15C)	109.5	C(22)-C(24)-H(24C)	109.5
H(15B)-C(15)-H(15C)	109.5	H(24A)-C(24)-H(24C)	109.5
O(1)-C(16)-C(17)	119.8(2)	H(24B)-C(24)-H(24C)	109.5
O(1)-C(16)-C(21)	119.6(2)	C(17)-C(25)-C(26)	114.7(2)

C(17)-C(25)-C(27)	110.1(2)	H(27A)-C(27)-H(27B)	109.5
C(26)-C(25)-C(27)	109.4(2)	C(25)-C(27)-H(27C)	109.5
C(17)-C(25)-H(25A)	107.5	H(27A)-C(27)-H(27C)	109.5
C(26)-C(25)-H(25A)	107.5	H(27B)-C(27)-H(27C)	109.5
C(27)-C(25)-H(25A)	107.5	N(4)-B(1)-N(6)	107.6(2)
C(25)-C(26)-H(26A)	109.5	N(4)-B(1)-N(2)	109.4(2)
C(25)-C(26)-H(26B)	109.5	N(6)-B(1)-N(2)	107.2(2)
H(26A)-C(26)-H(26B)	109.5	N(4)-B(1)-H(1)	113.0(13)
C(25)-C(26)-H(26C)	109.5	N(6)-B(1)-H(1)	109.2(13)
H(26A)-C(26)-H(26C)	109.5	N(2)-B(1)-H(1)	110.2(13)
H(26B)-C(26)-H(26C)	109.5		
C(25)-C(27)-H(27A)	109.5		
C(25)-C(27)-H(27B)	109.5		

Symmetry transformations used to generate equivalent atoms.

APPENDIX H: CRYSTAL STRUCTURE AND DATA REFINEMENT FOR
COMPLEX 4.1A

Table H1. Crystal data and structure refinement for 4.1a.

Empirical formula	C ₄₂ H ₄₅ B N ₆ Ni O	
Formula weight	719.36	
Temperature	123(2) K	
Wavelength	0.71073 Å	
Crystal system	Triclinic	
Space group	P $\bar{1}$	
Unit cell dimensions	$a = 10.7698(9)$ Å	$\alpha = 84.405(1)^\circ$
	$b = 11.1111(10)$ Å	$\beta = 78.857(1)^\circ$
	$c = 17.2505(15)$ Å	$\gamma = 65.717(1)^\circ$
Volume	1845.8(3) Å ³	
Z	2	
Density (calculated)	1.294 Mg/m ³	
Absorption coefficient	0.568 mm ⁻¹	
$F(000)$	760	
Crystal color, morphology	orange, irregular	
Crystal size	0.25 x 0.12 x 0.05 mm ³	
Theta range for data collection	2.10 to 27.48°	
Index ranges	$-13 \leq h \leq 13, -14 \leq k \leq 14, 0 \leq l \leq 22$	
Reflections collected	22004	
Independent reflections	8349 [$R(\text{int}) = 0.0310$]	
Observed reflections	6959	
Completeness to theta = 27.48°	98.6%	
Absorption correction	Multi-scan	
Max. and min. transmission	0.9722 and 0.8711	
Refinement method	Full-matrix least-squares on F^2	
Data / restraints / parameters	8349 / 0 / 467	
Goodness-of-fit on F^2	1.047	
Final R indices [$I > 2\sigma(I)$]	$R1 = 0.0364, wR2 = 0.0806$	
R indices (all data)	$R1 = 0.0471, wR2 = 0.0859$	
Largest diff. peak and hole	0.596 and -0.353 e.Å ⁻³	

Table H2. Atomic coordinates ($\times 10^4$) and equivalent isotropic displacement parameters ($\text{\AA}^2 \times 10^3$) for **4.1a**. U_{eq} is defined as one third of the trace of the orthogonalized U_{ij} tensor.

	x	y	z	U_{eq}
Ni1	4584(1)	6474(1)	2399(1)	17(1)
B1	4660(2)	4017(2)	1764(1)	21(1)
N1	3848(2)	4245(1)	2611(1)	20(1)
N2	3877(2)	5185(1)	3063(1)	20(1)
N3	6137(2)	3887(1)	1782(1)	20(1)
N4	6337(2)	4978(1)	1931(1)	20(1)
N5	3948(2)	5221(1)	1241(1)	19(1)
N6	3768(1)	6456(1)	1439(1)	19(1)
C1	3176(2)	3550(2)	3044(1)	22(1)
C2	2770(2)	4025(2)	3799(1)	25(1)
C3	3233(2)	5038(2)	3796(1)	22(1)
C4	2949(2)	2489(2)	2694(1)	27(1)
C5	3119(2)	5782(2)	4488(1)	23(1)
C6	2145(2)	5810(2)	5158(1)	35(1)
C7	2062(2)	6447(2)	5831(1)	42(1)
C8	2934(2)	7069(2)	5845(1)	36(1)
C9	3897(2)	7052(2)	5185(1)	30(1)
C10	3996(2)	6403(2)	4512(1)	25(1)
C11	7360(2)	2829(2)	1663(1)	22(1)
C12	8380(2)	3245(2)	1725(1)	24(1)
C13	7706(2)	4595(2)	1884(1)	20(1)
C14	7475(2)	1495(2)	1484(1)	26(1)
C15	8340(2)	5535(2)	1920(1)	22(1)
C16	9580(2)	5126(2)	2208(1)	30(1)
C17	10234(2)	5974(2)	2189(1)	35(1)
C18	9658(2)	7246(2)	1876(1)	33(1)
C19	8436(2)	7660(2)	1593(1)	29(1)
C20	7773(2)	6813(2)	1612(1)	25(1)
C21	3355(2)	5301(2)	606(1)	20(1)
C22	2782(2)	6608(2)	381(1)	21(1)

C23	3071(2)	7303(2)	907(1)	19(1)
C24	3359(2)	4134(2)	248(1)	28(1)
C25	2756(2)	8725(2)	854(1)	20(1)
C26	1563(2)	9581(2)	564(1)	22(1)
C27	1287(2)	10905(2)	435(1)	26(1)
C28	2194(2)	11401(2)	594(1)	32(1)
C29	3374(2)	10571(2)	891(1)	32(1)
C30	3655(2)	9244(2)	1021(1)	25(1)
O1	4331(1)	8043(1)	2783(1)	19(1)
C31	3660(2)	8962(2)	3338(1)	16(1)
C32	4436(2)	9475(2)	3673(1)	18(1)
C33	3764(2)	10394(2)	4269(1)	20(1)
C34	2354(2)	10826(2)	4529(1)	22(1)
C35	1589(2)	10362(2)	4176(1)	21(1)
C36	2217(2)	9441(2)	3575(1)	18(1)
C37	5975(2)	9027(2)	3359(1)	21(1)
C38	6818(2)	7695(2)	3724(1)	27(1)
C39	6529(2)	10056(2)	3464(1)	25(1)
C40	1326(2)	9029(2)	3168(1)	21(1)
C41	343(2)	8566(2)	3748(1)	30(1)
C42	513(2)	10182(2)	2656(1)	28(1)

Table H3. Bond lengths [Å] and angles [°] for **4.1a**

Ni(1)-O(1)	1.8214(11)	C(9)-H(9A)	0.9500
Ni(1)-N(4)	2.0174(14)	C(10)-H(10A)	0.9500
Ni(1)-N(6)	2.0246(14)	C(11)-C(12)	1.381(3)
Ni(1)-N(2)	2.0459(15)	C(11)-C(14)	1.493(2)
B(1)-N(1)	1.536(2)	C(12)-C(13)	1.400(2)
B(1)-N(5)	1.543(2)	C(12)-H(12A)	0.9500
B(1)-N(3)	1.543(2)	C(13)-C(15)	1.475(2)
B(1)-H(1A)	1.1200	C(14)-H(14A)	0.9800
N(1)-C(1)	1.348(2)	C(14)-H(14B)	0.9800
N(1)-N(2)	1.3762(19)	C(14)-H(14C)	0.9800
N(2)-C(3)	1.349(2)	C(15)-C(20)	1.392(3)
N(3)-C(11)	1.352(2)	C(15)-C(16)	1.396(3)
N(3)-N(4)	1.3700(19)	C(16)-C(17)	1.384(3)
N(4)-C(13)	1.344(2)	C(16)-H(16A)	0.9500
N(5)-C(21)	1.349(2)	C(17)-C(18)	1.390(3)
N(5)-N(6)	1.3729(19)	C(17)-H(17A)	0.9500
N(6)-C(23)	1.344(2)	C(18)-C(19)	1.374(3)
C(1)-C(2)	1.374(2)	C(18)-H(18A)	0.9500
C(1)-C(4)	1.498(2)	C(19)-C(20)	1.391(3)
C(2)-C(3)	1.405(2)	C(19)-H(19A)	0.9500
C(2)-H(2A)	0.9500	C(20)-H(20A)	0.9500
C(3)-C(5)	1.475(2)	C(21)-C(22)	1.373(2)
C(4)-H(4A)	0.9800	C(21)-C(24)	1.488(2)
C(4)-H(4B)	0.9800	C(22)-C(23)	1.400(2)
C(4)-H(4C)	0.9800	C(22)-H(22A)	0.9500
C(5)-C(10)	1.388(3)	C(23)-C(25)	1.470(2)
C(5)-C(6)	1.394(3)	C(24)-H(24A)	0.9800
C(6)-C(7)	1.388(3)	C(24)-H(24B)	0.9800
C(6)-H(6A)	0.9500	C(24)-H(24C)	0.9800
C(7)-C(8)	1.380(3)	C(25)-C(30)	1.397(2)
C(7)-H(7A)	0.9500	C(25)-C(26)	1.399(2)
C(8)-C(9)	1.380(3)	C(26)-C(27)	1.380(3)
C(8)-H(8A)	0.9500	C(26)-H(26A)	0.9500
C(9)-C(10)	1.390(3)		

C(27)-C(28)	1.380(3)	C(42)-H(42B)	0.9800
C(27)-H(27A)	0.9500	C(42)-H(42C)	0.9800
C(28)-C(29)	1.387(3)	O(1)-Ni(1)-N(4)	130.14(6)
C(28)-H(28A)	0.9500	O(1)-Ni(1)-N(6)	119.72(5)
C(29)-C(30)	1.382(3)	N(4)-Ni(1)-N(6)	88.63(6)
C(29)-H(29A)	0.9500	O(1)-Ni(1)-N(2)	121.91(5)
C(30)-H(30A)	0.9500	N(4)-Ni(1)-N(2)	91.52(6)
O(1)-C(31)	1.3409(19)	N(6)-Ni(1)-N(2)	95.53(6)
C(31)-C(36)	1.407(2)	N(1)-B(1)-N(5)	108.87(14)
C(31)-C(32)	1.415(2)	N(1)-B(1)-N(3)	108.20(14)
C(32)-C(33)	1.390(2)	N(5)-B(1)-N(3)	109.23(14)
C(32)-C(37)	1.522(2)	N(1)-B(1)-H(1A)	110.2
C(33)-C(34)	1.384(2)	N(5)-B(1)-H(1A)	110.2
C(33)-H(33A)	0.9500	N(3)-B(1)-H(1A)	110.2
C(34)-C(35)	1.386(2)	C(1)-N(1)-N(2)	110.64(14)
C(34)-H(34A)	0.9500	C(1)-N(1)-B(1)	129.19(15)
C(35)-C(36)	1.395(2)	N(2)-N(1)-B(1)	119.79(14)
C(35)-H(35A)	0.9500	C(3)-N(2)-N(1)	106.08(14)
C(36)-C(40)	1.520(2)	C(3)-N(2)-Ni(1)	140.71(12)
C(37)-C(39)	1.529(2)	N(1)-N(2)-Ni(1)	112.33(10)
C(37)-C(38)	1.531(3)	C(11)-N(3)-N(4)	110.18(14)
C(37)-H(37A)	1.0000	C(11)-N(3)-B(1)	130.46(14)
C(38)-H(38A)	0.9800	N(4)-N(3)-B(1)	119.36(13)
C(38)-H(38B)	0.9800	C(13)-N(4)-N(3)	106.70(13)
C(38)-H(38C)	0.9800	C(13)-N(4)-Ni(1)	137.67(12)
C(39)-H(39A)	0.9800	N(3)-N(4)-Ni(1)	113.40(10)
C(39)-H(39B)	0.9800	C(21)-N(5)-N(6)	110.22(14)
C(39)-H(39C)	0.9800	C(21)-N(5)-B(1)	130.11(14)
C(40)-C(41)	1.525(2)	N(6)-N(5)-B(1)	119.54(13)
C(40)-C(42)	1.530(3)	C(23)-N(6)-N(5)	106.31(13)
C(40)-H(40A)	1.0000	C(23)-N(6)-Ni(1)	139.61(12)
C(41)-H(41A)	0.9800	N(5)-N(6)-Ni(1)	114.08(10)
C(41)-H(41B)	0.9800	N(1)-C(1)-C(2)	107.50(15)
C(41)-H(41C)	0.9800	N(1)-C(1)-C(4)	122.10(16)
C(42)-H(42A)	0.9800	C(2)-C(1)-C(4)	130.39(17)

C(1)-C(2)-C(3)	106.40(16)	C(13)-C(12)-H(12A)	126.9
C(1)-C(2)-H(2A)	126.8	N(4)-C(13)-C(12)	109.47(16)
C(3)-C(2)-H(2A)	126.8	N(4)-C(13)-C(15)	122.60(15)
N(2)-C(3)-C(2)	109.35(15)	C(12)-C(13)-C(15)	127.66(16)
N(2)-C(3)-C(5)	124.47(16)	C(11)-C(14)-H(14A)	109.5
C(2)-C(3)-C(5)	126.09(16)	C(11)-C(14)-H(14B)	109.5
C(1)-C(4)-H(4A)	109.5	H(14A)-C(14)-H(14B)	109.5
C(1)-C(4)-H(4B)	109.5	C(11)-C(14)-H(14C)	109.5
H(4A)-C(4)-H(4B)	109.5	H(14A)-C(14)-H(14C)	109.5
C(1)-C(4)-H(4C)	109.5	H(14B)-C(14)-H(14C)	109.5
H(4A)-C(4)-H(4C)	109.5	C(20)-C(15)-C(16)	118.76(17)
H(4B)-C(4)-H(4C)	109.5	C(20)-C(15)-C(13)	120.64(16)
C(10)-C(5)-C(6)	118.61(17)	C(16)-C(15)-C(13)	120.42(17)
C(10)-C(5)-C(3)	122.11(16)	C(17)-C(16)-C(15)	120.74(19)
C(6)-C(5)-C(3)	119.21(17)	C(17)-C(16)-H(16A)	119.6
C(7)-C(6)-C(5)	120.40(19)	C(15)-C(16)-H(16A)	119.6
C(7)-C(6)-H(6A)	119.8	C(16)-C(17)-C(18)	119.84(19)
C(5)-C(6)-H(6A)	119.8	C(16)-C(17)-H(17A)	120.1
C(8)-C(7)-C(6)	120.4(2)	C(18)-C(17)-H(17A)	120.1
C(8)-C(7)-H(7A)	119.8	C(19)-C(18)-C(17)	119.88(18)
C(6)-C(7)-H(7A)	119.8	C(19)-C(18)-H(18A)	120.1
C(7)-C(8)-C(9)	119.72(19)	C(17)-C(18)-H(18A)	120.1
C(7)-C(8)-H(8A)	120.1	C(18)-C(19)-C(20)	120.54(19)
C(9)-C(8)-H(8A)	120.1	C(18)-C(19)-H(19A)	119.7
C(8)-C(9)-C(10)	120.08(19)	C(20)-C(19)-H(19A)	119.7
C(8)-C(9)-H(9A)	120.0	C(19)-C(20)-C(15)	120.23(17)
C(10)-C(9)-H(9A)	120.0	C(19)-C(20)-H(20A)	119.9
C(5)-C(10)-C(9)	120.75(17)	C(15)-C(20)-H(20A)	119.9
C(5)-C(10)-H(10A)	119.6	N(5)-C(21)-C(22)	107.78(15)
C(9)-C(10)-H(10A)	119.6	N(5)-C(21)-C(24)	123.48(16)
N(3)-C(11)-C(12)	107.52(15)	C(22)-C(21)-C(24)	128.73(16)
N(3)-C(11)-C(14)	122.64(16)	C(21)-C(22)-C(23)	106.13(15)
C(12)-C(11)-C(14)	129.82(16)	C(21)-C(22)-H(22A)	126.9
C(11)-C(12)-C(13)	106.11(15)	C(23)-C(22)-H(22A)	126.9
C(11)-C(12)-H(12A)	126.9	N(6)-C(23)-C(22)	109.55(15)

N(6)-C(23)-C(25)	124.81(15)	C(32)-C(33)-H(33A)	119.4
C(22)-C(23)-C(25)	125.49(16)	C(33)-C(34)-C(35)	119.57(16)
C(21)-C(24)-H(24A)	109.5	C(33)-C(34)-H(34A)	120.2
C(21)-C(24)-H(24B)	109.5	C(35)-C(34)-H(34A)	120.2
H(24A)-C(24)-H(24B)	109.5	C(34)-C(35)-C(36)	121.24(16)
C(21)-C(24)-H(24C)	109.5	C(34)-C(35)-H(35A)	119.4
H(24A)-C(24)-H(24C)	109.5	C(36)-C(35)-H(35A)	119.4
H(24B)-C(24)-H(24C)	109.5	C(35)-C(36)-C(31)	118.87(15)
C(30)-C(25)-C(26)	118.45(16)	C(35)-C(36)-C(40)	119.40(15)
C(30)-C(25)-C(23)	122.70(16)	C(31)-C(36)-C(40)	121.67(15)
C(26)-C(25)-C(23)	118.64(15)	C(32)-C(37)-C(39)	112.89(14)
C(27)-C(26)-C(25)	120.84(17)	C(32)-C(37)-C(38)	111.65(14)
C(27)-C(26)-H(26A)	119.6	C(39)-C(37)-C(38)	110.57(14)
C(25)-C(26)-H(26A)	119.6	C(32)-C(37)-H(37A)	107.1
C(28)-C(27)-C(26)	120.01(18)	C(39)-C(37)-H(37A)	107.1
C(28)-C(27)-H(27A)	120.0	C(38)-C(37)-H(37A)	107.1
C(26)-C(27)-H(27A)	120.0	C(37)-C(38)-H(38A)	109.5
C(27)-C(28)-C(29)	120.00(18)	C(37)-C(38)-H(38B)	109.5
C(27)-C(28)-H(28A)	120.0	H(38A)-C(38)-H(38B)	109.5
C(29)-C(28)-H(28A)	120.0	C(37)-C(38)-H(38C)	109.5
C(30)-C(29)-C(28)	120.24(18)	H(38A)-C(38)-H(38C)	109.5
C(30)-C(29)-H(29A)	119.9	H(38B)-C(38)-H(38C)	109.5
C(28)-C(29)-H(29A)	119.9	C(37)-C(39)-H(39A)	109.5
C(29)-C(30)-C(25)	120.46(17)	C(37)-C(39)-H(39B)	109.5
C(29)-C(30)-H(30A)	119.8	H(39A)-C(39)-H(39B)	109.5
C(25)-C(30)-H(30A)	119.8	C(37)-C(39)-H(39C)	109.5
C(31)-O(1)-Ni(1)	147.77(11)	H(39A)-C(39)-H(39C)	109.5
O(1)-C(31)-C(36)	121.74(15)	H(39B)-C(39)-H(39C)	109.5
O(1)-C(31)-C(32)	118.25(15)	C(36)-C(40)-C(41)	112.79(15)
C(36)-C(31)-C(32)	119.99(15)	C(36)-C(40)-C(42)	109.25(14)
C(33)-C(32)-C(31)	118.96(15)	C(41)-C(40)-C(42)	110.25(15)
C(33)-C(32)-C(37)	121.96(15)	C(36)-C(40)-H(40A)	108.1
C(31)-C(32)-C(37)	119.07(15)	C(41)-C(40)-H(40A)	108.1
C(34)-C(33)-C(32)	121.23(16)	C(42)-C(40)-H(40A)	108.1
C(34)-C(33)-H(33A)	119.4	C(40)-C(41)-H(41A)	109.5

C(40)-C(41)-H(41B)	109.5	C(40)-C(42)-H(42B)	109.5
H(41A)-C(41)-H(41B)	109.5	H(42A)-C(42)-H(42B)	109.5
C(40)-C(41)-H(41C)	109.5	C(40)-C(42)-H(42C)	109.5
H(41A)-C(41)-H(41C)	109.5	H(42A)-C(42)-H(42C)	109.5
H(41B)-C(41)-H(41C)	109.5	H(42B)-C(42)-H(42C)	109.5
C(40)-C(42)-H(42A)	109.5		

Symmetry transformations used to generate equivalent atoms

APPENDIX I: CRYSTAL STRUCTURE AND DATA REFINEMENT FOR
COMPLEX 4.2

Table I1. Crystal data and structure refinement for 4.2.

Empirical formula	$C_{60} H_{54} B_2 N_{12} Ni_2 O_2$	
Formula weight	1114.19	
Temperature	173(2) K	
Wavelength	0.71073 Å	
Crystal system	Tetragonal	
Space group	$P4_2/n$	
Unit cell dimensions	$a = 19.6818(18)$ Å	$\alpha = 90^\circ$
	$b = 19.6818(18)$ Å	$\beta = 90^\circ$
	$c = 13.5412(12)$ Å	$\gamma = 90^\circ$
Volume	$5245.5(8)$ Å ³	
<i>Z</i>	4	
Density (calculated)	1.411 Mg/m ³	
Absorption coefficient	0.776 mm ⁻¹	
<i>F</i> (000)	2320	
Crystal color, morphology	green, Needle	
Crystal size	0.45 x 0.12 x 0.10 mm ³	
Theta range for data collection	1.83 to 26.37°	
Index ranges	$-16 \leq h \leq 17, 0 \leq k \leq 24, 0 \leq l \leq 16$	
Reflections collected	60638	
Independent reflections	5365 [<i>R</i> (int) = 0.0500]	
Observed reflections	4145	
Completeness to theta = 26.37°	100.0%	
Absorption correction	Multi-scan	
Max. and min. transmission	0.9264 and 0.7215	
Refinement method	Full-matrix least-squares on <i>F</i> ²	
Data / restraints / parameters	5365 / 0 / 355	
Goodness-of-fit on <i>F</i> ²	1.020	
Final <i>R</i> indices [<i>I</i> > 2σ(<i>I</i>)]	<i>R</i> 1 = 0.0389, <i>wR</i> 2 = 0.0983	
<i>R</i> indices (all data)	<i>R</i> 1 = 0.0559, <i>wR</i> 2 = 0.1088	
Largest diff. peak and hole	0.436 and -0.260 e.Å ⁻³	

Table I2. Atomic coordinates ($\times 10^4$) and equivalent isotropic displacement parameters ($\text{\AA}^2 \times 10^3$) for **4.2**. U_{eq} is defined as one third of the trace of the orthogonalized U_{ij} tensor.

	x	y	z	U_{eq}
Ni1	5773(1)	5111(1)	5201(1)	30(1)
B1	7215(1)	5506(2)	5821(2)	33(1)
N1	6985(1)	5939(1)	4942(2)	34(1)
N2	6331(1)	5862(1)	4624(2)	35(1)
N3	6717(1)	5616(1)	6680(2)	34(1)
N4	6052(1)	5416(1)	6594(2)	33(1)
N5	7212(1)	4755(1)	5498(2)	33(1)
N6	6633(1)	4454(1)	5112(2)	33(1)
C1	7300(1)	6416(1)	4399(2)	36(1)
C2	6839(1)	6650(1)	3718(2)	40(1)
C3	6234(1)	6300(1)	3887(2)	34(1)
C4	8023(1)	6601(2)	4574(2)	50(1)
C5	5573(1)	6372(1)	3400(2)	36(1)
C6	5528(1)	6830(1)	2626(2)	42(1)
C7	4932(2)	6946(1)	2113(2)	43(1)
C8	4361(2)	6596(1)	2395(2)	43(1)
C9	4382(1)	6133(1)	3165(2)	42(1)
C10	4982(1)	5999(1)	3686(2)	38(1)
O1	4980(1)	5537(1)	4449(1)	38(1)
C11	6844(1)	5824(1)	7613(2)	36(1)
C12	6251(1)	5749(1)	8143(2)	38(1)
C13	5767(1)	5492(1)	7486(2)	33(1)
C14	7519(1)	6085(2)	7938(2)	49(1)
C15	5063(1)	5299(1)	7722(2)	34(1)
C16	4939(1)	4935(1)	8583(2)	38(1)
C17	4285(2)	4752(1)	8838(2)	44(1)
C18	3745(2)	4926(1)	8238(2)	44(1)
C19	3860(1)	5291(1)	7388(2)	44(1)
C20	4516(1)	5483(1)	7130(2)	39(1)
C21	7749(1)	4338(1)	5394(2)	37(1)

C22	7532(1)	3756(1)	4936(2)	41(1)
C23	6838(1)	3843(1)	4772(2)	35(1)
C24	8449(1)	4516(2)	5717(3)	52(1)
C25	6422(1)	3328(1)	4246(2)	39(1)
C26	6672(2)	3086(2)	3343(2)	50(1)
C27	6348(2)	2566(2)	2848(2)	55(1)
C28	5785(2)	2270(2)	3248(3)	62(1)
C29	5532(2)	2495(2)	4141(3)	71(1)
C30	5850(2)	3028(2)	4635(3)	56(1)

Table I3. Bond lengths [\AA] and angles [$^\circ$] for **4.2**.

Ni(1)-N(2)	2.000(2)	C(8)-H(8A)	0.9500
Ni(1)-O(1)#1	2.0104(17)	C(9)-C(10)	1.401(4)
Ni(1)-O(1)	2.0432(17)	C(9)-H(9A)	0.9500
Ni(1)-N(4)	2.054(2)	C(10)-O(1)	1.377(3)
Ni(1)-N(6)	2.134(2)	O(1)-Ni(1)#1	2.0104(17)
B(1)-N(1)	1.533(3)	C(11)-C(12)	1.377(4)
B(1)-N(3)	1.536(3)	C(11)-C(14)	1.493(4)
B(1)-N(5)	1.541(3)	C(12)-C(13)	1.399(3)
B(1)-H(1A)	1.1200	C(12)-H(12A)	0.9500
N(1)-C(1)	1.345(3)	C(13)-C(15)	1.472(3)
N(1)-N(2)	1.364(3)	C(14)-H(14A)	0.9800
N(2)-C(3)	1.333(3)	C(14)-H(14B)	0.9800
N(3)-C(11)	1.351(3)	C(14)-H(14C)	0.9800
N(3)-N(4)	1.373(3)	C(15)-C(20)	1.391(4)
N(4)-C(13)	1.339(3)	C(15)-C(16)	1.391(4)
N(5)-C(21)	1.345(3)	C(16)-C(17)	1.381(4)
N(5)-N(6)	1.387(3)	C(16)-H(16A)	0.9500
N(6)-C(23)	1.349(3)	C(17)-C(18)	1.380(4)
C(1)-C(2)	1.375(4)	C(17)-H(17A)	0.9500
C(1)-C(4)	1.488(4)	C(18)-C(19)	1.376(4)
C(2)-C(3)	1.394(4)	C(18)-H(18A)	0.9500
C(2)-H(2A)	0.9500	C(19)-C(20)	1.389(4)
C(3)-C(5)	1.466(3)	C(19)-H(19A)	0.9500
C(4)-H(4A)	0.9800	C(20)-H(20A)	0.9500
C(4)-H(4B)	0.9800	C(21)-C(22)	1.372(4)
C(4)-H(4C)	0.9800	C(21)-C(24)	1.488(4)
C(5)-C(6)	1.384(4)	C(22)-C(23)	1.394(4)
C(5)-C(10)	1.429(4)	C(22)-H(22A)	0.9500
C(6)-C(7)	1.382(4)	C(23)-C(25)	1.484(3)
C(6)-H(6A)	0.9500	C(24)-H(24A)	0.9800
C(7)-C(8)	1.372(4)	C(24)-H(24B)	0.9800
C(7)-H(7A)	0.9500	C(24)-H(24C)	0.9800
C(8)-C(9)	1.385(4)	C(25)-C(30)	1.377(4)

C(25)-C(26)	1.401(4)	C(13)-N(4)-N(3)	106.88(19)
C(26)-C(27)	1.380(4)	C(13)-N(4)-Ni(1)	138.48(17)
C(26)-H(26A)	0.9500	N(3)-N(4)-Ni(1)	114.63(15)
C(27)-C(28)	1.363(5)	C(21)-N(5)-N(6)	110.2(2)
C(27)-H(27A)	0.9500	C(21)-N(5)-B(1)	127.7(2)
C(28)-C(29)	1.380(5)	N(6)-N(5)-B(1)	121.30(19)
C(28)-H(28A)	0.9500	C(23)-N(6)-N(5)	105.3(2)
C(29)-C(30)	1.393(4)	C(23)-N(6)-Ni(1)	142.80(17)
C(29)-H(29A)	0.9500	N(5)-N(6)-Ni(1)	111.83(15)
C(30)-H(30A)	0.9500	N(1)-C(1)-C(2)	107.2(2)
N(2)-Ni(1)-O(1)#1	164.81(8)	N(1)-C(1)-C(4)	121.8(2)
N(2)-Ni(1)-O(1)	85.55(8)	C(2)-C(1)-C(4)	131.0(2)
O(1)#1-Ni(1)-O(1)	79.32(8)	C(1)-C(2)-C(3)	106.7(2)
N(2)-Ni(1)-N(4)	89.78(8)	C(1)-C(2)-H(2A)	126.6
O(1)#1-Ni(1)-N(4)	99.54(8)	C(3)-C(2)-H(2A)	126.6
O(1)-Ni(1)-N(4)	122.82(8)	N(2)-C(3)-C(2)	108.7(2)
N(2)-Ni(1)-N(6)	89.40(8)	N(2)-C(3)-C(5)	121.8(2)
O(1)#1-Ni(1)-N(6)	102.32(7)	C(2)-C(3)-C(5)	129.4(2)
O(1)-Ni(1)-N(6)	145.73(8)	C(1)-C(4)-H(4A)	109.5
N(4)-Ni(1)-N(6)	90.97(8)	C(1)-C(4)-H(4B)	109.5
N(1)-B(1)-N(3)	108.7(2)	H(4A)-C(4)-H(4B)	109.5
N(1)-B(1)-N(5)	108.2(2)	C(1)-C(4)-H(4C)	109.5
N(3)-B(1)-N(5)	110.4(2)	H(4A)-C(4)-H(4C)	109.5
N(1)-B(1)-H(1A)	109.9	H(4B)-C(4)-H(4C)	109.5
N(3)-B(1)-H(1A)	109.9	C(6)-C(5)-C(10)	119.2(2)
N(5)-B(1)-H(1A)	109.9	C(6)-C(5)-C(3)	117.5(2)
C(1)-N(1)-N(2)	109.9(2)	C(10)-C(5)-C(3)	123.4(2)
C(1)-N(1)-B(1)	132.5(2)	C(7)-C(6)-C(5)	122.9(3)
N(2)-N(1)-B(1)	117.52(19)	C(7)-C(6)-H(6A)	118.6
C(3)-N(2)-N(1)	107.4(2)	C(5)-C(6)-H(6A)	118.6
C(3)-N(2)-Ni(1)	133.76(17)	C(8)-C(7)-C(6)	118.1(3)
N(1)-N(2)-Ni(1)	118.48(15)	C(8)-C(7)-H(7A)	120.9
C(11)-N(3)-N(4)	110.0(2)	C(6)-C(7)-H(7A)	120.9
C(11)-N(3)-B(1)	129.3(2)	C(7)-C(8)-C(9)	121.1(3)
N(4)-N(3)-B(1)	120.25(19)	C(7)-C(8)-H(8A)	119.5

C(9)-C(8)-H(8A)	119.5	C(19)-C(18)-H(18A)	120.2
C(8)-C(9)-C(10)	121.8(3)	C(17)-C(18)-H(18A)	120.2
C(8)-C(9)-H(9A)	119.1	C(18)-C(19)-C(20)	120.4(3)
C(10)-C(9)-H(9A)	119.1	C(18)-C(19)-H(19A)	119.8
O(1)-C(10)-C(9)	120.0(2)	C(20)-C(19)-H(19A)	119.8
O(1)-C(10)-C(5)	123.1(2)	C(19)-C(20)-C(15)	120.2(3)
C(9)-C(10)-C(5)	116.9(2)	C(19)-C(20)-H(20A)	119.9
C(10)-O(1)-Ni(1)#1	126.75(15)	C(15)-C(20)-H(20A)	119.9
C(10)-O(1)-Ni(1)	129.96(15)	N(5)-C(21)-C(22)	108.1(2)
Ni(1)#1-O(1)-Ni(1)	100.68(8)	N(5)-C(21)-C(24)	123.5(2)
N(3)-C(11)-C(12)	107.5(2)	C(22)-C(21)-C(24)	128.3(3)
N(3)-C(11)-C(14)	122.9(2)	C(21)-C(22)-C(23)	106.0(2)
C(12)-C(11)-C(14)	129.6(2)	C(21)-C(22)-H(22A)	127.0
C(11)-C(12)-C(13)	106.4(2)	C(23)-C(22)-H(22A)	127.0
C(11)-C(12)-H(12A)	126.8	N(6)-C(23)-C(22)	110.4(2)
C(13)-C(12)-H(12A)	126.8	N(6)-C(23)-C(25)	127.5(2)
N(4)-C(13)-C(12)	109.3(2)	C(22)-C(23)-C(25)	122.1(2)
N(4)-C(13)-C(15)	124.1(2)	C(21)-C(24)-H(24A)	109.5
C(12)-C(13)-C(15)	126.6(2)	C(21)-C(24)-H(24B)	109.5
C(11)-C(14)-H(14A)	109.5	H(24A)-C(24)-H(24B)	109.5
C(11)-C(14)-H(14B)	109.5	C(21)-C(24)-H(24C)	109.5
H(14A)-C(14)-H(14B)	109.5	H(24A)-C(24)-H(24C)	109.5
C(11)-C(14)-H(14C)	109.5	H(24B)-C(24)-H(24C)	109.5
H(14A)-C(14)-H(14C)	109.5	C(30)-C(25)-C(26)	118.4(3)
H(14B)-C(14)-H(14C)	109.5	C(30)-C(25)-C(23)	124.0(3)
C(20)-C(15)-C(16)	118.8(2)	C(26)-C(25)-C(23)	117.3(2)
C(20)-C(15)-C(13)	122.5(2)	C(27)-C(26)-C(25)	120.9(3)
C(16)-C(15)-C(13)	118.7(2)	C(27)-C(26)-H(26A)	119.5
C(17)-C(16)-C(15)	120.5(2)	C(25)-C(26)-H(26A)	119.5
C(17)-C(16)-H(16A)	119.7	C(28)-C(27)-C(26)	119.9(3)
C(15)-C(16)-H(16A)	119.7	C(28)-C(27)-H(27A)	120.1
C(18)-C(17)-C(16)	120.4(3)	C(26)-C(27)-H(27A)	120.1
C(18)-C(17)-H(17A)	119.8	C(27)-C(28)-C(29)	120.4(3)
C(16)-C(17)-H(17A)	119.8	C(27)-C(28)-H(28A)	119.8
C(19)-C(18)-C(17)	119.7(3)	C(29)-C(28)-H(28A)	119.8

C(28)-C(29)-C(30)	119.9(3)
C(28)-C(29)-H(29A)	120.0
C(30)-C(29)-H(29A)	120.0
C(25)-C(30)-C(29)	120.5(3)
C(25)-C(30)-H(30A)	119.8
C(29)-C(30)-H(30A)	119.8

APPENDIX J: CRYSTAL STRUCTURE AND DATA REFINEMENT FOR
COMPLEX 4.3

Table J1. Crystal data and structure refinement for 4.3.

Empirical formula	$C_{31} H_{44} B_2 N_{12} Ni_2 O_3$	
Formula weight	771.82	
Temperature	173(2) K	
Wavelength	0.71073 Å	
Crystal system	Monoclinic	
Space group	$P2_1$	
Unit cell dimensions	$a = 8.053(5)$ Å	$\alpha = 90^\circ$
	$b = 30.944(19)$ Å	$\beta = 113.820(6)^\circ$
	$c = 8.073(5)$ Å	$\gamma = 90^\circ$
Volume	$1840.4(19)$ Å ³	
<i>Z</i>	2	
Density (calculated)	1.393 Mg/m ³	
Absorption coefficient	1.073 mm ⁻¹	
<i>F</i> (000)	808	
Crystal color, morphology	Green, Block	
Crystal size	0.45 x 0.12 x 0.10 mm ³	
Theta range for data collection	1.97 to 25.44°	
Index ranges	$-9 \leq h \leq 8, -33 \leq k \leq 37, 0 \leq l \leq 9$	
Reflections collected	14999	
Independent reflections	6484 [<i>R</i> (int) = 0.0528]	
Observed reflections	5206	
Completeness to theta = 25.44°	99.6%	
Absorption correction	Multi-scan	
Max. and min. transmission	0.89 and 0.87	
Refinement method	Full-matrix least-squares on <i>F</i> ²	
Data / restraints / parameters	6484 / 1 / 464	
Goodness-of-fit on <i>F</i> ²	1.061	
Final <i>R</i> indices [<i>I</i> > 2σ(<i>I</i>)]	<i>R</i> 1 = 0.0525, <i>wR</i> 2 = 0.1114	
<i>R</i> indices (all data)	<i>R</i> 1 = 0.0718, <i>wR</i> 2 = 0.1194	
Absolute structure parameter	0.00(2)	
Largest diff. peak and hole	0.579 and -0.627 e.Å ⁻³	

Table J2. Atomic coordinates ($\times 10^4$) and equivalent isotropic displacement parameters ($\text{\AA}^2 \times 10^3$) for **4.3**. U_{eq} is defined as one third of the trace of the orthogonalized U_{ij} tensor.

	x	y	z	U_{eq}
Ni1	3629(1)	3991(1)	7898(2)	43(1)
B1	2070(13)	3096(3)	6613(13)	42(3)
N1	3974(10)	3128(2)	6611(10)	39(2)
N2	4915(11)	3512(2)	7196(11)	48(2)
N3	2222(10)	3185(2)	8610(10)	40(2)
N4	2916(10)	3578(2)	9417(11)	40(2)
N5	865(8)	3445(2)	5279(9)	37(2)
N6	1293(8)	3878(2)	5716(8)	36(2)
C1	4984(15)	2837(4)	6125(15)	55(3)
C2	6605(14)	3032(4)	6429(16)	58(3)
C3	6542(13)	3440(4)	7041(15)	60(3)
C4	4340(19)	2395(4)	5414(16)	70(4)
C5	7914(16)	3810(4)	7630(20)	91(5)
C6	1813(13)	2930(3)	9751(14)	41(2)
C7	2246(12)	3176(4)	11331(14)	56(3)
C8	2945(13)	3570(3)	11144(14)	45(2)
C9	1060(16)	2477(3)	9289(17)	58(3)
C10	3567(13)	3956(4)	12352(13)	58(3)
C11	-697(11)	3430(3)	3708(12)	51(3)
C12	-1237(11)	3842(3)	3204(10)	52(3)
C13	5(10)	4124(3)	4439(12)	51(3)
C14	-1481(14)	2998(3)	2878(15)	74(3)
C15	9(12)	4600(3)	4459(15)	50(3)
Ni2	3791(1)	5342(1)	8764(1)	40(1)
B2	2140(14)	6220(3)	7232(14)	37(2)
N7	3833(10)	6289(2)	9015(10)	42(2)
N8	4818(9)	5927(2)	9922(10)	36(2)
N9	831(9)	5936(2)	7775(10)	37(2)

N10	1352(11)	5521(2)	8441(10)	39(2)
N11	2615(10)	5971(2)	5817(10)	38(2)
N12	3445(11)	5567(2)	6269(11)	40(2)
C16	4711(12)	6642(3)	9889(13)	50(2)
C17	6207(11)	6513(3)	11431(11)	47(2)
C18	6266(12)	6071(2)	11374(12)	44(2)
C19	3936(13)	7086(3)	9256(14)	57(3)
C20	7629(12)	5766(3)	12700(13)	52(2)
C21	-853(12)	6016(3)	7808(12)	41(2)
C22	-1409(13)	5658(4)	8412(11)	43(3)
C23	2(13)	5360(3)	8841(12)	42(2)
C24	-1831(15)	6445(3)	7129(17)	53(3)
C25	198(13)	4905(3)	9666(16)	50(3)
C26	2479(12)	6078(3)	4128(14)	47(2)
C27	3237(13)	5762(4)	3508(16)	57(3)
C28	3860(13)	5454(3)	4872(13)	43(3)
C29	1601(18)	6492(4)	3111(19)	76(5)
C30	4828(15)	5030(4)	4909(18)	65(3)
C31	5256(12)	4645(3)	9508(16)	51(3)
O1	3470(8)	4658(2)	8319(11)	56(2)
O2	5926(9)	4269(2)	9683(11)	78(3)
O3	5966(9)	4993(2)	10078(10)	66(2)

Table J3. Bond lengths [\AA] and angles [$^\circ$] for **4.3**.

Ni(1)-N(4)	2.009(7)	C(7)-H(7A)	0.9500
Ni(1)-N(2)	2.016(8)	C(8)-C(10)	1.493(15)
Ni(1)-N(6)	2.021(6)	C(9)-H(9A)	0.9800
Ni(1)-O(2)	2.021(7)	C(9)-H(9B)	0.9800
Ni(1)-O(1)	2.104(7)	C(9)-H(9C)	0.9800
Ni(1)-C(31)	2.477(10)	C(10)-H(10A)	0.9800
B(1)-N(1)	1.538(12)	C(10)-H(10B)	0.9800
B(1)-N(5)	1.557(11)	C(10)-H(10C)	0.9800
B(1)-N(3)	1.591(12)	C(11)-C(12)	1.354(12)
B(1)-H(1A)	1.1200	C(11)-C(14)	1.516(13)
N(1)-C(1)	1.374(11)	C(12)-C(13)	1.397(11)
N(1)-N(2)	1.385(10)	C(12)-H(12A)	0.9500
N(2)-C(3)	1.384(13)	C(13)-C(15)	1.471(12)
N(3)-C(6)	1.351(11)	C(14)-H(14A)	0.9800
N(3)-N(4)	1.385(10)	C(14)-H(14B)	0.9800
N(4)-C(8)	1.385(12)	C(14)-H(14C)	0.9800
N(5)-C(11)	1.380(10)	C(15)-H(15A)	0.9800
N(5)-N(6)	1.394(9)	C(15)-H(15B)	0.9800
N(6)-C(13)	1.361(9)	C(15)-H(15C)	0.9800
C(1)-C(2)	1.368(15)	Ni(2)-N(10)	1.955(8)
C(1)-C(4)	1.490(16)	Ni(2)-O(3)	1.963(6)
C(2)-C(3)	1.363(16)	Ni(2)-N(12)	2.041(8)
C(2)-H(2A)	0.9500	Ni(2)-N(8)	2.054(6)
C(3)-C(5)	1.529(16)	Ni(2)-O(1)	2.144(7)
C(4)-H(4A)	0.9800	Ni(2)-C(31)	2.413(10)
C(4)-H(4B)	0.9800	B(2)-N(7)	1.546(11)
C(4)-H(4C)	0.9800	B(2)-N(11)	1.549(14)
C(5)-H(5A)	0.9800	B(2)-N(9)	1.565(14)
C(5)-H(5B)	0.9800	B(2)-H(2B)	1.1200
C(5)-H(5C)	0.9800	N(7)-C(16)	1.336(10)
C(6)-C(7)	1.403(15)	N(7)-N(8)	1.397(9)
C(6)-C(9)	1.513(13)	N(8)-C(18)	1.352(10)
C(7)-C(8)	1.378(15)	N(9)-C(21)	1.389(11)

N(9)-N(10)	1.390(10)	C(30)-H(30A)	0.9800
N(10)-C(23)	1.348(12)	C(30)-H(30B)	0.9800
N(11)-C(26)	1.364(12)	C(30)-H(30C)	0.9800
N(11)-N(12)	1.394(10)	C(31)-O(3)	1.219(11)
N(12)-C(28)	1.346(12)	C(31)-O(2)	1.267(11)
C(16)-C(17)	1.396(12)	C(31)-O(1)	1.370(10)
C(16)-C(19)	1.509(12)	N(4)-Ni(1)-N(2)	90.6(3)
C(17)-C(18)	1.372(11)	N(4)-Ni(1)-N(6)	91.6(3)
C(17)-H(17A)	0.9500	N(2)-Ni(1)-N(6)	91.8(3)
C(18)-C(20)	1.514(10)	N(4)-Ni(1)-O(2)	103.9(3)
C(19)-H(19A)	0.9800	N(2)-Ni(1)-O(2)	95.0(3)
C(19)-H(19B)	0.9800	N(6)-Ni(1)-O(2)	162.9(3)
C(19)-H(19C)	0.9800	N(4)-Ni(1)-O(1)	118.3(3)
C(20)-H(20A)	0.9800	N(2)-Ni(1)-O(1)	146.9(3)
C(20)-H(20B)	0.9800	N(6)-Ni(1)-O(1)	102.3(2)
C(20)-H(20C)	0.9800	O(2)-Ni(1)-O(1)	64.2(2)
C(21)-C(22)	1.358(14)	N(4)-Ni(1)-C(31)	114.9(4)
C(21)-C(24)	1.526(14)	N(2)-Ni(1)-C(31)	121.7(3)
C(22)-C(23)	1.393(14)	N(6)-Ni(1)-C(31)	135.0(3)
C(22)-H(22A)	0.9500	O(2)-Ni(1)-C(31)	30.6(3)
C(23)-C(25)	1.538(14)	O(1)-Ni(1)-C(31)	33.6(3)
C(24)-H(24A)	0.9800	N(1)-B(1)-N(5)	107.3(7)
C(24)-H(24B)	0.9800	N(1)-B(1)-N(3)	108.7(7)
C(24)-H(24C)	0.9800	N(5)-B(1)-N(3)	110.6(7)
C(25)-H(25A)	0.9800	N(1)-B(1)-H(1A)	110.1
C(25)-H(25B)	0.9800	N(5)-B(1)-H(1A)	110.1
C(25)-H(25C)	0.9800	N(3)-B(1)-H(1A)	110.1
C(26)-C(27)	1.351(15)	C(1)-N(1)-N(2)	110.8(7)
C(26)-C(29)	1.532(14)	C(1)-N(1)-B(1)	131.6(8)
C(27)-C(28)	1.388(15)	N(2)-N(1)-B(1)	117.6(7)
C(27)-H(27A)	0.9500	C(3)-N(2)-N(1)	103.8(8)
C(28)-C(30)	1.520(15)	C(3)-N(2)-Ni(1)	139.2(8)
C(29)-H(29A)	0.9800	N(1)-N(2)-Ni(1)	117.0(5)
C(29)-H(29B)	0.9800	C(6)-N(3)-N(4)	110.9(7)
C(29)-H(29C)	0.9800	C(6)-N(3)-B(1)	130.4(8)

N(4)-N(3)-B(1)	118.7(7)	C(8)-C(7)-H(7A)	125.0
N(3)-N(4)-C(8)	107.4(7)	C(6)-C(7)-H(7A)	125.0
N(3)-N(4)-Ni(1)	115.6(6)	C(7)-C(8)-N(4)	106.5(9)
C(8)-N(4)-Ni(1)	137.1(6)	C(7)-C(8)-C(10)	132.9(10)
C(11)-N(5)-N(6)	107.7(7)	N(4)-C(8)-C(10)	120.6(8)
C(11)-N(5)-B(1)	134.0(8)	C(6)-C(9)-H(9A)	109.5
N(6)-N(5)-B(1)	118.1(6)	C(6)-C(9)-H(9B)	109.5
C(13)-N(6)-N(5)	108.1(6)	H(9A)-C(9)-H(9B)	109.5
C(13)-N(6)-Ni(1)	136.1(6)	C(6)-C(9)-H(9C)	109.5
N(5)-N(6)-Ni(1)	115.7(4)	H(9A)-C(9)-H(9C)	109.5
C(2)-C(1)-N(1)	106.8(10)	H(9B)-C(9)-H(9C)	109.5
C(2)-C(1)-C(4)	129.3(10)	C(8)-C(10)-H(10A)	109.5
N(1)-C(1)-C(4)	123.9(10)	C(8)-C(10)-H(10B)	109.5
C(3)-C(2)-C(1)	107.6(9)	H(10A)-C(10)-H(10B)	109.5
C(3)-C(2)-H(2A)	126.2	C(8)-C(10)-H(10C)	109.5
C(1)-C(2)-H(2A)	126.2	H(10A)-C(10)-H(10C)	109.5
C(2)-C(3)-N(2)	110.9(10)	H(10B)-C(10)-H(10C)	109.5
C(2)-C(3)-C(5)	132.9(10)	C(12)-C(11)-N(5)	108.0(8)
N(2)-C(3)-C(5)	116.2(11)	C(12)-C(11)-C(14)	132.2(8)
C(1)-C(4)-H(4A)	109.5	N(5)-C(11)-C(14)	119.8(9)
C(1)-C(4)-H(4B)	109.5	C(11)-C(12)-C(13)	108.9(7)
H(4A)-C(4)-H(4B)	109.5	C(11)-C(12)-H(12A)	125.6
C(1)-C(4)-H(4C)	109.5	C(13)-C(12)-H(12A)	125.6
H(4A)-C(4)-H(4C)	109.5	N(6)-C(13)-C(12)	107.3(7)
H(4B)-C(4)-H(4C)	109.5	N(6)-C(13)-C(15)	123.5(8)
C(3)-C(5)-H(5A)	109.5	C(12)-C(13)-C(15)	129.1(7)
C(3)-C(5)-H(5B)	109.5	C(11)-C(14)-H(14A)	109.5
H(5A)-C(5)-H(5B)	109.5	C(11)-C(14)-H(14B)	109.5
C(3)-C(5)-H(5C)	109.5	H(14A)-C(14)-H(14B)	109.5
H(5A)-C(5)-H(5C)	109.5	C(11)-C(14)-H(14C)	109.5
H(5B)-C(5)-H(5C)	109.5	H(14A)-C(14)-H(14C)	109.5
N(3)-C(6)-C(7)	105.2(8)	H(14B)-C(14)-H(14C)	109.5
N(3)-C(6)-C(9)	123.9(9)	C(13)-C(15)-H(15A)	109.5
C(7)-C(6)-C(9)	130.9(9)	C(13)-C(15)-H(15B)	109.5
C(8)-C(7)-C(6)	110.1(9)	H(15A)-C(15)-H(15B)	109.5

C(13)-C(15)-H(15C)	109.5	N(9)-N(10)-Ni(2)	116.4(5)
H(15A)-C(15)-H(15C)	109.5	C(26)-N(11)-N(12)	108.4(7)
H(15B)-C(15)-H(15C)	109.5	C(26)-N(11)-B(2)	132.3(8)
N(10)-Ni(2)-O(3)	149.0(3)	N(12)-N(11)-B(2)	119.2(7)
N(10)-Ni(2)-N(12)	92.4(3)	C(28)-N(12)-N(11)	105.7(8)
O(3)-Ni(2)-N(12)	117.2(3)	C(28)-N(12)-Ni(2)	139.1(7)
N(10)-Ni(2)-N(8)	90.5(3)	N(11)-N(12)-Ni(2)	115.2(5)
O(3)-Ni(2)-N(8)	97.5(3)	N(7)-C(16)-C(17)	108.7(7)
N(12)-Ni(2)-N(8)	90.9(3)	N(7)-C(16)-C(19)	120.4(8)
N(10)-Ni(2)-O(1)	102.2(3)	C(17)-C(16)-C(19)	130.6(8)
O(3)-Ni(2)-O(1)	64.5(3)	C(18)-C(17)-C(16)	106.5(7)
N(12)-Ni(2)-O(1)	102.3(3)	C(18)-C(17)-H(17A)	126.7
N(8)-Ni(2)-O(1)	161.1(2)	C(16)-C(17)-H(17A)	126.7
N(10)-Ni(2)-C(31)	130.6(3)	N(8)-C(18)-C(17)	109.1(6)
O(3)-Ni(2)-C(31)	30.2(3)	N(8)-C(18)-C(20)	122.3(7)
N(12)-Ni(2)-C(31)	114.2(4)	C(17)-C(18)-C(20)	128.6(7)
N(8)-Ni(2)-C(31)	127.5(3)	C(16)-C(19)-H(19A)	109.5
O(1)-Ni(2)-C(31)	34.3(3)	C(16)-C(19)-H(19B)	109.5
N(7)-B(2)-N(11)	111.6(8)	H(19A)-C(19)-H(19B)	109.5
N(7)-B(2)-N(9)	104.9(8)	C(16)-C(19)-H(19C)	109.5
N(11)-B(2)-N(9)	108.8(6)	H(19A)-C(19)-H(19C)	109.5
N(7)-B(2)-H(2B)	110.5	H(19B)-C(19)-H(19C)	109.5
N(11)-B(2)-H(2B)	110.5	C(18)-C(20)-H(20A)	109.5
N(9)-B(2)-H(2B)	110.5	C(18)-C(20)-H(20B)	109.5
C(16)-N(7)-N(8)	108.1(6)	H(20A)-C(20)-H(20B)	109.5
C(16)-N(7)-B(2)	133.2(7)	C(18)-C(20)-H(20C)	109.5
N(8)-N(7)-B(2)	118.5(6)	H(20A)-C(20)-H(20C)	109.5
C(18)-N(8)-N(7)	107.4(6)	H(20B)-C(20)-H(20C)	109.5
C(18)-N(8)-Ni(2)	137.1(5)	C(22)-C(21)-N(9)	109.0(8)
N(7)-N(8)-Ni(2)	115.5(4)	C(22)-C(21)-C(24)	129.9(9)
C(21)-N(9)-N(10)	107.6(7)	N(9)-C(21)-C(24)	121.0(9)
C(21)-N(9)-B(2)	132.7(8)	C(21)-C(22)-C(23)	106.0(9)
N(10)-N(9)-B(2)	119.6(7)	C(21)-C(22)-H(22A)	127.0
C(23)-N(10)-N(9)	106.7(7)	C(23)-C(22)-H(22A)	127.0
C(23)-N(10)-Ni(2)	136.7(7)	N(10)-C(23)-C(22)	110.6(9)

N(10)-C(23)-C(25)	119.3(9)	C(26)-C(29)-H(29C)	109.5
C(22)-C(23)-C(25)	130.1(9)	H(29A)-C(29)-H(29C)	109.5
C(21)-C(24)-H(24A)	109.5	H(29B)-C(29)-H(29C)	109.5
C(21)-C(24)-H(24B)	109.5	C(28)-C(30)-H(30A)	109.5
H(24A)-C(24)-H(24B)	109.5	C(28)-C(30)-H(30B)	109.5
C(21)-C(24)-H(24C)	109.5	H(30A)-C(30)-H(30B)	109.5
H(24A)-C(24)-H(24C)	109.5	C(28)-C(30)-H(30C)	109.5
H(24B)-C(24)-H(24C)	109.5	H(30A)-C(30)-H(30C)	109.5
C(23)-C(25)-H(25A)	109.5	H(30B)-C(30)-H(30C)	109.5
C(23)-C(25)-H(25B)	109.5	O(3)-C(31)-O(2)	131.0(8)
H(25A)-C(25)-H(25B)	109.5	O(3)-C(31)-O(1)	116.1(8)
C(23)-C(25)-H(25C)	109.5	O(2)-C(31)-O(1)	112.5(8)
H(25A)-C(25)-H(25C)	109.5	O(3)-C(31)-Ni(2)	54.0(5)
H(25B)-C(25)-H(25C)	109.5	O(2)-C(31)-Ni(2)	172.6(9)
C(27)-C(26)-N(11)	109.2(9)	O(1)-C(31)-Ni(2)	62.1(5)
C(27)-C(26)-C(29)	125.9(12)	O(3)-C(31)-Ni(1)	171.4(9)
N(11)-C(26)-C(29)	124.9(10)	O(2)-C(31)-Ni(1)	54.4(5)
C(26)-C(27)-C(28)	106.0(10)	O(1)-C(31)-Ni(1)	58.1(5)
C(26)-C(27)-H(27A)	127.0	Ni(2)-C(31)-Ni(1)	119.9(4)
C(28)-C(27)-H(27A)	127.0	C(31)-O(1)-Ni(1)	88.3(6)
N(12)-C(28)-C(27)	110.7(9)	C(31)-O(1)-Ni(2)	83.6(5)
N(12)-C(28)-C(30)	120.5(9)	Ni(1)-O(1)-Ni(2)	169.7(4)
C(27)-C(28)-C(30)	128.8(10)	C(31)-O(2)-Ni(1)	95.0(5)
C(26)-C(29)-H(29A)	109.5	C(31)-O(3)-Ni(2)	95.8(5)
C(26)-C(29)-H(29B)	109.5		
H(29A)-C(29)-H(29B)	109.5		

APPENDIX K: CRYSTAL STRUCTURE AND DATA REFINEMENT FOR
COMPLEX 4.4

Table K1. Crystal data and structure refinement for 4.4.

Empirical formula	C ₆₀ H ₅₆ B ₂ N ₁₂ Ni	
Formula weight	1025.50	
Temperature	173(2) K	
Wavelength	0.71073 Å	
Crystal system	Monoclinic	
Space group	C2/c	
Unit cell dimensions	$a = 18.0500(9)$ Å	$\alpha = 90^\circ$
	$b = 13.7439(7)$ Å	$\beta = 111.5050(10)^\circ$
	$c = 21.9848(15)$ Å	$\gamma = 90^\circ$
Volume	5074.3(5) Å ³	
Z, Z'	4, ½	
Density (calculated)	1.342 Mg/m ³	
Absorption coefficient	0.437 mm ⁻¹	
F(000)	2152	
Crystal color, morphology	green, block	
Crystal size	1.13 x 1.07 x 0.44 mm ³	
Theta range for data collection	1.94 to 27.48°	
Index ranges	$-23 \leq h \leq 23, -17 \leq k \leq 17, -28 \leq l \leq 28$	
Reflections collected	28593	
Independent reflections	5818 [$R(\text{int}) = 0.0221$]	
Observed reflections	5209	
Completeness to theta = 27.48°	99.8%	
Absorption correction	Multi-scan	
Max. and min. transmission	0.8317 and 0.6387	
Refinement method	Full-matrix least-squares on F^2	
Data / restraints / parameters	5818 / 0 / 346	
Goodness-of-fit on F^2	1.032	
Final R indices [$I > 2\sigma(I)$]	$R1 = 0.0308, wR2 = 0.0776$	
R indices (all data)	$R1 = 0.0356, wR2 = 0.0805$	
Largest diff. peak and hole	0.268 and -0.325 e.Å ⁻³	

Table K2. Atomic coordinates ($\times 10^4$) and equivalent isotropic displacement parameters ($\text{\AA}^2 \times 10^3$) for **4.4**. U_{eq} is defined as one third of the trace of the orthogonalized U_{ij} tensor.

	x	y	z	U_{eq}
Ni1	5000	7065(1)	7500	23(1)
N1	4217(1)	6023(1)	7680(1)	27(1)
N2	4055(1)	6262(1)	8223(1)	27(1)
N3	4405(1)	8223(1)	7803(1)	24(1)
N4	4404(1)	8038(1)	8416(1)	26(1)
N5	4139(1)	6943(1)	6475(1)	26(1)
N6	4548(1)	6776(1)	6069(1)	26(1)
C1	3697(1)	5307(1)	7376(1)	29(1)
C2	3203(1)	5114(1)	7724(1)	34(1)
C3	3441(1)	5723(1)	8253(1)	31(1)
C4	3112(1)	5831(1)	8783(1)	42(1)
C5	3677(1)	4767(1)	6788(1)	32(1)
C6	4349(1)	4599(1)	6639(1)	38(1)
C7	4310(1)	4063(1)	6093(1)	45(1)
C8	3597(1)	3681(1)	5684(1)	48(1)
C9	2925(1)	3828(1)	5830(1)	53(1)
C10	2960(1)	4362(1)	6376(1)	43(1)
C11	4157(1)	9154(1)	7668(1)	26(1)
C12	4009(1)	9553(1)	8197(1)	32(1)
C13	4181(1)	8839(1)	8663(1)	31(1)
C14	4183(1)	8888(1)	9343(1)	46(1)
C15	4051(1)	9700(1)	7062(1)	26(1)
C16	4076(1)	10715(1)	7095(1)	35(1)
C17	3987(1)	11278(1)	6551(1)	41(1)
C18	3865(1)	10838(1)	5959(1)	41(1)
C19	3827(1)	9835(1)	5915(1)	39(1)
C20	3915(1)	9267(1)	6458(1)	31(1)
C21	3361(1)	6791(1)	6104(1)	29(1)
C22	3291(1)	6527(1)	5471(1)	34(1)

C23	4044(1)	6517(1)	5465(1)	31(1)
C24	4316(1)	6241(1)	4925(1)	44(1)
C25	2676(1)	6926(1)	6313(1)	30(1)
C26	1924(1)	6610(1)	5899(1)	42(1)
C27	1259(1)	6759(1)	6056(1)	49(1)
C28	1318(1)	7224(1)	6625(1)	44(1)
C29	2056(1)	7520(1)	7048(1)	41(1)
C30	2726(1)	7376(1)	6891(1)	36(1)
B1	4561(1)	7014(1)	8717(1)	27(1)

Table K3. Bond lengths [Å] and angles [°] for 4.4.

Ni(1)-N(1)	2.1490(11)	C(8)-H(8A)	0.9500
Ni(1)-N(1)#1	2.1490(11)	C(9)-C(10)	1.389(2)
Ni(1)-N(3)#1	2.1568(11)	C(9)-H(9A)	0.9500
Ni(1)-N(3)	2.1568(11)	C(10)-H(10A)	0.9500
Ni(1)-N(5)	2.2260(11)	C(11)-C(12)	1.3974(18)
Ni(1)-N(5)#1	2.2260(11)	C(11)-C(15)	1.4790(17)
N(1)-C(1)	1.3540(17)	C(12)-C(13)	1.370(2)
N(1)-N(2)	1.3703(15)	C(12)-H(12A)	0.9500
N(2)-C(3)	1.3540(17)	C(13)-C(14)	1.4948(19)
N(2)-B(1)	1.5342(18)	C(14)-H(14A)	0.9800
N(3)-C(11)	1.3528(16)	C(14)-H(14B)	0.9800
N(3)-N(4)	1.3732(14)	C(14)-H(14C)	0.9800
N(4)-C(13)	1.3504(17)	C(15)-C(20)	1.3919(18)
N(4)-B(1)	1.5368(18)	C(15)-C(16)	1.3958(19)
N(5)-C(21)	1.3569(17)	C(16)-C(17)	1.384(2)
N(5)-N(6)	1.3708(15)	C(16)-H(16A)	0.9500
N(6)-C(23)	1.3530(17)	C(17)-C(18)	1.378(2)
N(6)-B(1)#1	1.5370(19)	C(17)-H(17A)	0.9500
C(1)-C(2)	1.3973(19)	C(18)-C(19)	1.381(2)
C(1)-C(5)	1.4809(19)	C(18)-H(18A)	0.9500
C(2)-C(3)	1.369(2)	C(19)-C(20)	1.387(2)
C(2)-H(2A)	0.9500	C(19)-H(19A)	0.9500
C(3)-C(4)	1.4964(19)	C(20)-H(20A)	0.9500
C(4)-H(4A)	0.9800	C(21)-C(22)	1.3990(19)
C(4)-H(4B)	0.9800	C(21)-C(25)	1.478(2)
C(4)-H(4C)	0.9800	C(22)-C(23)	1.364(2)
C(5)-C(6)	1.386(2)	C(22)-H(22A)	0.9500
C(5)-C(10)	1.395(2)	C(23)-C(24)	1.491(2)
C(6)-C(7)	1.388(2)	C(24)-H(24A)	0.9800
C(6)-H(6A)	0.9500	C(24)-H(24B)	0.9800
C(7)-C(8)	1.376(2)	C(24)-H(24C)	0.9800
C(7)-H(7A)	0.9500	C(25)-C(30)	1.387(2)
C(8)-C(9)	1.379(3)	C(25)-C(26)	1.3976(19)

C(26)-C(27)	1.380(2)	C(11)-N(3)-Ni(1)	142.38(8)
C(26)-H(26A)	0.9500	N(4)-N(3)-Ni(1)	110.34(8)
C(27)-C(28)	1.375(3)	C(13)-N(4)-N(3)	110.56(11)
C(27)-H(27A)	0.9500	C(13)-N(4)-B(1)	127.55(11)
C(28)-C(29)	1.377(2)	N(3)-N(4)-B(1)	121.62(10)
C(28)-H(28A)	0.9500	C(21)-N(5)-N(6)	105.59(10)
C(29)-C(30)	1.387(2)	C(21)-N(5)-Ni(1)	143.60(9)
C(29)-H(29A)	0.9500	N(6)-N(5)-Ni(1)	109.21(8)
C(30)-H(30A)	0.9500	C(23)-N(6)-N(5)	110.75(11)
B(1)-N(6)#1	1.5370(19)	C(23)-N(6)-B(1)#1	127.49(11)
B(1)-H(1B)	1.106(15)	N(5)-N(6)-B(1)#1	121.18(10)
		N(1)-C(1)-C(2)	109.57(12)
N(1)-Ni(1)-N(1)#1	96.32(6)	N(1)-C(1)-C(5)	125.76(12)
N(1)-Ni(1)-N(3)#1	169.84(4)	C(2)-C(1)-C(5)	124.58(12)
N(1)#1-Ni(1)-N(3)#1	89.96(4)	C(3)-C(2)-C(1)	106.50(12)
N(1)-Ni(1)-N(3)	89.96(4)	C(3)-C(2)-H(2A)	126.7
N(1)#1-Ni(1)-N(3)	169.84(4)	C(1)-C(2)-H(2A)	126.7
N(3)#1-Ni(1)-N(3)	85.00(6)	N(2)-C(3)-C(2)	107.49(12)
N(1)-Ni(1)-N(5)	82.71(4)	N(2)-C(3)-C(4)	123.34(13)
N(1)#1-Ni(1)-N(5)	91.48(4)	C(2)-C(3)-C(4)	129.16(13)
N(3)#1-Ni(1)-N(5)	89.17(4)	C(3)-C(4)-H(4A)	109.5
N(3)-Ni(1)-N(5)	97.25(4)	C(3)-C(4)-H(4B)	109.5
N(1)-Ni(1)-N(5)#1	91.48(4)	H(4A)-C(4)-H(4B)	109.5
N(1)#1-Ni(1)-N(5)#1	82.71(4)	C(3)-C(4)-H(4C)	109.5
N(3)#1-Ni(1)-N(5)#1	97.25(4)	H(4A)-C(4)-H(4C)	109.5
N(3)-Ni(1)-N(5)#1	89.17(4)	H(4B)-C(4)-H(4C)	109.5
N(5)-Ni(1)-N(5)#1	171.31(6)	C(6)-C(5)-C(10)	117.67(14)
C(1)-N(1)-N(2)	105.81(10)	C(6)-C(5)-C(1)	123.19(13)
C(1)-N(1)-Ni(1)	141.06(9)	C(10)-C(5)-C(1)	119.06(13)
N(2)-N(1)-Ni(1)	111.43(8)	C(5)-C(6)-C(7)	121.50(15)
C(3)-N(2)-N(1)	110.61(11)	C(5)-C(6)-H(6A)	119.2
C(3)-N(2)-B(1)	128.25(11)	C(7)-C(6)-H(6A)	119.2
N(1)-N(2)-B(1)	121.08(10)	C(8)-C(7)-C(6)	120.33(16)
C(11)-N(3)-N(4)	105.71(10)	C(8)-C(7)-H(7A)	119.8

C(6)-C(7)-H(7A)	119.8	C(17)-C(18)-C(19)	119.40(14)
C(7)-C(8)-C(9)	118.98(15)	C(17)-C(18)-H(18A)	120.3
C(7)-C(8)-H(8A)	120.5	C(19)-C(18)-H(18A)	120.3
C(9)-C(8)-H(8A)	120.5	C(18)-C(19)-C(20)	120.95(14)
C(8)-C(9)-C(10)	120.92(16)	C(18)-C(19)-H(19A)	119.5
C(8)-C(9)-H(9A)	119.5	C(20)-C(19)-H(19A)	119.5
C(10)-C(9)-H(9A)	119.5	C(19)-C(20)-C(15)	120.34(13)
C(9)-C(10)-C(5)	120.58(16)	C(19)-C(20)-H(20A)	119.8
C(9)-C(10)-H(10A)	119.7	C(15)-C(20)-H(20A)	119.8
C(5)-C(10)-H(10A)	119.7	N(5)-C(21)-C(22)	109.49(12)
N(3)-C(11)-C(12)	109.73(11)	N(5)-C(21)-C(25)	126.34(12)
N(3)-C(11)-C(15)	126.96(11)	C(22)-C(21)-C(25)	124.11(12)
C(12)-C(11)-C(15)	123.31(12)	C(23)-C(22)-C(21)	106.59(12)
C(13)-C(12)-C(11)	106.29(12)	C(23)-C(22)-H(22A)	126.7
C(13)-C(12)-H(12A)	126.9	C(21)-C(22)-H(22A)	126.7
C(11)-C(12)-H(12A)	126.9	N(6)-C(23)-C(22)	107.56(12)
N(4)-C(13)-C(12)	107.68(11)	N(6)-C(23)-C(24)	123.29(13)
N(4)-C(13)-C(14)	123.05(13)	C(22)-C(23)-C(24)	129.10(13)
C(12)-C(13)-C(14)	129.18(13)	C(23)-C(24)-H(24A)	109.5
C(13)-C(14)-H(14A)	109.5	C(23)-C(24)-H(24B)	109.5
C(13)-C(14)-H(14B)	109.5	H(24A)-C(24)-H(24B)	109.5
H(14A)-C(14)-H(14B)	109.5	C(23)-C(24)-H(24C)	109.5
C(13)-C(14)-H(14C)	109.5	H(24A)-C(24)-H(24C)	109.5
H(14A)-C(14)-H(14C)	109.5	H(24B)-C(24)-H(24C)	109.5
H(14B)-C(14)-H(14C)	109.5	C(30)-C(25)-C(26)	117.14(14)
C(20)-C(15)-C(16)	117.88(12)	C(30)-C(25)-C(21)	124.03(12)
C(20)-C(15)-C(11)	124.12(12)	C(26)-C(25)-C(21)	118.80(13)
C(16)-C(15)-C(11)	118.00(12)	C(27)-C(26)-C(25)	121.20(16)
C(17)-C(16)-C(15)	121.56(14)	C(27)-C(26)-H(26A)	119.4
C(17)-C(16)-H(16A)	119.2	C(25)-C(26)-H(26A)	119.4
C(15)-C(16)-H(16A)	119.2	C(28)-C(27)-C(26)	120.83(15)
C(18)-C(17)-C(16)	119.86(14)	C(28)-C(27)-H(27A)	119.6
C(18)-C(17)-H(17A)	120.1	C(26)-C(27)-H(27A)	119.6
C(16)-C(17)-H(17A)	120.1	C(27)-C(28)-C(29)	118.89(15)

C(27)-C(28)-H(28A)	120.6	N(2)-B(1)-N(4)	110.20(11)
C(29)-C(28)-H(28A)	120.6	N(2)-B(1)-N(6)#1	111.02(11)
C(28)-C(29)-C(30)	120.50(16)	N(4)-B(1)-N(6)#1	109.54(11)
C(28)-C(29)-H(29A)	119.8	N(2)-B(1)-H(1B)	108.3(8)
C(30)-C(29)-H(29A)	119.8	N(4)-B(1)-H(1B)	109.7(8)
C(25)-C(30)-C(29)	121.40(14)	N(6)#1-B(1)-H(1B)	108.1(8)
C(25)-C(30)-H(30A)	119.3		
C(29)-C(30)-H(30A)	119.3		

Symmetry transformations used to generate equivalent atoms:

#1 -x+1,y,-z+3/2



OHIO
UNIVERSITY

Thesis and Dissertation Services